

Unconventional Superconductivity and Magnetism in Lanthanide and Actinide Intermetallic Compounds

P. THALMEIER

Max-Planck-Institut für Chemische Physik fester Stoffe, 01187 Dresden

G. ZWICKNAGL

Institut für Mathematische Physik, Technische Universität Braunschweig,
38106 Braunschweig

Contents

1	Introduction	6
2	Theory and Techniques	10
2.1	Heavy quasiparticles in Ce, U compounds and their interactions	10
2.1.1	Kondo lattice model for Ce-compounds	10
2.1.2	Dual model for U-compounds	13
2.1.3	Fermi-liquid state and heavy quasiparticles: renormalized band theory	18
2.1.4	Quasiparticle interactions and spin fluctuation theory	20
2.2	Order parameters and their coexistence in strongly correlated electron systems	26
2.2.1	Order parameter classification	26
2.2.2	Pairing model for coexistence of SC and CDW/SDW	32
2.2.3	Coupled gap equations and results for coexistence	35
2.3	Methods to investigate the symmetry of order parameters	38
2.3.1	Detection of superconducting order parameter symmetry	38
2.3.2	Specific heat and magnetotransport in the vortex phase: a genuine angular resolved method	44
2.3.3	Detection of density wave type order parameters	49
3	Ce-based heavy-fermion superconductors	54
3.1	CeM ₂ X ₂	55
3.1.1	Electronic properties, Fermi surfaces and heavy quasiparticles	55
3.1.2	Superconductivity and itinerant antiferromagnetism in CeCu ₂ Si ₂	60
3.1.3	Pressure-induced superconductivity in CePd ₂ Si ₂ and CeNi ₂ Ge ₂	62
3.2	CeMIn ₅	64
3.2.1	Electronic properties and Fermi surfaces	65

3.2.2	Unconventional superconductivity in CeCoIn ₅	66
3.3	Superconductivity close to a quantum critical point	69
4	U-based heavy-fermion superconductors	71
4.1	Heavy fermion multicomponent superconductor UPt ₃	73
4.1.1	Dual model and heavy quasiparticles	73
4.1.2	Pairing and the spin-orbit coupling problem	77
4.1.3	Multicomponent superconducting order parameter	79
4.1.4	Small moment AF order	80
4.1.5	The superconducting state, coupled with AF order	81
4.1.6	The critical field curves and Ginzburg-Landau theory	84
4.1.7	The superconducting gap function	86
4.1.8	Low temperature transport properties	88
4.1.9	NMR Knight shift results	89
4.1.10	Magnetothermal properties in the vortex phase	90
4.2	Magnetic exciton mediated superconductivity in UPd ₂ Al ₃	92
4.2.1	AF structure and superconducting properties	92
4.2.2	Electronic structure, Fermi surface and effective mass	95
4.2.3	The dual model for UPd ₂ Al ₃ and induced moment AF	97
4.2.4	Induced moments and magnetic exciton dispersion in UPd ₂ Al ₃	98
4.2.5	Magnetic exciton anomalies in quasiparticle tunneling spectra	102
4.2.6	Possible symmetries of the superconducting order parameter	104
4.2.7	UNi ₂ Al ₃ : a possible triplet superconductor	105
4.3	Ferromagnetism and Superconductivity in UGe ₂	107
4.3.1	Electronic structure and band magnetism	109
4.3.2	Coexistence of FM order and superconductivity under pressure	111
4.3.3	Theoretical scenarios for superconductivity in UGe ₂	112
4.3.4	Symmetry properties of gap states and Ginzburg-Landau theory	113
4.3.5	Microscopic approaches	114
4.4	A case of ‘Hidden Order’ in URu ₂ Si ₂	115
4.4.1	Electronic structure and 5f-states	115
4.4.2	Phase transitions, field and pressure dependence	117
4.4.3	Theoretical models: localised vs. itinerant	118
4.4.4	High field phase diagram and metamagnetism	121
4.4.5	Collective excitations in the ordered phase	122
4.4.6	The superconducting state	122
4.5	Superconductivity in the non-Fermi liquid state of UBe ₁₃ and U _{1-x} Th _x Be ₁₃	124
4.5.1	Normal state and nFl properties of UBe ₁₃	124
4.5.2	The 5f-ground state of U	124
4.5.3	The superconducting state in UBe ₁₃	125
4.5.4	Superconducting phase diagram of Th-doped crystals	125
5	Rare Earth Borocarbide superconductors	129
5.1	Physical properties of the nonmagnetic borocarbides	130
5.1.1	Evidence for electron-phonon superconductivity	131

5.1.2	Anomalous H_{c2} -behaviour	132
5.1.3	Specific heat and thermal conductivity results	132
5.2	Theoretical analysis of nonmagnetic borocarbides	133
5.2.1	Electronic Structure of the Borocarbides	133
5.2.2	Nodal structure of the superconducting gap and impurity effects . .	134
5.2.3	Thermodynamics and transport in the vortex phase	136
5.3	Magnetic borocarbides	138
5.3.1	Metamagnetism and IC-C lock-in transition in $\text{HoNi}_2\text{B}_2\text{C}$	139
5.3.2	Weak Ferromagnetism in $\text{ErNi}_2\text{B}_2\text{C}$	143
5.4	Coexistence of superconductivity and magnetic order	143
5.4.1	Coexistence of helical SDW, antiferromagnetism and superconductivity in $\text{HoNi}_2\text{B}_2\text{C}$	144
5.4.2	Coexistence of superconductivity and weak ferromagnetism in $\text{ErNi}_2\text{B}_2\text{C}$	149
6	Rare Earth Skutterudite Superconductors	150
6.1	Electronic structure and HF behaviour of $\text{PrOs}_4\text{Sb}_{12}$	150
6.2	Pr-CEF states and antiferroquadrupolar order	151
6.3	The superconducting split transition	153
6.4	Thermal conductivity in the vortex phase and multiphase superconductivity in $\text{PrOs}_4\text{Sb}_{12}$	154
6.5	Gap models for SC A- and B-phases of $\text{PrOs}_4\text{Sb}_{12}$	156
7	Summary and Outlook	159

List of acronyms

AF	antiferromagnetic
AFQ	antiferroquadrupolar
ANNNI	anisotropic next nearest neighbor Ising
ARPES	angle resolved photoemission spectroscopy
BIS	Bremsstrahlung isochromat spectroscopy
BZ	Brillouin zone
CDW	charge density wave
CEF	crystalline electric field
dHvA	de Haas-van Alphen
DLRO	diagonal long range order
DOS	density of states
e-e	electron-electron
e-h	electron-hole
e-p	electron-phonon
FFLO	Fulde-Ferrell-Larkin-Ovchinnikov
FL	Fermi liquid
FLEX	fluctuation exchange
FM	ferromagnet
FS	Fermi surface
GL	Ginzburg-Landau
HF	heavy fermion
IC	incommensurate
INS	inelastic neutron scattering
LDA	local density approximation
LSDA	local spin density approximation
mf	mean field
MFS	magnetic Fermi surface
nFl	non-Fermi liquid
n.n.	next neighbor
n.n.n.	next nearest neighbor
NCA	non-crossing approximation
NMR	nuclear magnetic resonance
OAF	orbital antiferromagnet
ODLRO	off-diagonal long range order
OP	order parameter
PES	photoemission spectroscopy
QCP	quantum critical point
qp	quasi particle
RPA	random phase approximation
RKKY	Ruderman-Kittel-Kasuya-Yoshida
SBF	symmetry breaking field
SC	superconductivity
SDW	spin density wave
SN	spin nematic
s.o.	spin orbit
WFM	weak ferromagnetism

List of symbols

$\alpha(T)$	ultrasonic attenuation	$N(E)$	quasiparticle DOS
$\alpha_0, \beta, \gamma_0$	Landau free energy parameters	N_n	normal state quasiparticle DOS at E_F
B, H, M	magnetic induction, magnetic field and magnetisation	p	pressure
c, c^\dagger	conduction electron operators	Q	nesting or ordering wave vector
$C(T)$	specific heat	$\rho(T)$	electrical resistivity
δ	CEF splitting energy	$\rho_{\mathbf{Q}}$	conduction electron charge density
$\Delta(\mathbf{k})$	gap function (SC, SDW etc.; singlet, triplet etc.)	s_Q	conduction electron spin density
d(k)	vector of triplet gap functions	σ	vector of Pauli matrices
$\epsilon_{\mathbf{k}}$	quasiparticle energy in the normal state	θ, ϕ	polar angles of H
$E_{\mathbf{k}}$	quasiparticle energy in the ordered state (SC, SDW etc.)	ϑ, φ	polar angles of k
E_F	Fermi energy	t	nearest neighbor hopping matrix element
$f(\mathbf{k})$	form factor of gap functions	t'	next nearest neighbor hopping matrix element
$f(E_{\mathbf{k}})$	Fermi function	T	temperature
f_L, f_{GL}	Landau and Ginzburg-Landau free energy density	T*	characteristic or 'Kondo' temperature of HF compound
γ	linear specific heat (Sommerfeld) coefficient	T_c	superconducting transition temperature
Γ	quasiparticle scattering rate	T_N	Néel temperature
$ \Gamma\rangle$	CEF state	T_1^{-1}	NMR relaxation rate
η	SC vector order parameter	U	bare on-site Coulomb interaction
H_{c2}	upper critical field of the superconductor	$u(\omega)$	local CEF susceptibility
I	residual on-site quasiparticle repulsion or contact exchange	v_F	Fermi velocity
$J(\mathbf{q})$	effective interaction between quasiparticles or local moments	$\mathbf{v}_s(\mathbf{r})$	superfluid velocity field
J	total angular momentum of f-shell	V_l	effective quasiparticle interaction (l = angular momentum channel)
$\kappa(T)$	thermal conductivity	\tilde{v}	average Fermi velocity in uniaxial crystal
k, q	conduction electron wave vectors	$\chi_n, \chi_s(T)$	static homogeneous (q = 0) conduction electron spin susceptibility in normal and SC state
k_F	Fermi wave number	$\chi(\mathbf{q}, \omega)$	magnetic susceptibilities for conduction electrons or localised moments
λ	electron-phonon interaction	x	impurity or dopant concentration
μ, μ_B	magnetic moment, Bohr magneton	Y(T)	Yoshida function
m	free electron mass	ω	frequency
m_b	conduction electron band mass	$\omega_E(\mathbf{q})$	magnetic exciton dispersion
m^*	effective quasiparticle mass		
M_Q	staggered magnetization		

1. Introduction

The Fermi liquid state in metals has two common instabilities. Superconductivity (SC) is due to pair formation of electrons and (spin-, charge-) density waves (CDW, SDW) are formed by pairing electrons and holes. Theoretically it has been suspected quite early that pair-wave functions other than s-wave as in conventional superconductors and density waves may exist. However it has taken surprisingly long to identify such 'unconventional' condensed pair states in real materials.

Now there is an abundance of non-s-wave superconductors which are frequently associated with anisotropic 'nodal' gap functions where the quasiparticle excitations of the SC state vanishes on points or lines on the Fermi surface. This leads to low temperature 'power law' behaviour in many physical quantities. Heavy fermion (HF) lanthanide and actinide superconducting compounds were the first that were supposed to have unconventional SC pair states mediated by low energy spin fluctuations. High T_c cuprates which exhibit d-wave superconductivity are the most prominent and important examples. But nodal SC have also been found among the ruthenates and organic salts.

Conventional CDW and SDW states are ubiquitous in metals with the commensurate SDW or antiferromagnetic (AF) order being the most common. Compounds with confirmed unconventional density waves so far are rather scarce and with certainty have only been found in organic metals and perhaps in uranium HF compounds and the 'pseudo-gap' phase of underdoped cuprates. This may in part be due to the difficulty detecting such 'hidden' order parameters which leave no signature in standard neutron or x-ray diffraction experiments.

In this review article we will summarize the knowledge on a class of unconventional superconductors and their competition and coexistence with magnetism and hidden order phases that has accumulated over the last decade. To be comprehensive we will restrict ourselves exclusively to intermetallic lanthanide (4f) and actinide (5f) systems. Except for occasional remarks we will leave out completely the cuprate, cobaltate and ruthenate superconductors which are beyond the scope of our work on intermetallic compounds. The oxide superconductors are mostly close to a Mott insulator transition and the underlying microscopic physics is very different from the intermetallic f-electron compounds. Although on the phenomenological level of SC and density wave order parameter classification and investigation strong similarities exist. Likewise we do not discuss unconventional organic superconductors. The focus here is on stoichiometric 4f- and 5f-compounds where the lanthanide or actinide atoms occupy regular sublattices. With the exception of rare earth borocarbides the compounds reviewed are heavy fermion metals to a varying degree. In our review we do not want to provide an exhausting compilation of the physical properties in this whole class of materials. We rather focus on a few important compounds where each displays an important aspect of unconventional SC and its relation to magnetism or hidden order that will be discussed in detail in its physical and theoretical implications.

The complex low temperature phase diagrams of the HF metals results from the partially filled f-shells of the lanthanide and actinide ions which preserve atomic-like character. Occupying the states according to Hund's rules leads to magnetic moments. In a crystal their rotational degeneracy is partly lifted by the crystalline electric field (CEF) and the hybridisation with broad conduction bands corresponding to outer shell electrons. As a

result a large number of low-energy excitations appears. In the ideal Fermi liquid case these excitations correspond to heavy quasiparticles whose effective mass m^* is by orders of magnitude larger than the free electron mass m . The corresponding quasiparticle band width T^* is of the order meV for true HF metals. The mass enhancement is reflected in large increase of the specific heat γ -value, the Pauli susceptibility and the T^2 -coefficient of electrical resistivity. However close to a quantum critical point (QCP) which signifies the onset of density wave instabilities low temperature anomalies in these quantities appear which are characteristic signatures of a non-Fermi liquid state.

At this point, we emphasize that the Landau theory of Fermi liquids does not make assumptions concerning the microscopic nature of the ground state and the low-lying excitations, it merely gives a counting prescription. It does not address the question how they emerge in an interacting electron system, this requires a microscopic treatment. Generally speaking heavy quasiparticles arise from the lifting of local degeneracies which result as a consequence of strong local correlations. Various mechanisms for heavy mass generation have been suggested. While in Ce compounds with well localised $4f^1$ states the Kondo mechanism is appropriate, and there is increasing evidence that the dual, i.e. partly localised and partly itinerant, nature of $5f$ -states is responsible for the mass renormalization in the U compounds. In both scenarios it is assumed that the heavy quasiparticles predominantly have f -character.

Residual interactions among the quasiparticles lead to the pairing instabilities. Two candidates have been identified in HF compounds : Firstly pairing interactions via exchange of enhanced overdamped spin fluctuations of itinerant quasiparticles, presumably at an antiferromagnetic wave vector. This model is invoked for Ce-compounds, especially when SC appears near a quantum critical point. It may also contain some truth for the more itinerant U-HF compounds. However we now know for sure that in U-compounds with partly localised $5f$ -electrons a different mechanism is at work: pairing mediated by the exchange of propagating internal excitations ('magnetic excitons') of the localised $5f$ subsystem. A variant of this mechanism may also be appropriate for the recently discovered Pr-skutterudite HF superconductor with quadrupolar instead of magnetic excitons involved.

A major topic of our review is the critical discussion of existing evidence for unconventional SC order parameters as witnessed frequently by the presence of nodal gap functions. Previously the identification of gap symmetries has been an elaborate guess work mostly built on indirect evidence from low temperature 'power laws'. This situation has dramatically improved in recent years with the advent of genuine angular resolved magnetothermal and magnetotransport experiments in the vortex phase. They exploit the Doppler shift of SC quasiparticle energies which leads to field-angle oscillations in specific heat and thermal conductivity. Their analysis may lead to an unambiguous determination of nodal positions of the gap functions which facilitates a strong restriction and sometimes unique determination of the possible gap symmetry.

Superconductivity in HF-compounds frequently coexists with (spin-) density waves. In some cases they may be of the unconventional (hidden order) type. We discuss the competition and coexistence behaviour of these order parameters and related physical effects. Since both order parameters appear in the itinerant quasiparticle system this is a subtle interplay of Fermi surface geometry, pairing potentials and gap structures which

can only be schematically understood in simplified toy models.

Coexistence behaviour is much simpler in the relatively new class of rare earth borocarbide superconductors which have comparatively high T_c 's. Although as electron-phonon superconductors they are set aside from our main focus on HF systems, they have been included in this review for various reasons: Firstly magnetism and SC superconductivity are carried by different species of electrons which only interact weakly through contact exchange interaction leading to a small effect of the local moment molecular field on the SC conduction electrons. This can be nicely treated by perturbation theory and allows a much better understanding of coexistence behaviour as compared to the HF systems. Also they provide the first example of homogeneous coexistence of SC and ferromagnetism for all temperatures below T_c . Secondly the nonmagnetic rare earth borocarbides have extremely large gap anisotropy ratios $\geq 10^2$ which means that they are essentially nodal superconductors. In fact nonmagnetic borocarbides are the first which have been identified to have a SC gap with point nodes that is of fully symmetric s+g wave type. Surely the standard electron-phonon mechanism has to be supplemented by something else, perhaps anisotropic Coulomb interactions to achieve this 'quasi-unconventional' behaviour in borocarbides.

Considering the wide range of phenomena and questions involved we have to be quite selective in our review. We will concentrate on the exciting developments in 4f/5f intermetallic materials of the past decade referring to the literature for the earlier work. A general introduction to strongly correlated electron systems is given in the textbooks of Fulde (1995) and Fazekas (1999). Various aspects of heavy fermion physics are described in the previous review articles by Stewart et al. (1984), Ott (1987), Ott and Fisk (1987), Fulde et al. (1988) Grewe and Steglich (1991), Thalmeier and Lüthi (1991) and Zwicknagl (1992) as well as in the monographs by Kuramoto and Kitaoka (2000) and Hewson (1993). Reviews which focus on theories of unconventional HF superconductors are Sigrist and Ueda (1991), Sauls (1994) and Joynt and Taillefer (2002) and the monograph by Mineev and Samokhin (1999). Reviews discussing the rare earth borocarbide magnetic superconductors are given in Hilscher and Michor (1999) and Müller and Narozhnyi (2001). Earlier reviews of coexistence of superconductivity and localised magnetism can be found in Fulde and Keller (1982), Fulde and Zwicknagl (1990) and Fischer (1990).

Since we will not discuss oxide or organic unconventional superconductors we would like to refer to a few review articles where parallel developments, especially on pairing mechanism and gap function symmetries are discussed for these classes of materials: van Harlingen (1995), Scalapino (1995), Izyumov (1999), Moriya and Ueda (2000), Yanase et al. (2003) and Tsuei and Kirtley (2000) for cuprates, Mackenzie and Maeno (2003) for ruthenates and Maki and Won (1996) and Lang and Müller (2003) for unconventional organic superconductors.

The present review focuses on chosen topics of high current interest. We therefore select specific materials which allow us to discuss physical effects and theoretical concepts in detail.

The article is organized as follows: In sect. 2 we review the basic theoretical concepts and experimental techniques to identify pair condensate order parameters, especially we discuss the important new tool of angular resolved methods for SC gap investigation. Section 3 deals with the Ce-based heavy fermion compounds. The central question there

is the competition between magnetism and Fermi liquid states which may become superconducting. While superconducting ground states seem to occur rather rarely in Ce-based heavy fermion systems they are common in their U-based counterparts discussed in sect. 4. The major challenge in this context is the investigation of the unconventional and often exotic pairing mechanism and the identification of the symmetry of superconducting order parameters which may coexist with (hidden) long-range order. The low-temperature phases of rare earth borocarbides are reviewed in sect. 5. Of particular interest are the unusual magnetic ordering phenomena which may coexist with very anisotropic electron-phonon superconductivity. Section 6 is devoted to the newly discovered superconducting rare earth skutterudite cage compounds which may exhibit a quadrupolar pairing mechanism. We conclude in sect. 7 by giving a summary and an outlook.

2. Theory and Techniques

The theoretical understanding of superconductivity and magnetism in the Heavy Fermion systems is still in the state of rather schematic or illustrative models without real predictive power. The difficulty arises on two levels. Firstly the normal state quasiparticles themselves can so far be described only within effective one particle renormalised band pictures with empirical input parameters. For some compounds like URu_2Si_2 and Ce-compounds close to the quantum critical point the SC transition even takes place in a state without well defined quasiparticles as witnessed by the observation of non-Fermi liquid (nFL) behaviour. Secondly the effective pairing interactions can only be described in an oversimplified way as in the spin fluctuation models and its variants. They commonly neglect the internal orbital structure of f-electron compounds due to the intra-atomic spin orbit coupling and CEF potential. Attempts to include these terms have not been carried very far. Nevertheless it is important to understand these qualitative theories. We first discuss normal state quasiparticles, namely Kondo lattice models for Ce-compounds vs. dual 5f-electrons models for the U-compounds. Starting from this basis the renormalised band theory provides a way to describe the heavy quasiparticle bands within a Fermi liquid approach. From there approximate models for the effective pairing interactions may be obtained by standard many body techniques. The symmetry classification of pairing order parameters is an important step to understand the nodal structure of the gap and solve the gap equations. Models for coexistence and competition of SC and density wave order parameters frequently observed in HF metals will also be discussed. Finally we make a survey of theoretical ideas and experimental methods to identify the nodal structure of SC and density type order parameters which is the most important ingredient to understand the physics of HF superconductors.

2.1. Heavy quasiparticles in Ce, U compounds and their interactions

A prerequisite for a microscopic theory of superconductivity in heavy-fermion compounds is a description of the normal state and of the low-energy excitations at low temperatures. We begin by reviewing the physical processes which lead to the high density of low-energy excitations reflected in the strongly enhanced specific heat. The corresponding microscopic many-body problems, i. e. , the Kondo model and the dual model, can be solved for (effective) impurities but not for extended systems. The energy dispersion of the coherent quasiparticle states in a periodic lattice, however, can be calculated from an effective single-particle Hamiltonian where the effective and not necessarily local potential is devised to account for the relevant many-body effects. The residual interaction among the quasiparticles eventually leads to the instability of the normal Fermi liquid phase. We focus on Cooper pair formation induced by electron-electron interactions. Of particular importance are spin-fluctuation models which were adopted in the majority of papers during the past decade.

2.1.1. Kondo lattice model for Ce-compounds

The similarities in the behavior of Ce-based heavy-fermion systems to that of dilute magnetic alloys have led to the assumption that these systems are ‘Kondo lattices’ where the observed anomalous behavior can be explained in terms of periodically repeated resonant Kondo scattering. This ansatz provides a microscopic model for the formation of

a singlet ground state and the existence of heavy quasiparticles. In addition, it explains why there is no magnetic pairbreaking associated with the presence of the f-electrons. An extensive review is given by Hewson (1993). The Kondo picture for the Ce-based heavy-fermion compounds is supported by the fact that both the thermodynamic properties at low temperatures (e. g., the specific heat, the magnetic susceptibility) as well as the temperature-dependence of the spectroscopic data can be reproduced by an Anderson model with the same parameters (Gunnarsson and Schönhammer 1983). The most direct evidence, however, comes from photoelectron spectroscopy. The characteristic features of a Kondo system can be summarized as follows (Allen 1992, Malterre et al. 1996): At high temperatures, the combined PES/BIS spectra from photoemission and inverse photoemission exhibit two distinct peaks below and above the Fermi energy. These two features correspond to the valence transitions $f^n \rightarrow f^{n\pm 1}$, respectively. The changes in the occupation of the Ce 4f-shells are associated with energies of order eV. The high-temperature state can be modelled by weakly correlated conduction electrons which are weakly coupled to local f-moments. The f-derived low-energy excitations are those of a system of local moments. The direct manifestation of the low-energy scale is the appearance of a sharp peak in the f-spectral density near the Fermi energy when the temperature T is smaller than a characteristic ('Kondo') temperature T^* . In Ce systems, this many-body feature, i. e., the 'Abrikosov-Suhl' or 'Kondo' resonance, is centered at $E_F + kT^*$ slightly above the Fermi edge E_F with $T^* \simeq W \exp(\pi E_f / N_f \Delta)$ up to a constant of order unity. Here W is the conduction band width, $E_f < 0$ is the f-level position below the Fermi level $E_F \equiv 0$, N_f the f-level degeneracy and $\Delta = \pi |V|^2 N(E_F)$ is the hybridization or charge fluctuation width which can be estimated from the width of the transition $4f^1 \rightarrow 4f^0$ (V = hybridization matrix element, $N(E_F)$ = conduction electron DOS). This energy scale characterises the dynamical screening of the impurity spin by conduction electron spin fluctuations within a "screening cloud" that extends to distances $\sim \hbar v_F / T^*$ away from the impurity. The evolution of the Kondo resonance with temperature was recently observed by high-resolution photoemission experiments. The spectra displayed in fig. 1 provide direct evidence for the presence of a Kondo resonance in the lattice. The resonance is a genuine many-body feature reflecting the small admixture of f^0 -configurations to the ground state and the low-lying excitations which are mainly built from f^1 -configurations. By hybridization with conduction states via transitions $f^1 \leftrightarrow f^0$, the local magnetic degeneracies of the singly occupied 4f-shells are lifted. The characteristic energy $kT^* \simeq 1 - 10$ meV which can be surprisingly close to the value of the corresponding dilute system sets the scale for the anomalous low-temperature behavior. The width and the overall weight of the resonance are of the order $\pi kT^* / N_f$ and $\pi kT^* / N_f \Delta = 1 - n_f \ll 1$ respectively. Here n_f denotes the occupation of the f^1 state which in the Kondo limit $\Delta \ll |E_f|$ is slightly less than one due to the finite hybridisation matrix element V with conduction electrons. Impurity model calculations based on the NCA approximation for the Anderson model indicate that the Kondo resonance states exist as long as $n_f \geq 0.85$. For smaller n_f due to larger V one enters the mixed valent regime. At sufficiently low temperatures $T \ll T^*$, the contribution of the narrow resonance peak to the thermodynamic and transport properties can be described in terms of a Landau theory with heavy fermionic quasiparticles as suggested by the renormalization group calculations for magnetic impurities immersed in a metallic host (Wilson 1975). Based on the corresponding effective Hamiltonian Nozières

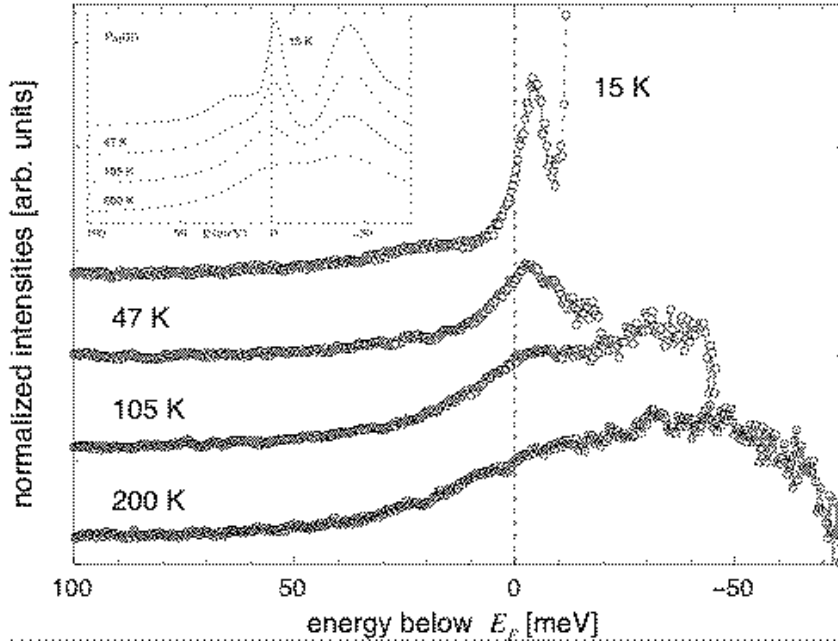


Figure 1. PES spectra at various temperatures showing the appearance of the low temperature Kondo resonance in CeCu_2Si_2 . The inset shows 4f-spectral density $\rho_{4f}(E)$ of the impurity Anderson model calculated within NCA (Reinert et al., 2001).

(1974) introduced a narrow resonant phase shift to account for the impurity contribution to the low-energy properties.

The novel feature observed in stoichiometric Ce-compounds is the formation of narrow coherent bands of low-energy excitations (Garnier et al. 1997, Garnier et al. 1998, Zwicky 1999). Following this line of thought, heavy fermions arise from a decoherence-coherence crossover. The strong local correlations in Kondo lattices lead to an observable many-body effect, i. e., the change with temperature of the volume of the Fermi surface. At high temperatures, the f -degrees of freedom appear as localized magnetic moments, and the Fermi surface contains only the itinerant conduction electrons. At low temperatures, however, the f degrees of freedom are now tied into itinerant fermionic quasi-particle excitations and accordingly, have to be included in the Fermi volume following Luttinger's theorem. Consequently the Fermi surface is strongly modified. This scenario (Zwicky 1993) was confirmed experimentally by measurements of the de Haas-van Alphen (dHvA) effect (Lonzarich 1988, Aoki et al. 1993, Tautz et al. 1995).

Competition between the formation of (local) Kondo singlets and the lifting of degeneracies by long-range magnetic order is clearly evident in many Ce-based heavy fermion compounds. In the high-temperature regime the moments of the Ce 4f-shells are coupled by the RKKY interaction which can favor parallel as well as antiparallel orientation of the moments at neighboring sites. In the majority of cases, there is a tendency towards antiferromagnetic alignment although also ferromagnetic HF systems are known. Model calculations for two Kondo impurities (Jayprakash et al. 1981, Jayprakash et al. 1982, Jones

and Varma 1987) showed that antiferromagnetic correlations between the magnetic sites weaken the Kondo singlet formation reducing the characteristic energy scale kT^* to rather small values. Since the latter plays the role of an effective Fermi energy for the heavy quasiparticles it is not surprising that the Fermi liquid description fails to be valid in systems with sufficiently strong antiferromagnetic correlations.

For Ce-based systems, the natural tuning parameter is the hybridization which measures the coupling between the strongly correlated f-electrons and the weakly correlated conduction states. This coupling, which can be increased by applying hydrostatic pressure or chemical pressure via proper element substitution, affects the f-electron system in two different ways. First, it is responsible for the indirect exchange interaction building up magnetic correlations between the moments at different sites. On the other hand, it leads to the formation of local singlets via the Kondo effect. The energy gain due to magnetic ordering follows a power law for weak hybridization whereas the Kondo temperature depends exponentially on the latter. Based on these considerations, Doniach (1977) suggested that for sufficiently weak hybridization the f-derived magnetic moments should order. With increasing hybridization, however, the magnetic ordering temperature should be suppressed and a Fermi liquid ground state characterized by Kondo-type correlations forms above a quantum critical point (QCP). At the QCP itself non-Fermi liquid behaviour is expected in the temperature dependence of physical quantities. The resulting schematic “Doniach” phase diagram has been widely used to understand qualitatively the variation with pressure of the anomalous low-temperature properties in heavy-fermion systems. It seems that in the majority of Ce-based heavy-fermion superconductors the superconducting phase develops in the vicinity of a quantum critical point.

2.1.2. Dual model for U-compounds

The Kondo picture, however, does not apply in the case of the actinide compounds. The difficulties with this model have been discussed in (Cox and Zawadowski 1999). The difference between the Ce-based heavy-fermion compounds and their U-counterparts can be seen directly from the photoemission spectra (Allen 1992). In U-based heavy-fermion compounds, the fingerprint character of the transitions $f^n \rightarrow f^{n\pm 1}$ is lost. Instead of the well-defined f-derived peaks familiar for the Ce systems, we encounter a rather broad f-derived feature. This fact shows that the f-valence in the actinide heavy-fermion systems is not close to integer value as it is the case in Ce-based compounds. In fact, the f-valence of the U ions has been discussed rather controversially.

There is growing evidence that actinide ions may have localized as well as delocalized $5f$ electrons. This picture which was suggested by susceptibility measurements (Schoenes et al. 1996) is supported by a great variety of experiments including, e. g., photoemission and neutron inelastic scattering experiments on UPd_2Al_3 (Takahashi et al. 1995, Metoki et al. 1998, Bernhoeft et al. 1998) as well as muon spin relaxation measurement in UGe_2 (Yaouanc et al. 2002). The assumption is further supported by quantum chemical calculations on uranocene $U(C_8H_8)_2$ (Liu et al. 1998) which exhibit a number of low-lying excitations which are due to intra-shell rearrangements of $5f$ electrons. There is clear evidence that the presence of localized $5f$ -states is even responsible for the attractive interactions leading to superconductivity (Sato et al. 2001). In addition the dual model should allow for a rather natural description of heavy fermion superconductivity coexisting

with 5f-derived magnetism.

The above-mentioned observations form the basis of the dual model which assumes the coexistence of both itinerant and localized 5f electrons. The former hybridize with the conduction states and form energy bands while the latter form multiplets to reduce the local Coulomb repulsion. The two subsystems interact which leads to the mass enhancement of the delocalized quasiparticles. The situation resembles that in Pr metal where a mass enhancement of the conduction electrons by a factor of 5 results from virtual crystal field (CEF) excitations of localized $4f^2$ electrons (White and Fulde 1981). The underlying hypothesis is supported by a number of experiments. Detailed Fermi surface studies for UGa_3 (Biasini 2003) show that the experimental data cannot be explained by assuming all 5f-electrons to be itinerant nor by treating them as fully localized. The basic assumptions underlying the dual model were recently confirmed by measurements of the optical conductivity (Dressel et al. 2002) which show the evolution of the high effective mass at low temperatures. The formation of the heavy quasiparticles is also observed in ARPES (Denlinger et al. 2001).

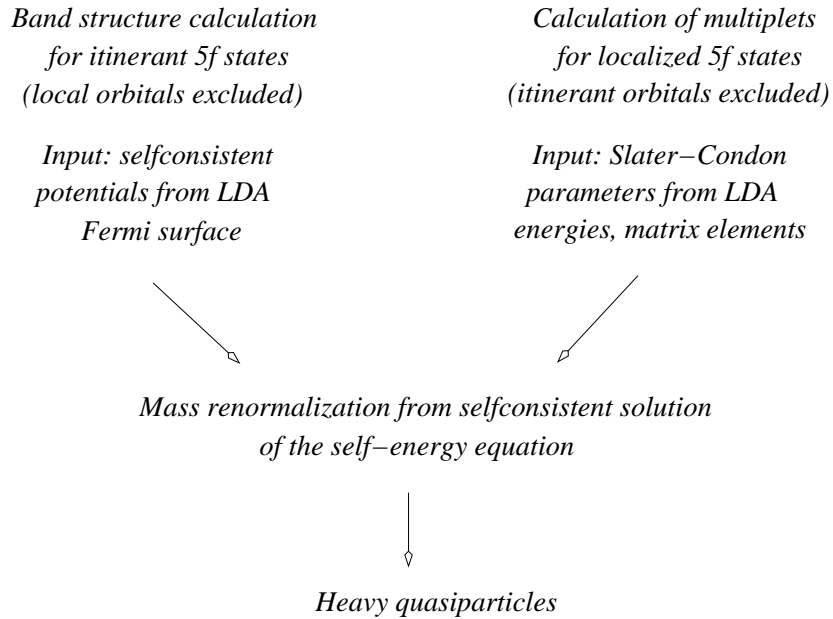


Figure 2. Calculational scheme for heavy quasiparticles in U-based heavy-fermion compounds

The dual model provides a microscopic theory for the heavy quasiparticles in U compounds. The method reproduces the dHvA data in UPt_3 (Zwicknagl et al. 2002) and UPd_2Al_3 (Zwicknagl et al. 2003). The calculation of the heavy bands proceeds in three steps schematically summarized in fig. 2. First, the band structure is determined by solving the Dirac equation for the self-consistent LDA potentials but excluding two U

$5f$ ($j=5/2$) states from forming bands. The choice of the itinerant and localized orbitals depends upon the symmetry of the crystal and the hybridization strengths. The localized $5f$ orbitals are accounted for in the self-consistent density and accordingly in the potential seen by the conduction electrons. The intrinsic bandwidth of the itinerant U $5f$ $j=5/2$ electrons is taken from the LDA calculation while the position of the corresponding band center is chosen such that the density distribution of the conduction states as obtained within LDA remains unchanged. For UPt₃ and UPd₂Al₃, the f-occupancy per U atom for the delocalized 5f-electrons amounts to $n_f = 0.65$ indicating that we are dealing with a mixed valent situation. The calculations yield the dHvA frequencies which can be directly compared with experimental data. In the second step, the localized U $5f$ states are calculated by diagonalizing the Coulomb matrix in the restricted subspace of the localized $5f$ states. Assuming the jj-coupling scheme, the Coulomb matrix elements are calculated from the radial functions of the ab-initio band structure potentials. In a crystal, the degeneracies of the ground-state may be lifted by a CEF. This is in fact the case for UPd₂Al₃ where the resulting singlet ground state of the localized $5f^2$ is given by $|g\rangle = (1/\sqrt{2})(|J_z = 3\rangle + |J_z = -3\rangle)$ in the $J = 4$ subspace. The coupling between the localized and delocalized $5f$ electrons is directly obtained from the expectation values of the Coulomb interaction H_C in the $5f^3$ states. Finally, the renormalization of the effective masses which results from the coupling between the two $5f$ subsystems is determined. The enhancement factor is calculated from the self-consistent solution of the self-energy equation (White and Fulde 1981) with the input taken from the ab-initio electronic structure calculations for the delocalized and the localized $5f$ electrons.

The coexistence of itinerant and localized $5f$ states is a consequence of the interplay between hybridization with the conduction electrons and local Coulomb correlations. This "partial localization" of the $5f$ states is found in many actinide intermetallic compounds. The underlying microscopic mechanism is an area of active current research (Lundin et al. 2000, Söderlind et al. 2000). LDA calculations show that the hopping matrix elements for different $5f$ orbitals vary. But it is of interest to understand why only the largest one of them is important and why the other ones are suppressed.

Partial localization may arise from the competition between hopping and angular correlations. This can be seen by exact diagonalization of small clusters which model the U sites in heavy fermion compounds (Efremov et al. 2003). We keep only the degrees of freedom of the $5f$ shells the conduction states being accounted for by (effective) anisotropic intersite hopping. The Hamiltonian reads

$$H = - \sum_{\langle nm \rangle, j_z} t_{j_z} \left(c_{j_z}^\dagger(n) c_{j_z}(m) + h.c. \right) + H_C \quad (1)$$

where the first sum is over neighboring sites $\langle nm \rangle$. Furthermore $c_{j_z}^\dagger(n)$ ($c_{j_z}(n)$), creates (annihilates) an electron at site n in the $5f$ $j = 5/2$ state with $j_z = -5/2, \dots, 5/2$. We will consider two and three sites models. Since the relevant correlations are local the results for these small clusters are qualitatively similar to those of four-site models. The effective hopping between sites results from the hybridisation of the $5f$ states with the orbitals of the ligands and depends generally on the crystal structure. Rather than trying to exhaust all possible different lattice symmetries, we shall concentrate here on the special case that hopping conserves j_z . While this is certainly an idealization, it allows us

to concentrate on our main interest, i. e., a study of the influence of atomic correlations on the renormalization of hybridization matrix elements. The parameters t_{j_z} ($= t_{-j_z}$) are chosen in accordance with density-functional calculations for bulk material which use jj_z basis states. The local Coulomb interactions can be written in the form

$$H_C = \frac{1}{2} \sum_n \sum_{j_{z1}, \dots, j_{z4}} U_{j_{z1}j_{z2}, j_{z3}j_{z4}} c_{j_{z1}}^\dagger(n) c_{j_{z2}}^\dagger(n) c_{j_{z3}}(n) c_{j_{z4}}(n) \quad (2)$$

with Coulomb matrix elements

$$U_{j_{z1}j_{z2}, j_{z3}j_{z4}} = \delta_{j_{z1}+j_{z2}, j_{z3}+j_{z4}} \sum_J \langle \frac{5}{2} \frac{5}{2} j_{z1} j_{z2} | J J_z \rangle U_J \langle J J_z | \frac{5}{2} \frac{5}{2} j_{z3} j_{z4} \rangle \quad . \quad (3)$$

Here J denotes the total angular momentum of two electrons and $J_z = j_{z1} + j_{z2} = j_{z3} + j_{z4}$. The sum is restricted by the antisymmetry of the Clebsch-Gordan coefficients $\langle \frac{5}{2} \frac{5}{2} j_{z1} j_{z2} | J J_z \rangle$ to even values $J = 0, 2, 4$. We use in the actual calculations U_J values which are determined from LDA wavefunctions for UPt₃ (Zwicknagl et al. 2002), i. e., $U_{J=4} = 17.21$ eV, $U_{J=2} = 18.28$ eV, and $U_{J=0} = 21.00$ eV. We expect $U_{J=4} < U_{J=2} < U_{J=0}$ always to hold for Coulomb interactions, independently of the chemical environment. In contrast, the relative order of the hopping matrix elements will vary strongly from one compound to the next. The average Coulomb repulsion of about 20 eV is irrelevant for the low-energy physics of the model. It simply restricts the relevant configurations to states such that each site is occupied either by 2 or 3 f electrons. The low-energy sector is exclusively determined by the differences of the U_J values, which are of the order of 1 eV and thus slightly larger than typical bare f -band widths. The latter are obtained, e.g., from LDA calculations for metallic uranium compounds like UPt₃. Restricting the model to f^2 and f^3 configurations is equivalent to let the various $U_J \rightarrow \infty$ while their differences remain finite. To mimic the situation in the U-based heavy-fermion compounds we consider the intermediate valence regime. Note that in the absence of a magnetic field all states of the two-site model with five electrons will be at least doubly degenerate because of Kramers' degeneracy.

The Hamiltonian eq. (1) conserves $\mathcal{J}_z = \sum_n J_z(n)$ where \mathcal{J}_z is the z -component of the total angular momentum of the system and the $J_z(n)$ refer to angular momentum projections on individual sites. We shall therefore characterize the eigenstates by their \mathcal{J}_z value. Since $t_{j_z} = t = \text{const}$ the system is rotationally invariant. Then \mathcal{J}^2 provides an additional good quantum number. Strong on-site correlations result in a considerable enhancement of anisotropies in the bare hopping matrix elements. This can lead to a localization of electrons in orbitals with relatively weak hybridization. The latter is effectively reduced to zero in those cases.

In order to quantify the degree of localization or, alternatively, of the reduction of hopping of a given j_z orbital by local correlations, we calculate the ratio of the j_z -projected kinetic energy T_{j_z} and the bare matrix element t_{j_z} and obtain

$$\frac{T_{j_z}}{t_{j_z}} = \sum_{\langle nm \rangle, \pm} \langle \Psi_{gs} | (c_{\pm j_z}^\dagger(n) c_{\pm j_z}(m) + h.c.) | \Psi_{gs} \rangle. \quad (4)$$

The ground-state wavefunction $|\Psi_{gs}\rangle$ contains the strong on-site correlations. A small ratio of T_{j_z}/t_{j_z} indicates partial suppression of hopping for electrons in the $\pm j_z$ orbitals.

Two kinds of correlations may contribute to that process. The first one is based on the reduction of charge fluctuations to atomic f^2 and f^3 configurations. This is a result for large values of U_J and can be studied by setting all U_J equal to a value much larger than the different t_{j_z} . The second one is due to differences in the U_J values, i. e. , $U_{J=4} < U_{J=2} < U_{J=0}$. The differences in the U_J values are the basis of Hund's rules. Hopping counteracts Hund's rule correlations and vice versa. What we want to stress is the fact that those correlations can lead to a complete suppression of hopping channels except for the dominant one which shows only little influence.

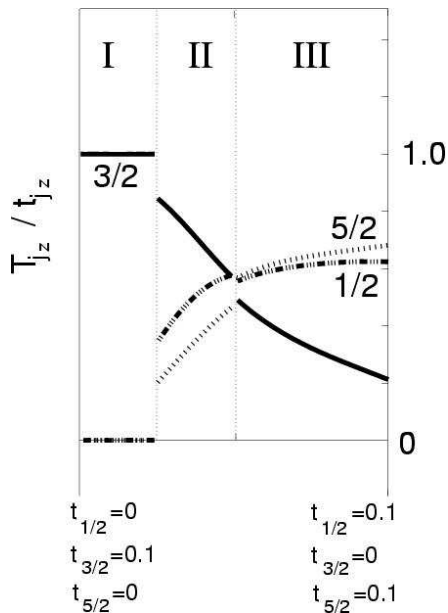


Figure 3. Values T_{j_z}/t_{j_z} for the two-site cluster along the line connecting linearly the points written below the figure. Regions with $\mathcal{J}_z = 15/2$, $5/2$ and $3/2$, are labeled with I, II and III respectively (Efremov et al. 2003).

Results for the ratios T_{j_z}/t_{j_z} are shown in fig. 3 for a two-site model. As the relevant correlations are local the general results qualitatively agree with those found for a three-site cluster and four-site clusters (Pollmann and Zwicknagl 2003). We can distinguish three different regimes with $\mathcal{J}_z = 15/2$, $5/2$ and $3/2$, labeled I, II and III respectively. One observes that in region I only the dominant hybridization of the $j_z = 3/2$ orbital survives while that of the $j_z = 1/2$ and $j_z = 5/2$ orbitals is completely suppressed. On the other hand in regions II and III the correlation effects on different orbitals are not very different. These findings demonstrate that in particular Hund's rule correlations strongly enhance anisotropies in the hopping. For a certain range of parameters this may result in a complete suppression of the effective hopping except for the largest one, which remains almost unaffected. This provides a microscopic justification of partial localization of $5f$ electrons which is observed in a number of experiments on U compounds and which is the basis for further model calculations described later.

2.1.3. Fermi-liquid state and heavy quasiparticles: renormalized band theory

Neither the Kondo model for Ce-based heavy-fermion systems nor the dual model for their U-based counterparts can be solved for extended systems described by lattice models. The excitation spectra of Ce metal in the α - and γ -phase were recently calculated applying the dynamical mean field theory (McMahan et al. 2003). The method yields a low-energy resonance but the experimentally observed change of the f-valence at the transition is not reproduced. A fully microscopic description is not available to describe experiments where inter-site effects become strongly manifest. Typical lattice effects are the formation of coherent heavy quasiparticle bands whose Fermi surfaces were observed experimentally.

The Landau Fermi liquid (FL) theory assumes a one-to-one correspondence between the states of the complex interacting system and those of a gas of independent fermions which may move in an external potential, Landau (1956, 1957, 1958), Abrikosov et al. (1975). The single-particle orbitals and energies are determined from an effective Hamiltonian. The characteristic properties of a system are reflected in an effective and not necessarily local potential V_{eff} which describes the field of the nuclei and the modifications arising from the presence of the other electrons. The essential many-body aspects of the problem are then contained in the prescription for constructing the effective potentials which have to be determined specifically for the problem under consideration.

The quasiparticle energies reflect the interaction among the fermions and therefore may be altered when the overall configuration is changed. A characteristic feature of interacting Fermi liquids is that the energy dispersion $\epsilon_\sigma(\mathbf{k})$ depends on how many other quasiparticles are present,

$$\epsilon_\sigma(\mathbf{k}) = E(\mathbf{k}) + \sum_{\mathbf{k}'\sigma'} f_{\sigma\sigma'}(\mathbf{k}, \mathbf{k}') \delta n_{\sigma'}(\mathbf{k}') \quad . \quad (5)$$

Here $E(\mathbf{k})$ denotes the energy dispersion of a dilute gas of quasiparticles. In systems with strong correlations it reflects the interactions and hence cannot be calculated from the overlap of single-electron wave functions. The interactions among the quasiparticles are characterized by the matrix $f_{\sigma\sigma'}(\mathbf{k}, \mathbf{k}')$. The deviations from the equilibrium distribution are given by $\delta n_\sigma(\mathbf{k})$.

Interaction effects must be accounted for in considering those situations where the quasiparticle distribution function deviates from that of the equilibrium case. In the phenomenological Landau FL theory the characteristic properties of the quasiparticles, which can hardly be calculated microscopically, are expressed in terms of parameters which are determined from experiment. Examples are the effective potentials, the interaction potential and the scattering amplitudes. An important property of the quasiparticles is that they can be considered as 'rigid' with respect to low-energy and long-wavelength perturbations. Only such processes can be described within this theoretical framework.

The energy dispersion $E(\mathbf{k})$ of a dilute gas of noninteracting quasiparticles is parametrized by the Fermi wave vector \mathbf{k}_F and the Fermi velocity \mathbf{v}_F

$$E(\mathbf{k}) = \mathbf{v}_F(\hat{\mathbf{k}}) \cdot (\mathbf{k} - \mathbf{k}_F) \quad (6)$$

where $\hat{\mathbf{k}}$ denotes the direction on the Fermi surface. The key idea of the renormalized band method is to determine the quasiparticle states by computing the band structure for a

given effective potential. Coherence effects which result from the periodicity of the lattice are then automatically accounted for. The quantities to be parametrized are the effective potentials which include the many-body effects. The parametrization of the quasiparticles is supplemented by information from conventional band structure calculations as they are performed for “ordinary” metals with weakly correlated electrons. The periodic potential leads to multiple-scattering processes involving scattering off the individual centers as well as the propagation between the centers which mainly depends on the lattice structure and is therefore determined by geometry. The characteristic properties of a given material enter through the information about single center scattering which can be expressed in terms of properly chosen set of phase shifts $\{\eta_\nu^i(E)\}$ specifying the change in phase of a wave incident on site i with energy E and symmetry ν with respect to the scattering center. Within the scattering formulation of the band structure problem the values of the phase shifts at the Fermi energy $\{\eta_\nu^i(E_F)\}$ together with their derivatives $\{(d\eta_\nu^i/dE)_{E_F}\}$ determine the Fermi wave vectors \mathbf{k}_F and the Fermi velocity \mathbf{v}_F .

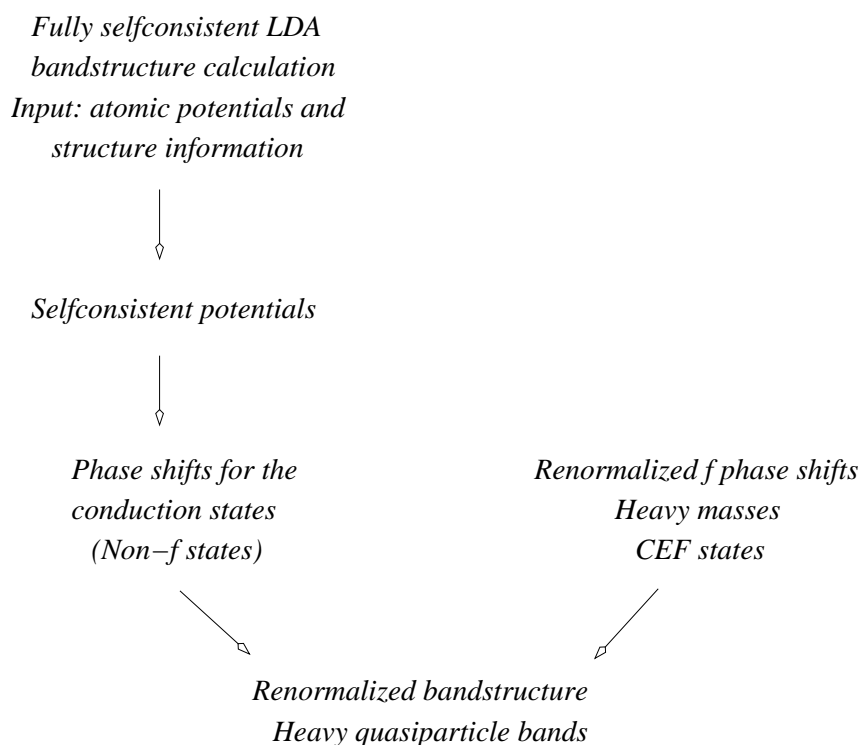


Figure 4. Schematic summary of renormalized band calculation for metals with strongly correlated electrons

The calculation of realistic quasiparticle bands proceeds in several steps as schematically summarized in fig. 4. The first step is a standard LDA band structure calculation by means of which the effective single-particle potentials are self-consistently generated.

The calculation starts, like any other ab-initio calculation, from atomic potentials and structure information. In this step, no adjustable parameters are introduced. The effective potentials and hence the phase shifts of the conduction states are determined from first principles to the same level as in the case of ‘ordinary’ metals. The f-phase shifts at the lanthanide and actinide sites, on the other hand, are described by a resonance type expression

$$\tilde{\eta}_f \simeq \arctan \frac{\tilde{\Delta}_f}{E - \tilde{\epsilon}_f} \quad (7)$$

which renormalizes the effective quasiparticle mass. One of the two remaining free parameters $\tilde{\epsilon}_f$ and $\tilde{\Delta}_f$ is eliminated by imposing the condition that the charge distribution is not significantly altered as compared to the LDA calculation by introducing the renormalization. The renormalized band method devised to calculate the quasiparticles in heavy-fermion compounds thus is essentially a one-parameter theory. We mention that spin-orbit and CEF splittings can be accounted for in a straight-forward manner (Zwicknagl 1992).

2.1.4. Quasiparticle interactions and spin fluctuation theory

The low-energy excitations of heavy-fermion systems are described in terms of quasiparticle bands which yield the high density of states and specific heat γ -value. The preceding sections focussed on the case of a dilute gas of quasiparticles whose energy dispersion can be explicitly calculated by means of the renormalized band method. The many-body effects, however, lead to deviations from the picture of independent fermions which fill the rigid bands of the dilute gas of quasiparticles. An important consequence of the quasiparticle interactions is the instability of the normal Fermi liquid with respect to charge or spin density waves or superconductivity. In heavy-fermion compounds, quasiparticle interactions are strongly evident in the electronic compressibility whose values are comparable to those of a normal metal and do not reflect the enhancement of the specific heat. This experimental fact indicates that there must be a strong repulsion between two quasiparticles at the same lattice site.

The influence of the quasiparticle interactions on observable quantities is usually described in terms of a small set of interaction parameters. According to Landau, the compressibility κ and susceptibility χ_s are given by

$$\frac{\kappa}{\kappa_0} = \frac{\frac{m^*}{m}}{1 + F_0^s} \quad \text{and} \quad \frac{\chi_s}{\chi_s^0} = \frac{\frac{m^*}{m}}{1 + F_0^a} \quad (8)$$

where κ_0 denotes the compressibility of independent fermions of mass m . From $\frac{\kappa}{\kappa_0} \simeq 1$ follows the order of magnitude estimate $F_0^s \simeq \frac{m^*}{m} \simeq 10^2 - 10^3$ for the spin-independent isotropic part of the quasiparticle interactions. The spin-dependent isotropic part of the interaction, on the other hand, is reflected in the enhancement of the spin susceptibility χ_s over the independent quasiparticle value χ_s^0 . From the observed value $\chi_s/\chi_s^0 \simeq m^*/m$ we infer that the enhanced spin susceptibility simply reflects the high density of quasiparticle states and that the corresponding Landau FL parameter F_0^a plays only a minor role in heavy-fermion compounds. Although these results are not sufficient to specify the effective interaction in an anisotropic Fermi liquid they nevertheless impose important constraints on theoretical models.

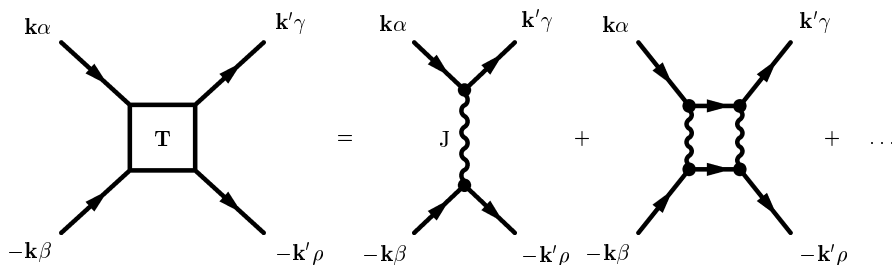


Figure 5. Left: two-particle (e-e) scattering matrix $T_{\alpha\beta;\gamma\rho}(\mathbf{k}_1\mathbf{k}_2; \mathbf{k}_3\mathbf{k}_4)$ for quasiparticle scattering with initial momenta $\mathbf{k}_3\mathbf{k}_4$ and spins $\gamma\rho$ to final momenta $\mathbf{k}_1\mathbf{k}_2$ and spins $\alpha\beta$. Right: SC transition corresponds to singular pair scattering with opposite momenta $\mathbf{k}_3 = -\mathbf{k}_4 = \mathbf{k}'$ and $\mathbf{k}_1 = -\mathbf{k}_2 = \mathbf{k}$. It is approximated by ladder diagrams involving the irreducible (with respect to e-e scattering) four-point vertex for the effective interaction (wiggly line) which is the central quantity in microscopic models of SC, see also fig. 6 and eqs. (12),(13).

The superconducting transition in a Fermi liquid is determined by a singularity in the scattering matrix of two quasiparticles with opposite momenta at the Fermi surface. In Landau FL theory a two-particle scattering matrix $T_{\alpha\beta;\gamma\rho}(\mathbf{k}_1\mathbf{k}_2; \mathbf{k}_3\mathbf{k}_4)$ is introduced which describes the scattering of two quasiparticles with momenta $\mathbf{k}_3\mathbf{k}_4$ and spins $\gamma\rho$ into states with momenta $\mathbf{k}_2\mathbf{k}_1$ and spins $\alpha\beta$ on the Fermi surface (see fig. 5). Assuming rotational invariance in spin space the general scattering matrix $T_{\alpha,\beta;\gamma,\rho}$ can be expressed in terms of two scalar amplitudes. Conventional choices are either the singlet and triplet amplitudes in the particle-particle channel ($\gamma\rho \rightarrow \alpha\beta$), T_s and T_t or alternatively, the singlet and triplet amplitudes in one of the particle-hole channels, $T^{(s)}$ and $T^{(a)}$,

$$\begin{aligned} T_{\alpha\beta;\gamma\delta} &= -\frac{1}{2}(\sigma_2)_{\alpha\beta}(\sigma_2)_{\gamma\rho}T_s + \frac{1}{2}(\boldsymbol{\sigma}\sigma_2)_{\alpha\beta} \cdot (\boldsymbol{\sigma}\sigma_2)_{\gamma\rho}T_t \\ &= \delta_{\alpha\beta}\delta_{\gamma\rho}T^{(s)} + \boldsymbol{\sigma}_{\alpha\beta} \cdot \boldsymbol{\sigma}_{\gamma\rho}T^{(a)} \end{aligned} \quad (9)$$

where $\sigma_\mu; \mu = 1 - 3$ denote the Pauli matrices. The two sets of scalar amplitudes are related by

$$T_s = T^{(s)} - 3T^{(a)} \quad ; \quad T_t = T^{(s)} + T^{(a)} \quad T^{(s)} = \frac{1}{4}(T_s + 3T_t) \quad ; \quad T^{(a)} = \frac{1}{4}(T_t - T_s) \quad (10)$$

The symmetries can be obtained directly from the symmetries of the two-particle Green's function. The Landau FL parameters F_0^s and F_0^a are determined by the isotropic Fermi surface averages $A_0^{s,a} = \langle T^{s,a}(\mathbf{k}_1\mathbf{k}_2; \mathbf{k}_1\mathbf{k}_2) \rangle_{FS}$ of the two particle forward-scattering amplitude by $F_0^{s,a} = A_0^{s,a}[1 - A_0^{s,a}]^{-1}$. As mentioned above, the transition to the superconducting state is caused by a singularity in the scattering of a pair with opposite momenta $\mathbf{k}_3 = -\mathbf{k}_4 = \mathbf{k}'$ into pair states with $\mathbf{k}_1 = -\mathbf{k}_2 = \mathbf{k}$.

The Fermi liquid approach which attempts to construct phenomenological models for the scattering amplitude has been reviewed (Fulde et al. 1988, Zwicky 1992). In the

present review we shall rather concentrate on microscopic models for the effective pairing interaction.

Microscopic theories of superconductivity focus on the attractive interaction which results from the motion of the (heavy) quasiparticle through a polarizable medium. The theories can be divided into two major groups depending on whether the polarizable medium is distinct from the particles which are participating in the attraction or not. The BCS theory (Bardeen et al. 1957, Schrieffer 1964) belongs to the former class where Cooper-pair formation is due to quasiparticle-phonon interactions which is appropriate for common metals. The spin fluctuation models assume that pairing is mediated by overdamped low lying magnetic excitations with a preferred wave vector in the itinerant electron system. The dual model for U-based heavy-fermion systems suggests a novel mechanism for the Cooper-pair formation, i.e., the exchange of weakly damped propagating magnetic excitons. In this case, the polarizable medium is provided by the CEF-split multiplets of the localized 5f-electrons. A model calculation for UPd₂Al₃ is presented in sect. (4.2). where we also compare theoretical predictions with experimental observations.

The majority of theoretical calculations for heavy-fermion systems adopts spin-fluctuation models for the quasiparticle attraction which belong to the second group. Early theoretical efforts (Anderson 1984a) emphasized an analogy with superfluid ³He. Even though a quantitative microscopic theory of suprafluidity is still lacking for ³He it is generally accepted that spin fluctuations qualitatively explain observed features in ³He, in particular odd-parity spin-triplet pairing (Anderson 1984b, Vollhardt and Wölfle 1990). The influence of spin fluctuations on the Cooper pair formation in metals was studied first by Berk and Schrieffer (1966) and Layzer and Fay (1971, 1974). It has found its most prominent applications in HF systems (Miyake et al. 1986) and especially in the theory of high-T_c superconductors (Monthoux et al. 1991, Monthoux and Pines 1994). The calculations proceed in close analogy to the strong-coupling theory of phonon-mediated superconductivity. At this point we have to add that the theory of spin fluctuation-mediated superconductivity does not have a natural small parameter which would allow for a systematic asymptotic expansion. In particular, there is no a priori justification for including only selected contributions in a diagrammatic expansion for the scattering matrix.

The pair scattering for two quasiparticles with opposite momenta at the Fermi surface is evaluated adopting the ladder approximation displayed in fig. 5. The problem is therefore reduced to finding the four-point vertex which is irreducible with respect to particle-particle scattering. The basic assumption is that the important structure in the scattering amplitudes comes from exchange of collective modes in the two particle-hole channels. The central quantity of these theories is the dynamic magnetic susceptibility $\chi(\mathbf{q}, \omega)$ which can be determined - in principle - by inelastic neutron scattering. Close to a magnetic instability, the susceptibility diverges for $\omega \rightarrow 0$ at some wave vector \mathbf{Q} . This behaviour results from a singularity in the particle-hole scattering matrix which accounts for the dynamic effects of the induced spin polarizations. The strong particle-hole correlations affect the pair scattering amplitude in the particle-particle channel. In explicit calculations, the effective interaction associated with $\chi(\mathbf{q}, \omega)$ originates in a residual on-site quasiparticle repulsion (I) described by the single band Hubbard model for the heavy

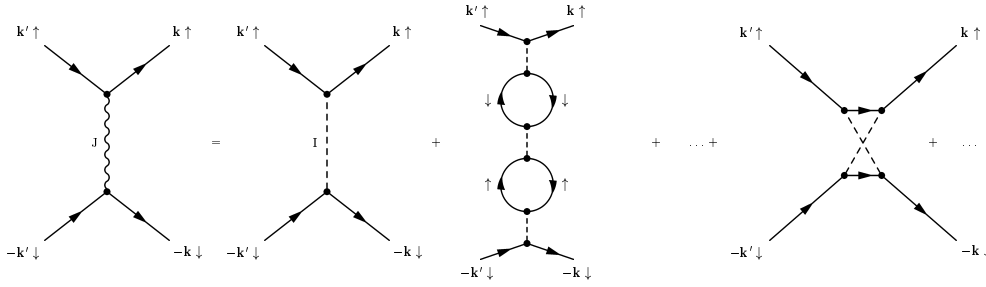


Figure 6. RPA diagrams for the effective interaction $J(\mathbf{k} - \mathbf{k}')$ between quasiparticles with opposite spins. The bare instantaneous interaction is denoted by I (dashed line) as in eq. (11). Contribution from polarisation (bubble) diagrams contains odd number and from (maximally crossed) exchange diagrams contain any number of interaction lines (I). For equal quasiparticle spins the RPA yields only a sum of bubble diagrams with an even number of interaction lines.

quasiparticle bands $\epsilon_{\mathbf{k}}$.

$$H_I = \sum_{\mathbf{k},s} \epsilon_{\mathbf{k}} n_{\mathbf{k}} + I \sum_i n_{i\uparrow} n_{i\downarrow} \quad (11)$$

This is also the starting point in the theory of high- T_c SC, albeit with bare Coulomb repulsion and 2D quasiparticle band. In the fluctuation exchange (FLEX) approach (Pao and Bickers 1994, Dahm and Tewordt 1995) the effective pair interactions and gap equations are obtained and solved selfconsistently in the context of a strong coupling approach. For the complicated 3D Fermi surfaces of HF materials this is too difficult and one is restricted to nonretarded model calculations. In this context the effective interaction is obtained within the random phase approximation (RPA) for pairs of quasiparticles with opposite and equal spins from the diagrams displayed in fig. 6. To conserve rotational invariance in spin space the maximally crossed particle exchange contributions in fig. 6 have to be included. These terms were studied by Berk and Schrieffer (1966) who considered the influence of spin-fluctuations on singlet pairing. The case of triplet scattering was discussed by Nakajima (1973) for ^3He . He showed that sufficiently close to a magnetic instability, the complete set of diagrams yields an effective spin-dependent interaction which is rotationally invariant in spin space

$$H_{eff} = \frac{1}{2} \sum_{\mathbf{k},\mathbf{k}'} J(\mathbf{k} - \mathbf{k}') \boldsymbol{\sigma}_{\alpha\gamma} \cdot \boldsymbol{\sigma}_{\beta\rho} c_{\mathbf{k}\alpha}^\dagger c_{-\mathbf{k}\beta}^\dagger c_{-\mathbf{k}'\rho} c_{\mathbf{k}'\gamma} \quad (12)$$

where

$$J(\mathbf{q}) = -\frac{1}{2} \frac{I}{1 - I\chi_0(\mathbf{q})} \simeq -\frac{1}{2} I^2 \chi(\mathbf{q}) \quad \text{and} \quad \chi(\mathbf{q}) = \frac{\chi_0(\mathbf{q})}{1 - I\chi_0(\mathbf{q})} \quad (13)$$

Here $\chi_0(\mathbf{q})$ is the static susceptibility of the non-interacting quasiparticles and $\chi(\mathbf{q})$ the RPA susceptibility of the interacting system. The approximation is valid for the enhanced

spin fluctuation regime $I\chi_0(\mathbf{q}) \leq 1$. In this regime the effective pairing is therefore completely determined by the collective static magnetic susceptibility $\chi(\mathbf{q})$.

Assuming a spherical FS the appropriate basis function for the SC order parameter are spherical harmonics of angular momentum l . The interaction in the l -wave channel is given by (P_l = Legendre polynomial)

$$V_l = a_l 2 \int_0^1 dx x P_l(1 - 2x^2) [-J(2k_F x)] \quad (14)$$

with $x=1-(q/2k_F)^2$ and $a_l=3$ (l even) or $a_l = -1$ (l odd). If the effective interaction $-J(\mathbf{q})$ strongly peaks for small q ($x \simeq 1$), i.e. for FM spin fluctuations, the integrand is positive in this region and hence $V_l < 0$ for odd l and $V_l > 0$ for even l .

Assuming that in HF systems the quasiparticle interaction is mediated by FM spin fluctuations one would expect odd-parity SC order parameters. For UPt₃ however, the odd parity state was originally claimed to be inconsistent with the power law behavior observed in thermodynamic and transport properties at low temperatures. This statement was based on the assumption that the superconducting phase should be characterized by one of the symmetry-adapted order parameters which were derived in the limit of strongly coupled orbital and spin moment of the Cooper pair (Volovik and Gor'kov 1985, Ueda and Rice 1985, Sigrist and Ueda 1991). We shall comment on this subtle point in the next section.

The discovery of antiferromagnetic spin fluctuations in UPt₃ (Aeppli et al. 1987) prompted Miyake et al. (1986) to study the nature of pairing due to antiferromagnetic spin fluctuations. The authors consider pairing in a single-band model with the effective electron interaction of eq. (12) where the nonretarded interaction $J(\mathbf{q})$ should have a maximum at an AF wave vector \mathbf{Q} , e.g. $\mathbf{Q}=(\frac{1}{2}, \frac{1}{2}, \frac{1}{2})$ or $\mathbf{Q}=(\frac{1}{2}, \frac{1}{2}, 0)$. In the vicinity of its maximum at \mathbf{Q} , $J(\mathbf{q})$ is approximated by

$$-J(\mathbf{q}) = J_0 - J_1 \gamma_{\mathbf{q}} \quad (15)$$

where J_0, J_1 are positive constants and the function $\gamma_{\mathbf{q}}$ has a minimum at $\mathbf{q} = \mathbf{Q}$. Examining this model for a parabolic single band Miyake et al. (1986) demonstrated that the resulting pairing interaction favors anisotropic even-parity SC order parameter in cubic symmetry ($V_l < 0$ for even $l > 0$). This turned out to be an influential result. Because of the general presence of AF spin fluctuations in HF metals it has led to the attitude to expect generally singlet (even parity) SC in these compounds.

There are, however, counter examples like UPt₃ and UNi₂Al₃ with AF spin fluctuations and experimentally identified triplet order parameter. The prediction of only even parity unconventional pair states therefore seems to be an artefact of the simplifications inherent in the model. One obvious deficiency is the assumption of cubic symmetry and basis functions adjusted for a spherical Fermi surface not appropriate for these compounds. More sophisticated versions of the model incorporating experimental data for the magnetic fluctuations via $\chi(\mathbf{q}, \omega)$ and realistic band structures for the quasiparticles failed to reproduce the symmetry of the superconducting order parameter in UPt₃. In particular, the calculations do not produce a multicomponent E₁ or E₂ order parameter as stable solution. This failure is discussed in detail in (Heffner and Norman 1996). Also the generalizations of standard spin-fluctuation theory which account for orbital effects (Norman 1994) do not resolve the difficulties encountered in real materials.

Aspects of strong coupling effects within spin-fluctuation theories, especially the pair breaking role of low frequency bosons have been discussed by Millis et al. (1988). More recently magnetically mediated superconductivity in materials close to a magnetic instability was investigated in a series of papers by Monthoux and Lonzarich (1999, 2001, 2002). A phenomenological form for the retarded generalized magnetic susceptibility $\chi(\mathbf{q}, \omega)$ defining the effective quasiparticle interaction is adopted

$$\chi(\mathbf{q}, \omega) = \frac{\chi_0 \kappa_0^2}{\kappa^2 + \hat{q}^2 - i \frac{\omega}{\eta(\hat{q})}} \quad (16)$$

where κ and κ_0 are the inverse correlation lengths (in units of the inverse lattice constant) with and without strong magnetic correlations, respectively. The functions \hat{q}^2 and $\eta(\hat{q})$ are parametrized so as to directly compare ferromagnetic and antiferromagnetic spin fluctuations. The instability of the normal state is determined by solving the linearized Eliashberg equations which yield the transition temperatures T_c and the mass renormalization. The questions addressed include the influence of dimensionality on the robustness of magnetic pairing and the relative stability of d-wave versus p-wave pairing.

Pairing instabilities may also appear in the electron-hole (Peierls-) rather than electron-electron (Cooper-) channel leading to CDW/SDW type instabilities described by $T^{(s)}$ and $T^{(a)}$ in eq. (10). They are strongly favored if the Fermi surface shows the nesting property $\epsilon_{\mathbf{k}+\mathbf{Q}} = -\epsilon_{\mathbf{k}}$ characteristic for flat FS portions connected by the nesting vector \mathbf{Q} as shown later in fig. 7. In this case the on-site interaction term in the Hamiltonian eq. (11) may be truncated in momentum space because the e-h scattering is dominated by processes with momentum transfer \mathbf{Q} . In mf approximation the effective CDW/SDW pairing Hamiltonian is given in eq. (33). To obtain the full variety of electron-hole pair states one needs more general microscopic interactions, replacing the on-site Hubbard model of eq. (11) by an extended Hubbard model which include inter-site Coulomb repulsion and exchange (Gulacsi and Gulacsi 1987, Schulz 1989, Ozaki 1992).

2.2. Order parameters and their coexistence in strongly correlated electron systems

Degenerate interacting Fermi systems are prone to instabilities due to pair condensation. The Pauli principle requires that states have to be filled up to the Fermi energy E_F leading to a large kinetic energy. Rearranging the occupation of noninteracting states around the Fermi level may reduce the interaction energy considerably. The large on-site Coulomb interactions will achieve this by reducing double occupancies of opposite spin states below the Hartree-Fock level. This leads to a strongly correlated electronic ground state which is ideally approached at low temperatures below a characteristic temperature scale T^* without breaking of spatial or internal symmetries. Excitations from this state may be described within the Landau Fermi liquid (FL) picture with quasiparticles that have a strongly enhanced effective electron mass $m^* \gg m$. Eventually however this state will become unstable against formation of electron (Cooper-) pairs or electron-hole (Peierls-) pairs due to the residual screened interactions between the quasiparticles. In the former case gauge symmetry is broken leading to a superconducting (SC) state, in the latter spatial symmetries and possibly spin rotational and time reversal symmetry are broken leading to charge-density wave (CDW) or spin-density wave (SDW) states. Which state is more favorable depends on the momentum and energy dependence of residual quasiparticle interactions and on the geometric properties of the Fermi surface and usually cannot be predicted with confidence for real materials. The effective Hamiltonian obtained previously describing the low energy pairing correlations of quasiparticles is most frequently used for studying possible SC states. The condensation into pairs is described by a gap function $\Delta(\mathbf{k})$ which characterises both the type of broken symmetry state and its new quasiparticle excitations. Its experimental determination is therefore of central importance. Unfortunately this is a difficult task except in the isotropic case where $\Delta(\mathbf{k})$ is a constant. In this section we outline the possible type of pair states and gap functions and their symmetry classification. We also discuss simple models of coexistence of SC and CDW/SDW type order parameters based on 2D FS models with nesting properties.

2.2.1. Order parameter classification

Many physical properties of superconducting materials are directly determined by the symmetry of the SC order parameter. The possible types of order parameters are restricted by crystal symmetry. This fact provides a classification scheme for different superconducting states and, in addition, allows one to construct the superconducting classes by means of group theory.

Superfluids are characterized by off-diagonal long range order (ODLRO) which leads to nonvanishing correlations in the two-particle density matrix for large separations of particles at points $\mathbf{r}_1, \mathbf{r}_2$ and $\mathbf{r}'_1, \mathbf{r}'_2$,

$$\langle \mathbf{r}_1 s_1; \mathbf{r}_2 s_2 \mid \rho^{(2)} \mid \mathbf{r}'_1 s'_1; \mathbf{r}'_2 s'_2 \rangle \rightarrow \psi_{s_1, s_2}^*(\mathbf{r}_1, \mathbf{r}_2) \psi_{s'_1, s'_2}(\mathbf{r}'_1, \mathbf{r}'_2) \quad (17)$$

Here, \mathbf{r}_i, s_i denote the fermion positions and spins, respectively. In systems with strong spin-orbit (s.o.) interactions, the indices s_i refer to pseudo spins associated with Kramers degeneracy of conduction bands. The ordered phase is characterized by the order parameter ψ which is a complex pseudo-wave function always connected with a spontaneous breaking of U(1) gauge symmetry. In general, it depends on the center-of mass and relative

coordinates, $\mathbf{R} = \frac{1}{2}(\mathbf{r}_1 + \mathbf{r}_2)$, $\mathbf{r} = \mathbf{r}_1 - \mathbf{r}_2$ and the pseudo spins s_1 and s_2 , respectively. We shall restrict ourselves to homogeneous systems neglecting the dependence on the center-of-mass variable of \mathbf{R} . Then the order parameter is a function of the relative coordinate \mathbf{r} only. Performing a Fourier transformation with respect to \mathbf{r} with $\psi_{s_1 s_2}(\mathbf{r}) \rightarrow \psi_{s_1 s_2}(\mathbf{k})$ and restricting the wave vector to the Fermi surface $\mathbf{k} = k_F(\hat{\mathbf{k}})\hat{\mathbf{k}}$ yields a pairing amplitude $\psi_{s_1 s_2}(\hat{\mathbf{k}})$ which depends upon the direction $\hat{\mathbf{k}}$ on the Fermi surface. In microscopic theories the gap function $\Delta_{s_1 s_2}$ which also determines the excitation spectrum is commonly used as order parameter. It is given by

$$\Delta_{s_1 s_2}(\hat{\mathbf{k}}) = - \sum_{\hat{\mathbf{k}}' s_3 s_4} V_{s_1 s_2 s_3 s_4}(\hat{\mathbf{k}}, \hat{\mathbf{k}}') \psi_{s_3 s_4}(\hat{\mathbf{k}}') \quad (18)$$

where V is the effective pairing interaction. For the spin fluctuation model we obtained $V_{s_1 s_2 s_3 s_4}(\mathbf{k}, \mathbf{k}') = -J(\mathbf{k} - \mathbf{k}') \boldsymbol{\sigma}_{s_1 s_4} \boldsymbol{\sigma}_{s_2 s_3}$ in eq.(12). Concerning the symmetry classification of the superconducting phases, one may use the gap function $\Delta_{s_1 s_2}$ or the pair amplitude $\psi_{s_1 s_2}$ as order parameter due to their identical transformation properties.

The fundamental property of $\psi_{s_1 s_2}$ or $\Delta_{s_1 s_2}$ is its behaviour as a two-fermion wave function in many respects. This expresses the fact that an ODLRO order parameter is not the thermal expectation value of a physical observable but rather a complex pseudo-wave function describing quantum phase correlations on the macroscopic scale of the SC coherence length. Its phase is a direct signature of the broken gauge invariance in the SC condensate. The Pauli principle then requires $\Delta_{s_1 s_2}$ to be antisymmetric under the interchange of particles

$$\Delta_{s_1, s_2}(\hat{\mathbf{k}}) = -\Delta_{s_2, s_1}(-\hat{\mathbf{k}}) \quad (19)$$

In addition, it transforms like a two-fermion wave function under rotations in position and spin space and under gauge transformations. The transformation properties yield a general classification scheme for the superconducting order parameter which is represented by a 2×2 -matrix in (pseudo-) spin space. It can be decomposed into an antisymmetric (s) and a symmetric (t) contribution according to $\boldsymbol{\Delta}(\hat{\mathbf{k}}) = \boldsymbol{\Delta}_s(\hat{\mathbf{k}}) + \boldsymbol{\Delta}_t(\hat{\mathbf{k}})$ with

$$\boldsymbol{\Delta}_s(\hat{\mathbf{k}}) = \phi(\hat{\mathbf{k}})i\sigma_2 \quad \text{and} \quad \boldsymbol{\Delta}_t(\hat{\mathbf{k}}) = \sum_{\mu=1}^3 d_\mu(\hat{\mathbf{k}})\sigma_\mu i\sigma_2 \quad (20)$$

where σ_μ denote the Pauli matrices. Antisymmetry $\boldsymbol{\Delta}(\hat{\mathbf{k}}) = -\boldsymbol{\Delta}^T(-\hat{\mathbf{k}})$ requires

$$\phi(\hat{\mathbf{k}}) = \phi(-\hat{\mathbf{k}}) \quad \text{and} \quad d_\mu(\hat{\mathbf{k}}) = -d_\mu(-\hat{\mathbf{k}}) \quad (21)$$

for the complex orbital functions $\phi(\hat{\mathbf{k}})$ and $d_\mu(\hat{\mathbf{k}})$ ($\mu = 1-3$). For brevity we will frequently write $\Delta(\hat{\mathbf{k}})$ for $\phi(\hat{\mathbf{k}})$ or $|\mathbf{d}(\hat{\mathbf{k}})|$. The physical meaning of the order parameters ϕ and \mathbf{d} for singlet and triplet state respectively is evident from the identity

$$\frac{1}{2}\text{Tr} \left| \boldsymbol{\Delta}_s(\hat{\mathbf{k}}) \right|^2 = \left| \phi(\hat{\mathbf{k}}) \right|^2 \quad \text{and} \quad \frac{1}{2}\text{Tr} \left| \boldsymbol{\Delta}_t(\hat{\mathbf{k}}) \right|^2 = \left| \mathbf{d}(\hat{\mathbf{k}}) \right|^2 \quad (22)$$

Therefore the modulus of ϕ and \mathbf{d} is a measure for the total gap amplitude of the Cooper pairs at a given point $\hat{\mathbf{k}}$ on the Fermi surface. In addition, the direction of the vector \mathbf{d} specifies the relative contributions of the three triplet pair states. The above relation

holds for triplet states which satisfy $\mathbf{d}^* \times \mathbf{d} = 0$. They are called ‘unitary states’ because they are invariant under time reversal. In this case the vector \mathbf{d} defines a unique direction in spin space for every point on the Fermi surface.

The order parameter can be chosen either as purely antisymmetric Δ_s or purely symmetric Δ_t when spin-orbit interaction can be neglected. Then the total spin is a good quantum number and may be used to classify the pair states. Accordingly the states Δ_s and Δ_t are called spin singlet and spin triplet states, respectively. In crystals which have an inversion center, pair states can also be classified with respect to their parity as even-parity (Δ_s) and odd-parity states (Δ_t).

In the 4f- and 5f-based heavy fermion superconductors the spin-orbit interaction is strong. As a consequence classification according to physical pair spins cannot be used. If their high-temperature crystal structures, however, have an inversion center then classification according to parity is still possible. We note here that recently the first example of a HF superconductor (CePt₃Si) which lacks inversion symmetry was discovered (Bauer et al. 2003) and its theoretical implications were discussed by Frigeri et al. (2003).

The simplest even-parity state is the isotropic state encountered in ordinary superconductors. This state is often referred to as ‘s-wave state’. The isotropic order parameter does not depend on the direction $\hat{\mathbf{k}}$ and reduces to a complex constant $\phi = |\phi|e^{i\varphi}$. Its only degree of freedom is the Josephson phase φ . By far the most extensively studied examples of anisotropic pairing are the p-wave states realized in the superfluid phases of ³He, the d-wave pair state in high- T_c superconductors and the f-wave states in UPt₃ and SrRu₂O₄. The odd parity (p,f) states among these examples are characterised by more than one order parameter component with internal phase degrees of freedom which appear in addition to the overall Josephson phase.

The general classification scheme for superconducting order parameters proceeds from the behavior under the transformations of the symmetry group \mathcal{G} of the Hamiltonian. It consists of the crystal point group G , the spin rotation group $SU(2)$, the time-reversal symmetry group \mathcal{K} , and the gauge group $U(1)$. The latter two are respectively defined by

$$K\Delta(\hat{\mathbf{k}}) = \sigma_2\Delta^*(-\hat{\mathbf{k}})\sigma_2 \quad \text{and} \quad \Phi\Delta(\hat{\mathbf{k}}) = e^{i\varphi}\Delta(\hat{\mathbf{k}}) \quad (23)$$

Concerning rotations in \mathbf{k} - and spin space we distinguish two different cases: (1) If spin-orbit coupling is negligible spatial and spin rotations can be applied independently. For the elements $g \in G$ of the point group which act on $\hat{\mathbf{k}}$ one has

$$g\Delta(\hat{\mathbf{k}}) = \Delta(D_G^{(-)}(g)\hat{\mathbf{k}}) \quad (24)$$

where $D_G^{(-)}(g)$ is the three-dimensional representation of G in $\hat{\mathbf{k}}$ -space. For the elements $g \in SU(2)$ of the spin rotation group which act on the spin indices we obtain

$$g\Delta(\hat{\mathbf{k}}) = D_{(s)}^T(g)\Delta(\hat{\mathbf{k}})D_{(s)}(g) \quad (25)$$

where $D_{(s)}(g)$ denotes the representation of $SU(2)$ for spin $\frac{1}{2}$. This transformation leaves even-parity states invariant. For odd-parity states where the order parameter can be represented by a vector \mathbf{d} in spin space the transformation gives a conventional orthogonal rotation of the \mathbf{d} -vector according to

$$g\mathbf{d}(\hat{\mathbf{k}}) = D_G^{(+)}(g)\mathbf{d}(\hat{\mathbf{k}}) \quad (26)$$

(2) In the presence of spin-orbit interaction the transformations of $\hat{\mathbf{k}}$ and the spin rotations are no longer independent. The spins are frozen in the lattice and the operations of the point group amount to simultaneous rotations in $\hat{\mathbf{k}}$ space and spin space:

$$g\mathbf{d}(\hat{\mathbf{k}}) = D_G^{(+)}(g)\mathbf{d}(D_G^{(-)}(g)\hat{\mathbf{k}}) \quad (27)$$

The appropriate choice of rotations corresponding to weak or strong spin-orbit coupling case is determined by microscopic considerations. Using the above transformation properties the singlet and triplet gap functions $\phi(\hat{\mathbf{k}})$ and $\mathbf{d}(\hat{\mathbf{k}})$ respectively may further be decomposed into basis functions $\phi_\Gamma^n(\hat{\mathbf{k}})$ or $\mathbf{d}_\Gamma^n(\hat{\mathbf{k}})$ of the irreducible representations Γ (degeneracy index n) of $G \times \text{SU}(2)$ (weak s.o. coupling) or G (strong s.o. coupling).

The occurrence of long-range order at a phase transition described by an order parameter is most frequently associated with spontaneous symmetry breaking. The simplest superconductors where only gauge symmetry is broken are called *conventional*. In this case the SC order parameter has the same spatial symmetry as the underlying crystal, i.e. it transforms as a fully symmetric even parity singlet A_{1g} representation of G . It should be noted, however, that conventional is not a synonym for isotropic, for any G one can form A_{1g} representations from angular momentum orbitals of higher order l , for example $l \geq 2$ for tetragonal and hexagonal symmetry and $l \geq 4$ for cubic symmetry. On the other hand, a superconductor with additional broken symmetries besides gauge symmetry is called *unconventional*. It can have either parity. Any odd-parity SC state which has broken inversion symmetry is unconventional in this sense. From the effective attractive interactions as eq. (12) obtained from model Hamiltonians like eq. (11) containing ‘high energy’ interaction parameters the symmetry can be obtained by directly minimizing the free energy and solving the resulting gap equations. These calculations depend on the model parameters and approximation schemes and cannot make predictions for real compounds.

The usual procedure described in detail in the next section to determine the symmetry of SC order parameters is to select plausible candidate states corresponding to irreducible representations (or mixtures) of the symmetry group, calculate the expected (temperature, field) behavior of physical quantities and compare the predictions with experiment. The selection of candidate states exploits Michel’s theorem (Michel 1980) according to which stable points of the free energy should correspond to states which are invariant under subgroups of the full symmetry group. However the theorem was only proven for free energy expressions which are polynomial in the order parameter. As long as we work sufficiently close to the transition temperature, where a Ginzburg-Landau expansion is valid the systematic construction of gap functions in terms of basis functions which are invariant under subgroups is a useful guideline. Exhaustive lists of the superconducting classes for the relevant crystal symmetries were given by Volovik and Gor’kov (1985), Ueda and Rice (1985), Blount (1985), Gorkov (1987), Sigrist and Ueda (1991), Annett (1990) and Ozaki and Machida (1985), Machida and Ohmi (1998), Machida et al. (1999) and references cited therein. A recent summary is found in the textbook of Mineev and Samokhin (1999).

Quite generally the results as given above can be divided into two groups (1,2) according to their treatment of spin-orbit interaction. Group (1) treats the orbital and (pseudo-) spin degrees of freedom separately, while group (2) assumes that the spin of the Cooper

pair is frozen in the lattice. In mathematical terms: (1) assumes the symmetry group to be the direct product $G \times SU(2)$, while (2) considers the point group of the crystal to be the double group. The two schemes yield different predictions for the node structures. Treating the Cooper pair spin or \mathbf{d} as frozen in the lattice leads to odd-parity order parameters which vanish only in isolated points on the Fermi surface. This fact which was first pointed out by Blount (1985) and is usually referred to as Blount's theorem. Even-parity states, on the other hand, have gap functions which may vanish on lines and at isolated points on the Fermi surface.

Blount's theorem seems to rule out odd-parity states in UPt_3 at first glance since there is strong evidence for node lines on the Fermi surface. As a consequence, the majority of early order parameter models for UPt_3 adopted multicomponent even-parity states. However the anisotropy of thermal conductivity, reversal of upper critical field anisotropy and Knight shift results in UPt_3 are better accounted for by an odd-parity order parameter. For an extensive discussion of this problem we refer to Sect. 4.1. Another more recent case is UNi_2Al_3 where evidence for an odd parity state exists. It seems that Blount's theorem is not respected in real HF superconductors.

Concerning this ambiguity we add the following remark. Doubtlessly spin-orbit interaction plays an important role in U compounds. However, the energy $\xi_{so} \simeq 2$ eV associated with this relativistic effect is large compared to the HF quasiparticle band width $k_B T^* \simeq 10$ meV. In fact it is even larger than the hybridization energies, leading to separate 5f LDA bands belonging to different total angular momenta $j = \frac{5}{2}$ and $\frac{7}{2}$ where the latter is almost empty (Albers et al. 1986). With respect to pair formation spin orbit coupling is therefore to be treated as a high-energy effect. This suggests that spin orbit coupling should be included already in the properties of the normal state quasiparticle states. The latter can be classified according to the pseudo spins connected with Kramers degeneracy of band states.

The transformation properties of the odd-parity order parameters under spatial rotations is reduced to considering the behavior of the quasiparticle states. To leading order in the small ratio kT^*/ξ_{so} we include the spin-orbit interaction in the calculation of the local atomic basis states, in a second step they are coherently superposed to form extended states. For bands derived from one doubly (Kramers-) degenerate orbital the elements of the point group should act only on the propagation vector. When the Cooper pairs, i. e., the two-particle states, are formed the orbital and spin degrees of freedom can be treated independently. With the spin-orbit interaction already included in the normal state quasiparticles one can use Machida's states derived for vanishing spin-orbit interaction.

The two different methods in treating the spin-orbit interaction have their counterparts in atomic physics. The scheme put forward by Volovik and Gor'kov parallels Russell-Saunders coupling where the orbital momenta and spins of the individual electrons are coupled to the total orbital momentum \mathbf{L} and total spin \mathbf{S} , respectively. These two quantities are coupled to form the total angular momentum $\mathbf{J} = \mathbf{L} + \mathbf{S}$. Including the spin-orbit interaction in the quasiparticle states, on the other hand, closely parallels jj -coupling.

The symmetry classification of density wave order parameters may proceed in a similar way. Charge and spin density are physical observables, hence the CDW/SDW order

parameter describe diagonal long range order (DLRO) meaning that they correspond to expectation values of diagonal elements in the one-particle density matrix according to

$$\langle \mathbf{r}_{s_1} | \rho^{(1)} | \mathbf{r}_{s_2} \rangle \rightarrow A_{s_1 s_2} \exp(i\mathbf{Q}\mathbf{r}) \quad (28)$$

where \mathbf{Q} is the wave vector of the density modulation and its amplitude is given by

$$A_{s_1 s_2} = \sum_{\mathbf{k}} F_{s_1 s_2}^{\mathbf{Q}}(\mathbf{k}) \quad \text{and} \quad F_{s_1 s_2}^{\mathbf{Q}}(\mathbf{k}) = \langle c_{\mathbf{k}s_1}^\dagger c_{\mathbf{k}+\mathbf{Q}s_2} \rangle \quad (29)$$

The electron-hole pair amplitude $\mathbf{F}_{\mathbf{Q}}(\mathbf{k})$ may again be decomposed into singlet (CDW) and triplet (SDW) components $\rho_{\mathbf{Q}}(\mathbf{k})$ and $\mathbf{s}_{\mathbf{Q}}(\mathbf{k})$ respectively in analogy to SC pair amplitudes. Their corresponding gap functions are then given by the gap equations (c.f. eq. (52))

$$\Delta_C(\mathbf{k}) = -I \langle \rho_{\mathbf{Q}}(\mathbf{k}) \rangle \quad \text{and} \quad \Delta_S(\mathbf{k}) = -I \langle s_{\mathbf{Q}}^z(\mathbf{k}) \rangle \quad (30)$$

for CDW and SDW (\mathbf{d} vector along z) respectively, where I is the on-site Hubbard interaction. Likewise the \mathbf{k} -dependence of gap functions may be classified according to the irreducible representations of the point group G with even and odd parity type when it contains the inversion symmetry. Several interesting aspects arise here: (1) Since gauge symmetry is obviously not broken its phase cannot be chosen arbitrarily, it rather is tied to the spatial transformation properties of the representation considered. Commonly the gap functions will either be real or imaginary for commensurate density waves. (2) On the other hand for electron-hole pairing there is no antisymmetry requirement hence the gap function for singlet (CDW) or triplet (SDW) can *both* be odd or even. (3) Conventional CDW and SDW states correspond to gap functions $\Delta_C(\mathbf{k})$ and $\Delta_S(\mathbf{k})$ which transform as fully symmetric (A_{1g}) representations, in the simplest case they are constants, independent of \mathbf{k} . In this case the amplitude of the CDW/SDW density modulation in real space obtained from the summation in Eq. (29) is nonzero because the gap function does not change sign. If the gap functions belong to *nontrivial* representations, e.g. $d_{x^2-y^2}$ in two dimensions they do change sign and the sum in Eq. (29) is zero, i.e. there is *no density modulation* although there is a ‘hidden’ order parameter $\Delta_C(\mathbf{k})$ or $\Delta_S(\mathbf{k})$ which characterizes the electron-hole condensate. Such states have been given the misleading name ‘unconventional density waves’ in analogy to the usage for SC states. These hidden order parameters have recently been under intense discussion for both underdoped cuprates, organic materials and U-HF systems.

2.2.2. Pairing model for coexistence of SC and CDW/SDW

In U-HF compounds the coexistence of SC and SDW order parameters is frequently observed. In a purely itinerant picture this phenomenon is well studied on the basis of a mean field (mf) pairing Hamiltonian which allows for both type of instabilities. It has first been proposed for SC/CDW coexistence (Bilbro and McMillan 1976) and then for conventional SC/SDW (Machida 1981, Machida and Matsubara 1981) coexistence and later generalized to unconventional anisotropic gap functions for both SC and CDW/SDW (Kato and Machida 1988, Thalmeier 1994).

The effective mf Hamiltonian for pair formation in both electron-hole (e-h or Peierls) and electron-electron (e-e or Cooper) channels is given by

$$H = \sum_{\mathbf{k},s} \epsilon_{\mathbf{k}} c_{\mathbf{k}s}^{\dagger} c_{\mathbf{k}s} + H_{e-h} + H_{e-e} \quad (31)$$

Introducing the charge and spin-densities (polarised along z)

$$\begin{aligned} \rho_{\mathbf{k}}(\mathbf{Q}) &= c_{\mathbf{k}\uparrow}^{\dagger} c_{\mathbf{k}+\mathbf{Q}\uparrow} + c_{\mathbf{k}\downarrow}^{\dagger} c_{\mathbf{k}+\mathbf{Q}\downarrow} \\ s_{\mathbf{k}}(\mathbf{Q}) &= c_{\mathbf{k}\uparrow}^{\dagger} c_{\mathbf{k}+\mathbf{Q}\uparrow} - c_{\mathbf{k}\downarrow}^{\dagger} c_{\mathbf{k}+\mathbf{Q}\downarrow} \end{aligned} \quad (32)$$

the electron-hole part can be separated in singlet (CDW) and triplet (SDW) part

$$H_{e-h} = - \sum_{\mathbf{k}} [\Delta_C(\mathbf{k}) \rho_{\mathbf{k}}(\mathbf{Q}) + \text{h.c.}] - \sum_{\mathbf{k}} [\Delta_S(\mathbf{k}) s_{\mathbf{k}}(\mathbf{Q}) + \text{h.c.}] \quad (33)$$

Likewise the electron-electron part which, for example, is the mf approximation of Eq. 12 is given by

$$H_{e-e} = - \sum_{\mathbf{k}} \Delta_{SC}^{ss'}(\mathbf{k}) [c_{\mathbf{k}s}^{\dagger} c_{-\mathbf{k}s'}^{\dagger} + \text{h.c.}] \quad (34)$$

Here $\Delta_C(\mathbf{k})$, $\Delta_S(\mathbf{k})$ and $\Delta_{SC}^{ss'}$ are the CDW, SDW and SC gap functions which in general will depend on the momentum \mathbf{k} . The former two simply correspond to spin singlet (CDW) and triplet pairing (SDW) in the e-h channel. Analogously the superconducting gap matrix $\hat{\Delta}_{SC}(\mathbf{k})$ may be decomposed into singlet and triplet parts described previously.

If only a single nonzero OP is present diagonalisation of H leads to quasiparticle excitations ($A \equiv C, S$)

$$E_{\mathbf{k}} = [\epsilon_{\mathbf{k}}^2 + \Delta_{SC}^{\mathbf{k}2}]^{\frac{1}{2}}; \quad \text{or} \quad E_{\mathbf{k}} = [\epsilon_{\mathbf{k}}^2 + \Delta_A^{\mathbf{k}2}]^{\frac{1}{2}}; \quad (35)$$

in the ordered phase. Here $\Delta_{SC}^{\mathbf{k}}$ represents $\phi(\mathbf{k})$ in the singlet case and $|\mathbf{d}(\mathbf{k})|$ in the (unitary) triplet case respectively. The general case of coexisting order parameters and coupled gap equation is discussed below.

In the spirit of the Landau theory of 2^{nd} order phase transitions one has to assume that each of the gap functions transforms as an irreducible representation of the underlying symmetry group which consists of gauge transformations U(1), time reversal K , spin rotations SU(2) and spatial transformations G as introduced before. For e-h pairing the former is preserved, for e-e pairing it is at least partly broken. If the gap functions belong to a fully symmetric or trivial representation (A_{1g} or Γ_1^+) i.e. if they are invariant under all spatial symmetry operations (including parity) of G then the condensed state

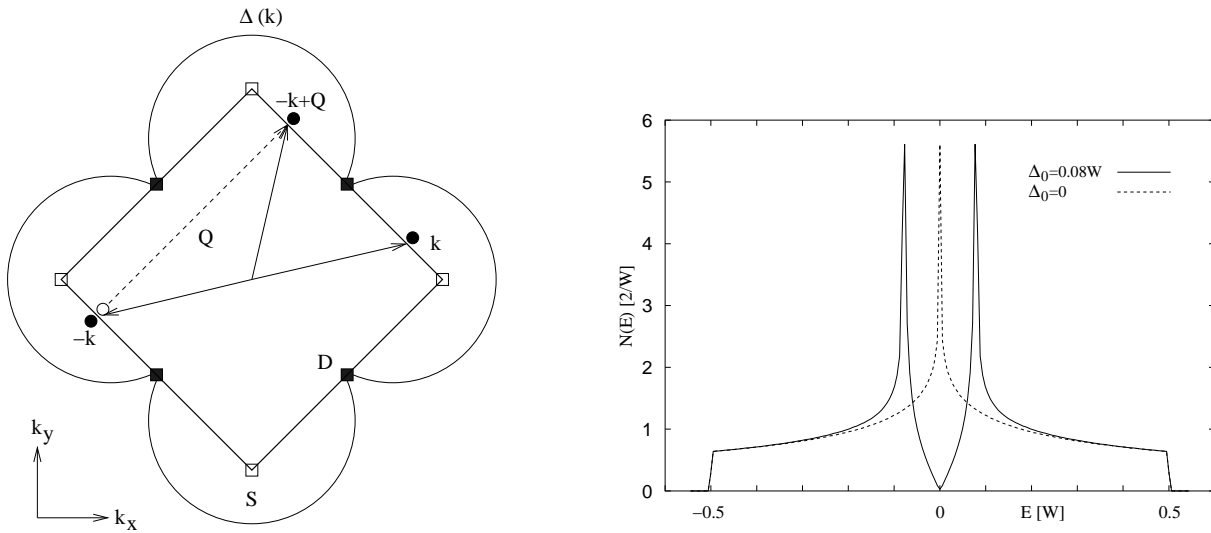


Figure 7. Left panel: Cooper pairs $(-\mathbf{k}, \mathbf{k})$ and electron-hole (Peierls) pairs $(-\mathbf{k}, -\mathbf{k}+\mathbf{Q})$ for the n.n. tight binding Fermi surface (thick line) with perfect nesting vector \mathbf{Q} . Saddle points (S) of $\epsilon(\mathbf{k})$ at $(0, \pm\pi)$ and $(\pm\pi, 0)$ lead to DOS peak at the Fermi energy. Therefore unconventional pair states can only have nodes away from S, i.e. at the ‘Dirac’ points D $(\pm\frac{\pi}{2}, \pm\frac{\pi}{2})$ where the quasiparticle spectrum takes the form of eq. (54). This is the case for a $d_{x^2-y^2}$ -type gap function $\Delta(\mathbf{k})$ which is indicated schematically. Right panel: corresponding quasiparticle DOS $N(E)$ (W = tight binding band width) for normal state (dotted) and with $d_{x^2-y^2}$ -gap with amplitude Δ_0 . The Fermi level is at $E_F=0$.

describes a conventional CDW, SDW or superconductor, for all other representations the pair state is called unconventional as mentioned before. The most important difference in the two cases is due to their generally different nodal structure. Whereas for A_{1g} in general $|\Delta_i(\mathbf{k})| > 0$ ($i = A, SC$) and hence quasiparticle excitations are gapped, for the unconventional states frequently zeroes of the gaps $\Delta_i(\mathbf{k}) = 0$ or $\mathbf{d}(\mathbf{k}) = 0$ on points or lines on the Fermi surface are *possible* but not necessary. In the SC case one basically has two types of nodes: (i) symmetry enforced gap nodes which always appear when the gap function transforms as an irreducible representation whose remaining symmetry group in the SC phase contains elements composed of spatial transformation and discrete gauge transformations and/or time reversal. (ii) accidental nodes which depend on the specific choice of basis functions within a single representation or which appear as a result of superposition of different representations ('hybrid gap functions'). Then gap nodes exist only for special superposition parameters ('fine tuning'). Such nodes (or at least very large gap anisotropies $\Delta_{max}(\mathbf{k}_{max})/\Delta_{min}(\mathbf{k}_{min})$) may also be present in conventional superconductors where the hybrid gap function is constructed from fully symmetric representations A_{1g} of various degree and only U(1) symmetry is broken. Both types of nodes have been found and examples will be discussed in later sections. The precise conditions for the symmetry enforced gap nodes are discussed in Mineev and Samokhin (1999). On the other hand in some compounds, for example borocarbides (sect.5) and possibly skutterudites (sect.6) the second type of SC gap nodes is observed. The quasiparticle spectrum of eq. (35) around the nodes defined by $\Delta_{SC}^{\mathbf{k}} = 0$ or $\Delta_A^{\mathbf{k}} = 0$ determines completely the low temperature physics of the ordered state. Knowledge about their position, multiplicity and dimension (points or lines) is therefore essential.

2.2.3. Coupled gap equations and results for coexistence

The interplay between superconductivity and antiferromagnetism has been in the focus of interest for a long time. The coexistence of the two ordering phenomena is well understood in those materials where they occur in different electronic subsystems which, in addition, are not coherently coupled. Wellknown examples are the Chevrel phases RMO_6S_8 , the rhodium borides RRh_4B_4 or the borocarbides $\text{RNi}_2\text{B}_2\text{C}$ where the influence of local moments of the lanthanide elements (R) on SC can be modelled by a molecular magnetic field acting on the SC conduction electrons (sect. 5). This results in a weaker pair interaction as compared to the paramagnetic phase and therefore leads to anomalies in the upper critical field H_{c2} below the onset of magnetic order.

The interplay of superconductivity with itinerant-electron magnetism where *both* SC and CDW/SDW are carried by conduction electrons continues to be a theoretical challenge. Qualitative phase diagrams reflecting the dominant order parameters and their mutual coexistence or expulsion have been derived within a mf approximation in order to interpret experiments. The concepts developed for transition metal alloys or organic superconductors have been extended to the case of heavy-fermion systems (Kato and Machida 1988, Konno and Ueda 1989). The basic assumption is that the long-range order, i. e. , superconductivity or spin-density wave results from an instability of the Fermi surface of the strongly renormalized heavy quasiparticles. This assumption implies that we have at least an approximate separation of energy scales with $T_c(T_N) \ll T^*$ where T_c , and T_N denote the superconducting and magnetic transition temperatures while T^* is the HF quasiparticle band width.

Kato and Machida (1988) adopt a two-dimensional (t,t')-tight binding model for the quasiparticle bands resulting in a Fermi surface that exhibits nesting features with the commensurate wave vector $\mathbf{Q} = (\frac{1}{2}, \frac{1}{2}, 0)$. The effective interaction which consists of an on-site repulsion and an attractive pairing leads to both SDW and SC instabilities, the former supported by the nesting feature. The formation of a spin-density wave changes the symmetry of the system. This requires a modified classification scheme for the superconducting order parameters which can appear in a second order phase transition within the SDW state. The presence of both types of order parameters Δ_A (A=C,S) and Δ_{SC} may lead to induced SC pair amplitudes with pair momentum \mathbf{Q} which strongly influence the coexistence behaviour. The competing order parameters for various symmetry types are determined from coupled gap equations for $\Delta_A(\mathbf{k})$ and $\Delta_{SC}(\mathbf{k})$. In Kato and Machida (1988) the former was taken as constant (conventional SDW) while the latter allowed to belong to any nonconventional representation. In Thalmeier (1994) the coexistence study was generalised to include also unconventional density waves $\Delta_A(\mathbf{k})$. In the general case coexistence, competition as well as expulsion of the two order parameters may be observed.

For the tight binding model described above there are two types of coupled gap equations which are due to the different even/odd transformation properties of $\Delta_{SC}(\mathbf{k})$, $\Delta_A(\mathbf{k})$ under the two discrete transformations $\mathbf{k} \rightarrow -\mathbf{k}$ (inversion) and $\mathbf{k} \rightarrow \mathbf{k} + \mathbf{Q}$ (translation). Case (I): there is no induced SC pairing with nonzero wave vector. Case (II): a finite induced pairing amplitude $\langle c_{\mathbf{k}s_1} c_{\mathbf{k}+\mathbf{Q}s_2} \rangle$ for SC pairs with nonzero pair momentum exists. Competition of SC and density wave pairs is much stronger in the second case because the induced pairing inevitably leads to a large loss in condensation energy.

In case I for the perfect nesting model ($t^{\prime}=0$) the gap equations are given simply by

$$1 = V \sum_{\mathbf{k}} \frac{f_{SC}(\mathbf{k})^2}{2E_{\mathbf{k}}} \tanh \frac{E_{\mathbf{k}}}{2T} \quad \text{and} \quad 1 = I \sum_{\mathbf{k}} \frac{f_A(\mathbf{k})^2}{2E_{\mathbf{k}}} \tanh \frac{E_{\mathbf{k}}}{2T} \quad (36)$$

where $E_{\mathbf{k}} = [\epsilon_{\mathbf{k}}^2 + |\Delta_{SC}^{\mathbf{k}}|^2 + |\Delta_A^{\mathbf{k}}|^2]^{\frac{1}{2}}$ is the quasiparticle energy and the form factors $f_{SC}(\mathbf{k})$, $f_A(\mathbf{k})$ which correspond to irreducible basis functions of D_{4h} point group are defined via $\Delta_{SC}(\mathbf{k}) = \Delta_{SC}^0 f_{SC}(\mathbf{k})$ and $\Delta_A(\mathbf{k}) = \Delta_A^0 f_A(\mathbf{k})$. Furthermore interaction constants I and V determine whether SDW or SC transition happens first. In HF compounds frequently we have $T_N > T_c$. In this weakly competitive case coupled gap equations are formally the same as for each of the gap functions individually. They influence each other only through the quasiparticle energies where both gap functions appear. Numerical solution shows that for this case coexistence is always possible and (assuming $T_N > T_c$) the transition from SDW to SDW+SC coexistence phase happens always in a second order phase transition, irrespective how small T_c is.

In case II the gap equations are formally different from individual gap equations:

$$\begin{aligned} 1 &= V \sum_{\mathbf{k}} \frac{f_{SC}(\mathbf{k})^2}{4|\Delta_{SC}^{\mathbf{k}}|} \left(\frac{|\Delta_{SC}^{\mathbf{k}}| + |\Delta_A^{\mathbf{k}}|}{E_{\mathbf{k}}^+} \tanh \frac{E_{\mathbf{k}}^+}{2T} + \frac{|\Delta_{SC}^{\mathbf{k}}| - |\Delta_A^{\mathbf{k}}|}{E_{\mathbf{k}}^-} \tanh \frac{E_{\mathbf{k}}^-}{2T} \right) \\ 1 &= I \sum_{\mathbf{k}} \frac{f_A(\mathbf{k})^2}{4|\Delta_A^{\mathbf{k}}|} \left(\frac{|\Delta_A^{\mathbf{k}}| + |\Delta_{SC}^{\mathbf{k}}|}{E_{\mathbf{k}}^+} \tanh \frac{E_{\mathbf{k}}^+}{2T} + \frac{|\Delta_A^{\mathbf{k}}| - |\Delta_{SC}^{\mathbf{k}}|}{E_{\mathbf{k}}^-} \tanh \frac{E_{\mathbf{k}}^-}{2T} \right) \end{aligned} \quad (37)$$

where the two quasiparticle bands $E_{\pm}^{\mathbf{k}} = [\epsilon_{\mathbf{k}}^2 + (|\Delta_{SC}^{\mathbf{k}}| \pm |\Delta_A^{\mathbf{k}}|)^2]^{\frac{1}{2}}$ are now split due to the presence of two order parameters. Numerical solutions for case II show a much more competitive behaviour of gap functions Δ_A and Δ_{SC} . If T_c is comparable in size to T_N the SDW state may be destroyed at T_c and replaced by the SC phase in a first order phase transition. For smaller T_c again a coexistence state SDW+SC appears in a second order phase transition but generally the order parameters in this regime show strong competition resulting in nonmonotonic temperature behaviour of gap functions.

The coexistence/competition behaviour of $\Delta_A(\mathbf{k})$ and $\Delta_S(\mathbf{k})$ is therefore quite different in case I and II and it also depends strongly on the relative nodal structure of $\Delta_A(\mathbf{k})$ $\Delta_S(\mathbf{k})$. Generally speaking if their nodes are on the same positions on the FS (or if at least one of them is a conventional gap function without nodes) this enhances competition, nonmonotonic temperature behaviour and tendency to expulsion of one OP. On the other hand an ‘orthogonal’ nodal structure for both (e.g. d_{xy} symmetry for SDW and $d_{x^2-y^2}$ for SC) supports coexistence because the two gaps become maximal at different parts of the FS and this also favors monotonic temperature dependence of the gap amplitudes.

To illustrate this behaviour we briefly discuss an example which may be relevant to CeCu_2Si_2 . Qualitatively the complex phase diagram of CeCu_2Si_2 can be described by a simple mean-field model for a conventional spin density wave ground state (competing with d-wave superconductivity within a two band model proposed by Dahm (2001). The calculated phase diagram displayed in fig. 8 shows that a state with d_{xy} symmetry can become stable within the SDW phase. This is in contrast to the pairing states with $d_{x^2-y^2}$ symmetry considered by Kato and Machida (1988) in a one band model. The experimentally observed unusual stability of the (A+SC) phase might follow from the peculiar Fermi surface of the heavy quasiparticles displayed in fig. 18. This is suggested

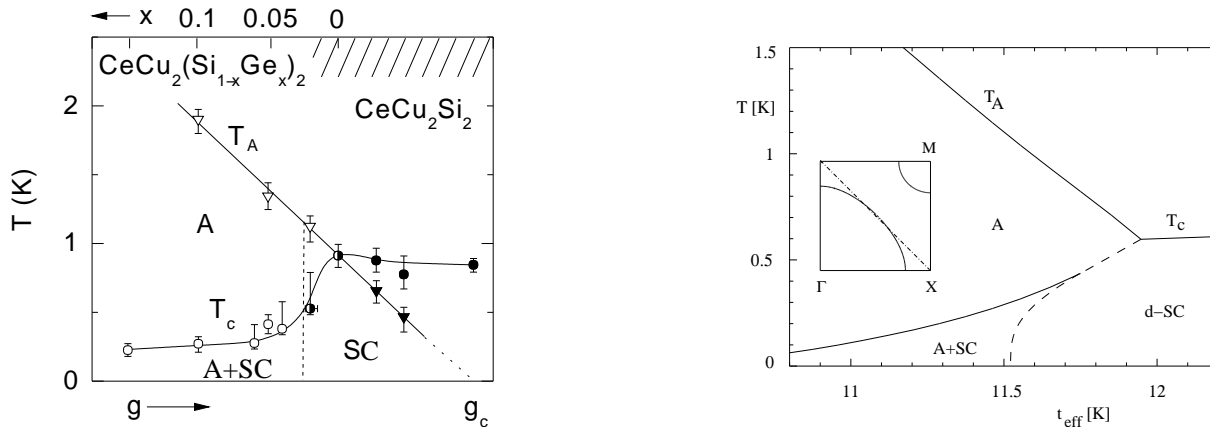


Figure 8. Left panel: experimental results for coexistence and competition between superconductivity and SDW in $\text{CeCu}_2(\text{Si}_{1-x}\text{Ge}_x)_2$ (Gegenwart et al. 1998). Ge substitution acts like a (negative) chemical pressure. Here A = SDW and SC is the superconducting state. T_A depends linearly chemical pressure, hence $g \sim 1-x$. Right panel: two band model for A and d-SC order in mf theory from Steglich et al, (2001b). Here A denotes a conventional SDW state with constant Δ_A and d-SC has $\Delta_{SC}(\mathbf{k}) = \Delta_{SC}^0 \sin k_x \sin k_y$; A+SC denotes the coexistence region. Solid and dashed lines correspond to second and first order transitions respectively. The effective tight-binding hopping integral is t_{eff} , it should also scale linearly with $1-x$. Inset: FS topology with two bands. Dash-dotted line indicates location of SDW gapping.

by model calculations which start from a more complex Fermi surface model. Assuming two well-separated sheets centered at Γ and M, respectively, allows for a solution where the SDW gaps exist only on part (centered around Γ) of the Fermi surface while the quasiparticles on the remaining parts (centered around M) condense into a superconducting state. The calculated temperature-'pressure' phase diagram (assuming that the electron band width $\sim t_{\text{eff}}$ scales linearly with pressure) is qualitatively in agreement with experimental results (Gegenwart et al. 1998) for CeCu_2Si_2 . Indeed the A-phase has now been identified as conventional SDW state with an incommensurate propagation vector $\mathbf{Q} = (0.22, 0.22, 0.55)$ and a moment of $0.1\mu_B$ per Ce-atom by neutron diffraction experiments (Stockert et al. 2003). The experimentally determined magnetic structure therefore requires a more refined treatment of the SDW/SC coexistence behaviour.

2.3. Methods to investigate the symmetry of order parameters

Phase transitions with the appearance of a spontaneous symmetry breaking are characterised by order parameters. In the spirit of Landau theory they belong to representations of the high temperature symmetry group and also characterise the class of remaining symmetries in the low temperature phase. Furthermore they partly determine the type of possible excitations in the ordered phase which in turn influence the low temperature thermodynamic and transport properties. The investigation of the order parameter symmetry is therefore of singular importance. In the case of order parameters corresponding to expectation values of physical observables like spin- and charge densities this is in principle straightforward as they reveal their existence and symmetry in x-ray and neutron diffraction experiments. However for ‘hidden’ order e.g. quadrupole ordering or ‘unconventional’ density waves (orbital antiferromagnetism) there is no large obvious signature in diffraction experiments and evidence for its presence has to be obtained indirectly by other means. The superconducting order parameter does not correspond to the expectation value of a classical observable but rather to the appearance of quantum mechanical phase rigidity of Cooper pairs on a macroscopic scale (the coherence length). For unconventional superconductors determination of the gap function dependence on the momentum of paired states is of fundamental importance. It is also extraordinarily difficult. The classical experimental techniques which we discuss in this section rely on the interpretation of temperature dependences of physical quantities obtained by *averaging* over the gap function momentum dependence and, therefore, the conclusion about their proper symmetry is always ambiguous. Recently a much more powerful method relying on the field angle resolved measurement of specific heat and thermal conductivity in the vortex phase for $T \ll T_c$ has been developed. It leads directly to the determination of the relative position of node lines and/or points of the SC gap function with respect to crystal axes. This leads to a strong reduction of the number of possible SC order parameters and possibly allows a unique determination. Therefore we devote an extra subsection to this new technique. On the other hand we shall not discuss phase sensitive methods based on Josephson tunneling which have been unsuccessful in HF compounds and point contact spectroscopy or μ SR methods due to their difficult interpretation. For unconventional density waves which also correspond to gap functions of nontrivial momentum dependence in the particle-hole channel, the field angle dependent investigation of magnetoresistance has similar potential but is less developed.

2.3.1. Detection of superconducting order parameter symmetry

In conventional electron-phonon superconductors with an almost isotropic gap numerous thermodynamic, static and dynamic transport measurements and also resonance methods can give information about the superconducting gap. The SC transition affects these quantities in two ways: i) the quasiparticle DOS exhibits a gap Δ with a square root singularity of the DOS: $N_s(E) = N_0 E / (E^2 - \Delta^2)$ ($E \geq \Delta$) ii) coupling of external probe fields to the quasiparticles involves a coherence factor $\frac{1}{2}(1 \mp \Delta^2/EE')$ where \mp corresponds to perturbations even or odd under time reversal respectively. In the former case (I) the DOS singularity and the vanishing coherence factor for $E \simeq \Delta$ compensate leading to a steep drop of the corresponding physical quantity, e.g. ultrasonic attenuation below T_c . In the latter case (II) the coherence factor is unity and therefore a Hebel-Slichter type

anomaly as e.g. in the NMR-relaxation rate develops below T_c . At low temperatures ($T \ll T_c$) invariably experimental quantities determined by electron-hole excitations tend to zero exponentially due to the finite superconducting gap. Therefore the most obvious and seemingly easiest method to look for evidence of unconventional superconductivity is the search for deviations from the exponential low temperature dependence. This strategy relies on the fact that nontrivial (unconventional) \mathbf{k} -dependent gap functions $\Delta(\mathbf{k})$ in many cases (though not always) exhibit node points or lines on the Fermi surface leading to a nonvanishing $N_s(E)$ for all energies $E > 0$ even in the superconducting state. The asymptotic behaviour of $N_s(E)$ for $E/\Delta \ll 1$ is $\sim E^2$ for (first order) point nodes and $\sim E$ for line nodes. Then this should ideally lead to ‘power law’ behaviour $\sim T^n$ for physical quantities like specific heat, penetration depth, NMR relaxation rate and many others for $T \ll T_c$. The experimentally observed exponent n would then allow to determine whether $\Delta(\mathbf{k})$ has point nodes ($n=3$), line nodes ($n=2$) or both if the exponent n is in between, or whether gapless regions of the Fermi surface ($n=1$) exist. For nondirectional quantities like $C(T)$ this would however say nothing about the position of nodes relative to the crystal axes. Unfortunately this picture is so oversimplified as to make it useless. Firstly, experimental determination of the exponent n very often includes temperatures where $T \ll T_c$ is not valid and more importantly impurity scattering in anisotropic superconductors has dramatic effects (Sigrist and Ueda 1991, Fulde et al. 1988). In conventional superconductors Anderson’s theorem ensures that the low temperature thermodynamic properties are not affected by impurity scattering. On the other hand normal impurities for unconventional pairs act strongly pairbreaking. This is especially important in HF compounds where the normal state electrons are already strongly correlated and impurities act as unitary scattering centers. Their effect for anisotropic superconductors has originally been studied by Buchholtz and Zwicknagl (1981) for p-wave states and later extended and applied (Hirschfeld et al. 1986, Scharnberg et al. 1986, Schmitt-Rink et al. 1986, Hotta 1993, Sun and Maki 1995) for other cases like d-wave. In the unitary scattering limit a resonant residual quasiparticle DOS at low energies develops (Hirschfeld et al. 1986) invalidating the abovementioned power laws. On the other hand hybrid nodal superconductors like s+g wave type in borocarbides exhibit the opposite behaviour: Impurity scattering immediately leads to the opening of a gap (Yuan et al. 2003) with resulting low temperature exponential behaviour. It is therefore more reasonable to investigate the T-dependence of physical quantities depending on the gap anisotropy for the whole temperature range below T_c and compare with experiments, rather than looking at the often ill-defined and contradictory low-T power laws. This will be discussed now in a few cases.

Specific heat: The specific heat in the anisotropic SC state is given by an expression formally identical to the s-wave case:

$$C_s = 2k\beta \sum_{\mathbf{k}} \left(-\frac{\partial f_{\mathbf{k}}}{\partial E_{\mathbf{k}}} \right) \left[E_{\mathbf{k}}^2 + \frac{1}{2}\beta \frac{\partial \Delta_{\mathbf{k}}^2}{\partial \beta} \right] \quad \text{and} \quad \frac{\Delta C_s}{C_n} = \frac{3}{2} \frac{8}{7\zeta(3)} \frac{\langle f_{\mathbf{k}}^2 \rangle_{FS}}{\langle f_{\mathbf{k}}^4 \rangle_{FS}} \quad (38)$$

where $\beta = 1/kT$, $E_{\mathbf{k}} = (\epsilon_{\mathbf{k}}^2 + \Delta_{\mathbf{k}}^2)^{\frac{1}{2}}$, $f_{\mathbf{k}} = f(E_{\mathbf{k}})$ is the Fermi function and $C_n = \gamma T$. The specific heat jump given by the second formula has the BCS value $\frac{\Delta C_s}{C_n} = 1.43$ for the isotropic s-wave gap. In fig. 9 model calculations for $C_s/\gamma T$ by (Hasselbach 1993) for all possible gap symmetries in tetragonal D_{4h} group are shown and compared with experi-

Table 1

BCS ratio $2\Delta(0)/kT_c$ and specific heat ratio $\Delta C_s/C_n$ for some common order parameter models (Einzel 2002) characterised by the gap form factor $f(\vartheta, \varphi)$ as function of polar angles of \mathbf{k} and normalised on the unit sphere ($a = 3\sqrt{3}/2$).

	isotropic	axial	polar	$E_{1g}(D_{6h})$	$E_{2u}(D_{6h})$
$f(\vartheta, \varphi)$	1	$\sin \vartheta$	$\cos \vartheta$	$2\sin \vartheta \cos \vartheta$	$a\sin^2 \vartheta \cos \vartheta$
$2\Delta(0)/kT_c$	3.52	4.06	4.92	4.22	4.26
$\Delta C_s/C_n$	1.43	1.19	0.79	1.00	0.97

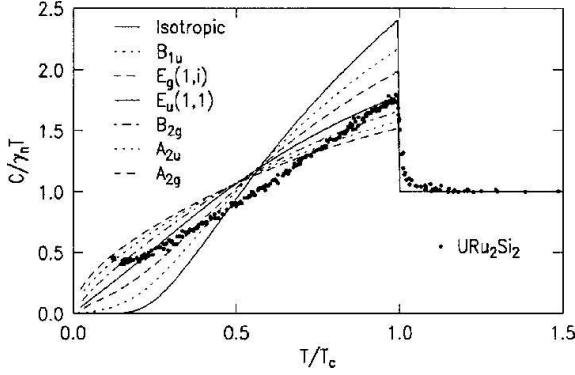


Figure 9. Calculated specific heat for various superconducting order parameters in comparison to experimental results for URu_2Si_2 (Hasselbach et al. 1993). The specific heat jump $\Delta C_s(T_c)$ agrees best for $E_u(1,1)$ or B_{1g} state.

mental results for URu_2Si_2 . The latter show remarkably linear behaviour over the whole experimental temperature range. It is obvious that a perfect fit is not possible with any gap representation and at low T a tendency for saturation due to an impurity induced residual DOS is visible. A comparison of theoretical and experimental $\Delta C(T_c)$ jumps however favors either a $E_u(1,1)$ state $\Delta(\mathbf{k}) = \Delta(k_x + k_y)^2$ or B_{1g} state $\Delta(\mathbf{k}) = \Delta(k_x^2 - k_y^2)^2$ for which one has $2\Delta(0)/kT_c = 4.92$ or 5.14 respectively. Since the presence of nodes reduces T_c compared to s-wave case for the same gap amplitude the BCS ratio (table 1) is always larger for anisotropic SC. However for real compounds this increase may also be partly due to strong coupling effects. Likewise the ratio $\Delta C_s/C_n$ is always maximal for isotropic SC.

Thermal conductivity: The thermal conductivity tensor is a directional quantity depending on the orientation of temperature gradient and heat current. At low temperatures its anisotropy may contain important information on the relative position of nodal points or lines with respect to crystal axes. For example this has proved decisive in the identification of the E_{2u} SC order parameter of UPt_3 (sect. 4.1). The uniaxial thermal conductivity tensor in the unitary scattering limit for a spherical Fermi surface is explicitly given (Norman and Hirschfeld 1996, Kübert and Hirschfeld 1998, Machida et al. 1999, Graf

et al. 2000, Wu and Joynt 2002) as

$$\begin{aligned}\frac{\kappa_i(T)}{\kappa_n} &= \frac{9}{2\pi^2 T_c} \int_0^\infty d\omega \left(\frac{\omega}{T}\right)^2 \text{sech}^2 \frac{\omega}{2T} K_i(\omega, T) \\ K_i(\omega, T) &= \frac{\langle \hat{k}_i^2 \text{Re}[\omega^2 - |\Delta_{\mathbf{k}}(T)|^2]^{\frac{1}{2}} \rangle}{\langle \text{Re}[\omega^2 - |\Delta_{\mathbf{k}}(T)|^2]^{-\frac{1}{2}} \rangle}\end{aligned}\quad (39)$$

where $\hat{k}_i = (\hat{\mathbf{i}} \cdot \hat{\mathbf{k}}) = \cos \theta_i$ and $\hat{\mathbf{i}}$ are the unit vectors along x,y,z axes.

At low temperatures the \mathbf{k} -averaging in $\kappa_i(T)$ is determined only by the quasiparticles close to the nodal region. Because of the direction cosines in the averages of eq. (39) coming from the quasiparticle velocities, κ_i depend on the position of the nodal points or lines with respect to the axis $\hat{\mathbf{i}}$. When the nodal direction in \mathbf{k} -space is parallel to the direction $\hat{\mathbf{i}}$ of the heat current a large contribution to $\kappa_i(T)$ is obtained and a small one if it is perpendicular. This may lead to a uniaxial thermal conductivity anisotropy characterised by the ratio (Norman and Hirschfeld 1996)

$$\frac{\kappa_c(0)}{\kappa_a(0)} = \lim_{\omega \rightarrow 0} \frac{\text{Re} \langle \hat{k}_z^2 [\omega^2 - |\Delta_{\mathbf{k}}(T)|^2]^{\frac{1}{2}} \rangle}{\text{Re} \langle \hat{k}_x^2 [\omega^2 - |\Delta_{\mathbf{k}}(T)|^2]^{\frac{1}{2}} \rangle}\quad (40)$$

As discussed in sect. 4.1 this anisotropy ratio of thermal conduction has proved quite useful in the identification of the order parameter symmetry in UPt₃ (see fig. 31).

Ultrasonic attenuation: Sound attenuation has in addition to the propagation direction ($\hat{\mathbf{q}}$) another polarization ($\hat{\mathbf{e}}$) degree of freedom and may therefore give even more information on the gap nodes than the thermal conductivity. In HF metals sound attenuation can generally be considered in the hydrodynamic limit where $\omega\tau$, $ql \ll 1$ with q , ω denoting wave number and frequency (~ 100 MHz) of the sound wave respectively and $l = v_F\tau$ is the mean free path in the normal state. In this case conduction electrons act like a viscous medium to the sound waves and the attenuation coefficient may be expressed as a correlation function of the electronic stress tensor (Tsuneto 1961, Kadanoff and Falko 1964). Its evaluation for unconventional SC states using a quasiclassical approximation leads to (Machida et al. 1999, Graf et al. 2000)

$$\begin{aligned}\frac{\alpha_{ij}(T)}{\alpha_n} &= \frac{1}{2T} \int_0^\infty d\omega \text{sech}^2 \frac{\omega}{2T} A_{ij}(\omega, T) \\ A_{ij}(\omega, T) &= \frac{1}{\langle \Pi_{ij}^2 \rangle} \langle \Pi_{ij}^2 \frac{1}{\omega} \text{Re}[\omega^2 - |\Delta_{\mathbf{k}}(T)|^2]^{\frac{1}{2}} \rangle \\ \Pi_{ij} &= \hat{k}_i \hat{k}_j - \frac{1}{3} \delta_{ij}\end{aligned}\quad (41)$$

The projection factor Π_{ij} ($i = \text{polarisation}$, $j = \text{propagation direction}$) determines which of the quasiparticles having a $\hat{\mathbf{k}}$ -vector described by polar and azimuthal angles ϑ , φ contribute strongly to the attenuation. Consider two cases with $ij = ab$ where $\Pi_{ij}^2 \sim \sin^2(2\varphi)$ and $ij = ac$ with $\Pi_{ij}^2 \sim \sin^2(2\vartheta)$. The quasiparticle contribution to $\alpha_{ij}(T)$ therefore vanishes for nodal directions $\varphi = n(\frac{\pi}{2})$ and $\vartheta = n(\frac{\pi}{2})$ respectively. For example if the gap has a node line in the basal plane ($\vartheta = \frac{\pi}{2}$) it gives maximal contribution to the attenuation for $ij=ab$ but minimal contribution for $ij=ac$. The same argument holds for point nodes

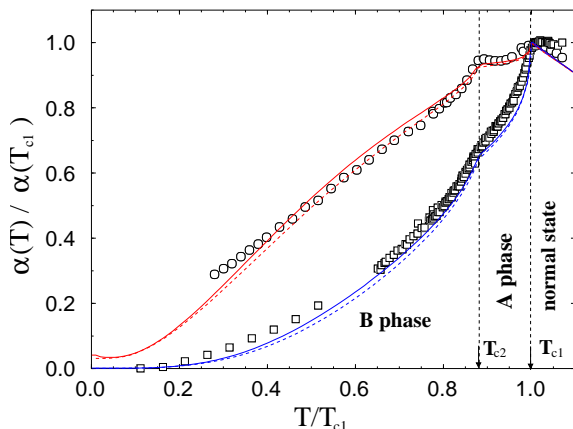


Figure 10. Temperature dependence of ultrasonic attenuation in B-phase of UPt_3 for transverse waves with propagation along a-axis and polarisation along b-axis (ab: circles) or c-axis (ac: squares), from Graf et al. (2000). Here $T_{c1,2}$ denotes the split SC transition temperature.

on the c-axis where $\vartheta=0,\pi$. This situation is indeed realized in the E_{2u} type B phase of UPt_3 (sect. 4.1) and one can see in fig. 10 that the attenuation for ac configuration is much smaller than for ab. The anomalies around the split T_c are complicated and analyzed in (Graf et al. 2000). Therefore polarization and propagation dependence of ultrasonic attenuation is a powerful method to distinguish between gap representations with different nodal structure. Finally it should be mentioned that collective modes in unconventional superconductors hardly contribute to the attenuation since one has an off-resonance situation due to $v_s \ll v_F$ (Kee et al. 2000).

NMR relaxation and Knight shift:

In an external field nuclear spins exhibit a Larmor precession with a frequency ω_0 . In metals this is modified by the hyperfine coupling to conduction electrons which leads to spin-flip processes as witnessed by the NMR-relaxation rate T_1^{-1} and the Knight shift of the resonance frequency $\delta\omega_0$. A review of these important effects for HF superconductors is given by Tou et al. (2003). The relaxation rate T_1^{-1} is determined by the availability of resonant electron-hole excitations. In the normal state this leads to the Korringa law $T_{1n}^{-1} \sim T$. In the superconducting state the presence of $\Delta(\mathbf{k})$ should lead to a faster decrease with temperature depending on the type of node structure, i.e. the low energy behaviour of the quasiparticle DOS. According to Sigrist and Ueda (1991) for singlet pairs one has

$$\frac{T_{1n}}{T_1} = \frac{2}{N_n^2} \int_0^\infty dE \left(-\frac{\partial f}{\partial E} \right) N_s(E) N_s(E + \omega_0) \left[1 + \frac{|\langle \Delta_{\mathbf{k}} \rangle_{FS}|^2}{E(E + \omega_0)} \right] \quad (42)$$

For s-wave pairs the type II-coherence factor together with the singular DOS leads to the appearance of the Hebel-Slichter peak. Because for unconventional pair states the Fermi surface average in eq. (42) vanishes, there is no difference between type I and II coherence

factors and the relaxation rate is determined by the DOS alone. Because in the presence of nodes there is no divergence in $N_s(E)$ no Hebel-Slichter peak will appear below T_c . Its absence may therefore be taken as a sign of an unconventional pair state. Furthermore the low temperature behaviour of T_1^{-1} should be $\sim T^3$ for line nodes and $\sim T^5$ for point nodes. Invariably the former is observed in HF systems, often in conflict with ‘power laws’ of other quantities. A puzzling feature is the absence of any crossover for $T \ll T_c$ to Korringa behaviour in the impurity dominated gapless regime.

In addition to the relaxation the hyperfine interaction leads to a Knight shift of the resonance frequency given by

$$\delta\omega_0(T) \sim |\psi_0|^2 \chi_s(T) H \quad (43)$$

where ψ_0 is the conduction electron wave function at the nucleus and $\chi_s(T)$ is the *spin* susceptibility of conduction electrons. Without spin orbit coupling present in an s-wave singlet state this drops to zero exponentially below T_c , leading to a pronounced T-dependence of $\delta\omega_0$. For a triplet SC state the condensate spin or the \mathbf{d} -vector of the pair can be freely rotated and $\chi_s(T)$ should not change leading to T-independent $\delta\omega_0$. Therefore the existence or non-existence of a T-dependent Knight shift below T_c is usually interpreted as direct evidence for singlet or triplet superconductivity respectively. In the former case the Knight shift should be proportional to the Yoshida function given by the FS average

$$Y(T) = \left\langle \frac{1}{2T} \int_0^\infty d\epsilon \cosh^{-2} \frac{E_{\mathbf{k}}}{2T} \right\rangle_{FS} \quad (44)$$

with a low T behaviour $Y(T) \sim T^2$ for point nodes and $\sim T$ for line nodes. Unfortunately the situation may be completely changed under the presence of strong spin orbit (s.o.) coupling, for both the conduction electrons themselves and for the conduction electron-impurity scattering. If the mean free path due to conduction electron-impurity s.o. scattering is much smaller than the coherence length, the Knight shift variation with temperature approaches zero also for singlet pairing (Abrikosov 1988). On the other hand in a triplet pair state a conduction electron s.o. coupling may lead to the pinning of the triplet pair \mathbf{d} -vector along one of the crystal axis. Then the T-dependence of $\delta\omega_0$ should be very anisotropic, vanishing for $\mathbf{H} \perp \mathbf{d}$ and large for $\mathbf{H} \parallel \mathbf{d}$. A moderately anisotropic Knight shift is indeed found in UPt₃ (sect. 4.1). These complications make a quantitative analysis as for the previous quantities difficult, in fact it is rarely performed for HF compounds. The arguments for or against singlet or triplet pairing using Knight shift results should therefore be taken with caution.

Upper critical field: The temperature dependence and anisotropy of the upper critical field H_{c2} may contain important information both about the question of singlet vs. triplet pairing and the anisotropy of the gap function $\Delta(\mathbf{k})$. A general discussion of the problem within the semiclassical approach has been given in Rieck et al. (1991). Theoretical analysis in the context of a generalized Ginzburg Landau theory depends very much on the crystal symmetry and order parameter model. It will be briefly discussed in sect. 4.1 for UPt₃. In this case the importance of uniaxial anisotropy to decide between singlet and triplet pairing has been realized (Choi and Sauls 1991, Sauls 1994, Yang and Maki 1999).

In a pure isotropic superconductor the upper critical field $H_{c2}(0)$ is limited by orbital effects leading to

$$\mu_B H_{c2}(0) = 0.58 T_c |dH_{c2}/dT|_{T_c} \quad (45)$$

The actual critical field may be much lower caused by the effect of paramagnetic ‘Pauli-limiting’ due to the Zeeman energy of the Cooper pair. If the field is larger than $\mu_B H_P = \Delta_0/\sqrt{2} = 1.25 T_c$ the upper critical field is limited by the breaking up of singlet Cooper pairs. According to eq. (45) a large critical field slope should also lead to a larger $H_{c2}(0)$. In UPt₃ the opposite is true leading to a ‘crossing’ of $H_{c2}(T)$ curves for a- and c-directions. This led to the proposal that $H_{c2}(0)$ is strongly reduced by Pauli-limiting effects for field along c but not along a. This can only be explained by assuming triplet pairing with strongly pinned **d**-vector parallel to c. As will be discussed in sect. 4.1 this interpretation is not undisputed. In addition to the question of the spin state a nontrivial **k**-dependence of the gap should also lead to anisotropies in the upper critical field (slope) beyond those due to effective mass anisotropies. This proved difficult or inconclusive for HF superconductors investigated so far (Keller et al. 1995).

2.3.2. Specific heat and magnetotransport in the vortex phase: a genuine angular resolved method

The classical methods to determine $\Delta(\mathbf{k})$ discussed above all suffer under the same major deficiency: the angular dependence, or at least nodal positions in **k**-space are never determined directly. Instead the physical quantities investigated are obtained by *averaging* over the quasiparticle and hence gap energies in **k**-space. And then it is hoped that the averaged quantities still show clear signatures depending on the gap symmetry. Naturally this leads to ambiguous results for any one method and only a comparison of all gap models for a number of methods may lead to a conclusion on the gap symmetry.

However recently a new and powerful method has been established that is able to locate directly the nodal positions of the SC gap in **k**-space Izawa et al. (2001, 2001a, 2002). In this method the *field-angle* dependence of specific heat or thermal conductivity is investigated. Typical oscillations are observed whose periodicity, phase and shape give direct information on the type of nodes (point- or line-like) and their direction in **k**-space. Therefore possibilities for allowed gap functions can be much more restricted. Notice however that still the full **k**-dependence of $\Delta(\mathbf{k})$ cannot be determined.

At the heart of this method is the ‘Volovik effect’ in the vortex state of the superconductor, it was first proposed by Volovik (1993) for d-wave superconductors. There it was shown that for nodal gap functions a continuum of quasiparticle states exists outside the vortex cores which dominate the specific heat and can easily carry a thermal current even perpendicular to the vortex lines. These states are due to quasiparticles channeling out of the vortex core region through the nodal points or lines. This is an important new aspect as compared to conventional nodeless gap functions where one has only bound states in the vortex core. For the quasiclassical limit $\xi_0 k_F \gg 1$ they also form a quasi-continuum but they can carry a heat current only parallel to the vortex direction. The theory of magnetothermal transport has subsequently been developed by many authors (Barash et al. 1997, Kübert and Hirschfeld 1998, Vekhter et al. 2001, Won and Maki 2000, Dahm et al. 2000, Won and Maki 2001a, Won and Maki 2001b). The

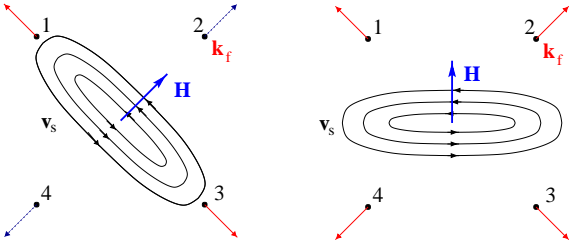


Figure 11. Illustration of the Volovik effect (Vekhter et al., 2000). \mathbf{k}_i ($i=1-4$) denote the nodal directions of the gap. Left: field \mathbf{H} along nodal direction where \mathbf{v}_s is orthogonal to $\mathbf{k}_2, \mathbf{k}_4$; these nodal directions do not contribute to the Doppler shift, the residual DOS will be at minimum. Right: Field along antinodal direction, all \mathbf{k}_i ($i=1-4$) directions contribute to the Doppler shift, the residual DOS is maximal.

Volovik effect can nicely be explained within the quasiclassical picture where momentum (\mathbf{k}) and position (\mathbf{r}) coordinates commute and the quasiparticle energy $E(\mathbf{k}, \mathbf{r})$ and occupation $f(\mathbf{k}, \mathbf{r})$ depends on both. The dependence on \mathbf{r} comes from the fact that the energy of quasiparticles channeling into the inter-vortex region gets Doppler shifted due to the \mathbf{r} -dependent superfluid velocity field $\mathbf{v}_s(\mathbf{r})$. This leads to $E(\mathbf{k}, \mathbf{r}) = E(\mathbf{k}) - \mathbf{v}_s(\mathbf{r}) \cdot \mathbf{k}$. Here $E(\mathbf{k})$ is the zero-field quasiparticle energy and the second term is the Doppler shift energy. This position dependent shift leads to a finite residual DOS which will depend both on field magnitude and direction:

$$\frac{N_s(E, \mathbf{H})}{N_n} \simeq \frac{1}{\Delta} \langle \langle |E(\mathbf{k}) - \mathbf{v}_s(\mathbf{r}) \cdot \mathbf{k}| \rangle \rangle \quad (46)$$

The double average is performed both over the velocity field coordinate \mathbf{r} and the quasiparticle momentum. It will depend on the direction of the magnetic field $\mathbf{H}(\theta, \phi)$ with respect to the nodal directions (θ and ϕ are polar and azimuthal angles of \mathbf{H} with respect to the c -axis). An illustration of this direction dependence is given in fig. 11. The variation of the field angles (θ, ϕ) is therefore expected to lead to a periodic variation in $N(E, \theta, \phi)$ and hence in the specific heat and thermal conductivity components. Oscillations will be strongest i) in the low temperature limit $T \ll \tilde{v}\sqrt{eH} \ll \Delta(0)$ when only quasiparticle from the nodal regions contribute to the residual DOS and ii) if the node structure is not smeared to much by impurity scattering, i.e. one is in the ‘superclean limit’ with $(\Gamma\Delta)^{\frac{1}{2}} \ll \tilde{v}\sqrt{eH}$ where Γ is the impurity scattering rate and $\tilde{v} = \sqrt{v_a v_c}$ with v_a and v_c giving the Fermi velocities along a - and c -axis in uniaxial symmetry. This limit can also be expressed as $\Gamma/\Delta \ll H/H_{c2} \ll 1$. For hybrid nodal gaps such as $s+g$ wave gap in the borocarbides the superclean condition should be replaced by $\Gamma \ll T \ll \tilde{v}\sqrt{eH}$ due to the completely different effect of impurities in this case (sect. 5). Including the effect of impurity scattering one obtains for the residual DOS at the Fermi level (Won and Maki 2000):

$$\frac{N_s(0, \mathbf{H})}{N_n} = \text{Re}[g(0, \mathbf{H})]$$

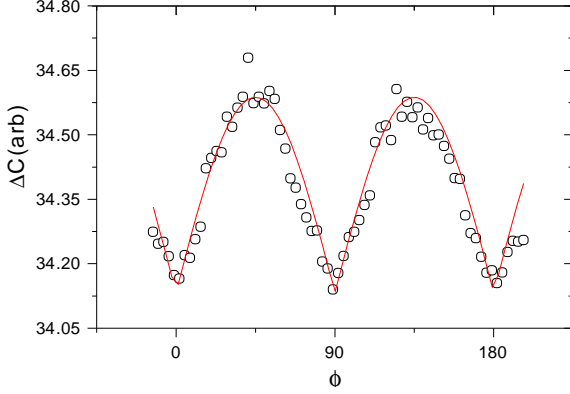


Figure 12. Specific heat oscillation $\Delta C(\phi)$ in $\text{YNi}_2\text{B}_2\text{C}$ for field \mathbf{H} in the ab-plane as function of the azimuthal field angle ϕ . Full line is a fit using a phenomenological cusp function (Park et al. 2003).

$$g(0, \mathbf{H}) = \left\langle \frac{C_0 - ix}{\sqrt{(C_0 - ix)^2 + f^2}} \right\rangle \quad (47)$$

$$C_0 = \frac{\Gamma}{\Delta g(0, \mathbf{H})}$$

Here $f(\mathbf{k}) = \Delta(\mathbf{k}) / \Delta$ and $x = |\mathbf{v}_s \cdot \mathbf{k}| / \Delta$ are the normalized gap function and Doppler shift energy respectively while C_0 is a normalized scattering rate. The above condition for the superclean limit can be expressed as $C_0 \ll x$.

The averaging is performed by restricting the \mathbf{k} -integration to the node region (since $T \ll \Delta$) and approximating the \mathbf{r} -integration over the superfluid velocity field of the vortex lattice by that of a single vortex (assuming $H \ll H_{c2}$) with cutoff $d = 1/\sqrt{eH}$ given by the half-distance between two vortices (Won and Maki 2001a). It is important to note that the averaging of the Doppler shift energy has to be done simultaneously in \mathbf{r} and \mathbf{k} . The field (angle-) dependent specific heat C_s , spin susceptibility χ_s and superfluid density are then given by

$$\frac{C_s(\mathbf{H})}{\gamma T} = \frac{\chi_s(\mathbf{H})}{\chi_n} = g(0, \mathbf{H}) \quad \text{and} \quad \frac{\rho_s(\mathbf{H})}{\rho_s(0)} = 1 - g(0, \mathbf{H}) \quad (48)$$

The explicit expression for $C_s(H, \theta, \phi)$ depends on the node structure of $\Delta(\mathbf{k})$ and is, up to numerical constants of order unity, obtained as

$$C_s(H, \theta, \phi) = \frac{\tilde{v}\sqrt{eH}}{\Delta} I(\theta, \phi) \quad (49)$$

Where for example for the d-wave order parameter with $f(\mathbf{k}) = \cos(2\varphi)$ and two orthogonal line nodes parallel to c one has for planar magnetic field (Won and Maki 2000)

$$I\left(\frac{\pi}{2}, \phi\right) \simeq 0.95 + 0.028 \cos(4\phi) \quad (50)$$

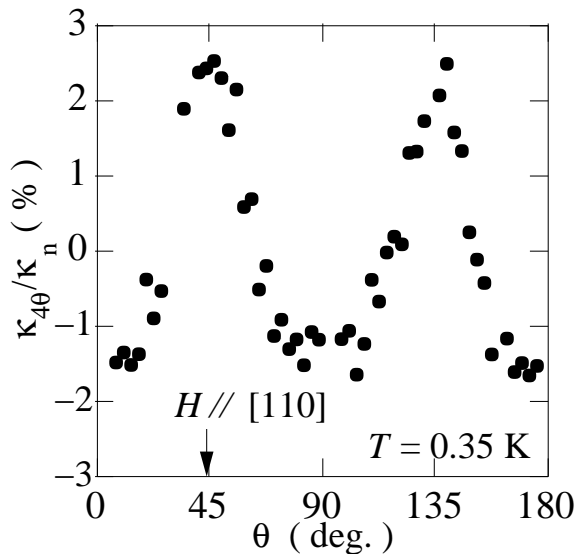


Figure 13. Thermal conductivity $\kappa_{xx}(\phi)$ for field in the ab-plane as function of the azimuthal angle ϕ for CeCoIn₅ (Izawa et al 2001a). A fourfold oscillation compatible with $d_{x^2-y^2}$ SC state is clearly seen.

Thus the specific heat should exhibit a fourfold oscillation with field rotation in the ab-plane with a minimum in the nodal and the maximum in the anti-nodal direction. The amplitude of the oscillation is not large because of the \mathbf{k} -averaging in eq. (47) along the node line. It may be larger for a gap function with point nodes as in the case of borocarbides which is discussed in detail in sect. 5. This has been experimentally investigated by Park et al. (2003) as shown in fig. 12. It also shows the typical cusp-like minima of point nodes as opposed to smooth minima observed for gap functions with line nodes. The smoothing is also due to the additional averaging along the line node. A most significant result is the observed \sqrt{H} dependence of the specific heat magnitude which is also a fingerprint of nodal superconductivity (fig. 55). However one must keep in mind that this should be observed for $H \ll H_{c2}$, a global approximate behaviour over the whole field range as sometimes found in conventional superconductors has no relation to the above effect.

Similar field-angle dependence of thermal conductivity can be calculated starting from the Ambegaokar-Griffin formula generalized to anisotropic gap functions. In the d-wave case one obtains in the superclean limit (Won and Maki 2000).

$$\frac{\kappa_{xx}}{\kappa_n} = \frac{2}{\pi} \langle x \rangle^2 = \frac{2}{\pi} \frac{\tilde{v}^2}{\Delta^2} I\left(\frac{\pi}{2}, \phi\right)^2 \quad (51)$$

Due to the magnetic field there is also an off-diagonal ‘thermal Hall conductivity’ κ_{xy} which has been identified in high- T_c compounds (Ocana and Esquinazi 2002). The fourfold oscillations in $\kappa_{xx}(\phi)$ have been found in the HF superconductor CeCoIn₅ with node directions $\phi = 0, \frac{\pi}{2}$ corresponding to maxima in $\kappa_{xx}(\phi)$ in the anti-nodal directions $\phi = \pm \frac{\pi}{4}$ as shown in fig. 13. This lead to the proposal of a $d_{x^2-y^2}$ gap functions as in high- T_c

compounds. For this geometry, where both field and heat current are in the *ab*-plane, there is also a term that shows a twofold rotation $\sim \cos(2\phi)$ which is possibly due to the heat current contribution of vortex core states. This contribution is zero or finite for heat current perpendicular or parallel to vortex lines respectively. Therefore a more favorable geometry is to rotate the field around the heat current direction, e.g. measuring κ_{zz} as function of the azimuthal angle for a given polar angle θ . In this case only oscillations due to the nodes should appear. Various examples will be discussed later (sect. 4.1, sect. 5 and sect. 6)

Finally we note that the field angle-oscillations in specific heat and thermal conductivity cannot be explained by normal state Fermi surface effects. Calculations based on the Kubo formula indicate that the angle variation of thermal conductivity is determined by the anisotropy of the gap function and not by that of the Fermi velocity which enters only as secondary effect. This can be checked experimentally by measuring the angle dependence in the *normal* state for fields above H_{c2} . Also the (planar) angle dependence of H_{c2} is usually of a few percent and for fields $H \ll H_{c2}$ this does not contribute significantly to the angle dependence of the thermal conductivity.

The field angle dependence of specific heat and thermal transport in the vortex phase have revolutionized the investigation of superconducting gap structure in nodal superconductors. Many ambiguities from the previous methods which have persisted over years have been resolved in a short time. This method certainly has enormous potential, it remains to be seen whether it can also be tried for other quantities, e.g. ultrasonic attenuation in the vortex phase as function of magnetic field direction.

2.3.3. Detection of density wave type order parameters

Density wave order parameters are of ‘diagonal long range order’ (DLRO) type and correspond to the expectation value of a physical observable, i.e. the charge or spin density operator in eq. (32). Their gap functions for e-h pair states are determined by selfconsistent equations formally identical to the BCS gap equations as obvious from eq. (36). The physical meaning of the gap function in the e-h pairing case becomes obvious by calculating the expectation values of charge (C) and spin (S) densities in eq. (32):

$$\langle \rho_{\mathbf{Q}} \rangle = \sum_{\mathbf{k}} \Delta_C(\mathbf{k}) F(\mathbf{k}) \quad \text{and} \quad \langle M_{\mathbf{Q}}^z \rangle = \sum_{\mathbf{k}} \Delta_S(\mathbf{k}) F(\mathbf{k}) \quad (52)$$

with $F(\mathbf{k}) = \tanh(E_{\mathbf{k}}/2T)/2E_{\mathbf{k}}$ and $E_{\mathbf{k}} = \sqrt{\epsilon(\mathbf{k})^2 + \Delta_i(\mathbf{k})^2}$ ($i = C, S$) denoting the quasi-particle energy and the gap functions $\Delta_i(\mathbf{k})$ are given by eq. (30).

Conventional density waves :

In the conventional ‘s-wave’ CDW and SDW case with \mathbf{k} -independent gap functions $\Delta_{C,S}(\mathbf{k}) = \Delta$ the sum in eq. (52) leads to a finite charge or spin density Fourier component for the modulation vector \mathbf{Q} . This also holds for a fully symmetric (A_{1g}) gap function which is \mathbf{k} -dependent but satisfies $\Delta(g\mathbf{k}) = \Delta(\mathbf{k})$ for any group element $g \in G$. Due to nonvanishing $\langle \rho_{\mathbf{Q}} \rangle$ and $\langle M_{\mathbf{Q}}^z \rangle$ conventional CDW and SDW states are straightforward to identify because macroscopic densities either couple to the electric and magnetic fields of external probes or, as in the case of CDW, lead to observable distortions of the underlying crystal lattice. In neutron and (magnetic) x-ray diffraction experiments one can therefore observe additional lattice or magnetic superstructure Bragg reflections that originate in the scattering from density modulations $\langle \rho_{\mathbf{Q}} \rangle \cos(\mathbf{Q} \cdot \mathbf{r})$ and $\langle M_{\mathbf{Q}}^z \rangle \cos(\mathbf{Q} \cdot \mathbf{r})$. This is the standard method to observe broken spatial and time reversal symmetries, i.e. structural and magnetic phase transitions. There are also numerous other physical quantities, both static and dynamic which are affected by the appearance of conventional CDW and SDW modulations for which we refer to the book by Grüner (1994) and references cited therein.

Unconventional density waves:

These order parameters also correspond to DLRO of density operators but the gap functions $\Delta_{\mathbf{k}}$ now belong to a nontrivial representation of G sometimes called ‘unconventional density waves’. In this case there will be elements $g \in G$ with $\Delta(g\mathbf{k}) = -\Delta(\mathbf{k})$ signifying a sign change of $\Delta_i(\mathbf{k})$ between different sectors of \mathbf{k} -space. Under these circumstances cancellation in eq. (52) occurs and macroscopic charge and spin-densities $\langle \rho_{\mathbf{Q}} \rangle$ and $\langle M_{\mathbf{Q}}^z \rangle$ vanish even though the order parameter corresponds to a physical observable (therefore the name convention for these states is misleading). A more formal proof of this cancellation effect was given in Thalmeier (1994). Now one has a perplexing situation of ‘hidden order’. Although there is a condensation of e-h pairs associated with quasiparticle energies and thermodynamic signatures similar to conventional (s-wave) CDW and SDW, the order parameter cannot be identified by the usual diffraction type experiments. This makes the search for such ‘hidden order’ a difficult task, and in fact it has not been unambiguously successful in any specific material. Some of the most prominent candidates for unconventional density waves are; the HF compound URu₂Si₂ (Ikeda and Ohashi 1998) to be discussed in sect. 4.4; the underdoped pseudo-gap phase of high- T_c materials (Benfatto et al. 2000, Chakravarty et al. 2001); and the organic conductors (Dóra and Virosztek 2001, Basletic et al. 2002, Korin-Hamzic et al. 2002), especially Bechgaard-

salts (Maki, Dora, Kartsovnik, Virosztek, Korin-Hamzic and Basletic (2003, 2003a)). To discuss the properties of unconventional CDW and SDW e-h pair states and their physical signature we restrict ourselves in the following to the 2D tight binding model with nearest neighbor (n.n.) hopping which in this respect is the only model sofar investigated in any detail. In this case the tight-binding band $\epsilon_{\mathbf{k}} = -2t(\cos k_x + \cos k_y)$ has the important perfect nesting property $\epsilon_{\mathbf{k} \pm \mathbf{Q}} = -\epsilon_{\mathbf{k}}$ leading to parallel Fermi surface sections at half filling ($E_F=0$) as shown in fig. 7. This also leads to a singular behaviour of the DOS according to $N(0) \sim \ln(t/|\epsilon|)$ due to the saddle points (S) of $\epsilon_{\mathbf{k}}$ at $\mathbf{k}=(0, \pm\pi)$ and $(\pm\pi, 0)$. The various possibilities of density wave and superconducting pair states assuming three types of interactions (U = on-site Coulomb, V = n.n. Coulomb, J = n.n. exchange) were studied and classified (Gulacsi and Gulacsi 1987, Schulz 1989, Ozaki 1992). From the many possible phases the most important ones are conventional s-SC, s-CDW, SDW, and unconventional d-SC, d-CDW, SDW states. Historically the latter two states have also been called orbital antiferromagnet (OAF) and spin-nematic (SN) states respectively (Nersesyan and Vachnadze 1989, Nersesyan et al. 1991, Gor'kov and Sokol 1992) which points to their physical origin in staggered charge or spin currents on the 2D square lattice respectively. Their pairing amplitudes or gap functions have a d-wave like \mathbf{k} -dependence given by

$$\Delta_{C,S}^d(\mathbf{k}) = i\Delta_0(\cos k_x - \cos k_y) \quad (53)$$

and illustrated in fig. 7. The d-wave gaps have nodes which are located at the four ‘Dirac’ points (D) $\mathbf{k} = (\pm\frac{\pi}{2}, \pm\frac{\pi}{2})$. The node points are in ‘orthogonal’ (rotated by $\frac{\pi}{4}$) configuration to the saddle points (S) because at the latter with their singular DOS the gap value of a density wave state (and also SC state) has to achieve maximum value to be stable. In other words the ordered state consists mostly of e-h pairs $(\mathbf{k}, \mathbf{k}+\mathbf{Q})$ with \mathbf{k} close to the saddle point regions. This allows one to study the problem in a simplified continuum theory (Schulz 1989, Thalmeier 1996). As indicated the phase of gap function for d-density waves with commensurate nesting \mathbf{Q} is not arbitrary. Because of the symmetry $\Delta_{C,S}^d(\mathbf{k})^* = -\Delta_{C,S}^d(\mathbf{k})$ the gap function has to be purely imaginary. Due to this property the ordered states are connected with staggered persistent charge (C) or spin (S) currents around the lattice plaquettes. In real space the pattern of currents at the lattice links is indicated in fig. 14.

As a means of identification of d-density wave states one then has to look for signatures of persistent currents in the ground state and for evidence of nodes in the quasiparticle excitation spectrum in thermodynamic and (magneto-) transport properties.

Neutron diffraction: For d-CDW the charge currents break time reversal symmetry while the spin-currents in d-SDW do not (under time reversal both current and spin direction are reversed leaving the spin current invariant), they do, however, break spin rotational symmetry. Therefore d-CDW state may lead to the appearance of staggered *orbital* moments. Because the currents are spread out over a whole plaquette, the generated magnetic fields are of the order ~ 10 G associated with orbital moments $\sim 10^{-2}\mu_B$ per plaquette. The contribution to elastic and inelastic neutron cross section has been discussed (Chakravarty et al. 2001) in context with the d-CDW scenario for the spin gap phase of underdoped cuprates (Chakravarty et al. 2001a), but it is generally valid for the

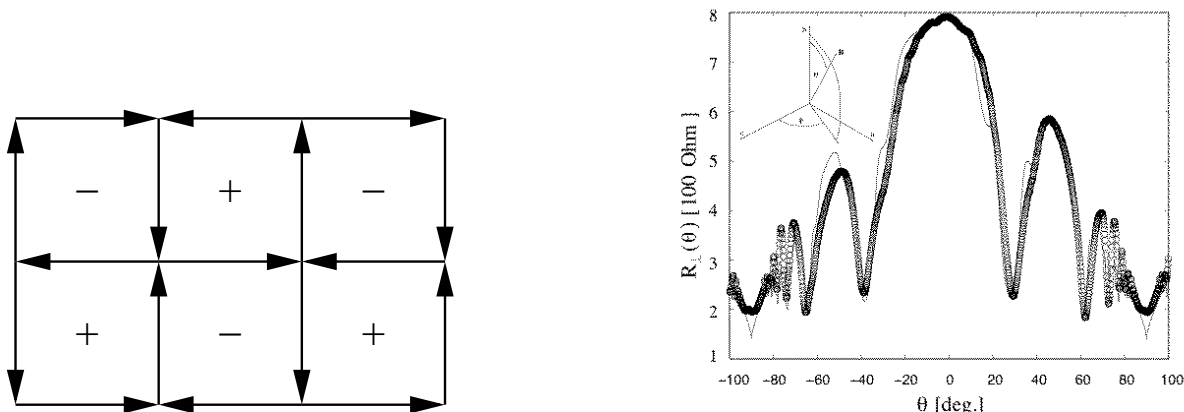


Figure 14. Left: illustration of staggered charge or spin current pattern in the square lattice for d-CDW or d-SDW. Right: magnetoresistance ($\mathbf{j} \perp ac$ -plane) oscillations in the low temperature d-CDW state of the organic quasi-1D conductor α -(BEDT-TTF) $_2$ KHg(SCN) $_4$. The oscillations result from the Landau quantisation of energy levels eq. (55) around the nodal Dirac points in fig. 7. The circles are from experiment ($T = 1.4$ K, $B = 15$ T, $\phi = 45^\circ$), and the full line from d-CDW calculations (Maki et al. 2003).

tight binding model used here. While the scattering from spin moments is determined by the form factor $g(\mathbf{q})$ of atomic electron densities which falls off moderately fast with momentum transfer \mathbf{q} , the scattering cross section from orbital moments is determined by the orbital current distribution $\mathbf{j}(\mathbf{q})$ namely proportional to $|\langle \mathbf{j}(\mathbf{q}) \rangle|^2 / \mathbf{q}^2 \sim 1/\mathbf{q}^4$ which falls off much more quickly with momentum transfer due to the spread-out orbital moment density. Although this method would be rather straightforward it is quantitatively difficult due to the small orbital moment size and only applicable for d-CDW.

A more indirect but more versatile method consists in looking for signatures of the gap nodes in the d-density wave states. For low temperatures $T \ll \Delta$ the nodal regions dominate thermodynamics and transport properties. Specific heat and thermal conductivity is equivalent to that of d-SC which have been discussed before. Susceptibility and frequency dependent electrical conductivity however are characteristic for the d-density wave states. Of course there is no vortex phase and the Doppler shift method cannot be applied.

Giant diamagnetism: The susceptibility has been analysed in detail (Nersesyan and Vachnadze 1989, Nersesyan et al. 1991). Strong anomalies in the diamagnetic susceptibility for both d-CDW and -SDW are predicted at low fields. This is due to the peculiar conical or ‘relativistic’ quasiparticle spectrum around the nodal Dirac points (D) in fig. 7. For $T \ll \Delta_0$ the spectrum can be linearized and consists of two bands

$$E_{\pm}(\mathbf{k}) = \pm \sqrt{v_F^2 k_x^2 + v_{\Delta}^2 k_y^2} \quad (54)$$

with $v_F = 2\sqrt{2}ta$ and $v_{\Delta} = \sqrt{2}\Delta_0 a$ giving the group velocity perpendicular and parallel to the original Fermi surface in fig. 7 respectively which are related to the effective mass

via $m^* = \Delta_0/2v_Fv_\Delta$. Here the lower band (-) is completely filled and the upper band (+) empty, thus the Fermi surface in the ordered state ($\Delta_0 > 0$) consists of two inequivalent points $\mathbf{k}_{1,2} = (\frac{\pi}{2}, \pm\frac{\pi}{2})$, the other Dirac points are equivalent since \mathbf{Q} is now a reciprocal lattice vector. The linearization corresponds to restricting to a (2+1) dimensional continuum field theory of chiral massless relativistic fermions with 'anisotropic' velocities v_F and v_Δ (Nersesyan and Vachnadze 1989). The quasiparticle DOS close to the Fermi level $E_F = 0$ is given by $N(E) = |E|/(\pi v_F v_\Delta)$ therefore one has low-T power laws $C \sim T^2/(t\Delta_0)$ and $\chi_P^\parallel \sim \mu_B^2 T/\Delta_0$ for the specific heat and the in-plane spin susceptibility. The most striking effect however should appear in the diamagnetic susceptibility anomaly caused by the persistent plaquette currents. This is obtained through the relativistic Landau quantisation of the spectrum which leads to Landau levels

$$E_n^\pm = \pm\sqrt{|\Omega_\perp|n} \quad \text{and} \quad \Omega_\perp = 2eH_\perp v_F v_\Delta / c \quad (55)$$

which have a degeneracy $\nu(H) = |eH|/2\pi c$ (c = speed of light) per unit area. Furthermore, $H_\perp = H\cos\theta$ where θ = polar field angle with respect to the plane normal vector $\hat{\mathbf{n}}$. This equation holds for fields with $\sqrt{|\Omega_\perp|} \ll \Delta_0$. From eq. (55) the H-dependent total energy is obtained leading to a (2D) diamagnetic susceptibility

$$\chi_{2D} \sim \frac{\sqrt{\Delta_0}}{|H|^{1/2}} \cos^{3/2}\theta \quad (56)$$

which predicts an enhancement factor of $(\Delta/\Omega_c) \gg 1$ compared to the normal state diamagnetic susceptibility. The divergence in eq. (56) will be arrested below a tiny crossover field where 3D behaviour due to interlayer hopping sets in and perfect diamagnetism with $\chi_{3D}(H \rightarrow 0) = -1/4\pi$ will be approached. Thus for temperatures $T \ll \Delta_0$ and almost zero field the staggered currents of d-CDW or SDW should achieve a similar perfect screening effect as supercurrents in the d-SC state.

The conical quasiparticle spectrum and associated 'relativistic' Landau quantisation should also leave its mark on the (magneto-) resistance which we only briefly mention since so far it has only been applied to d-CDW candidates among quasi-1D organic conductors. In this case a finite carrier concentration ($|E_F| > 0$) should be present. This is achieved by including a finite next-nearest-neighbor (n.n.n.) hopping element t' in the model. It does not appear in the linearized spectrum eq. (55) however. Analogous to the susceptibility, the magnetoresistance is determined by the Landau levels of the d-CDW state leading to typical oscillations (fig. 14) in its angular dependence which have been identified in two examples (Dóra et al. 2002, Basletic et al. 2002, Maki, Dora, Kartsovnik, Virosztek, Korin-Hamzic and Basletic 2003).

Finite frequency probes: Finally we discuss finite frequency probes for d-DW states like optical conductivity (Yang and Nayak 2002). It exhibits non-Drude like behaviour at low frequencies because of arbitrary low excitation energies for $\mathbf{q} = 0$ interband ($E_- \leftrightarrow E_+$) transitions at the nodal (Dirac) points. For perfect nesting ($E_F = 0$) at low temperatures one obtains (for $\omega\tau \gg 1$, τ = quasiparticle lifetime)

$$\sigma(\omega, T) = (\ln 2)e^2\alpha T\delta(\omega) + \frac{1}{8}e^2\alpha|f(-\frac{\omega}{2}) - f(+\frac{\omega}{2})| \quad (57)$$

where $\alpha \simeq (v_F/v_\Delta)$ and f denotes the Fermi function. The first part is the Drude term and the second is the interband term which should extend to arbitrary low frequencies and contribute to the d.c. conductivity because of the vanishing gap at the node points. The weight of the Drude peak vanishes for $T \rightarrow 0$ while the interband contribution stays finite at zero frequency. Since the thermal conductivity has only a Drude contribution, the Wiedemann-Franz law $\kappa \sim \sigma T$ should be strongly violated in the d-DW state and one would rather expect $\kappa \sim \sigma T^2$. This result holds as long as $E_F < kT$ and also for finite quasiparticle scattering rate $\Gamma = 1/\tau$ if $\Gamma < E_F$. In addition the d-DW state may lead to anomalous field dependence of electrical and thermal Hall conductivity.

The peculiar excitation spectrum eq. (55) of a d-DW should also leave its imprint in the inelastic neutron scattering cross section (Chakravarty et al. 2001) which is proportional to the imaginary part of the dynamical spin susceptibility.

3. Ce-based heavy-fermion superconductors

The discovery of superconductivity in CeCu_2Si_2 by Steglich et al. (1979) initiated the rapid development of heavy fermion physics. For nearly two decades, this material was the only Ce-based heavy fermion superconductor at ambient pressure. Only recently, superconductivity at ambient pressure was found in the new class of heavy fermion materials $\text{Ce}_n\text{M}_m\text{In}_{3n+2m}$ where M stands for the transition metal ion Ir or Co and $m = 1$ while $n = 1$ or $n = 2$ (Thompson et al. 2001). Typical examples are CeCoIn_5 (Petrovic et al. 2001a) and CeIrIn_5 (Petrovic et al. 2001).

The SC phases are characterized by BCS-type pair correlations among the heavy quasiparticles. In addition the strong on-site correlations introduced by the partially filled Ce-4f shells are reflected in several aspects. Firstly, the SC gap functions are anisotropic due to the local quasiparticle repulsion. Secondly, the competition between the non-magnetic Fermi liquid state and magnetically ordered phases leads to pronounced strong-coupling effects. They highlight the complex low-frequency dynamics in these systems which result from the competition between Kondo effect and long-range magnetic order.

The main emphasis of the current experimental and theoretical studies is on the fundamental question which factors actually determine the low-temperature phases, i. e., when does a Ce compound become a heavy fermion superconductor or why does it order magnetically. The subtle interplay between Kondo effect and long-range magnetic order can be monitored experimentally in pressure studies where isostructural relatives of the heavy-fermion superconductors are tuned from magnetic phases at ambient pressure to superconducting states. Similar behavior is found in doping experiments where constituents of the metallic host are successively replaced. Examples for pressure-induced superconductors are CeCu_2Ge_2 (Jaccard et al. 1992), CePd_2Si_2 (Grosche et al. 1996, Mathur et al. 1998), CeNi_2Ge_2 (Grosche et al. 2000) and CeRh_2Si_2 (Movshovich et al. 1996) CeSn_3 (Walker et al. 1997) and CeIn_3 (Grosche et al. 1996).

Finally, a different type of competition between superconductivity and magnetic order may be realized in CeCu_2Si_2 . In this compound, the strongly renormalized Fermi liquid seems to be unstable with respect to the formation of both superconducting pairs and an (incommensurate) spin-density wave. The actual ground state depends sensitively on the composition of the sample.

In the present section, we review the properties of the stoichiometric Ce compounds exhibiting competition between heavy fermion superconductivity and long-range magnetic order. We shall not discuss the highly complex phase diagrams obtained in alloy systems. In addition, we summarize recent attempts at a theoretical description of the complex low-frequency dynamics resulting from the competition between Kondo effect and RKKY interaction.

3.1. CeM_2X_2

The archetype heavy fermion superconductor CeCu_2Si_2 as well as the pressure-induced superconductors CeCu_2Ge_2 , CePd_2Si_2 , CeNi_2Ge_2 and CeRh_2Si_2 crystallize in the tetragonal ThCr_2Si_2 structure. The unit cell is shown in fig. 15. The isostructural compounds CeM_2X_2 with $M=\text{Ru, Ni, Pd, Cu, Ag, Au}$ and $X=\text{Si, Ge}$ exhibit a great variety of possible ground states and have been extensively studied to clarify the interplay between the formation of magnetic order and heavy fermion behavior.

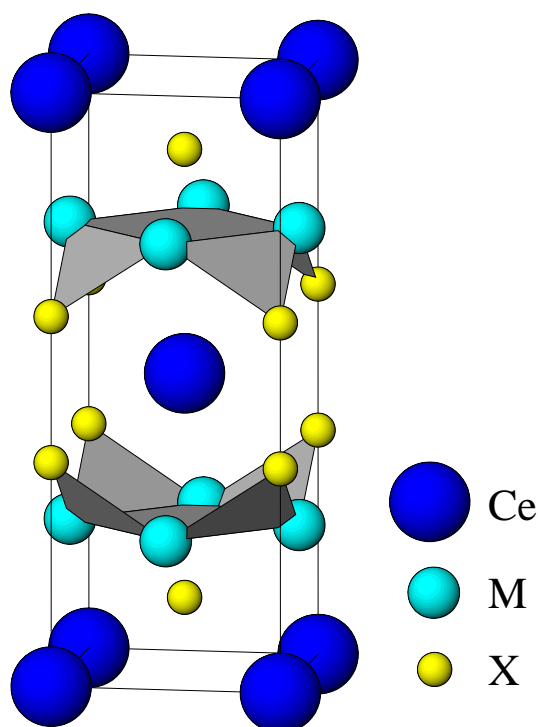


Figure 15. Conventional unit cell of the ThCr_2Si_2 and CeM_2X_2 structure where $M = \text{Cu, Ni, Ru, Rh, Pd, Au, ..}$ and $X = \text{Si, Ge}$. This is also the unit cell of URu_2Si_2 (sect. 4.4)

3.1.1. Electronic properties, Fermi surfaces and heavy quasiparticles

To study the electronic structure, we compare the results for two different models treating the Ce 4f degrees of freedom as localized (atomic like) states and as delocalized yet strongly renormalized electrons. The first procedure provides a good quantitative description of the properties at elevated temperatures, high excitation energies, and above the metamagnetic transition. The latter ansatz yields a model for the Fermi liquid state.

With respect to the electronic properties, the compounds CeM_2X_2 fall into two distinct categories, the key feature being the presence or absence of transition metal d-states at the Fermi level. We apply this criterion to classify the CeM_2X_2 compounds exhibiting superconductivity. The first group is formed by CePd_2Si_2 , CeNi_2Ge_2 and CeRh_2Si_2 which have a large conduction electron density of states at the Fermi level. A well-studied

model for the normal state of these systems is provided by CeRu_2Si_2 which we shall consider in detail below. The macroscopic properties of this compound closely resemble those of CeNi_2Ge_2 and CePd_2Si_2 . The general conclusions derived for CeRu_2Si_2 should therefore apply also to the pressure-induced superconductors. The second group is given by CeCu_2Si_2 and CeCu_2Ge_2 where the metal d-bands are filled.

The low-temperature behavior of CeRu_2Si_2 is well described by a paramagnetic Fermi liquid with weak residual interactions. The relevant low-energy excitations are heavy quasiparticles as inferred from the linear specific heat coefficient $\gamma \simeq 350 \text{ mJ/molK}^2$ (Steglich et al. 1985). The electronic structure was calculated both for the local moment regime at high temperatures and for the Fermi liquid state. Both types of calculations start from ab-initio crystal potentials which are determined selfconsistently within the LDA. Details of the calculation can be found in (Runge et al. 1995). In the local moment regime, the Fermi surface is determined exclusively by the conduction states. The strongly renormalized Fermi liquid state, on the other hand, is described by the renormalized band method using $\tilde{\Delta}_f \simeq 10 \text{ K}$ in eq. (7) for the intrinsic width of the quasiparticle band. The value is consistent with inelastic neutron data (Regnault et al. 1988) as well as thermopower and specific heat data (Steglich 1985). CEF effects are accounted for by adopting a Γ_7 ground state. The details of the calculation are described in (Zwicknagl 1992).

The renormalized band scheme gives the correct Fermi surface topology for CeRu_2Si_2 and thus consistently explains the measured dHvA data (Zwicknagl et al. 1990, Zwicknagl 1993). The Fermi surface consists of five separate sheets among which are four closed hole surfaces centered around the Z point. The remaining one is a complex multiply-connected surface where extremal orbits of rather different character exist. In particular, one can find typical particle-like orbits as well as others for which a hole picture would be more appropriate. The agreement between calculated and experimental results with respect to general topology is rather good (for further details see (Zwicknagl 1992, Zwicknagl 1993)).

The character of quasiparticles in CeRu_2Si_2 varies quite strongly over the Fermi surface. There are three Z-centered hole ellipsoids with rather light quasiparticles. The states on the pillow-shaped Z-centered hole surface displayed in fig. 16, however, have predominantly f-character and therefore yield the dominant contribution to the specific heat. Experimentally, one finds heavy and light quasiparticles coexisting on the multiply-connected sheet.

The validity of the Fermi liquid picture is concluded from a comparison of the effective masses on the fourth pillow-shaped sheet as given in table 2. From the large linear specific heat the renormalized band scheme deduces a characteristic energy $kT^* \simeq 10 \text{ K}$ which in turn implies heavy masses of the order of $m^*/m \simeq 100$. This value was confirmed by experiments (Albessard et al. 1993, Aoki et al. 1993, Tautz et al. 1995) where the ψ orbit with $m^*/m \simeq 120$ was observed. The corresponding Fermi surface cross section is in agreement with estimates from the renormalized band theory. This proves that the heavy quasiparticles exhaust the low-energy excitations associated with the f-states in HF systems. The shape of the Fermi surface of heavy quasiparticles implies the existence of nesting vectors. This fact suggests that the Fermi liquid state might become unstable with respect to particle-hole pairing, leading for example to the formation of a SDW state.

The change in the volume of the Fermi surface when going from $T \ll T^*$ to $T \gg T^*$

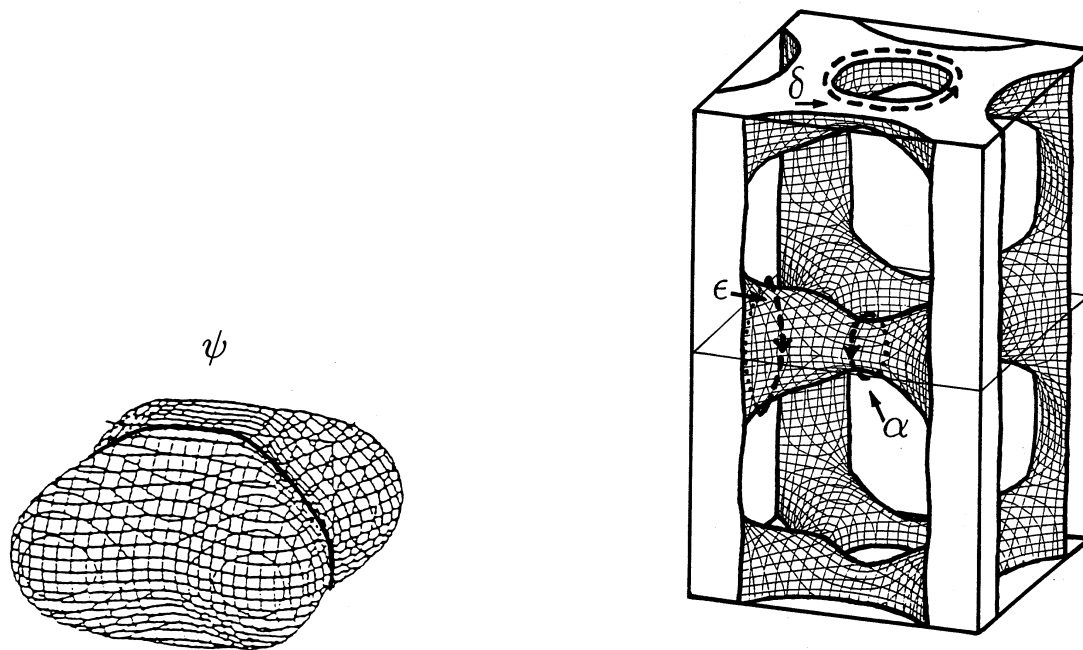


Figure 16. CeRu_2Si_2 : Fermi surface sheets for quasiparticles with f-character. The labels ψ and α , δ , ϵ refer to the branches observed in dHvA experiments (Lonzarich 1988, Albessard et al. 1993). Left: hole surface centered around the Z-point of the Brillouin zone with effective mass $m^* \sim 100 m$ which dominates the specific heat γ -value. For localized f-electrons at elevated temperatures, the hole surface expands extending to the boundaries of the Brillouin zone while the multiply connected electron-like surface shrinks. The expansion of ψ is confirmed by photoemission experiments. Right: multiply-connected electron-like sheet

is observed by comparing the Fermi surface of CeRu_2Si_2 to that of its ferromagnetic isostructural counterpart CeRu_2Ge_2 where the f-states are clearly localized. In a series of beautiful experiments (King and Lonzarich 1991) it was demonstrated that the Fermi surfaces of these two compounds are rather similar. However, the enclosed Fermi volume is smaller in the case of CeRu_2Ge_2 , the difference being roughly one electron per unit cell. More direct evidence is provided by recent photoemission experiments (see fig. 17). Denlinger et al. (2001) have shown that at temperatures around 25 K, the Fermi surface of CeRu_2Si_2 , is that of its counterpart LaRu_2Si_2 which has no f-electrons.

The similarity of the Fermi surface topologies for localized and itinerant Ce 4f states is a characteristic feature of the CeM_2X_2 systems with partially filled M d-bands. In addition, we mention that the topology of the Fermi surface for the heavy quasiparticles is qualitatively reproduced by standard band structure calculations based on the LDA (Zwicknagl 1988).

This, however, is not the case for CeCu_2Si_2 . As the Cu d bands are filled there are only two major twofold degenerate bands crossing the Fermi energy, and the effective hy-

Table 2

CeRu₂Si₂: Effective masses of the heavy quasiparticles. Comparison of experiment (Albessard et al. 1993) and theory (Zwicknagl et al. 1990). The heavy quasiparticles explain the specific heat at low temperatures. There are no further low-energy excitations involved.

ψ	experiment	theory (approx.)
area [MG]	53.6	62
m^*/m	120	100



Figure 17. Photoemission results for LaRu₂Si₂ (a) in comparison to CeRu₂Si₂ (b) at T = 25 K above the Kondo temperature T* = 15 K of CeRu₂Si₂. Band structures are similar for both compounds (Denlinger et al. 2001).

bridization becomes rather anisotropic. To calculate the quasiparticle bands in CeCu₂Si₂ by means of the renormalized band method, we adopt the doublet-quartet CEF scheme suggested by Goremychkin and Osborn (1993). The ground state is separated from the excited quartet by $\delta \simeq 340$ K.

The results for the Fermi surface (Zwicknagl and Pulst 1993, Pulst 1993) can be summarized as follows: two separate sheets of the Fermi surface for heavy and light quasiparticles are found. The light quasiparticles have effective masses of the order of $m^*/m \simeq 5$. They can be considered as weakly renormalized conduction electrons and the corresponding Fermi surface is rather similar to the LDA prediction (Harima and Yanase 1991). The observed Fermi surface cross sections (Hunt et al. 1990) can be explained by both the renormalized band structure as well as by the LDA bands. There is, however, a characteristic difference between the Fermi surfaces for the light quasiparticles as derived from the two schemes: The LDA calculation predicts a small closed surface centered around the Γ -point which is absent in the dHvA-experiment although the corresponding cross sections are rather small and the masses are expected to be light.

Of particular interest are heavy quasiparticles of effective masses $m^*/m \simeq 500$ which are found on a separate sheet. The topology of this surface is rather different from the corresponding LDA result as can be seen from fig. 18. It mainly consists of columns parallel to the tetragonal axis and small pockets. The topology of the Fermi surface suggests that the strongly correlated Fermi liquid state should become unstable at sufficiently low

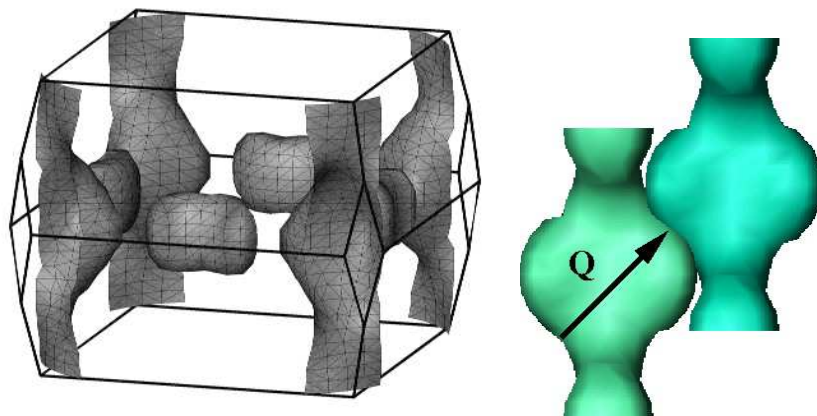


Figure 18. CeCu_2Si_2 : Left: FS of heavy quasiparticles ($m^*/m \simeq 500$) calculated by using the renormalized band method. It consists of ellipsoids and modulated columns which are oriented parallel to the tetragonal axis. The calculations adopt the CEF scheme suggested by Goremychkin and Osborn (1993) consisting of a singlet ground state separated from an excited quartet by a CEF splitting $\delta \sim 340$ K. Therefore $\delta \gg T^* \simeq 10$ K (obtained from the γ -value). Consequently quasiparticle properties are strongly anisotropic. The topology of the renormalized band FS differs qualitatively from LDA results. Right: enlarged FS columns exhibiting nesting between a column and its counterpart shifted by the nesting vector $\mathbf{Q} = (0.23, 0.23, 0.52)$ (Zwicknagl and Pulst 1993).

temperatures. Firstly, it exhibits pronounced nesting features which may eventually lead to the formation of a ground state with a spin density modulation. This will be discussed in detail below. Secondly, the topology of this surface depends rather sensitively on the position of the Fermi energy. The band filling and hence the f-valence are critical quantities. Reducing the f-occupancy from the initial value of $n_f \simeq 0.95$ by $\simeq 2\%$ leads to changes in the topology as shown by Pulst (1993) and Zwicknagl and Pulst (1993). As a result, the quasiparticle density of states (DOS) should exhibit rather pronounced structures in the immediate vicinity of the Fermi energy which, in turn, can induce instabilities (Kaganov and Lifshits 1979).

An external magnetic field couples to the f-degrees of freedom. It leads to a Zeeman splitting of order $\mu_{eff}B$ of the heavy quasiparticle bands and hence can move the structures in the DOS relative to the Fermi energy. The effective moment μ_{eff} of the f-states which contains the CEF effects depends on the direction of the external magnetic field. From the renormalized band calculation we determine the values of the critical magnetic fields when the pronounced structures are moved to the Fermi energy. Due to CEF effects on the f-states this critical value of the external magnetic field will depend upon its orientation. The explicit values of the critical fields B_{crit}^c and B_{crit}^a for field directions parallel to the c- and a-axes as listed in table 3 agree rather well with the observed critical magnetic fields for the transition into the ‘B-phase’ (see fig. 19).

Having discussed the basic electronic structure of the CeM_2X_2 heavy fermion compounds we now turn to their low-temperature properties.

Table 3

Low-temperature values of the critical magnetic fields for the transition into the high-field ‘B-phase’. Comparison with experiment of the renormalized band prediction for the approximate critical magnetic fields for field directions along the tetragonal axis (B_{crit}^c) and in the basal plane (B_{crit}^a) (Zwicknagl and Pulst 1993)

critical field	renormalized bands	experiment
B_{crit}^a [T]	8.0	7.0
B_{crit}^c [T]	6.5	4.0

3.1.2. Superconductivity and itinerant antiferromagnetism in $CeCu_2Si_2$

$CeCu_2Si_2$ exhibits highly complex phase diagrams at low temperatures. This fact partially results from an extreme sensitivity of the physical properties with respect to variations of the stoichiometry. Thorough investigations of the ternary chemical phase diagram (for a review see (Steglich et al. 2001)) showed that the actual ground state is mainly determined by the average occupation of the non-f sites surrounding the Ce-ion.

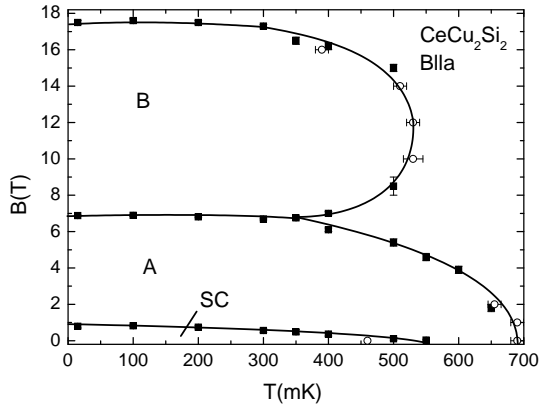


Figure 19. B-T phase diagram of $CeCu_2Si_2$ for $B \parallel a$. The original version of this phase diagram is from Bruls et al. (1990) while the completed version is from Weickert et al. (2003). For this sample the A-phase is expelled from the SC region (no coexistence).

Apart from the composition, the phases are strongly affected by magnetic fields. The B-T-phase diagram (Bruls et al. 1994) for a high-quality single-crystal is displayed in fig. 19. The phase transitions were deduced from anomalies in thermodynamic quantities including the elastic constants, thermal expansion and magnetostriction coefficients. In the low temperature regime, there is a SC phase surrounded by a phase ‘A’ which becomes unstable in high magnetic fields. Similar phase diagrams are obtained from resistivity measurements, e. g. (Steglich et al. 2000a). In addition to these ‘A-SC-type’ crystals, there exist also ‘A-type’ systems which do not superconduct as well as ‘SC-type’ compounds

where the A phase is suppressed (fig. 8). The high-field phase B, on the other hand, is present in all three cases. It is interesting to note that the transition into the B-phase occurs close to the calculated critical fields B_{crit}^a and B_{crit}^c listed in table 3. At these values, the Fermi surface of the heavy quasiparticles is expected to change drastically.

Much effort has been devoted to the characterization of the A phase which originally had the appearance of another ‘hidden order’ phase. However later the spin density wave character first inferred from resistivity results (Gegenwart et al. 1998) was supported by specific heat and high-resolution magnetization measurements (Steglich et al. 2000). The transition temperature T_A is suppressed by increasing the 4f-conduction electron hybridization and eventually vanishes. This can be achieved by applying hydrostatic pressure or choosing a few percent excess of Cu. The ordered moments are expected to be rather small. The propagation vector \mathbf{Q} can be estimated by extrapolation from neutron diffraction studies in single-crystalline $\text{CeCu}_2(\text{Si}_{1-x}\text{Ge}_x)_2$. The central result is that the wave vector of the magnetic order changes only slightly with the Ge concentration while the ordered moment per Ce site, however, decreases strongly from $\mu \simeq 0.5\mu_B$ for $x = 0.5$ to $\mu \simeq 0.1\mu_B$ for $x = 0$.

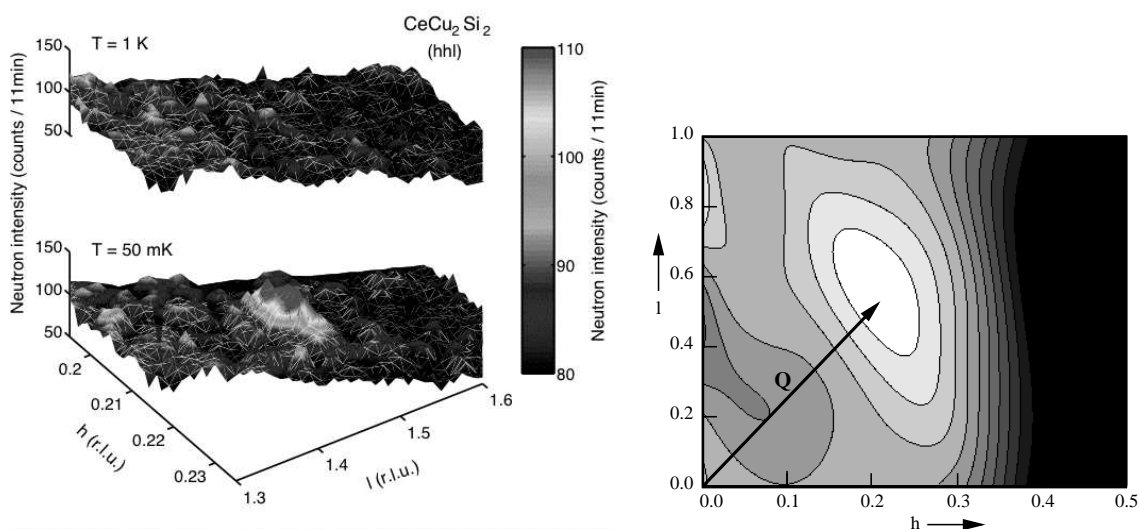


Figure 20. Left panel: Neutron diffraction intensity in CeCu_2Si_2 at temperatures above and below the A-phase transition temperature T_A . Incommensurate peak is at $\mathbf{Q} = (0.22, 0.22, 0.55)$ (Stockert et al. 2003). Right panel: Nesting of heavy FS columns (fig. 18) leads to a peak in the static susceptibility $\chi(\mathbf{q})$ at $\mathbf{q} = \mathbf{Q}$. The intensity map of $\chi(\mathbf{q})$ (value increasing from dark to bright) in the reciprocal (h, h, l) -plane as calculated for the renormalized bands at $T = 100$ mK. The *experimental* \mathbf{Q} at 50 mK from the left panel shows perfect agreement with the calculated maximum position of $\chi(\mathbf{q})$.

Recent neutron scattering experiments (Stockert et al. 2003) (fig. 20) for the stoichiometric compound ($x=0$) show a spin density wave which forms below $T_N \simeq 0.7$ K. The experimental propagation vector \mathbf{Q} is close to $(0.22, 0.22, 0.55)$ and the ordered moment

amounts to $\mu \simeq 0.1\mu_B$. The instability of the Fermi liquid state with respect to the SDW state follows from the nesting properties of the heavy quasiparticle surface shown in fig. 18 which leads to peaks at $\mathbf{q} = \mathbf{Q}$ in the static susceptibility $\chi(\mathbf{q})$ with \mathbf{Q} close to the above experimental value (fig 20).

3.1.3. Pressure-induced superconductivity in CePd_2Si_2 and CeNi_2Ge_2

The compounds CeNi_2Ge_2 and CePd_2Si_2 offer the possibility for studies of the antiferromagnetic instability in a heavy-fermion system. In the vicinity of the quantum critical point, non-Fermi liquid behaviour and superconductivity are observed. At ambient pressure, CePd_2Si_2 orders in an antiferromagnetic structure below a Néel temperature $T_N \simeq 8.5$ K. The magnetic structure is characterized by a propagation vector $\mathbf{Q} = (1/2, 1/2, 0)$. The ordered moment lying in the basal plane is reduced to $\sim 0.66 \mu_B$ by CEF effects and possibly Kondo screening (van Dijk et al. 2000). The coefficient of the linear specific heat $\gamma \simeq 250$ mJ/mol K² and the quasielastic line width suggest a Kondo temperature $T^* \simeq 10$ K which is close to the Néel temperature T_N . The interplay between the Kondo effect and the RKKY interaction is reflected in the depression of T_N with increasing pressure. The antiferromagnetic order is suppressed by a critical pressure p_c between 28 and 29.5 kbar. There is a superconducting phase between 23 and 33 kbar with a maximum $T_c \simeq 290$ K close to p_c . This fact indicates that the appearance of superconductivity should be related to the magnetic instability (Demuer et al. 2001).

CeNi_2Ge_2 has a slightly smaller lattice constant than CePd_2Si_2 and exhibits non-Fermi liquid behavior at ambient pressure (Gegenwart et al. 1999). No phase transition is found down to lowest temperatures. However magnetic correlations appear gradually with decreasing temperature (Fak et al. 2000). They have a characteristic energy of 4 meV and an incommensurate wave vector $\mathbf{Q} = (0.23, 0.23, 0.5)$ which is rather similar to the ordering vector in CeCu_2Ge_2 . They also exhibit quasi-two dimensional character with strong correlations between moments in the [110] planes. The electronic structure was recently studied by angle-resolved photoemission (Ehm et al. 2001). The low-temperature data ($T \simeq 20$ K) exhibit strongly dispersing bands in agreement with LDA band structure calculations. Close to the Fermi level two features with high spectral intensity can be distinguished one of which has predominantly Ni-3d character. The other one can be assigned to a non-dispersive Kondo resonance. These findings indicate that CeNi_2Ge_2 is in the intermediate temperature regime below the single-site Kondo temperature T^* and above the coherence temperature where extended heavy band states form. The magnetic moments of the Ce ions are already screened by the Kondo effect as indicated by the f-spectral weight at the Fermi level. The coherence between the sites in the periodic lattice, on the other hand, is not yet fully developed.

Traces of possible superconductivity at ambient pressure have been found in resistivity measurements (Steglich et al. 1997, Gegenwart et al. 1999, Grosche et al. 2000). The preliminary phase diagram (Braithwaite et al. 2000) shows that the transition temperature T_c goes through a maximum around 30 kbar and vanishes above 65 kbar. The upper critical field data $H_{c2}(T)$ of the system under pressure are analyzed by comparing them with calculated curves assuming weak coupling in the clean limit. The analysis reveals two interesting points. First, the values of H_{c2} at low temperatures considerably exceed the Pauli limit which indicates the possibility of triplet pairing. Second, the initial slope

$\left(-\frac{dH_c2}{dT}\right)_{T=T_c}$ exhibits only a weak decrease in the range between 0 kbar and 23 kbar which is much weaker than the change expected from the variation of the specific heat.

3.2. CeMIn₅

The compounds CeMIn₅ (M=Co,Ir,Rh) are a newly reported family of heavy fermion systems (Hegger et al. 2000, Petrovic et al. 2001) which exhibit a superconducting transition at comparatively high temperatures. The values of the critical temperatures reach $T_c = 2.3$ K in CeCoIn₅ (Petrovic et al. 2001a). We mention that the isostructural compound PuCoGa₅ is the first Pu-based superconductor with $T_c = 18.5$ K (Sarrao et al. 2003). The discovery of this new class of heavy-fermion compounds has opened a way to systematically investigate the evolution from the antiferromagnetic to superconducting state as a function of pressure.

The structurally layered compounds CeMIn₅ crystallize in the tetragonal HoCoGa₅-structure (Grin' et al. 1979) which is displayed in fig. 21. They belong to the broader family of materials Ce_nM_mIn_{3n+2m} which can be considered as built from 'CeIn₃' and 'MIn₂' layers stacked along the tetragonal c-axis. The infinite-layer parent CeIn₃ crystallizes in the cubic AuCu₃ structure. The layering introduces pronounced anisotropies in the electronic and structural properties which, in turn, influence the magnetic and superconducting properties as well as the behavior in the quantum critical regime. Varying the stacking sequence, i. e. , the parameters n and m, allows for a study of the general role on dimensionality in the competition between the various ground states.

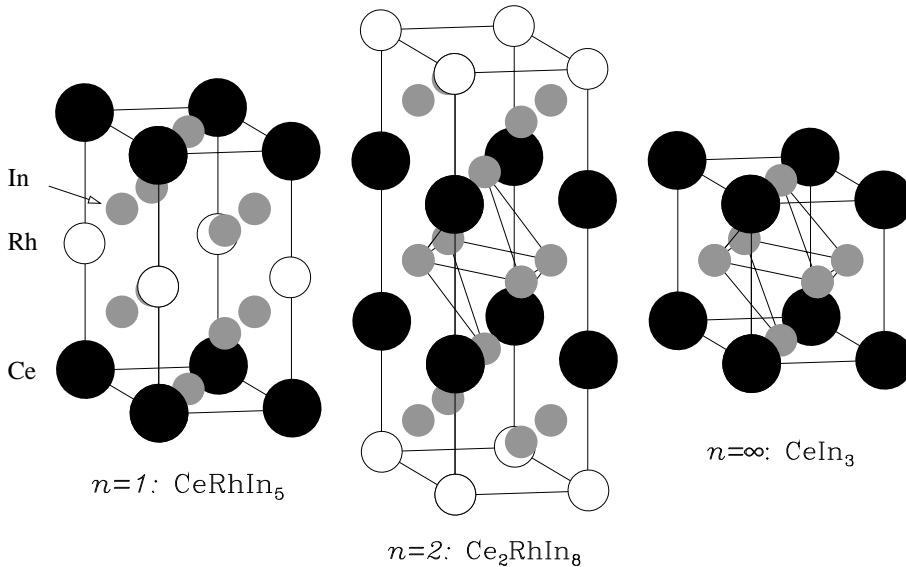


Figure 21. Unit cell of typical Ce_nM_mIn_{3n+2m} (here for M = Rh) compounds which are built from n 'CeIn₃' and m 'MIn₂' subunits stacked along the tetragonal axis. CeCoIn₅ has n = 1.

The subsequent section is mainly devoted to the properties of the n = m = 1 materials commonly referred to as single-layer systems. We begin, however, by briefly summarizing the properties of the infinite-layer parent CeIn₃. At ambient pressure it orders antiferromagnetically at $T_N \simeq 10$ K with an ordering vector $\mathbf{Q} = (0.5, 0.5, 0.5)$ (Morin et al. 1988)

and an ordered moment of $0.4\mu_B$. The magnetic ordering temperature decreases monotonically with pressure. In a narrow range around a critical pressure $p_c = 2.6$ GPa resistivity vanishes below the onset temperature at 0.2 K. Recent measurements of T_1^{-1} and the ac-susceptibilities (Kawasaki et al. 2002) confirm the bulk character of superconductivity. The results, however, yield a much lower value $T_c = 95$ mK than the onset temperature. The absence of the coherence peak is taken as evidence of an unconventional pair state.

The single-layer ($n=1$) members with $M = \text{Rh, Ir, Co}$ and the bilayer ($n=2$) member with $M = \text{Rh}$ can be considered as pressure variants of the parent CeIn_3 . This is suggested by the lattice constants of CeIn_3 ($a = 4.689$ Å), CeRhIn_5 ($a = 4.652$ Å, $c = 7.542$ Å), CeIrIn_5 ($a = 4.668$ Å, $c = 7.515$ Å), CeCoIn_5 ($a = 4.62$ Å, $c = 7.56$ Å) and Ce_2RhIn_8 ($a = 4.665$ Å, $c = 12.244$ Å). Like the parent, the compounds CeRhIn_5 and Ce_2RhIn_8 order antiferromagnetically at ambient pressure and become pressure-induced superconductors. The magnetic ordering temperatures T_N , however, are reduced while the superconducting transition temperatures T_c are an order of magnitude higher than the maximum value found in CeIn_3 . CeIrIn_5 ($T_c = 0.4$ K) and CeCoIn_5 ($T_c = 2.3$ K) become superconducting at ambient pressure.

Structure data as well as pressure studies indicate that superconductivity in CeMIn_5 occurs close to a quantum critical point (QCP). The lattice parameters suggest that the antiferromagnetic compound CeRhIn_5 and the superconductor CeCoIn_5 fall on different sides of the QCP in the Doniach phase diagram.

Finally we want to add two comments. The layered crystal structure of the materials seems to suggest that the compounds may be approximately described as 2-dimensional systems. However, this is not justified in view of magnetic properties. Neutron scattering data on CeRhIn_5 and Ce_2RhIn_8 have shown that these materials are magnetically 3-dimensional despite their layered structure. The Fermi surface topologies of the alloys $\text{Ce}_x\text{La}_{1-x}\text{RhIn}_5$ (Alver et al. 2001) are found to be nearly independent of the composition parameter x .

3.2.1. Electronic properties and Fermi surfaces

The electronic properties of the CeMIn_5 compounds have been studied theoretically by band structure calculations based on the LDA. Of particular interest are the Fermi surfaces which can be directly compared with experimental dHvA data. The central result is the confirmation of the qualitative picture that Ce 4f-degrees of freedom should be considered as localized moments in CeRhIn_5 (at ambient pressure) while a description in terms of itinerant, strongly renormalized fermions is more appropriate in CeIrIn_5 and CeCoIn_5 . The conclusions are based on the following findings by Shishido et al. (2002) and references therein: For the reference compound LaRhIn_5 without f electrons the Fermi surface as well as the effective masses of the quasiparticles are well described by the LDA band structure. The quasi-two-dimensional character reflects the tetragonal lattice structure. The topology of the main Fermi surfaces is also in good agreement with that of the Ce-counterpart CeRhIn_5 indicating the localized nature of the Ce-4f electron in this system. A detailed quantitative comparison between calculated and measured cross-sections, however, is difficult due to the complicated antiferromagnetic structure. Angle-resolved photoemission experiments (Fujimori et al. 2003) performed at 15 K showed rather small 4f weight close to E_F . The presence of the localized 4f-states in CeRhIn_5 is

reflected in the rather large quasiparticle masses m^* which are enhanced by a factor 7-9 over those of LaRhIn_5 . The Fermi surfaces of LaRhIn_5 and the localised 4f-compound CeRhIn_5 are highly different from those of the HF systems CeIrIn_5 and CeCoIn_5 which are reasonably well explained by the itinerant 4f-band model.

Let us now turn to the properties of the 4f-electrons in the local moment regime. In the tetragonal CEF the degeneracy of the 4f $j=5/2$ state is lifted. The level scheme has been determined using susceptibility and thermal expansion coefficient data for CeRhIn_5 , CeIrIn_5 and CeCoIn_5 (Takeuchi et al. 2001, Shishido et al. 2002). In all three compounds, the CEF ground state has predominantly $j_z = \pm 5/2$ - character while the first and second excited states are mainly derived from $j_z = \pm 3/2$ - and $j_z = \pm 1/2$ - states. However the CEF level schemes differ with respect to their excitation energies. In the Rh and Ir systems, the $j = 5/2$ - manifold is split into three Kramers doublets with the excitation energies $E(\pm \frac{3}{2}) \sim 60$ K and $E(\pm \frac{1}{2}) \sim 300$ K whereas these excited states are (almost) degenerate in the Co-compound separated by ~ 150 K from the ground state.

Finally, we mention angle-resolved photoemission studies of CeRhIn_5 and CeIrIn_5 (Fujimori et al. 2003, Fujimori et al. 2002a). The spectral contributions from the ligand states, i.e., from the Rh, Ir and In states, agree rather well with the results of LDA band structure calculations. However, no feature originating from the Ce 4f-states is observed near the Fermi level. This fact may have an explanation within the Kondo scenario: The experiments were carried out at $T = 14$ K which is already equal to the estimated Kondo temperature of CeIrIn_5 given by $T^* \simeq 15$ K.

3.2.2. Unconventional superconductivity in CeCoIn_5

CeCoIn_5 appears to be a typical heavy-fermion material. The effective magnetic moment of $\sim 2.59\mu_B$ as determined at high temperatures ($T > 200$ K) from a polycrystalline average is consistent with the free-ion value for Ce^{3+} ($2.54\mu_B$). The $\rho(T)$ dependence is rather weak above a characteristic temperature $T^* \simeq 30$ K. The crossover to a coherent state is reflected in a rapid decrease at lower temperatures. The electronic contribution to the low-temperature specific heat in the normal state ($T > 2.3$ K) varies linearly $C \sim \gamma T$ with a large coefficient $\gamma \sim 350$ mJ/molK² indicating substantial mass renormalization (Petrovic et al. 2001). The normal Fermi liquid becomes unstable at $T_c = 2.3$ K where the heavy quasiparticles form Cooper pairs. This can be seen from the discontinuity in the specific heat with $\Delta C(T_c)/\gamma T_c \simeq 5$ as shown in fig. 22. The enhancement over the universal BCS values for isotropic SC points to pronounced strong coupling effects. The BCS value of 1.43 for isotropic superconductors should be considered as an upper bound on weak-coupling theory which is reduced for anisotropic pair states as obvious from table 1.

The superconducting state seems to be of unconventional $d_{x^2-y^2}$ singlet type. The presence of line nodes is inferred from the power-law behavior exhibited by various thermodynamic and transport properties at low temperatures. The latter include the specific heat (Petrovic et al. 2002, Hegger et al. 2000) and NMR relaxation rate (Kohori et al. 2001, Zheng et al. 2001). The most direct evidence, however, is provided by thermal conductivity measurements in a magnetic field rotating within the a-b plane (Izawa et al. 2001, Matsuda and Izawa 2003) (fig. 13). In addition, the observation of a zero-bias conductance anomaly in point-contact spectroscopy supports the hypothesis of an

unconventional pair state (Goll et al. 2003). This is also suggested by the Knight shift measurements of Kohori et al. (2001) which give support for an even singlet SC order parameter with line nodes such as the $d_{x^2-y^2}$ gap function deduced from the above thermal conductivity results.

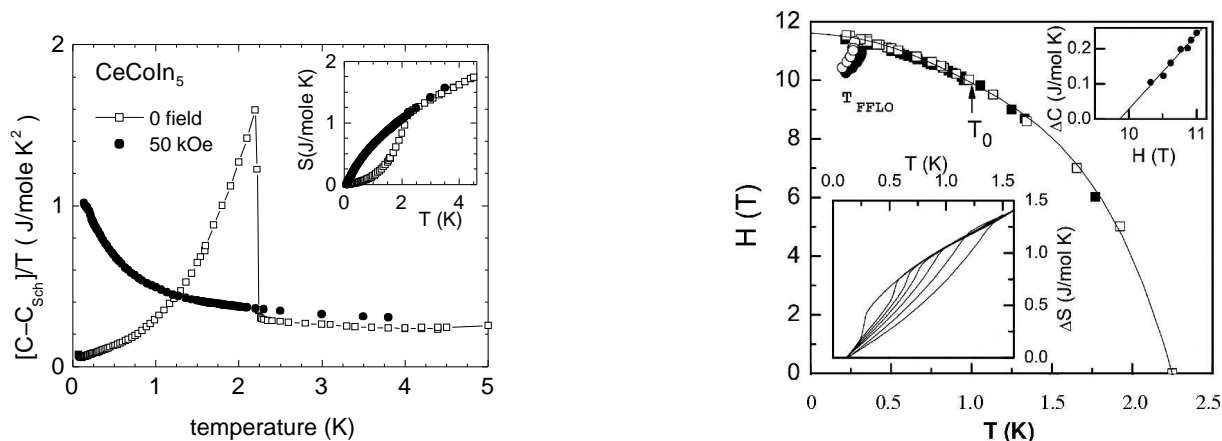


Figure 22. Left panel: Linear specific heat coefficient of CeCoIn_5 vs temperature, for zero field anomalous nFI behaviour is observed. $\Delta C(T_c)/\gamma T_c \simeq 5$ is strongly enhanced over the isotropic BCS value 1.43. Inset shows corresponding entropies. Right panel: H_{c2} curve from specific heat data. At $T_0 \simeq 1.1$ K the transition changes from second to first order. lower inset shows entropy gain as function of T starting from 0.13 K, for increasing field (right to left: 8.6 T - 11.4 T) a step is evolving. Upper inset shows specific heat jump at the transition line T_{FFLO} to the Fulde-Ferrell-Larkin-Ovchinnikov state (Bianchi et al. 2003).

The properties of this unconventional superconductor are of great interest. A first issue is the sensitivity to nonmagnetic impurities which are expected to act as strong pairbreakers. Substitution of Ce-ions with La-ions results in a depression of the transition temperature T_c (Petrovic et al. 2002). However the measured T_c -reduction is weaker than the value expected for isotropic (s-wave) scatterers in a $d_{x^2-y^2}$ -state. This suggests that La-substitution introduces anisotropic scattering. Anisotropies in the scattering matrix element may strongly reduce pairbreaking as compared with pure s-wave scattering (Fulde and Zwicknagl 1990, Fulde et al. 1988). The upper critical field H_{c2} is simply reduced by the impurities while its anisotropy remains unaltered.

A magnetic field can suppress superconductivity by acting on the orbits of the charged quasiparticles and by acting on their spins. Both mechanisms determine the upper critical magnetic field $H_{c2}(T)$ which separates the normal state for $H > H_{c2}(T)$ from the superconducting vortex phase at $H < H_{c2}(T)$. The relative importance of the two depairing effects determines the order of the phase transition in a type-II superconductor. While the omnipresent and usually dominating orbital pairbreaking is associated with a second order phase transition, a first order transition is anticipated for dominant spin depairing.

In superconductors with sufficiently weak orbital pairbreaking a change from second order at $T_0 < T \leq T_c$ to first order at $T < T_0$ should be observed (for a review see Saint-James et al. (1969)). The crossover, however, was not observed in conventional superconductors due to the presence of strong spin-orbit scattering. CeCoIn₅ appears to be an ideal candidate for the observation of the first order phase transition in a magnetic field. Firstly, it is a very clean type-II superconductor where the orbital pairbreaking is rather weak due to the high effective mass of the quasiparticles. Secondly, the magnetic susceptibility is enhanced which further lowers the Chandrasekhar-Clogston field. The first order phase transition at T_0 shown in the phase diagram of fig. 22 was originally inferred from a step in thermal conductivity by Izawa et al. (2001). It is reflected in a pronounced sharpening of both the specific heat and thermal expansion, a large magnetoelastic effect and a steplike change in the sample volume (Bianchi et al. 2002).

The change from the second-order nature of the transition observed at zero and low magnetic field to first order at high fields occurs at $T_0 \simeq 1.1 \text{ K} = 0.48 T_c$. This value should be compared with the estimate of $0.33 T_c$ deduced from the Chandrasekhar-Clogston field of a d-wave order parameter and the orbital critical field obtained from extrapolating the behavior close to the zero-field transition to low temperatures.

The structure of the flux line lattice which forms at low temperatures in the presence of an external magnetic field is of particular interest. A comprehensive review of this topic for s-wave superconductors has been given by Brandt (1995). An ideal isotropic type-II superconductor favors the hexagonal flux lattice. However, as the energy gain with respect to the square lattice is only 2%, relatively weak perturbations like FS or gap anisotropies may lead to distorted hexagonal or even square vortex lattices. CeCoIn₅ is a clean type-II superconductor for which one anticipates a rather complex variation with magnetic field of the flux line lattice. Recent small-angle neutron scattering experiments (Eskildsen et al. 2003) have imaged the vortex lattice of CeCoIn₅. At low fields, a hexagonal lattice is observed. The latter undergoes a “phase transition” to a square lattice when the field is increased. The orientation of the square flux line lattice relative to the crystal lattice is consistent with the expectations for the suggested d-wave order parameter. The square lattice for d-wave superconductors has been predicted theoretically by Won and Maki (1995) and Berlinsky et al. (1995). Finally at low temperatures and close to H_{c2} specific heat measurements (Bianchi et al. 2003) seem to indicate the presence of another inhomogeneous phase for both a- and c-field directions which was interpreted as the long-sought Fulde-Ferrell-Larkin-Ovchinnikov (FFLO) phase which is characterised by Cooper pairs with finite net momentum. The FFLO phase for d-wave SC order parameter of CeCoIn₅ was studied theoretically in Won et al. (2003a).

3.3. Superconductivity close to a quantum critical point

The symmetry and mechanism of SC in the CeMIn₅ compounds have not yet been identified in any comprehensive way. However there are strong indications of unconventional order parameters. The interest in the SC of these compounds results from the observation that under pressure and chemical substitution the SC pair correlations develop in the vicinity of a QCP. Recently a few U-compounds have been found which fall also in this class. Theories to describe SC at the QCP are at present highly controversial and will be discussed there to some extent (sect. 4.3).

Here we shall briefly focus on the genuine QCP phenomenon in Ce-systems and its theoretical description. The compounds under consideration have a tendency to AF order. Two different scenarios are discussed for the transition from the HF state to a phase with long-range magnetic order.

The first approach views the magnetic order as itinerant magnetism of the heavy quasi-particle system. The theory starts on the Fermi liquid side which is characterized by a large Fermi surface including the f-degrees of freedom. The low-energy excitations are fermionic quasiparticles and their collective excitations. Close to the QCP, the static susceptibility is assumed to diverge at a specific wave vector \mathbf{Q} which signifies the transition to a spin density wave state. The quasiparticles are strongly scattered by spin fluctuations along "hot lines" which are connected by \mathbf{Q} . This scattering modifies the low-temperature thermodynamic and transport properties which exhibit anomalous scaling relations close to QCP. They differ from those of the familiar Fermi liquid and therefore are at the focus of experimental interest. The theoretical derivation of the QCP scaling relations proceeds in close analogy to the spin-fluctuation theory of ferromagnetism (Moriya 1985) starting from the self consistent RPA expression for the magnetic susceptibility of the heavy Fermi liquid (Moriya and Takimoto 1995). The theory was recast in the renormalization group language (Hertz 1976, Millis 1993). The ansatz yields scaling relations for the specific heat, the susceptibility, and the Wilson ratio which differ from the well-known Fermi liquid results (Continentino 2001, Sachdev 1999). The scaling behavior obtained for various different models and many non-Fermi liquid compounds are summarized in Stewart (2001). The anomalous transport properties exhibited by metals near antiferromagnetic quantum phase transitions are of particular interest in the experimental study of Ce-based heavy fermion systems. The theory (Rosch 1999) exploits the fact that in the vicinity of the magnetic instability the magnetic susceptibility reduces to the simple form

$$\chi^{-1}(\mathbf{q}, \omega) \simeq \frac{1}{(q_0\xi)^2} + \omega_{\mathbf{q}} - \frac{i\omega}{\Gamma} \quad (58)$$

with

$$\frac{1}{(q_0\xi)^2} \simeq r + c \left(\frac{T}{\Gamma}\right)^{3/2} \quad \text{and} \quad \omega_{\mathbf{q}} \simeq \frac{1}{q_0^2} (\mathbf{q} - \mathbf{Q})^2 \quad (59)$$

Here r measures the (almost T-independent) distance from the quantum critical point, Γ denotes the characteristic energy scale of the fluctuations and c is a constant. The frequency $\omega_{\mathbf{q}}$ vanishes at the ordering vector \mathbf{Q} of the antiferromagnetic structure. In the dirty limit the variation with temperature of the resistivity

$$\rho(T) = \rho(0) + \Delta\rho(T) \quad \text{with} \quad \Delta\rho(T) \sim T^{3/2} \quad (60)$$

In the clean limit, on the other hand, the transport is dominated by the carriers with the longest life times, i. e. , by the quasiparticles far away from the ‘hot’ regions on the Fermi surface yielding $\rho(T) \sim T^2$. Eq. (60) is valid only at very low temperatures $T/\Gamma < 1/\hat{\rho}_0$ where $\hat{\rho}_0$ denotes the residual resistivity ratio $\hat{\rho}_0 = \rho(0)/\rho(273K)$. At intermediate temperatures $1/\hat{\rho}_0 < T/\Gamma < 1/\sqrt{\hat{\rho}_0}$ the resistivity rises linearly with temperature

$$\Delta\rho(T) \sim T\sqrt{\rho} \quad (61)$$

The important feature of the weak-coupling picture as described above is that Γ , which is related to the characteristic energy of the Fermi liquid phase still plays the role of the scaling energy. This fact is not surprising since only parts of the Fermi surface contribute to the anomalous properties. One should note however that this theory is not fully self consistent because the AF fluctuation wave vector is not connected with any FS feature since the latter is assumed as spherical.

The loss of the energy scale Γ is a characteristic feature of an alternative scenario which emphasizes the role of local correlations in quantum critical behavior (Si et al. 1999, Si et al. 2001, Coleman 1999). The dynamical competition between the Kondo and RKKY interactions is analyzed by an extension (Smith and Si 2000, Chitra and Kotliar 2000) of the dynamical mean-field theory (see (Georges et al. 1996) and references therein). The resulting momentum-dependent susceptibility has the general form

$$\chi^{-1}(\mathbf{q}, \omega) = M(\omega) + J(\mathbf{q}) \quad (62)$$

where the spin self energy $M(\omega)$ is calculated from the effective impurity problem. A zero-temperature phase transition will occur when $\chi(\mathbf{q}, \omega = 0)$ diverges. Anomalous behavior is expected whenever the (effective) local dynamics has an anomalous frequency dependence. Different scenarios are discussed in Si (2001). We finally mention that the compound YbRh_2Si_2 (where Yb has one f-hole instead of one f-electron as in Ce) has been identified as one of the most promising and cleanest QCP systems where these theoretical models can be tested (Custers et al. 2003)

4. U-based heavy-fermion superconductors

Heavy Fermion superconductivity is found more frequently in intermetallic U-compounds than in Ce-compounds. This may be related to the different nature of heavy quasiparticles in U-compounds where the 5f-electrons have a considerable, though orbitally dependent, degree of delocalisation. The genuine Kondo mechanism is not appropriate for heavy quasiparticle formation as in Ce-compounds. This may lead to more pronounced delocalised spin fluctuations in U-compounds which mediate unconventional Cooper pair formation as discussed in sect. 2. The AF quantum critical point scenario invoked for Ce compounds previously also does not seem to be so important for U-compounds with the possible exception of UGe_2 . On the other hand AF order, mostly with small moments of the order $10^{-2}\mu_B$ is frequently found to envelop and coexist with the SC phase in the B-T plane.

A common trait of U-compounds is the varying degree of localisation of 5f-electrons. It has recently become clear that Fermi surface properties of e.g. UPt_3 (Zwicknagl et al. 2002) and UPd_2Al_3 (Zwicknagl et al. 2003) can be well described by treating two of the three 5f-electrons as localised in orbitals of specific symmetry and small CEF splitting of the order of meV. This approach also leads to a natural mechanism for the formation of heavy quasiparticles via the scattering of delocalised 5f-electrons by the internal CEF excitations of their localised 5f-electrons. This type of ‘dual model’ seems much closer to the truth than either a purely delocalised LDA type description which fails to explain the large masses or Kondo lattice models with fully localised 5f-states whose associated Kondo type anomalies above the Kondo temperature in transport and thermodynamics are not present in U-compounds.

In the following we will discuss to some length a number of prominent examples of U-compounds which have extensively been investigated experimentally and partly theoretically, mostly in the context of phenomenological Ginzburg-Landau (GL) theories or BCS type theories with magnetic effective pairing interactions. One is however far from being able to predict the spin state (parity) or even symmetry type of the gap function. Simple models of AF spin fluctuations would predict singlet even parity gap functions but well characterised examples of triplet odd parity U-superconductors exist.

Indeed the hexagonal compound UPt_3 (Stewart et al. 1984) exhibits triplet pairing and it sticks out as the most interesting case of unconventional SC with a multicomponent order parameter whose degeneracy is lifted by a symmetry breaking field due to the small moment AF order. On the other hand in UPd_2Al_3 (Geibel et al. 1991a) SC coexists with large moment AF and probably spin singlet pairing is realised, it also exhibits a new kind of magnetic pairing mechanism mediated by propagating magnetic exciton modes. The sister compound UNi_2Al_3 (Geibel et al. 1991) is an example of coexistence of large moment AF with a SC triplet order parameter. In URu_2Si_2 (Palstra et al. 1985) the SC order parameter symmetry is still undetermined. The interest in this compound is focused more on the enveloping phase with a ‘hidden’ order parameter presumably of quadrupolar type or an ‘unconventional’ SDW. The oldest cubic U-HF superconductor UBe_{13} (Ott et al. 1983) and its thorium alloy $\text{U}_{1-x}\text{Th}_x\text{Be}_{13}$ is also the most mysterious one. While for the pure system there is a single SC phase of yet unknown symmetry, in the small Th concentration range two distinct phases exist which may either correspond

to two different SC order parameters or may be related to a coexistence of SC with a SDW phase. In addition in UBe_{13} SC order appears in a state with clear non-Fermi liquid type anomalies. More recently the coexistence of ferromagnetism and SC in UGe_2 (Saxena et al. 2000) has been found. This is the only case of U-compounds where quantum critical fluctuations might be involved in the SC pair formation. Due to the FM polarisation the triplet gap function contains only equal spin pairing.

4.1. Heavy fermion multicomponent superconductor UPt₃

The intermetallic compound UPt₃ which crystallizes in the hexagonal Ni₃Sn structure is regarded as the archetype of a strongly correlated Fermi liquid. The existence of heavy quasiparticles is inferred from enhanced thermodynamic and transport coefficients, for example $\gamma \sim 420 \text{ mJ}/(\text{molU K}^2)$ (Frings et al. 1983) and anisotropic Pauli-like susceptibility $\chi_c \sim 50 \cdot 10^{-9} \text{ m}^3/(\text{molU})$ and $\chi_{a,b} \sim 100 \cdot 10^{-9} \text{ m}^3/(\text{molU})$ (Frings et al. 1983, Stewart et al. 1984). In addition, the resistivity rises quadratically with temperature with a T^2 -coefficient $A \simeq 0.49 \mu\Omega/(\text{cm K}^2)$ (Taillefer and Lonzarich 1988). The formation of the coherent heavy Fermi liquid state is clearly seen in the optical conductivity (Marabelli et al. 1987, Degiorgi 1999, Dressel et al. 2002) and in the dynamical magnetic susceptibility as measured by neutron scattering (Bernhoeft and Lonzarich 1995). Direct evidence for the existence of heavy quasiparticles comes from the observation of quantum oscillations (Taillefer et al. 1987, Taillefer and Lonzarich 1988, McMullen et al. 2001, Kimura et al. 1998) where Fermi surfaces and effective masses up to $m^* = 135 m$ were determined. The average dHvA mass enhancement $m^*/m_b \simeq 20$ compared to the band mass m_b is found to be consistent with the specific heat enhancement $\gamma_{exp}/\gamma_{calc} = 17$ (Norman et al. 1988). These results prove convincingly that UPt₃ in its normal state is a heavy Fermi liquid.

The normal Fermi liquid state becomes unstable at low temperatures. At $T_N \simeq 5.8$ K an antiferromagnetic phase with extremely small ordered moments $\mu \simeq 0.035 \mu_B/\text{U}$ develops (Heffner et al. 1989, Hayden et al. 1992, Lussier et al. 1996). The most exciting phenomena are associated with the superconducting state. The existence of two clearly distinct transition temperatures $T_{c1} = 530$ mK and $T_{c2} = 480$ mK (Fisher et al. 1989, Brison et al. 1994) implies that the superconducting phases are characterized by a multicomponent order parameter. The discontinuities in the specific heat at the superconducting transitions show that the Cooper pairs are formed by the heavy quasiparticles of the normal heavy Fermi liquid state.

From this we conclude that a quantitative theory for the origin of the heavy quasiparticles in UPt₃ is a prerequisite for a detailed understanding of the fascinating low-temperature properties of this compound.

4.1.1. Dual model and heavy quasiparticles

Although a comprehensive picture of the low temperature ordered phases of UPt₃ has emerged, a complete theoretical understanding of the origin of 5f-derived heavy quasiparticles is still missing. The number of itinerant U 5f electrons as well as the microscopic mechanism yielding the high effective masses are still controversial. It has been considered a success of the LDA that de Haas van Alphen (dHvA) frequencies can be related to the areas of extremal orbits on the Fermi surface obtained by band-structure calculation which treats the U 5f states as itinerant (Albers et al. 1986, Norman et al. 1988). From these findings, however, one should not conclude that the U 5f states are ordinary weakly correlated band states. The calculated energy bands are much too broad for explaining the effective masses while on the other hand, they are too narrow to fit the photoemission data (Allen 1992).

The key feature is likely the dual nature of the U 5f states, i. e., the presence of both localized and delocalized U 5f electrons. The theoretical investigation proceeds in

three steps. Firstly, band-structure calculations have been performed starting from the self-consistent LDA potentials but excluding the U $5f$ $j=\frac{5}{2}$, $j_z=\pm\frac{5}{2}$ and $j_z=\pm\frac{1}{2}$ states from forming bands. The localized $5f$ orbitals are accounted for in the self-consistent density and likewise in the potential seen by the conduction electrons. The $5f$ bands are calculated by solving the Dirac equation (Albers et al. 1986). The intrinsic bandwidth of the itinerant U $5f$ $j=\frac{5}{2}$, $j_z=\pm\frac{3}{2}$ is taken from the LDA calculation while the position of the corresponding band center is chosen such that the density distribution of the conduction states as obtained within LDA remains unchanged. The resulting position of the f band relative to the calculated Pt d states is consistent with photoemission data. It was found that the U $5f$ bands with $j_z = \pm\frac{3}{2}$ hybridize strongly near the Fermi level so that the f occupancy per U atom for the delocalized $5f$ electrons amounts to $n_f = 0.65$ indicating that we are dealing with a mixed valent situation. The theoretical Fermi surface shown in fig. 23 is formed by two bands which are doubly degenerate and which are derived from the $5f$ $|j = \frac{5}{2}, j_z = \pm\frac{3}{2}\rangle$ states. The thermodynamically most important orbit is assigned to the Γ -centered strongly anisotropic electron surface shown in the left part of fig. 23. The A-centered part of the Fermi surface shown in the right part of fig. 23 has open orbits spanning the entire Brillouin zone for magnetic fields oriented along the a -direction in the basal plane. This feature is consistent with magnetoresistance measurements (McMullen et al. 2001). Now we turn to the discussion of the localized U $5f$ states. The multiplet

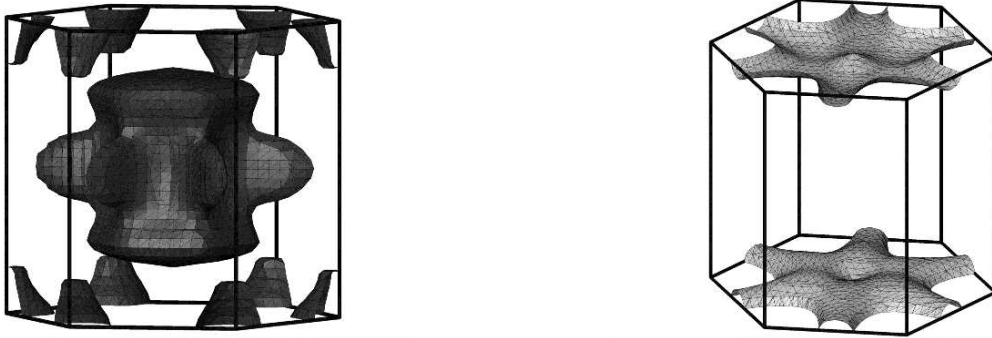


Figure 23. UPt_3 : FS of heavy quasiparticles as calculated within the dual model (Zwicknagl et al. 2002). One of the U $5f$ -electrons ($j = 5/2$, $j_z = 3/2$) is treated as itinerant and is included in the FS while the remaining two are localized. Then two bands contribute to the FS. Left: Γ -centered heavy electron sheet which dominates γ . Right: A-centered open orbit sheet consistent with magnetoresistance results (Mc Mullen et al. 2001).

structure of the localized f^2 states is calculated by diagonalizing the Coulomb matrix. The spin-orbit splitting is rather large and therefore a jj -coupling scheme is used. This simplification gives six 2-particle states built from $|j = \frac{5}{2}, j_z = \pm\frac{5}{2}\rangle$ and $|j = \frac{5}{2}, j_z = \pm\frac{1}{2}\rangle$. The resulting eigenstates are generally no longer eigenstates of the total angular momentum \mathbf{J}^2 , but remain eigenstates of J_z . The Coulomb matrix elements are calculated following Condon and Shortley (1957). Inputs are the Slater-Condon parameters F^K

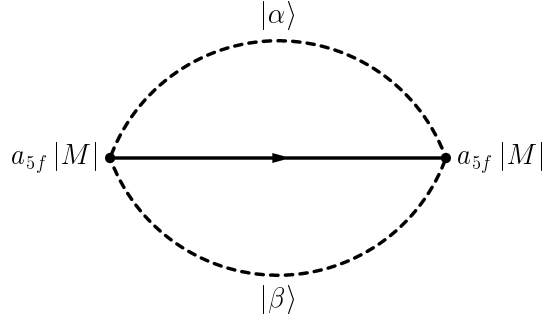


Figure 24. Self energy due to virtual CEF excitations $|\alpha\rangle \leftrightarrow |\beta\rangle$ leading to the enhanced m^* . Full line and dashed bubble represent conduction electron propagator and local $5f$ susceptibility of eq. (66), respectively. The self consistent solution of eq. (65) yields the leading order in an expansion in terms of the small ratio δ/W^* (δ = CEF-splitting, W^* = effective conduction band width). Input parameters: matrix element $\alpha_{5f}|M|$, DOS $N(E)$ and (effective) CEF splitting δ . The former two are determined from first principles calculations while δ is taken from experiment.

(Coulomb integrals) and G^K (exchange integrals) which are evaluated with the radial function $R_{f, \frac{5}{2}}^U(r)$ for U which is determined from a self-consistent band structure potential. Diagonalization of the matrix yields a doubly degenerate ground state $J_z = \pm 3$ which must be an eigenstate of $J = 4$. Note that the Pauli principle permits even values of J only, i.e., $J = 0, 2, 4$ in our case. The states $|j = \frac{5}{2}, j_z = \frac{5}{2}; J = 4, J_z = \pm 3\rangle$ have an overlap of 0.865 with the Hund's rule ground state 3H_4 derived from the LS-coupling scheme. Therefore the choice of jj vs. LS coupling should only weakly affect the results obtained for the ground-state multiplet. The two-fold degeneracy of the ground-state is lifted by a CEF yielding the two singlet states

$$\begin{aligned}
 |\Gamma_3\rangle &= \frac{1}{\sqrt{2}}(|J = 4; J_z = 3\rangle + |J = 4; J_z = -3\rangle) \\
 |\Gamma_4\rangle &= \frac{1}{\sqrt{2}}(|J = 4; J_z = 3\rangle - |J = 4; J_z = -3\rangle).
 \end{aligned} \tag{63}$$

Note that $|\Gamma_4\rangle$ has also been suggested as ground state of UPd_2Al_3 (Grauel et al. 1992, Böhm et al. 1992). The excited eigenstates of the Coulomb matrix are neglected, they are assumed to be separated by a rather high excitation energy from the ground state. The coupling between the localized and delocalized f electrons is directly obtained from the expectation values of the Coulomb interaction H_C (eq. 2) in the $5f^3$ states yielding the transition matrix element

$$|M| = \left| \langle f^1; \frac{5}{2}, \frac{3}{2} | \otimes \langle \Gamma_4 | H_C | \Gamma_3 \rangle \otimes | f^1; \frac{5}{2}, \frac{3}{2} \rangle \right| = 0.19 \text{ eV}. \tag{64}$$

Finally, we determine the mass enhancement which arises from the scattering of the itinerant U $5f$ electrons due to virtual excitations of the localized f^2 subsystem. The

latter are characterized by a CEF splitting energy δ while the relevant energy scale for the ‘itinerant’ 5f states is set by the effective band width W^* . To leading order in the ratio δ/W^* the mass enhancement m^*/m is obtained from the fluctuation exchange (FLEX) contribution to the band self energy as shown in fig. 24 in close analogy to the case of Pr metals (White and Fulde 1981). This leads to an expression

$$\begin{aligned} \frac{m^*}{m_b} &= 1 - \left(\frac{\partial \Sigma}{\partial \omega}\right)_{\omega=0} \\ \Sigma(i\omega_n) &= a_{5f}^2 |M|^2 T \sum_{n'} \chi(i\omega_n - i\omega_{n'}) g(i\omega_{n'}) \end{aligned} \quad (65)$$

where ω_n are Matsubara frequencies, m_b is the LDA band mass and a_{5f} denotes the 5f weight of conduction electron states close to E_F . Furthermore the local 5f susceptibility and conduction electron propagator are given, respectively, by

$$\begin{aligned} \chi(i\omega_n - i\omega_{n'}) &= \tanh \frac{\delta}{2T} \frac{2\delta}{\delta^2 - (i\omega_n - i\omega_{n'})^2} \\ g(i\omega_n) &= \int dE \frac{N(E)}{i\omega_n - E - \Sigma(i\omega_n)} \end{aligned} \quad (66)$$

Here $2N(E)$ is the total electronic DOS obtained from the LDA bandstructure with two of the 5f electrons kept localised.

This calculation procedure leads to a good agreement of theoretical and observed quasi-particle masses (Zwicknagl et al. 2002) for the main Fermi surface sheets. The results are summarized in fig. 25 as well as in Table 4. If the dependence upon the wave vector \mathbf{k}

Table 4
Mass renormalisation in UPt_3 from dHvA experiments and dual model calculations for field along hexagonal symmetry directions.

m^*/m	c	a	b
Experiment	110	82	94
Theory	128	79	104

is neglected one obtains an isotropic enhancement of the effective mass m^* over the band mass m_b . The explicit evaluation requires as input parameters the density of states and the f-weight per spin and U-atom at the Fermi energy, $N(0)$ and $4a_{5f}^2$, respectively, as well as the average energy δ of CEF excitations. Solving for the selfconsistent conduction electron propagator with the input determined from the ab-initio calculations of the electronic structure ($N(0) \simeq 15.5$ states/ (eV cell), $|M|^2 = 0.036$ eV², $4a_{5f}^2 = 0.13$) and the estimate $\tilde{\delta} \simeq 20$ meV) we finally obtain the effective masses listed above.

The dual model and its partial 5f localisation scenario therefore provides for a satisfactory explanation for both the FS structure and mass renormalisation of the heavy quasiparticles observed in UPt_3 . The physical reason for the strongly orbital dependent effect of local electron correlations on the different LDA hybridization matrix elements has been investigated separately (sect. 2). Finally we want to point out that the prescribed

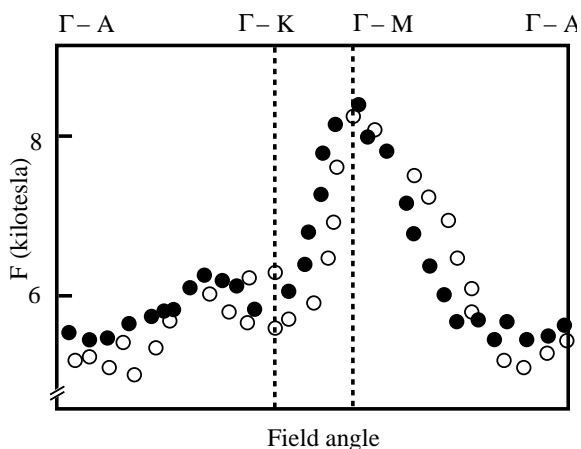


Figure 25. UPt_3 : dHvA cross sections of heavy quasiparticle FS (Γ -centered closed sheet in fig. (23) from experiment (filled symbols) (Kimura et al. 1998) and from dual model calculation (Zwicknagl et al. 2002) (empty symbols). Field direction is turned from c -direction (Γ -A) to a -direction (Γ -K) and then rotated in the basal plane from a -direction to b -direction (Γ -M) and finally turned back to c -direction. The calculated splitting for magnetic field orientations in the a - c -plane (Γ -A to Γ -K sector) is indeed observed in recent dHvA experiments (McMullen et al. 2001).

way of treating the $5f$ electrons in UPt_3 is also applicable to other uranium compounds, notably UPd_2Al_3 (sect. 4.2).

4.1.2. Pairing and the spin-orbit coupling problem

There is little doubt that UPt_3 is an unconventional superconductor with a multicomponent superconducting order parameter. Theoretical models which have been proposed are reviewed by Sauls (1994) and Joynt and Taillefer (2002) and will be discussed in the next section. Here we shall briefly comment on the issue of the importance of spin orbit coupling in the pairing scheme. In all theoretical treatments the superconducting phases of UPt_3 are characterized by BCS-type gap functions $\Delta_{s_1, s_2}(\hat{\mathbf{k}})$ which satisfies the anti-symmetry relation eq.(19). The wave vector $\mathbf{k} = k_F(\hat{\mathbf{k}})\hat{\mathbf{k}}$ is restricted to the Fermi surface since the coherence length ξ_0 is much larger than the interatomic distance or, equivalently, the Fermi wave length $\lambda_F = 2\pi/k_F$ satisfies

$$\xi_0 = \frac{\hbar v_F}{k_B T_c} \gg \lambda_F \quad . \quad (67)$$

As a consequence, the gap function $\Delta(\hat{\mathbf{k}})$ is a matrix function of $\hat{\mathbf{k}}$ only or its corresponding polar and azimuthal angles ϑ and φ . We have neglected indices for interband pairing because the available phase space is much smaller than in the case of intraband pairs.

The indices s_1, s_2 refer to the (pseudo-) spin labels of the quasiparticles. Due to the large spin-orbit interaction the quasiparticle states are no longer eigenstates of the spin. In the absence of an external magnetic field the states $|\mathbf{k}s\rangle$ and $|-\mathbf{k}-s\rangle$ show Kramers degeneracy. In UPt_3 , the crystal structure has inversion symmetry. This fact implies that

all four quasiparticle states $|\mathbf{k}s\rangle$, $|\mathbf{-k}s\rangle$, $|\mathbf{k}-s\rangle$ and $|\mathbf{-k}-s\rangle$ are degenerate. As a result, the superconducting order parameter can be decomposed into the contributions

$$\begin{aligned} \text{even-parity (pseudo-spin singlet, } S = 0) : \quad & \Delta_{s_1 s_2}(\mathbf{k}_F) = \Delta(\mathbf{k}_F) (i\sigma_y)_{s_1 s_2} \\ \text{odd-parity (pseudo-spin triplet, } S = 1) : \quad & \Delta_{s_1 s_2}(\mathbf{k}_F) = \Delta(\mathbf{k}_F) \cdot (i\sigma\sigma_y)_{s_1 s_2} \end{aligned} \quad (68)$$

Because the energy splitting of $j=\frac{5}{2}$ and $j=\frac{7}{2}$ states due to spin orbit coupling is larger than the bandwidth due to hybridisation and overlap (Albers et al. 1986) their mixing can be neglected. Consequently the pseudospin indices s_1, s_2 are good quantum numbers and effectively the classification of the gap function can proceed as for the weak spin orbit coupling case (sect. 2).

4.1.3. Multicomponent superconducting order parameter

The hexagonal heavy Fermion compound UPt_3 can justly be called the flagship of unconventional superconductivity, despite having a critical temperature less than one Kelvin. It is set aside from all other unconventional superconductors so far because it exhibits *two* superconducting phase transitions which have to be interpreted as a direct signature of the fact that the SC order parameter is a complex vector with more than one component. In all other unconventional superconductors, e.g. in high- T_c compounds the order parameter is still a complex scalar as in ordinary superconductors, albeit belonging to a nontrivial (but one-dimensional) representation of the symmetry group as witnessed by nodes in the anisotropic gap function. Only recently another example of a multicomponent superconductor, the Pr-skutterudite compound $\text{PrOs}_4\text{Sb}_{12}$ (sect. 6), may have been found. The exciting discovery of the split SC transitions in UPt_3 at $T_{c1} = 530$ mK and $T_{c2} = 480$ mK in specific heat measurements by (Fisher et al. 1989) has led to an enormous amount of experimental and theoretical work on UPt_3 whose historical evolution has been described in detail in a recent review by Joynt and Taillefer (2002). Therefore in the following discussion we shall restrict to the essential aspects of SC in UPt_3 . The additional small moment AF observed in UPt_3 ($T_N = 5.8$ K, $\mu = 0.035\mu_B$) plays a key role in the identification of the SC order parameter since the in-plane staggered magnetisation acts as a symmetry breaking field (SBF) to the SC multicomponent order parameter. The SBF is believed to be responsible for the appearance of two SC transitions which otherwise would merge into one, in fact this has later been proven by specific heat pressure experiments (Trappmann et al. 1991) on the SC $T_{c1,2}(p)$ and by complementary neutron diffraction under pressure (Hayden et al. 1992). Naturally there are also two critical-field curves. They intersect at a tetracritical point in the B-T plane that is present for all field directions. Therefore one can identify three distinct SC phases A,B,C in the B-T plane (fig. 29) corresponding to different choices of the orientation of the complex vector SC-order parameter. These phase boundaries have first been identified by ultrasound velocity measurements (Bruls et al. 1990) and have been confirmed using the same method (Adenwalla et al. 1990). Subsequently many different methods like thermal expansivity (van Dijk et al. 1993, van Dijk 1994), field dependent specific heat (v. Löhneysen 1994) etc. have yielded equivalent B-T phase diagrams. An important observation is a crossover of the anisotropy ratio of upper critical fields as function of temperature indicating that H_{c2} shows Pauli limiting for $\mathbf{H}\parallel c$ but not for $\mathbf{H}\perp c$ (Shivaram et al. 1987, Choi and Sauls 1991). Again the asymptotic ($T \ll T_c$) low temperature behaviour of thermodynamic and transport coefficients, most notably thermal conductivity (Lussier et al. 1996, Graf et al. 1999) with power law behaviour points to a gap function with nodes. The precise node structure is different for the three phases due to the internal degrees of freedom for a multicomponent order parameter. Despite the wealth of experimental results on UPt_3 there is no unequivocal consensus on the symmetry and node structure of the superconducting gap. The many different proposals that have been put forward at various times are summarized in (Joynt and Taillefer 2002). Here we restrict to the most commonly accepted E_{2u} (f-wave) model for the order parameter which was originally proposed by (Choi and Sauls 1991, Sauls 1994) and in the form used here by (Norman and Hirschfeld 1996). This odd parity spin triplet order parameter is consistent with ^{195}Pt Knight shift measurements and the observed linear in T dependence of the

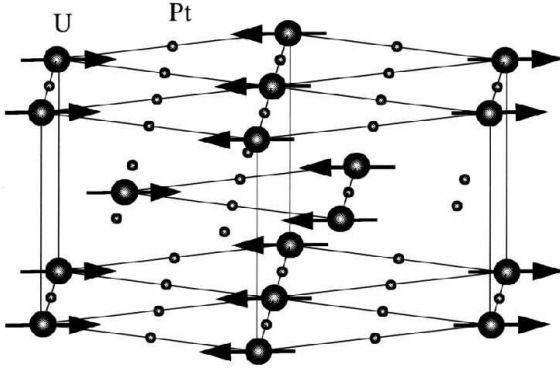


Figure 26. Crystal structure and AF magnetic structure of UPt_3 below $T_N = 5.8$ K. The hexagonal axis defines the \mathbf{c} direction and the moments are oriented along $\mathbf{b} \perp \mathbf{a}$ (using orthogonal \mathbf{a} , \mathbf{b} , \mathbf{c} lattice vectors where $a = b = 5.764 \text{ \AA}$ and $c = 4.884 \text{ \AA}$). Hexagonal planes are separated by $c/2$. The AF order leads to a doubling of the unit cell along \mathbf{b} (moment direction) resulting in orthorhombic (D_{2h}) symmetry of the AF crystal.

thermal conductivity for both a and c directions. The corresponding B-phase (e.g. $H = 0$, $T < T_{c2}$) has a gap function with an equatorial node line and polar second order node points. The anisotropic paramagnetic limiting of the upper critical field suggests that its \mathbf{d} -vector is pinned along the c axis by an anisotropy potential due to spin orbit coupling. This interpretation is however in conflict with a nearly isotropic constant Knight shift for larger fields (Kitaoka et al. 2000). Further investigations, notably field-angle dependent thermal conductivity experiments are necessary to confirm the node structure of the E_{2u} model.

The underlying normal heavy fermion state of UPt_3 , which was the first system where heavy quasiparticles have directly been seen in dHvA oscillations (Taillefer and Lonzarich 1988), has been described above. It was argued that the picture of heavy quasiparticle mass generation in 5f-metals has to be revised. This is due to a considerably different degree of localisation of 5f electrons in different orbital states as opposed to the simple LDA picture which assumes complete delocalisation for all 5f orbitals.

4.1.4. Small moment AF order

UPt_3 crystallizes in the hexagonal MgCd_3 structure (D_{6h} point group) and has two inequivalent U-sites with C_{3v} site symmetry. As in most other U-based superconductors the SC phase is embedded in an antiferromagnetic phase with very small moments ($\mu = 0.035\mu_B$). The commensurate AF order of hcp UPt_3 with moments parallel to the hexagonal b -axis is indicated in fig. 26. The D_{6h} sixfold symmetry of the paramagnetic phase is reduced to an orthorhombic D_{2h} symmetry by the AF order with modulation vector $\mathbf{Q} = (\frac{1}{2}, 0, 0)$. Although the AF intensity shows mean field behaviour $\sim (T_N - T)$ (Aeppli et al. 1988) AF Bragg peaks retain a finite width pointing to imperfect AF

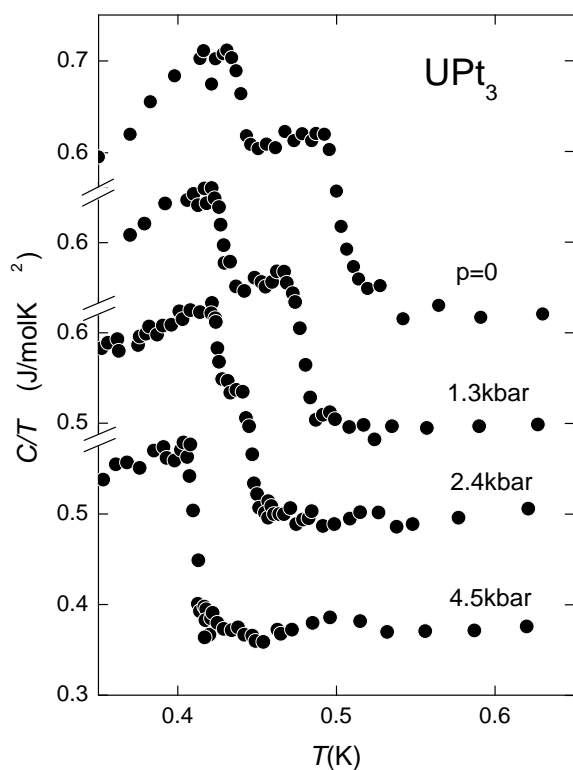


Figure 27. Disappearance of the double-peak structure of specific heat under hydrostatic pressure (Trappmann et al. 1991) from which the pressure dependence of $T_{c1,2}(p)$ shown in fig. 28 is obtained.

ordering with a correlation length of $\xi_{AF} \sim 150 \text{ \AA}$. Only below 50 mK ξ_{AF} starts to diverge (Koike et al. 1998) and true long range magnetic order develops at 28 mK according to specific heat measurements (Schuberth et al. 1992). Still in the imperfect ordered regime the Bragg intensity starts to decrease below the superconducting transition (Aeppli et al. 1988) which signifies a coupling of superconducting and AF order parameters, this has also been observed in URu_2Si_2 , UPd_2Al_3 and UNi_2Al_3 (Metoki 2001). Thus the small moment AF itself is a rather unconventional magnetic state but in the following discussions its influence on the superconducting state will be treated as ordinary AF order though with small moment.

4.1.5. The superconducting state, coupled with AF order

The exceptional nature of the superconducting state was already obvious from the two specific heat jumps first observed by (Fisher et al. 1989) of comparable size indicating two SC transitions at $T_{c1,2}$. Later it was shown (Trappmann et al. 1991) that under hydrostatic pressure the two transitions merge at a critical pressure of $p_c \simeq 3.8 \text{ kbar}$ (fig. 27). It is important to note that above p_c the two transitions do not separate again. Together with the pressure dependence of the AF moments observed in neutron diffraction (Hayden et al. 1992) this gives a clue about the nature of the two superconducting transitions as

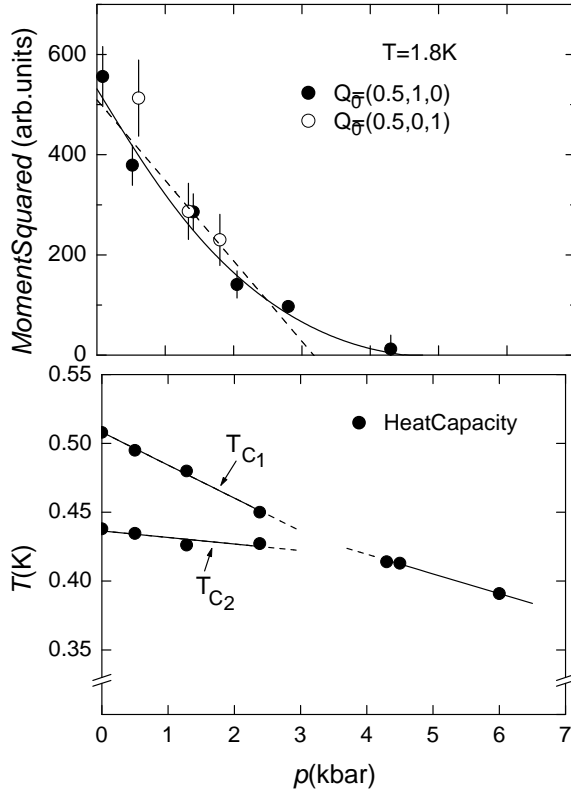


Figure 28. Reduction of the squared AF moment in UPt_3 with hydrostatic pressure p (above), it vanishes at a critical pressure of $p_c \simeq 3.8$ kbar. Simultaneously the SC T_c splitting is reduced and also vanishes at p_c staying zero for larger pressures (Hayden et al. 2002). This supports the idea that a twofold degenerate SC order parameter (e.g. E_{2u}) is split by an AF symmetry breaking field according to eqs. (69),(70)

well as the role of AF order. If the two transitions would correspond to two SC phases whose order parameters belong to one-dimensional representations with accidentally close transition temperatures then one would expect simply a crossing of $T_{c1,2}(p)$ at p_c , there would be no symmetry reason why the two transitions should merge above p_c as is actually seen in (fig. 28). The observation (Hayden et al. 1992) that the magnetic moment vanishes at about the same critical pressure (fig. 28) then suggests a natural scenario: at large hydrostatic pressure $p > p_c$ which preserves hexagonal symmetry the SC order parameter belongs to a two-dimensional hexagonal representation, E_1 or E_2 , i.e. it is a complex 2-component vector $\boldsymbol{\eta} = (\eta_1, \eta_2) = (|\eta_1|, |\eta_2|e^{i\Phi})e^{i\varphi}$ rather than a complex scalar $\eta e^{i\varphi}$ as for one-dimensional representations associated with a single T_c . Here φ is the overall Josephson-phase of the order parameter and Φ is an intrinsic phase which is a novel feature of the 2-component order parameter. At pressures $p < p_c$ the AF moments appear, since they are aligned in the b-direction they reduce hexagonal symmetry to orthorhombic symmetry. The AF order parameter acts as a symmetry breaking field (SBF), any small coupling between the AF and SC order parameters will then lead to a splitting of T_c into $T_{c1,2}$ which are associated with two SC order parameters of different symmetry with respect to the orthorhombic group. Therefore the small moment magnetism with its easy-plane anisotropy is a lucky coincidence which helps to unveil the complex vector nature of the SC order parameter. This scenario may generically be described within the Landau theory characterised by a free energy density (Machida et al. 1989, Hess et al. 1989, Joynt 1990)

$$f_L(\boldsymbol{\eta}, \mathbf{M}_{\mathbf{Q}}) = \alpha_0(T - T_c)\boldsymbol{\eta} \cdot \boldsymbol{\eta}^* + \beta_1(\boldsymbol{\eta} \cdot \boldsymbol{\eta}^*)^2 + \beta_2|\boldsymbol{\eta} \cdot \boldsymbol{\eta}|^2 - \gamma_0\mathbf{M}_{\mathbf{Q}}^2(\eta_x^2 - \eta_y^2) \quad (69)$$

Here $\mathbf{M}_{\mathbf{Q}} = M_{\mathbf{Q}}\hat{\mathbf{y}}$ is the AF order parameter which has already reached saturation in the SC temperature range, furthermore a shift of the critical temperature $T_c \sim M_{\mathbf{Q}}^2$ has already been included in T_c . There are two fourth order terms characterized by the Landau parameters β_1, β_2 as compared to only one in the case of a scalar SC order parameter. The last term is a phenomenological coupling of the SBF to the E-type SC order parameter. This type of theory is the same for each of the even or odd two-dimensional E-representations. The different \mathbf{k} -dependence of the respective SC-gap function enters only via the parameters of the Landau free energy in eq. (69) where $\alpha_0, \beta_1 > 0$. The ratio β_2/β_1 selects the SC ground state in the two dimensional manifold of possible order parameters $\boldsymbol{\eta}$. First we discuss the decoupled case $\gamma_0 = 0$ where a single transition at T_c into a state belonging to that manifold takes place. Then all possible SC ground states have $|\eta_1| = |\eta_2| \equiv |\eta|$. For $-1 < \beta_2/\beta_1 < 0$ the 'unitary' state with intrinsic phase $\Phi=0$ is stable whereas for $\beta_2/\beta_1 > 0$ the 'non-unitary' state with $\Phi = \pm\frac{\pi}{2}$ and $\boldsymbol{\eta} \times \boldsymbol{\eta}^* \neq 0$ is the stable one which is the case in UPt₃. The SBF splits the degenerate E-representations through the last term in eq. (69). Whereas at low temperature the stable state is determined by the fourth order terms, close to T_{c1} the second order terms $\sim \gamma_0 > 0$ dominate and favor a single component state, only below T_{c2} will the second component be nonzero. One has two phases (A) $\boldsymbol{\eta} = \eta(1,0)$ below T_{c1} and (B) $\boldsymbol{\eta} = \eta(1,ai)$ below T_{c2} . The $T_{c1,2}$ -splitting and the difference in amplitudes ($a < 1$) in the B-phase are determined by the Landau parameters according to

$$\Delta T_c = T_{c1} - T_{c2} = \left(1 + \frac{\beta_1}{\beta_2}\right)\lambda_0 T_c$$

$$\begin{aligned}
a &= (1 - \frac{\beta_1}{\beta_2}\lambda_0)/(1 + \frac{\beta_1}{\beta_2}\lambda_0) \\
\lambda_0 &= \frac{\gamma_0 M_{\mathbf{Q}}^2}{\alpha_0 T_c}
\end{aligned}
\tag{70}$$

Using the somewhat smaller transition temperatures $T_{c1,2}$ of van Dijk (1994) with $\Delta T_c = 0.054$ K (fig. 29) one obtains for the dimensionless coupling parameter of SC and AF order parameters $\lambda_0 = 0.038$. The smallness of this parameter is primarily due to the small AF moment in UPt_3 . If it would be only slightly larger the lower B-phase of UPt_3 would be completely suppressed and only one SC transition would be observable. Furthermore one has $\frac{\beta_1}{\beta_2} = \frac{T_c - T_{c2}}{\lambda_0 T_c} \simeq 2$ and the amplitude ratio $a = 0.86$ which will be set to 1 in the following. The ratio of the SC specific heat jumps at $T_{c1,2}$ is given by

$$\frac{\Delta_2 C}{\Delta_1 C} = \frac{T_{c2}}{T_{c1}} \left(1 + \frac{\beta_2}{\beta_1}\right)
\tag{71}$$

Here $\Delta_i C$ ($i=1,2$) are both counted from the normal state. Using the experimental values this also leads to a ratio $\frac{\beta_1}{\beta_2}=2$. This type of phenomenological theory can be extended to include also the pressure dependence (Thalmeier et al. 1991). From the two different slopes of $T_{c1,2}$ vs. pressure one may infer a magnetic Grüneisen parameter $\Omega_M = -(\partial \ln M_{\mathbf{Q}}^2 / \partial \epsilon_v) = -385$ which is in reasonable agreement with $\Omega_M = -260$ as determined directly from the pressure dependence of Bragg intensities which are $\sim M_{\mathbf{Q}}^2$. This gives further support that the AF order provides the SBF that leads to the observed splitting into (1,0) and (1,i) superconducting phases at zero field.

4.1.6. The critical field curves and Ginzburg-Landau theory

Naturally the two superconducting transitions at $T_{c1,2}$ will lead to two different critical field curves $H_{c2}^{1,2}$ which have been investigated by experimental methods mentioned before. The most obvious feature is a crossing of the critical field curves at a tetracritical point for all field directions. As a consequence there are three distinct SC regions in the H-T plane with phases A (high T, low H), B (low T, low H) and C (low T, high H). This important result has first been obtained by Bruls et al. (1990) with ultrasonic experiments. In fig. 29 we show the phase diagram for $H \perp c$ and $H \parallel c$ obtained by van Dijk (1994) using thermal expansion measurements. Its most important properties may be summarized as follows: (i) The existence of a tetracritical point (T_t, H_t) . Purely thermodynamical analysis of its vicinity (Yip et al. 1991) leads to the conclusion that if all four phase boundaries meeting at (T_t, H_t) are of second order, relations between their slopes and the specific heat jumps across them exist. They were confirmed by van Dijk (1994) which proved the second order nature of transitions. The change of slopes leads to pronounced kinks in the phase boundaries for $H \parallel a$. (ii) Defining the upper critical field $H_{c2}(T)$ as the upper phase boundary in fig. 29 for a,c directions one notices a reversal of the a-c anisotropy ratio $H_{c2}^a(T)/H_{c2}^c(T)$ as function of temperature. This ratio is < 1 for $T/T_c > 0.4$ and > 1 for $T/T_c < 0.4$. This reversal has been advanced as a major argument for spin triplet pairing by Sauls (1994). For the explanation of the structure of the A,B,C phase diagram an appropriate Ginzburg-Landau theory for a SC 2-component vector order parameter has to be constructed (Machida et al. 1989, Hess et al. 1989). It is obtained by adding all appropriate hexagonal invariants formed from η_j and its covariant gradient operators

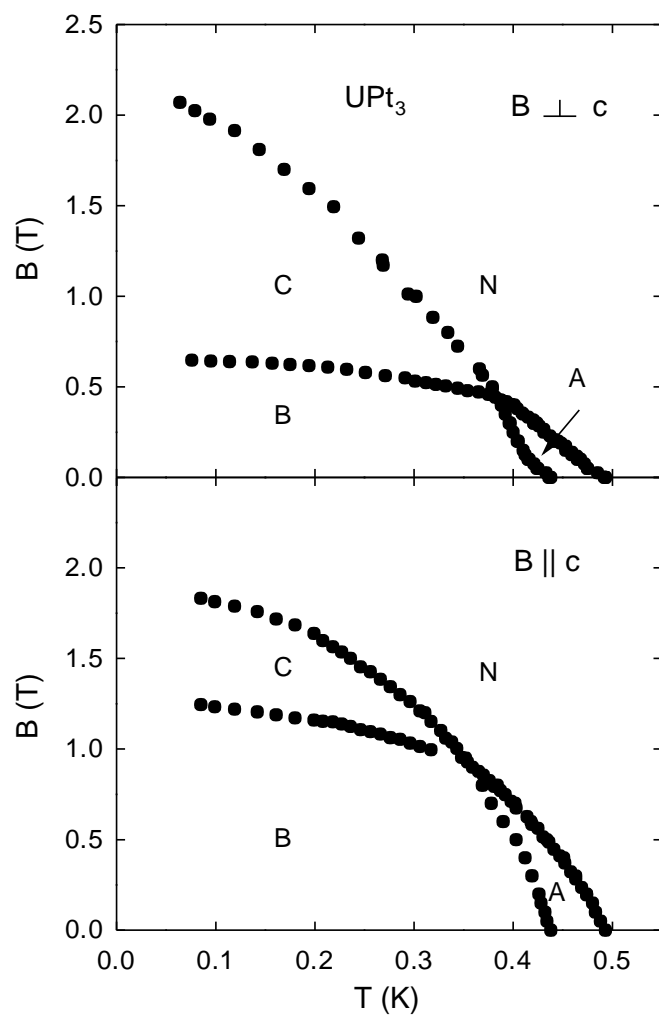


Figure 29. Superconducting B-T phase diagram as obtained from thermal expansion and magnetostriction (van Dijk et al. 1993a and 1993b, van Dijk 1994). Critical field curves cross at a tetracritical point which is present for all field directions, therefore three distinct SC phases A(1,0), B(1,i) and C(0,1) with different E_{2u} order parameters η exist.

$D_j = \partial_j - i\mathbf{A}_j$ with \mathbf{A} denoting the vector potential corresponding to the field \mathbf{B} given in units of $\phi_0/2\pi$ where $\phi_0 = \frac{hc}{2e}$ is the flux quantum. The homogeneous terms of the GL free energy density are again given by eq. (69) to which we have to add the gradient terms

$$\begin{aligned} f_G(\boldsymbol{\eta}, \mathbf{M}_Q) = & K_1(|D_x\eta_1|^2 + |D_y\eta_2|^2) + K_2(|D_x\eta_2|^2 + |D_y\eta_1|^2) \\ & + K_3(D_x\eta_1 D_y^*\eta_2^* + D_x\eta_2 D_y^*\eta_1^* + c.c) + K_4(|D_z\eta_1|^2 + |D_z\eta_2|^2) \\ & - \kappa M_Q^2 (|D_x\eta_1|^2 - |D_y\eta_1|^2 + |D_x\eta_2|^2 - |D_y\eta_2|^2) \end{aligned} \quad (72)$$

The expression for the total GL free energy density $f_{GL} = f_L + f_G$ is valid for both E_1 and E_2 type order parameters of odd and even parity but in the whole section we restrict discussion to the most likely E_{2u} case. The last term in eq. (72) with $K_M = \kappa M_Q^2$ describes the coupling of the SBF to the gradients of the SC order parameter. In a conventional GL theory for a scalar order parameter one has only one GL parameter $K = \frac{\hbar c}{2m^*}$ determined by the effective electron mass. For the vector order parameter $\boldsymbol{\eta}$ one has altogether 5 parameters. It is therefore obvious that a GL theory for a multicomponent superconductor has little real predictive power, but it may be used as a convenient frame for qualitative discussion. In weak coupling BCS theory the coefficients K_i can be expressed as angular averages of Fermi velocities (Sauls 1994) which leads to the conclusion that in the E_{2u} -case one has $K_2, K_3 \ll K_1$. In this case the terms mixing η_x and η_y can be neglected and the solution of the linearized GL-equations corresponding to eqs. (69),(72) lead to two parallel critical field curves without the term $\sim K_M$ for all directions of the field. The tetracritical point in this model is therefore entirely due to the coupling of gradient terms $D_{x,y}\eta_i$ to the SBF where the sign of κ is negative, i.e. it has to be opposite to that of γ in the homogeneous coupling term of eq. (69) in order to obtain a crossing at T_t . Using eq.(72) and the quadratic part of eq.(69) one obtains the critical field curves

$$\begin{aligned} H_{c2}^1 &= \frac{\phi_0}{2\pi} \frac{\alpha_0(T_{c1} - T)}{\sqrt{(K_1 + K_M)K_4}} \\ H_{c2}^2 &= \frac{\phi_0}{2\pi} \frac{\alpha_0(T_{c2}^0 - T)}{\sqrt{(K_1 - K_M)K_4}} \end{aligned} \quad (73)$$

Here $T_{c2}^0 > T_{c2}$ is the second transition temperature without inclusion of quartic terms of eq.(69) (Machida et al. 1989). For fields parallel to the c-axis similar expressions hold with $\sqrt{(K_1 \pm K_M)K_4}$ replaced by $(K_1 \pm K_M)$. Ignoring K_M for the moment the a-c anisotropy of H_{c2}^1 is given by a slope ratio $H_{c2}^{1c}/H_{c2}^{1a} = \sqrt{K_4/K_1} = \sqrt{\langle v_c^2 \rangle / \langle v_a^2 \rangle} = \sqrt{m_a/m_c}$. The experimental slope ratio 1.64 is indeed exactly equal to the root of the mass anisotropy $m_a/m_c = 2.7$ as obtained from transport measurements. The linearized version of the E_{2u} model has however no natural explanation for the slope changes ($B \perp c$) at the tetracritical point. On the other hand it explains the basic observation of the three (A,B,C) phases in the B-T plane for all field directions. In addition to the low- (or zero-) field phases (A,B) discussed before a high field phase (C) with an order parameter $\boldsymbol{\eta} = |\eta|(0,1)$ appears which is stabilized by the gradient coupling term $\sim K_M$.

4.1.7. The superconducting gap function

A detailed understanding of thermodynamics and transport properties requires the \mathbf{k} -dependent gap functions of the three phases. Their node structure determines the low

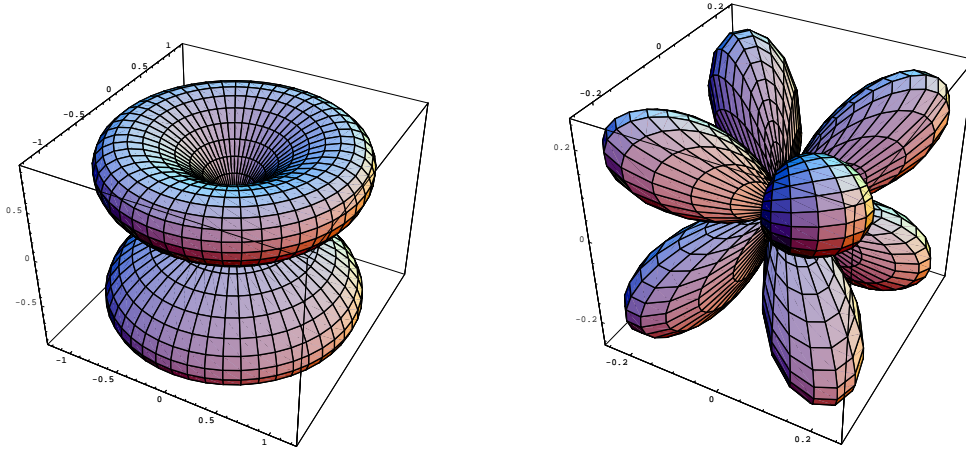


Figure 30. Spherical plots of $|\Delta(\vartheta, \varphi)|$ for B-phase (left) and C-phase (right). B-phase has node line $\vartheta = \frac{\pi}{2}$ ($k_z=0$) and 2^{nd} order node points along c-axis ($\vartheta = 0, \pi$). C-phase has additional node lines at $k_x=0, k_y=0$ ($\varphi = 0, \frac{\pi}{2}$) (Yang and Maki 1999).

temperature behaviour of thermodynamic and transport coefficients. The most commonly proposed triplet f-wave gap function with E_{2u} symmetry is given by

$$\mathbf{d}(\mathbf{k}) = \eta_1 [k_z \hat{\mathbf{z}}(k_x^2 - k_y^2) + \eta_2 (2k_z \hat{\mathbf{z}} k_x k_y)] \quad (74)$$

The orientation of the \mathbf{d} -vector is assumed to be \mathbf{k} -independent and pinned along the hexagonal c-axis ($\hat{\mathbf{z}}$) by an anisotropy potential acting on the (Kramers degeneracy) pseudospin of the heavy quasiparticles which has its origin in the spin-orbit coupling of 5f-electrons. This pinning effect leads to a large paramagnetic limiting effect for $\mathbf{B} \parallel \mathbf{d}$, $\hat{\mathbf{z}}$ and to no effect for $\mathbf{B} \perp \mathbf{d}$, $\hat{\mathbf{z}}$ which was suggested (Graf et al. 2000) as origin of the crossover in the a-c upper critical field anisotropy mentioned before. This is claimed as strong evidence for triplet pairing (Graf et al. 2000) and as argument against the singlet d-wave (E_{1g}) gap function. Defining $\mathbf{d}(\mathbf{k}) = \Delta(\mathbf{k}) \hat{\mathbf{z}} = \Delta(\vartheta, \varphi) \hat{\mathbf{z}}$ where ϑ, φ are the polar and azimuthal angles of \mathbf{k} one has explicitly the following E_{2u} gap functions (without normalization) for the A,B($a=1$) and C phases ($\Delta_0 \equiv |\eta_{1,2}|$)

$$\begin{aligned} A(1, 0) : \Delta(\vartheta, \varphi) &= \Delta_0 k_z (k_x^2 - k_y^2) = \Delta_0 \cos \vartheta \sin^2 \vartheta \cos(2\varphi) \\ B(1, i) : \Delta(\vartheta, \varphi) &= \Delta_0 k_z (k_x + ik_y)^2 = \Delta_0 \cos \vartheta \sin^2 \vartheta \exp(2i\varphi) \\ C(0, 1) : \Delta(\vartheta, \varphi) &= 2\Delta_0 k_z k_x k_y = \Delta_0 \cos \vartheta \sin^2 \vartheta \sin(2\varphi) \end{aligned} \quad (75)$$

An angular plot of these gap functions is shown in fig. 30 which also exhibits their node structure described in the caption. In the above equation the equal amplitude approximation $a = 1$ was made for the B-phase which leads to a gap with full rotational symmetry around c. As an effect of the SBF which leads to $a < 1$ the rotational symmetry is slightly broken, one has to multiply the (B-phase) gap function by a factor $(1 - \epsilon^2 \sin^2(2\varphi))^{\frac{1}{2}}$ with fourfold symmetry around c and $\epsilon^2 = 1 - a^2 = 0.26$. The node structure is unchanged, it consists of an equatorial line node and two second order node points at the poles. Both

contribute to the linear behaviour of the quasiparticle DOS $N(E)$ for $E \ll \Delta_0$. It was calculated (Yang and Maki 2001) including the effect of impurity scattering which quickly leads to a residual DOS $N(0)$. Indeed in UPt_3 large residual γ values are usually obtained by extrapolation from temperatures above the magnetic ordering at 28 mK. Finally one should note that the presence of a node line is not required by symmetry if one assumes the strong spin-orbit coupling case (Blount 1985), it is rather a result of a special choice of the E_{2u} order parameter in the allowed subspace. Forming a linear combination of all possible E_{2u} representations there are in general only point nodes. However, as argued above and in sect. 2, the weak spin orbit coupling case is more realistic in the effective quasiparticle pseudo spin picture for UPt_3 and then the appearance of node lines is natural. It is obvious from fig. 30 and eq.(75) that the non-unitary B-phase has fewer nodes than the unitary A- or C-phases. This general feature of non-unitary phases means that they are preferred as stable low temperature states in unconventional SC because fewer nodes lead to a larger condensation energy.

The ratio of fourth order Landau coefficients $\beta_1/\beta_2 \simeq 2$ was taken as evidence for the weak coupling nature of superconductivity. Therefore the question arises whether it is possible to calculate the symmetry of the order parameter within a microscopic weak coupling Hamiltonian starting from an on-site effective quasiparticle interaction which is repulsive. Such attempts have originally been made without the inclusion of the orbital degeneracy of U-5f states and within one band models with the static susceptibility tensor used as an input. However, not surprisingly the gap functions obtained are sensitive to the input function and also the E_{2u} gap function is not the favored one (Norman 1991, Norman 1994) in such models. Attempts to include orbital degrees of freedom to remedy this situation have been made (Norman 1994). As mentioned before it has now become clear that 5f-states in UPt_3 have also a dual nature, partly localised in $5f^2$ configurations and partly itinerant states which have heavy masses due to renormalisation by low lying CEF excitations of the $5f^2$ states. It is therefore possible that, as in the case of UPd_2Al_3 , exchange of localised $5f^2$ excitation modes play an essential role for the formation of unconventional Cooper pairs in UPt_3 .

4.1.8. Low temperature transport properties

The quasiparticle energies vanish at the nodes of the superconducting gap. Therefore the low temperature ($T \ll T_c$) behaviour of thermodynamic and transport coefficients may give information on the node structure. Specific heat analysis has proved of little use due to the presence of the huge 28 mK peak caused by the onset of true long range magnetic order of the small moments. Thermal conductivity measurements for $0.1 < T/T_{c2} < 0.3$ (Lussier et al. 1996) have been more successful. The temperature dependence in this asymptotic regime requires the presence of node lines and/or second order node points, furthermore comparison of the anisotropy ratio $\kappa_c(T)/\kappa_a(T)$ shown in fig. 31 with the calculated ones (Norman and Hirschfeld 1996) gives good agreement for the E_{2u} gap function of the B-phase in eq. (75). Extrapolation for zero temperature leads to a ratio ~ 0.5 contrary to the older E_{1g} model which extrapolates to zero. This difference is due to the presence of second order node points with $\Delta(\vartheta) \sim \vartheta^2$ or $(\pi - \vartheta)^2$ at the poles in the E_{2u} case. Finally for $T/T_{c2} < 0.1$ one reaches the gapless regime where the pair breaking energy scale $\sqrt{\Gamma} \hbar \Gamma k T > kT$ with Γ denoting the normal state impurity scattering rate.

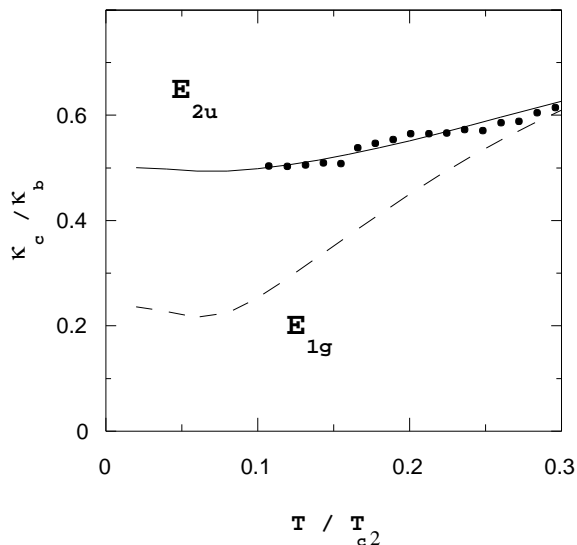


Figure 31. Anisotropy ratio κ_c/κ_b of thermal conductivities as function of the reduced temperature. Data from (Lussier et al. 1996).

In this case a behaviour $\kappa/T \sim \alpha + \beta T^2$ is predicted (Graf et al. 1996) in good agreement with observations (Suderow et al. 1997).

4.1.9. NMR Knight shift results

The Knight shift (KS) in the superconducting regime is a direct measure of the change $\delta\chi_s$ in the spin susceptibility of the SC condensate. It can be measured by μ SR or NMR experiments. In the latter the NMR resonance frequency is shifted due to the contact interaction of nuclear and electronic spin moment (sect. 2). Ideally when spin orbit coupling can be neglected, the KS should drop to zero for a singlet SC state and should be unchanged for a triplet state. Spin orbit coupling complicates the interpretation and may lead to only a partial reduction for a singlet state and an observable anisotropic reduction in the triplet state (Mineev and Samokhin 1999). In the latter case for a rigid $\mathbf{d}(\mathbf{k})$ with respect to \mathbf{H} one has for the susceptibility tensor (i,j=x,y,z):

$$\chi_{sij} = \chi_n \int \frac{d\Omega}{4\pi} [(P_{ij}^\perp(\mathbf{k}) + Y(\hat{\mathbf{k}}, T)P_{ij}^\parallel(\mathbf{k}))] \quad (76)$$

Where χ_n is the normal state spin susceptibility (assumed isotropic for simplicity). Furthermore $P_{ij}^\perp(\mathbf{k}) = \mathbf{d}_\alpha^*(\mathbf{k})\mathbf{d}_\beta^*(\mathbf{k}) / |\mathbf{d}(\mathbf{k})|^2$ and $P_{ij}^\parallel(\mathbf{k}) = [\delta_{\alpha\beta} - P_{ij}^\perp(\mathbf{k})]$ are the projectors to the direction perpendicular and parallel to $\mathbf{d}(\mathbf{k})$ respectively and $Y(\hat{\mathbf{k}}, T)$ is related to the Yoshida function of sect. 2.

In the strong spin-orbit coupling case with the \mathbf{d} -vector pinned along c one would expect a suppression of the KS for \mathbf{H} applied parallel to the c direction due to the effect of $Y(\hat{\mathbf{k}}, T)$ but not for $\mathbf{H} \perp c$, i.e. for \mathbf{H} in the hexagonal plane. The Knight shift should therefore be quite anisotropic for pinned \mathbf{d} -vector. However it was found (Tou et al. 1996, Tou et al. 1998, Kitaoka et al. 2000) that for large fields (in the C-phase) there is almost no

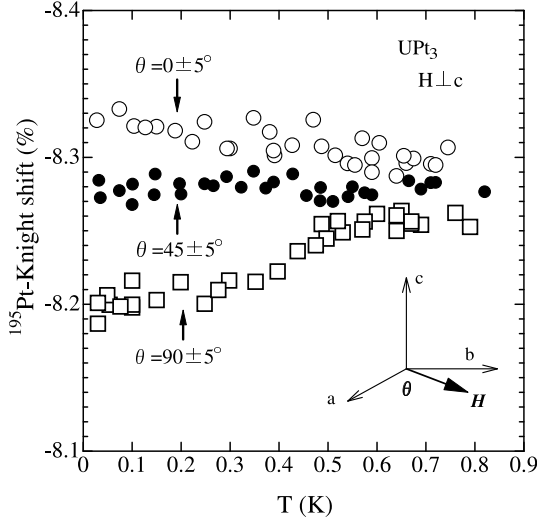


Figure 32. Anisotropic Knight shift for field in the hexagonal plane ($H = 0.19$ T) (Kitaoka et al. (2000)). The field angle dependence of $\sim 1\%$ of the Knight shift is possibly a sign of weak \mathbf{d} -vector pinning by the SBF.

change for both field directions. This was interpreted as evidence that the weak spin orbit coupling case is realized in UPt_3 . In this case the \mathbf{d} -vector may be rotated by the field. For large fields it is always perpendicular to \mathbf{H} and therefore no KS reduction will take place. On the other hand for low fields (in the B-phase) it may be pinned by the SBF (parallel to a) and therefore rotation of \mathbf{H} in the hexagonal ab -plane will produce an anisotropic Knight shift as shown in fig. 32. The weak spin orbit coupling scenario has also been theoretically investigated (Ohmi and Machida 1996, Ohmi and Machida 1996a). On the other hand this interpretation seems to be in conflict with the anisotropic paramagnetic limiting which leads to the reversal for the upper critical field anisotropy as explained before. This discrepancy has so far not been resolved.

4.1.10. Magnetothermal properties in the vortex phase

The a - c anisotropy of the zero-field thermal conductivity in the B-phase has provided a major argument for the E_{2u} SC order parameter with its second order nodal points at the poles. These node points (and also the equatorial node line) have, however, not been seen directly until now. As explained in sect. 2 magnetothermal conductivity or specific heat measurements in the vortex phase as function of field angles can provide such direct evidence. Due to the comparatively low T_c of UPt_3 experiments have to be done at 50 mK or below, so far they have not been performed. Calculations of the field angle dependence for the B-phase (Maki and Thalmeier 2003) and the C-phase (Thalmeier and Maki 2003a) have been carried out however. For simplicity we discuss only the former since the modulus of the gap function in the B-phase is isotropic in the hexagonal plane according to eq. (75). This means that specific heat and c -axis thermal conductivity κ_{zz} depend only on the polar field angle θ . They are given in the low temperature and

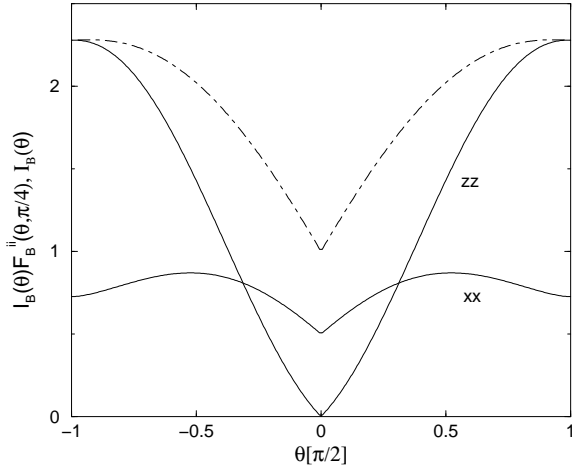


Figure 33. Angular dependence of specific heat (dot-dashed) and thermal conductivity κ_{ii} ($i=x,z$) polar field angle θ . Cusps at $\theta=0$ are due to polar node points of the gap in eq. (75). While κ_{zz} is independent of ϕ , κ_{xx} is shown for $\phi = \frac{\pi}{4}$ (Thalmeier and Maki 2003a).

superclean limit of sect. 2 by

$$\begin{aligned}
 \frac{C_s(\theta)}{\gamma T} &= \frac{1}{\sqrt{3}} \tilde{v} \sqrt{eH} I_B(\theta) \\
 \frac{\kappa_{zz}(\theta)}{\kappa_n} &= \frac{2 v_a v_c}{3 \Delta^2} (eH) I_B(\theta) F_B^{zz}(\theta) \\
 I_B(\theta) &= \alpha \sin \theta + \frac{2}{\pi} E(\sin \theta)
 \end{aligned} \tag{77}$$

where $F_B^{zz}(\theta) = \sin \theta$ and $E(\sin \theta)$ is the complete elliptic integral. The θ -dependent factors in the above equation are shown in fig. 33. Sharp cusps for $\theta = 0, \pi$ are indeed seen in these functions which if observed in the corresponding specific heat $C_s(\theta)$ and thermal conductivity $\kappa_{zz}(\theta)$ would constitute a direct and unambiguous proof for the polar node points in the B-phase of UPt_3 . Likewise the equatorial line node of the B-phase will lead to a flat minimum (without a cusp) for $\theta = \frac{\pi}{2}$ in $\kappa_{xx}(\theta)$. Observing these features in UPt_3 as ultimate proof for the node structure is an experimental challenge.

4.2. Magnetic exciton mediated superconductivity in UPd₂Al₃

Among the U-based HF superconductors UPd₂Al₃ (Geibel et al. 1991a) is a rather special case. In this HF compound with a moderate $\gamma = 120$ mJ/mole K² there is also AF order below $T_N = 14.3$ K with almost atomic size local moments ($\mu = 0.85\mu_B$) in contrast to the small moments in other U-compounds. The entropy release is $\Delta S(T_N) = 0.67R\ln 2$ per mole, much larger than in the itinerant SDW sister compound UNi₂Al₃. The AF order coexists with superconductivity below $T_c = 1.8$ K. This suggests that in addition to the heavy itinerant quasiparticles nearly localised 5f-electrons should be present. They result from the dominating 5f² configuration of the U⁴⁺ ion (Grauel et al. 1992). This dual nature of 5f-electrons is even more obvious than in UPt₃ as is seen from various experimental investigations like susceptibility (Grauel et al. 1992), Knight shift (Feyerherm et al. 1994) and optical measurements (Dressel et al. 2002). The former exhibit a pronounced a-c axis anisotropy (Grauel et al. 1992) shown in fig. 34 with a much larger $\chi_a(T)$ whose T-dependence is very reminiscent of CEF-effects. A CEF scheme with two low lying singlets split by δ was proposed for the 5f² localized states. Later investigations (Shiina 2001) indicate that the first excited state is rather a doublet with $\delta = 6$ meV. Since the ground state is a singlet the local 5f-moment magnetism must be of the induced type caused by the mixing with the excited doublet via inter-site exchange. A direct confirmation of this dual nature of 5f-electrons in UPd₂Al₃ was obtained from inelastic neutron scattering (INS) (Mason and Aeppli 1997) which found excitations that originate in local CEF transitions of energy δ and disperse into bands of ‘magnetic excitons’ due to intersite exchange. This band extends up to 8 meV and along the c direction the modes are propagating with little damping. Later high resolution INS experiments (Sato et al. 1997, Sato et al. 1997a, Bernhoeft et al. 1998, Bernhoeft 2000) have shown that below T_c a resonance like structure in the dynamical structure function of localised moments appears which is linked to the superconducting quasiparticles. Complementary tunneling experiments probe the response of the itinerant quasiparticles and their superconducting gap. In a breakthrough experiment this has been achieved the first time for a HF superconductor using an epitaxially grown UPd₂Al₃-AlO_x-Pb tunneling device (Jourdan et al. 1999). Typical strong coupling features in the tunneling DOS have been observed which appear at an energy related to the excitations of local moments seen in INS. Together both experiments strongly suggest that the magnetic excitons identified in INS are the bosonic ‘glue’ which binds the electrons together to Cooper pairs (Sato et al. 2001). This is a new mechanism for superconductivity distinctly different from both the electron-phonon and spin fluctuation mechanism known sofar. The pairing potential is mediated by a propagating boson (the magnetic exciton) as in the former but depends on the spin state of conduction electrons as in the latter. It is the main purpose of this section to present the evidence for this important new mechanism for unconventional superconductivity. Before considering this in detail we summarize some essential physical facts known about UPd₂Al₃.

4.2.1. AF structure and superconducting properties

The AF magnetic structure of UPd₂Al₃ consists of FM ordered hexagonal planes with moments ($\mu = 0.83\mu_B$) in [100] direction and stacked antiferromagnetically along the c-axis (Krimmel et al. 1992, Kita et al. 1994). It corresponds to an AF wave vector

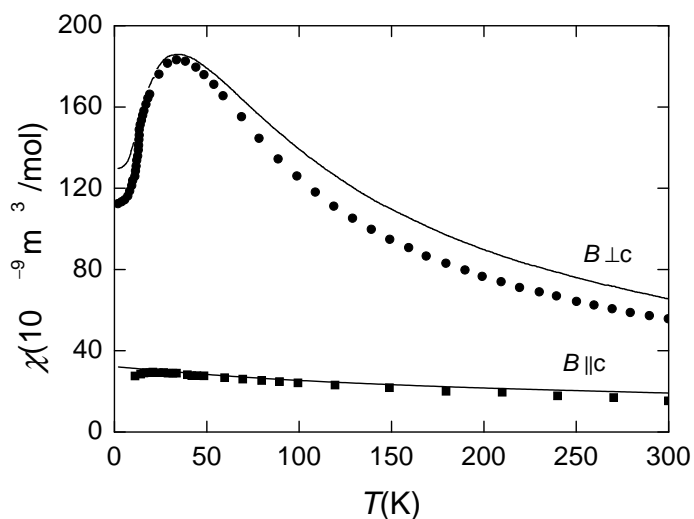


Figure 34. Magnetic susceptibility of UPd_2Al_3 for field parallel to a- and c-axis. The pronounced maximum for $\chi_{\perp}(T)$ is a typical signature of CEF split localised 5f-states (Grauel et al. 1992). The full line is a fit using a U^{3+} CEF level scheme containing singlet ground state and first excited state (33 K).

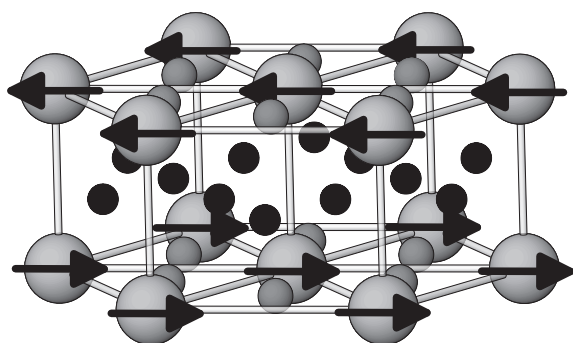


Figure 35. Conventional unit cell of UPd_2Al_3 ($a = 5.350 \text{ \AA}$, $c = 4.185 \text{ \AA}$) and simple AF magnetic structure with propagation vector $\mathbf{Q} = (0, 0, \frac{1}{2})$. The large and small grey spheres in hexagonal planes correspond to the U and Pt atoms respectively, intercalated by Al atoms (small black spheres).

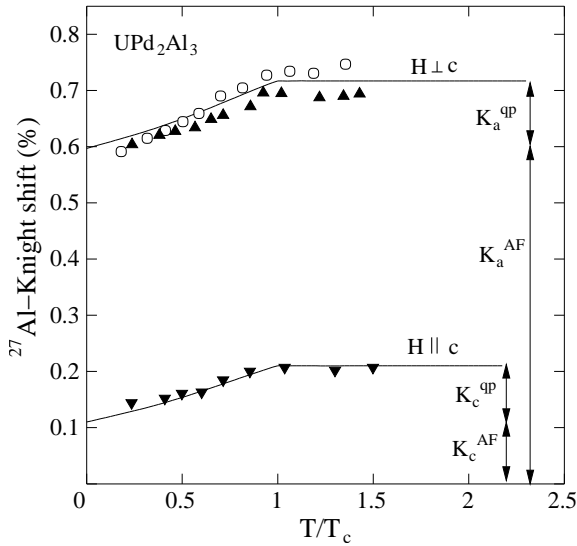


Figure 36. ^{27}Al Knight shift from NMR below T_c (Kitaoka et al. (2000)). The arrows indicate the suggested separation in localised (AF) and itinerant quasiparticle (qp) contributions. The AF and qp parts cannot be independently determined experimentally. Therefore the complete suppression of K^{qp} is a conjecture.

$\mathbf{Q}=(0,0,\frac{1}{2})$ (in r.l.u.) and is shown in fig. 35. As expected from the large a-c anisotropy of the susceptibility in fig. 34 the AF structure does not change in applied magnetic fields \mathbf{H} along c . For fields in the easy ab-plane the hexagonal in-plane anisotropy is much smaller and moment reorientation can be seen. The magnetic B-T phase diagram has been determined by Kita et al. (1994) and no effects of the superconducting transition at $T_c = 1.8$ K on the magnetic structure has been found supporting the idea of two separate superconducting (itinerant) and magnetic (localised) 5f-subsystems.

The superconducting state of UPd_2Al_3 has been investigated by thermodynamic and transport measurements (Casparly et al. 1993, Hessert et al. 1997, Hiroi et al. 1997), NMR (Tou et al. 1995, Matsuda et al. 1997), μsR experiments (Feyerherm et al. 1994) and tunneling studies (Jourdan et al. 1999). Despite this great effort the symmetry of the order parameter is not reliably known so far.

The upper critical field exhibits flattening for low temperatures which has been interpreted as a Pauli limiting effect and hence evidence for singlet pairing (Hessert et al. 1997). The angular dependence $H_{c2}(\theta)$, where θ is the polar angle, changes dramatically from $T = 1.5$ K to $T = 0.5$ K which was interpreted as a gradual change from d-wave to s-wave character of the order parameter when temperature is lowered. Within this picture the effect of background AF order was ignored which may not be permissible because the critical fields for localized 5f-spin reorientation are of the same order as H_{c2} (Grauel et al. 1992, Kita et al. 1994).

The Knight shift in the SC phase is a direct probe for the reduction of the spin susceptibility $\chi_s(T)$ in the SC state (Tou et al. 2003). Ideally there should be a complete suppression of $\chi_s(T)$ for singlet pairing and no effect for triplet pairing (sections 2,4.1).

This picture is however complicated by the effect of spin-orbit coupling which may lead to intermediate cases. The result for $\Delta K_s(T)$ as obtained from ^{27}Al NMR experiments (Tou et al. 1995) is shown in fig. 36. Although a reduction is clearly visible, large (anisotropic) residual Knight shift values remain. This is attributed to the localized 5f-susceptibility which cannot be independently determined. Therefore these results and similar ones from μSR experiments (Feyerherm et al. 1994) are difficult to interpret. It is not possible to say with certainty how strong the Knight shift caused by the itinerant quasiparticles is actually reduced in the SC phase. But the conclusion concerning singlet pairing seems unaffected by this ambiguity.

The ^{27}Al NMR relaxation rate T_1^{-1} was found to exhibit a T^3 behaviour in the SC state over four orders of magnitude down to $0.1 T_c$ (Tou et al. 1995) where the gap amplitude will be constant. This means that $\Delta(\mathbf{k})$ should have a node line implying a low quasiparticle energy DOS $N_s(E) \sim |E|$. This conclusion was confirmed by ^{105}Pd NMR/NQR experiments (Matsuda et al. 1997) which also observed a T^3 behaviour of the relaxation rate and the absence of a coherence peak immediately below T_c was noticed, both facts are naturally explained by the existence of a node line in $\Delta(\mathbf{k})$.

Commonly in HF compounds the low temperature behaviour of the specific heat is not easily explained by simple models that involve only the topology of gap nodes. Very often residual γ - values exist where they should not due to node points or lines in $\Delta(\mathbf{k})$. This is ascribed to the presence of a residual density of states induced by impurity scattering. Extracting the true low temperature behaviour of the electronic specific heat C_s is also complicated by the presence of nuclear terms due to the hyperfine splitting which lead to a low temperature upturn $\sim \alpha T^{-2}$. This situation has also been encountered in UPd_2Al_3 . Originally the existence of a residual γ - value was concluded in (Casparly et al. 1993) but later measurements extending to lower temperatures (Sato 1993) have shown that the data can be well fitted without the residual γ but assuming instead a dominant T^2 term in $C_S(T)$ which is compatible with the node line hypothesis for UPd_2Al_3 . It is not known yet whether the field dependence of $C_S(T,H)$ is dominated by field induced $\gamma(H) \sim \sqrt{H}$ expected in the presence of nodes.

Thermal conductivity measurements for parallel heat current and field lying in the hexagonal plane (Hiroi et al. 1997) have shown a dominating temperature dependence $\kappa(T) \sim T^2$ and a linear behaviour $\kappa(T,H) \sim H$ at low temperatures. This is again in agreement with the existence of node lines in $\Delta(\mathbf{k})$. However their exact position on the FS is not yet known. This has to be investigated by field-angle dependent thermal conductivity measurements which has been successful in this task in other unconventional superconductors as described in sect. 2.

4.2.2. Electronic structure, Fermi surface and effective mass

In LDA type electronic band structure calculations for intermetallic U-compounds all 5f-electrons are treated in the same way and their degree of (de-)localisation is not much different. This is in contradiction to the behaviour observed in UPd_2Al_3 just as described above. Nevertheless LDA calculations give usually reasonable results for the Fermi surface topology. This can be understood in the context of model calculations as a result of many body correlations. For example within the Anderson lattice model it may be shown that the Fermi volume comprises both the f-electrons and conduction electrons ('Luttinger's

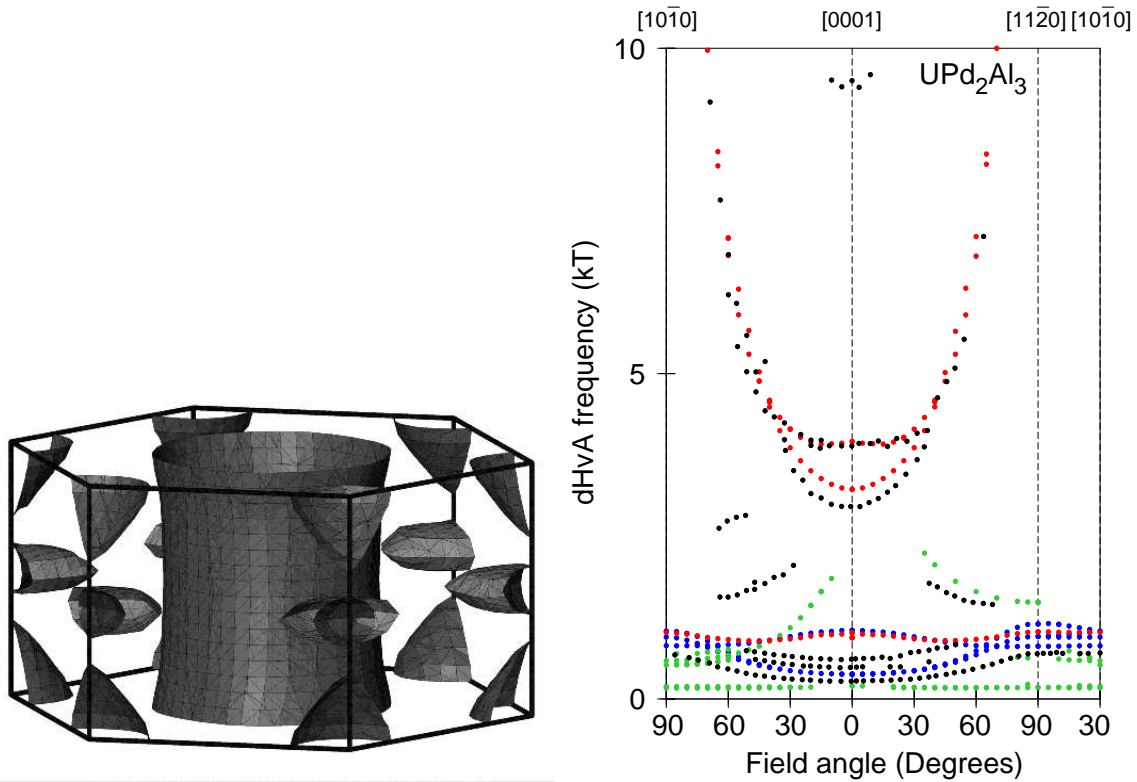


Figure 37. Left panel: Fermi surface of UPd_2Al_3 calculated within the dual approach method (Zwicknagl et al 2003). The main cylinder part has also a heavy mass with $m^* = 19 - 33 m$. Right panel: comparison of experimental dHvA frequencies (black symbols) from (Inada et al. 1999) and calculated frequencies (color symbols compatible with FS sheets on left panel) from the dual approach model (Zwicknagl et al 2003). Large parabola corresponds to the main FS cylinder.

theorem'), even in the Kondo limit when the f-electron is localised (Fazekas 1999). Therefore it looks as if the Fermi wave vector, and more generally the Fermi surface is the same as if both type of electrons were delocalised. This is indeed assumed in LDA calculations for UPd₂Al₃ which we discuss now. FS sheets and associated angle dependent de Haas-van Alphen (dHvA) frequencies have first been calculated by Sandratskii and Kübler (1994), Knöpfle et al. (1996) and compared to the experimental dHvA results (Inada et al. 1995). Similar calculations (Inada et al. 1999) obtain the same main FS sheets but differ in the positions of smaller sheets. The larger sheets are also those with experimentally found heavy masses, which the LDA calculation naturally cannot explain. The largest sheet which also has the strongest 5f-admixture is shown in fig. 37 in the AF Brillouin zone. It has the shape of a corrugated cylinder if one ignores the hexagonal in-plane anisotropy. In the subsequent model calculations we assume this simplified FS for UPd₂Al₃ and neglect all other sheets. The LDA approach to the 5f-electronic structure does not include the different degree of localisation evident from experiments discussed before. Progress in the treatment of partial localisation of 5f-electrons has recently been made for a number of U-compounds including UPt₃ (Zwicknagl et al. 2002) (sect. 4.1) and UPd₂Al₃ (Zwicknagl et al. 2003). Due to the strong spin orbit coupling 5f electrons occupy total angular momentum orbitals $|j = \frac{5}{2}, j_z\rangle$. The two localised 5f electrons are put into $j_z = \pm\frac{5}{2}$ and $j_z = \pm\frac{1}{2}$ localized states and the remaining $j_z = \pm\frac{3}{2}$ states is included in the LDA basis of band electrons. This treatment is justified by the larger hybridisation of the $j_z = \pm\frac{3}{2}$ orbitals as compared to $j_z = \pm\frac{1}{2}, \pm\frac{5}{2}$ already on the LDA level. It has been shown within model calculations (Efremov et al. 2003) that intraatomic correlations strongly increase the orbital dependence of the effective hybridisation, leading to the dual character of the 5f-electrons (sect. 2). Although two of the 5f-electrons are localised, the Fermi surface obtained from this calculation shows good agreement with the experimental results of the dHvA experiments. They are presented in fig. 37 together with the theoretical calculations.

This is reassuring for the dual 5f model approach, however the FS is also in good agreement with standard LDA calculations as discussed before. The decisive advantage of the former is that it also provides a basically parameter free explanation for the mass enhancement which cannot be obtained within LDA. The enhancement is due to the coupling of the delocalised with the localised 5f-electrons characterised by a matrix element $\alpha = 2a_{5f}M$. As explained below the latter are split into two low lying CEF singlet states with an excitation energy δ which is known from INS. Then the global mass enhancement factor (m^*/m_b) (independent of the FS sheet) with respect to the band mass m_b may be calculated according to eqs. (65),(66) as in the case of UPt₃. The comparison of experimental and theoretical total mass enhancement m^*/m is presented in table 5.

4.2.3. The dual model for UPd₂Al₃ and induced moment AF

The dual model for UPd₂Al₃ which comprises both localised 5f² electrons with total angular momentum \mathbf{J} and itinerant heavy 5f-electrons created by $c_{\mathbf{k}\sigma}^\dagger$ is described by the model Hamiltonian

$$H = H_c + H_{CEF} + H_{ff} + H_{cf}$$

Table 5

Effective masses for $\mathbf{H} \parallel c$. Notation for FS sheets and experimental values from (Inada et al. 1999). Theoretical values from (Zwicknagl et al. 2003)

FS sheet	m^*/m (exp.)	m^*/m (theory)
ζ	65	59.6
γ	33	31.9
β	19	25.1
ϵ_2	18	17.4
ϵ_3	12	13.4
β	5.7	9.6

$$H = \sum_{\mathbf{k}\sigma} \epsilon_{\mathbf{k}\sigma} c_{\mathbf{k}\sigma}^\dagger c_{\mathbf{k}\sigma} + \delta \sum_i |e\rangle \langle e|_i \quad (78)$$

$$- \sum_{\langle\langle ij \rangle\rangle} J_{ff}(ij) \mathbf{J}_i \mathbf{J}_j - 2I_0(g-1) \sum_i \mathbf{s}_i \mathbf{J}_i$$

where

$$\epsilon_{\mathbf{k}\sigma} = \epsilon_\perp(\mathbf{k}_\perp \sigma) - 2t_\parallel \cos k_z \quad (79)$$

is a model for the heavy conduction band energies whose FS is a corrugated cylinder along the hexagonal c -axis. Here t_\parallel is the effective hopping along c which determines the amount of corrugation. The form of the dispersion $\perp c$ is not important. The localised $5f^2$ electrons show a CEF splitting $\delta = 6$ meV into a singlet ground state $|g\rangle$ and an excited singlet $|e\rangle$ at δ . The remaining terms describe a superexchange J_{ff} between localised and an on-site exchange $I = I_0(g-1)$ between itinerant and localised $5f$ -electrons. The total effective inter-site exchange has therefore an additional RKKY contribution:

$$J(\mathbf{q}) = J_{ff}(\mathbf{q}) + I_0^2(g-1)^2 \chi_e(\mathbf{q}) \quad (80)$$

Here $\chi_0(\mathbf{q})$ is the conduction electron susceptibility. $\mathbf{J}(\mathbf{q})$ may be fitted to the experimentally observed magnetic excitations.

4.2.4. Induced moments and magnetic exciton dispersion in UPd_2Al_3

First we consider the magnetism of the localised $5f$ moments without dynamic effects of coupling to itinerant $5f$ electrons. In a nonmagnetic singlet ground state system with $\langle g|\mathbf{J}|g\rangle \equiv 0$ the moments have to be induced via nondiagonal matrix elements $\langle e|J_x|g\rangle = -i\langle e|J_y|g\rangle = \frac{1}{2}\alpha$ between ground state and excited state singlets. In UPd_2Al_3 the maximum of $\mathbf{J}(\mathbf{q})$ is at the AF wave vector $\mathbf{Q} = (0,0,\frac{1}{2})$ with $J_e \equiv J_e(\mathbf{Q})$. In the resulting AF state the CEF ground state will then be a superposition of $|g\rangle$ and $|e\rangle$. This type of magnetism is well known for Pr-metal and its compounds where one has two CEF split singlets from the $\text{Pr}^{3+}(4f^2)$ configuration (Jensen and Mackintosh 1991). This induced moment AF is only possible if the control parameter

$$\xi = \frac{\alpha^2 J_e}{2\delta} \quad (81)$$

exceeds a critical value, i.e. $\xi > \xi_c = 1$. Then the Néel temperature T_N and saturation moment $\langle J \rangle_0$ oriented along the a-axis (x-direction) are given by

$$T_N = \frac{\delta}{2 \tanh^{-1}(\frac{1}{\xi})} \quad \text{and} \quad \langle J \rangle_0 = \frac{1}{2} \alpha \frac{1}{\xi} (\xi^2 - 1)^{\frac{1}{2}} \quad (82)$$

When ξ is only slightly larger than $\xi_c = 1$ ($T_N/\delta \ll 1$) the saturation moment will be $\sim \alpha \exp(-\delta/2T_N)$ and hence decreases exponentially with T_N . This is the major difference from the usual local moment AF where the saturation moment is independent of T_N .

The signature of singlet-singlet induced moment magnetism is the existence of a paramagnetic excitation that grows soft on approaching T_N . The excitation spectrum is obtained from the dynamical local moment susceptibility

$$\chi_{ij;\alpha\beta}^{\lambda\mu}(\tau) = -\langle T \{ J_{i\alpha}^{\lambda}(\tau) J_{j\beta}^{\mu}(0) \} \rangle \quad (83)$$

where i,j = lattice site, λ, μ = AF sublattices (A,B) and α, β = x,y,z denotes cartesian components. Within RPA its Fourier transform is obtained as

$$\chi(\mathbf{q}, \omega) = [1 - \mathbf{u}(\omega) \mathbf{J}(\mathbf{q})]^{-1} \mathbf{u}(\omega) \quad (84)$$

Here $\chi(\mathbf{q}, \omega)$ and the single ion dynamical susceptibility $\mathbf{u}(\omega)$ are tensors in both sublattice (A,B) and transverse (xy) cartesian coordinates. The poles of eq. (84) determine the collective excitations of 5f-local moments. In the paramagnetic phase they are given by the *magnetic exciton* dispersion

$$\omega_E(\mathbf{q}) = \delta [1 - \frac{\alpha^2 J(\mathbf{q})}{2\delta} \tanh \frac{\beta}{2} \delta] \quad (85)$$

The physical origin and nature of magnetic excitons is illustrated in the inset of fig. 38 and described in the caption. When T_N is approached the exciton energy at \mathbf{Q} (PM zone boundary or AF zone center) becomes soft as a precursor to the appearance of the AF moment according to

$$\omega_E(\mathbf{Q}, T) = \frac{1}{2} \left(\frac{\delta}{T_N} \right)^2 \left(\xi - \frac{1}{\xi} \right) (T - T_N) \quad (86)$$

Below T_N an induced staggered moment leading to two magnetic sublattices appears. Its saturation value is given by eq. (82). Then $\mathbf{Q} = (0, 0, \frac{1}{2})$ becomes the center of the new AF Brillouin zone $[\frac{\pi}{2c}, -\frac{\pi}{2c}]$. In reality the softening of $\omega_E(\mathbf{Q}, T)$ will be arrested at a finite value at T_N by Curie type contributions to the static susceptibility which contribute to the AF instability but not to the exciton dispersion. Therefore a magnetic excitation gap at \mathbf{Q} will appear. Below T_N the dispersion is somewhat modified due to the effect of the molecular field, however for ξ only marginally above the critical value this modification is not important. This is indeed the case for the dual model of UPd₂Al₃ where $T_N/\delta = 0.22$ and hence $\xi = 1.015$. The magnetic exciton dispersion including the molecular field and exchange anisotropy has been derived (Thalmeier 2002) and compared to the experimental results obtained in INS experiments (Mason and Aeppli 1997). In this work the excitations were measured up to 10 meV in the whole BZ and it was found that well defined propagating modes exist along the hexagonal c*-axis. For wave vector in the hexagonal

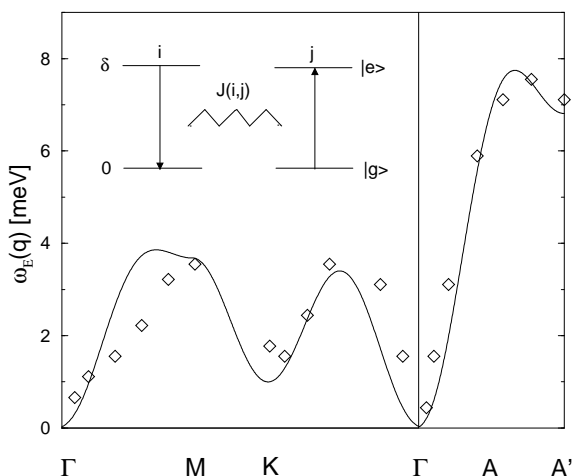


Figure 38. Magnetic exciton dispersion of UPd_2Al_3 in the AF BZ. The diamonds are data from Mason and Aeppli (1997). The solid line is a calculation using a generalized version of eq. (85) with an appropriate model for the exchange function $J(\mathbf{q})$ (Thalmeier (2002)). The inset illustrates the principle of magnetic (Frenkel-) exciton propagation: A CEF singlet-singlet excitation (δ) propagates between lattice sites i, j through the action of intersite exchange $J(i,j)$ and thereby acquires a dispersion $\omega_E(\mathbf{q})$.

plane $\perp c^*$ the line width of excitations was found to be much bigger. No excitation gap at the AF zone center \mathbf{Q} could be identified in these early experiments. This conclusion had to be revised in later high resolution experiments around \mathbf{Q} as discussed below. The comparison to the theoretical calculation using a parametrized exchange function $J(\mathbf{q})$ was given in Thalmeier (2002) and is shown in fig. 38. There the extended BZ was used which allows one to plot only the acoustic mode. It should be mentioned that it is not clear whether the dip at the K-point is realistic because the line width of magnetic excitons becomes rather large.

The damping of magnetic exciton modes has two sources: (i) intrinsic dynamical effects in the localised moment system beyond RPA, e.g. damping by thermal fluctuations in the singlet occupation. (ii) extrinsic damping due to the coupling to conduction electrons described by the last term in eq. (78). For low temperatures the latter is the dominating part. In addition it leads to a renormalized exciton mode frequency. Both effects can be described in extending the previous RPA approach including the last coupling term in eq. (78). This leads to coupled RPA equations (Buyers and Holden 1985), the solution for the localised dynamical susceptibility is given by

$$\chi(\mathbf{q}, \omega) = \frac{u(\omega)}{1 - J_{ff}(\mathbf{q})u(\omega) - I^2 u(\omega)\chi_e(\omega)} \quad (87)$$

with

$$u(\omega) = \frac{\alpha \langle S \rangle}{\delta - \omega} \quad \text{and} \quad \chi_e(\omega) = \frac{1}{i\omega - \Gamma} \quad (88)$$

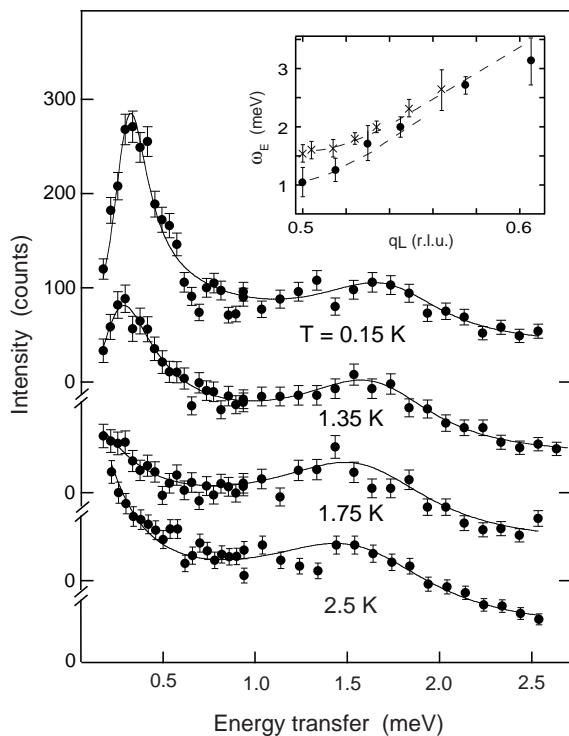


Figure 39. INS spectrum for various temperatures above and below $T_c = 1.8$ K (Sato et al. 2001). The momentum transfer was varied around the AF point $\mathbf{q} = (0,0,q_L)$. The solid line is the result of a calculation using eq. (87) from which the magnetic exciton energy $\omega_E(\mathbf{q})$ is determined for every \mathbf{q} . The result is shown in the inset for $T = 2.5$ K (crosses) and $T = 0.15$ K (circles).

where $u(\omega)$ is the single ion local moment susceptibility and $\chi_e(\omega) \equiv \chi_e(\mathbf{Q}, \omega)$ is the low frequency conduction electron susceptibility at $\mathbf{q} = \mathbf{Q}$ and Γ is a phenomenological damping rate. If one neglects its imaginary part and uses $\chi_e(\mathbf{q}) \sim \Gamma^{-1}$ for $\mathbf{q} \simeq \mathbf{Q}$ then, with eqs. (88), (80) the poles of eq. (87) again lead to the undamped magnetic exciton dispersion $\omega_E(\mathbf{q})$ of eq. (85). Inclusion of the imaginary part of $\chi_e(\omega)$ leads to a shift of the mode frequency and a damping. For a large coupling constant I , a part of the spectral weight of the magnetic exciton is shifted to low energies leading to an additional quasielastic peak.

The INS intensity is then proportional to the *localised* 5f-dynamical structure factor $S(\mathbf{q}, \omega) = (1+n(\omega))Im\chi(\mathbf{q}, \omega)$ where $n(\omega) = (\exp(\beta\omega) - 1)^{-1}$ is the Bose factor. The experimental high resolution magnetic INS intensity for wave vectors close to \mathbf{Q} as obtained by (Sato et al. 1997, Sato et al. 1997a, Bernhoeft et al. 1998) is shown in fig. 39. At the AF vector \mathbf{Q} above T_c (2.5 K) one can observe a strongly broadened inelastic peak at around 1.5 meV which is interpreted as the (upward) shifted magnetic exciton energy. In addition, as a signature of the strong coupling to conduction electrons one observes a quasielastic peak around $\hbar\omega \simeq 0$. The full line is a calculation of $S(\mathbf{Q}, \omega)$ using eq.

(87) for $\chi(\mathbf{q}, \omega)$ and taking I and $\omega_E(\mathbf{Q})$ as adjustable parameters. The INS intensity was also measured for other wave vectors close to \mathbf{Q} along c^* . Repeating the same fitting procedure one may determine the *unrenormalized* magnetic exciton dispersion $\omega_E(\mathbf{q})$ which is shown in the inset of fig. 39. Obviously the magnetic excitons have a gap at the AF zone center of about 1 meV. As mentioned before in the original experiments (Mason and Aeppli 1997) this gap was not identified due to insufficient resolution. In the singlet-singlet CEF model, even including a uniaxial anisotropy of the exchange, this relatively large gap cannot be explained. Its most probable origin is an arrested softening of $\omega_E(\mathbf{Q}, T)$ due to higher lying CEF states.

In fig. 39 another important feature is obvious: As temperature is lowered below $T_c = 1.8$ K the quasielastic peak evolves into a low energy inelastic peak. This is due to the appearance of the SC quasiparticle gap function $\Delta(\mathbf{k})$ which possibly may have node lines or points. Its influence on the conduction electron susceptibility may be described in a simple manner by shifting the diffusive pole at $-i\Gamma$ in $\chi_e(\omega)$ to $-i\Gamma + \Delta_{av}$ where the real part corresponds to the \mathbf{k} -averaged SC gap. The calculated intensity in the SC phase (e.g. at $T = 0.15$ K) is then again shown as a full line from which the size of Δ_{av} may be extracted. The result $\Delta_{av} \simeq \omega_E(\mathbf{Q})$ shows that magnetic exciton energy and SC gap are almost degenerate, which means that there will be a strong mixing of magnetic excitons with SC quasiparticle excitations. This explains why the lower peak appears with a large intensity.

4.2.5. Magnetic exciton anomalies in quasiparticle tunneling spectra

The near degeneracy of SC gap and magnetic exciton energy suggests that the latter might play a role in the formation of Cooper pairs in UPd_2Al_3 . Knowing only the INS results this would only be a hypothesis. However in a breakthrough experiment (Jourdan et al. 1999) the first SC quasiparticle tunneling in a HF system by using epitaxially grown UPd_2Al_3 was achieved. This experiment is complementary to INS measurements as it probes the itinerant 5f-electrons. The resulting tunneling spectra which ideally are proportional to the SC quasiparticle DOS are shown in fig. 40. The tunneling current is parallel to the c -axis and a real gap is seen in dI/dV in this direction. Therefore, if node lines of $\Delta(\mathbf{k})$ exist they should be perpendicular to the c -axis at k_z positions where the velocity $v_c(k_z)$ vanishes. The most striking result is the presence of typical ‘strong coupling anomalies’ around 1 meV which are well known from ordinary electron-phonon superconductors like Pb. These anomalies are connected to the frequency spectrum of the exchanged boson which is responsible for the formation of Cooper pairs in UPd_2Al_3 . The Debye energy of UPd_2Al_3 $k\theta_D = 13$ meV is much too large to be connected with the observed modulation around 1 meV, however it agrees perfectly with the magnetic exciton energy $\omega_E(\mathbf{Q})$ found by INS (inset of fig. 39). Furthermore the average gap energy and mode energy determined in INS are of the same order. This leads to the conclusion that UPd_2Al_3 is a magnetic exciton mediated strong coupling superconductor. This is the first time that a non-phononic mechanism for superconductivity has been proven in a direct way by identifying the non-phononic boson (magnetic exciton) that provides the ‘glue’ for the formation of Cooper pairs in UPd_2Al_3 . These arguments can be made more quantitative by using Eliashberg theory to calculate the SC quasiparticle DOS. The retarded effective potential due to magnetic exciton exchange can be described by a

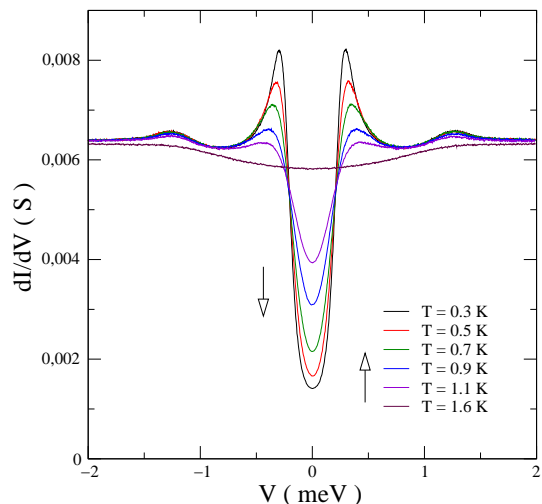


Figure 40. Differential conductivity dI/dV of a UPd_2Al_3 - AlO_x -Pb tunneling contact as function of the voltage across the tunneling contact for different temperatures (Jourdan et al. 1999). At low temperatures dI/dV is proportional to the quasiparticle DOS.

factorized ansatz

$$V_E(\mathbf{q}, \omega) = \frac{V_0 \omega_0}{(\omega - \omega_E(\mathbf{Q}))^2 + \omega_0^2} f(\mathbf{k}) f(\mathbf{k}') \quad (89)$$

which exhibits a maximum at the observed exciton frequency $\omega_E(\mathbf{Q})$ with a width ω_0 and strength V_0 . Here $\mathbf{q} = \mathbf{k}' - \mathbf{k}$ and $f(\mathbf{k})$ is the form factor which describes the \mathbf{k} -dependence of the superconducting singlet gap function $\Delta(\mathbf{k}) = \Delta f(\mathbf{k})$. For an isotropic conventional e-p superconductor $f(\mathbf{k}) \equiv 1$. As explained in the next section in UPd_2Al_3 the gap function should have a node line perpendicular to the c -axis. For tunneling current along c the tunneling DOS can be determined from the *isotropic* Eliashberg equations using eq. (89) if one replaces $f(\mathbf{k})$ by the averaged constant $\langle f(\mathbf{k})^2 \rangle_{FS}^{1/2}$ which may then be absorbed into the coupling strength V_0 that is adjusted to obtain the experimental T_c . The result of this analysis is shown in fig. 41 which nicely explains the experimental results in fig. 40, especially: (i) The width of the gap does not depend much on temperature but is rather filled up with increasing temperature. This is characteristic for a strong coupling superconductor, the ratio $\Delta/2T_c = 5.6$ obtained here is rather high and agrees well with the ratio $\Delta/2T_c = 6$ obtained previously from the analysis of INS spectra. (ii) In the calculated tunneling DOS of fig. 41 typical modulations above the gap due to the retardation of the potential in eq. (89) appear at a voltage that corresponds to the magnetic exciton energy at \mathbf{Q} which is about 1 meV.

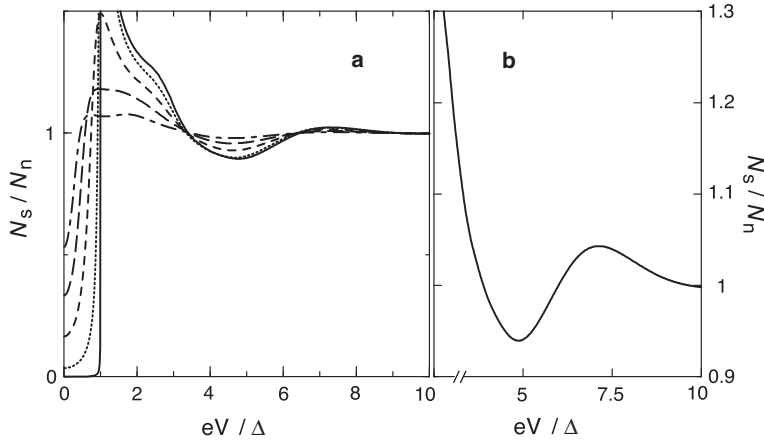


Figure 41. Calculated tunneling DOS N_s using isotropic Eliashberg equations and the retarded potential of eq.(89). N_n is the DOS in the normal state. (a) The various lines correspond to temperatures $T/T_c = 0.25, 0.6, 0.9, 0.95$ from top to bottom at $eV/\Delta = 2$. (b) Enlarged strong coupling anomaly due to magnetic exciton exchange for $T = 0.25T_c$ (Sato et al. 2001).

4.2.6. Possible symmetries of the superconducting order parameter

The existence of node lines of $\Delta(\mathbf{k})$ in UPd_2Al_3 was suggested by various thermodynamic properties discussed previously. Other evidence was proposed by Bernhoeft (2000) where it is claimed that the symmetry property $\Delta(\mathbf{k} \pm \mathbf{Q}) = \pm\Delta(\mathbf{k})$ has to be fulfilled to explain the large intensity of the low energy quasiparticle-like peak in fig. 39. This implies a node line orthogonal to the c -axis which is compatible the appearance of a gap in the c -axis tunneling geometry as used for fig. 40. In the ansatz of eq. (89) the energy and momentum dependences are factorized and therefore the form factor $f(\mathbf{k})$, i.e. gap function symmetry is put in by hand. Considering the presence of a strong AF ordered moment \parallel x -axis the appropriate symmetry group is orthorhombic D_{2h} . The simplest spin singlet even parity irreducible representation appropriate for the FS with cylindrical symmetry (fig. 37) has the form

$$\Delta(\mathbf{k}) = \Delta \cos k_z \quad \text{with} \quad A_{1g}(\Gamma_1^+) - \text{symmetry} \quad (90)$$

This gap function is independent of k_x and k_y . A more general $\Delta(\mathbf{k})$ with the same symmetry can be obtained by multiplying eq.(90) with any fully symmetric function $f_{\Gamma_1^+}(k_x, k_y)$. $\Delta(\mathbf{k})$ has the required behaviour under the transformation $\mathbf{k} \rightarrow \mathbf{k} \pm \mathbf{Q}$ and it has a node line at the AF zone boundary $k_z = \pm \frac{1}{2}Q_z = \pm \frac{\pi}{2c}$. A theoretical investigation of possible gap functions based on a nonretarded weak coupling theory of the magnetic exciton mediated pair potential was undertaken in Thalmeier (2002). It was found that due to the CEF-anisotropy and the action of the AF local moment order the degeneracy of odd parity triplet states is lifted and one of them would be favored against the above even parity singlet state. However this may be due to the neglect of retardation which is not a good approximation for UPd_2Al_3 as evident from the previous discussion. As

mentioned before Pauli limiting of H_{c2} and Knight shift reduction below T_c favor an even parity A_{1g} (singlet) state.

As in the borocarbides the gap function will be modified by the background magnetic order due to the reconstruction of Bloch states close to the magnetic Bragg planes $k_z = \pm \frac{1}{2}Q_z$. The AF modified gap function for the even parity state is given by eq. (117) which in the present case reduces to

$$\Delta(\mathbf{k}) = \Delta \cos k_z \left(\frac{\cos^2 k_z}{\lambda_{AF}^2 + \cos^2 k_z} \right)^{\frac{1}{2}} \quad (91)$$

Here the dimensionless interaction parameter $\lambda_{AF} = (I\langle J \rangle_0)/(\alpha W_{\parallel})$ describes the strength of the AF influence on $\Delta(\mathbf{k})$. It is interesting to note that despite the presence of a node line the above order parameter is fully symmetric (A_{1g}) because it is invariant under all symmetry transformations of the *magnetic* unit cell. Thus in a strict sense UPd_2Al_3 cannot be called a superconductor with unconventional gap symmetry, although the novel magnetic exciton mechanism certainly is unconventional. Various possible nodal structures in addition to eq. (90) have been discussed by Thalmeier and Maki (2002) in the context of magnetothermal properties.

4.2.7. UNi_2Al_3 : a possible triplet superconductor

The HF superconductor UNi_2Al_3 (Geibel et al. 1991) ($\gamma = 120 \text{ mJ/K}^2 \text{ mole}$) is isostructural to its hexagonal sister compound UPd_2Al_3 (fig. 35) but it has rather different physical properties. It exhibits an incommensurate SDW below $T_m = 4.6 \text{ K}$ ($\mu = 0.2 \mu_B$) with a modulation wave vector $\mathbf{Q}_m = (0.39, 0, 0.5)$, like in UPd_2Al_3 the moments are pointing to n.n. along the a direction of the hexagonal plane. Superconductivity sets in below $T_c = 1.2 \text{ K}$ and coexists with magnetic order. The T-dependence of $1/T_1$ in NMR (Kyogaku et al. 1993) and the small entropy release of $\Delta_S = 0.12R\ln 2$ at T_m (Tateiwa et al. 1998) points to an itinerant character of magnetic order in contrast to UPd_2Al_3 ($\Delta_S = 0.67R\ln 2$) which exhibits local moment magnetism of the induced type with large ordered moment. This view is supported by INS experiments (Gaulin et al. 2002) which do not show any evidence for propagating collective modes in the SDW state unlike the magnetic exciton mode discussed previously for UPd_2Al_3 . The magnetic excitation spectrum in UNi_2Al_3 consists of quasielastic spin fluctuations for all wave vectors and its energy width of about 6 meV corresponds to the coherence temperature $\sim 80 \text{ K}$ associated with the γ value. For temperatures not too close to T_m the spin fluctuations are centered around odd multiples of the commensurate AF wave vector $\mathbf{Q} = (0, 0, 0.5)$ and also extending along ridges in q_x - direction.

From the spin fluctuation spectrum of UNi_2Al_3 observed in INS which is located around an AF Bragg point one might expect it should be a textbook example of spin fluctuation mediated superconductivity. However as in the case of UPt_3 the spin singlet pairing predicted by AF spin fluctuation type theories (Miyake et al. 1986) is probably not realised. According to the ^{27}Al -Knight shift measurements of (Ishida et al. 2002) which did not observe any drop in the spin susceptibility below T_c UNi_2Al_3 should have a spin triplet SC order parameter. This is supported by the observed lack of Pauli paramagnetic limiting effect on $H_{c2}(T)$ (Sato et al. 1996). As in the case of UPd_2Al_3 the position of gap nodes is not known with certainty, but NMR results suggest the presence of a node line

in UNi_2Al_3 as in UPd_2Al_3 . In the simplest scenario then the latter might correspond to the singlet gap function of eq. (90) while the former has one of the triplet gap functions.

$$\mathbf{d}(\mathbf{k}) = \Delta \hat{d} \sin k_z \quad (92)$$

With the possibilities $\hat{d} = \hat{x}, \hat{y}, \hat{z}$ due to the AF orthorhombic symmetry. These gap functions have all an equatorial node line at $k_z = 0$. Confirmation of the node structure has to await the results of angle resolved magnetotransport or specific heat measurements in the vortex phase and for a confirmation of the spin state the Knight shift measurements on high quality single crystals are necessary.

4.3. Ferromagnetism and Superconductivity in UGe₂

The possibility of coexisting ferromagnetism (FM) and superconductivity was first considered by Ginzburg (Ginzburg 1957) who noted that this is only possible when the internal FM field is smaller than the thermodynamic critical field of the superconductor. Such a condition is hardly ever fulfilled except immediately below the Curie temperature T_C where coexistence has been found in a few superconductors with local moment FM and $T_C < T_c$ such as ErRh₄B₄ and HoMo₆S₈. If the temperature drops further below T_C the internal FM molecular field rapidly becomes larger than H_{c2} and SC is destroyed. The reentrance of the normal state below T_C has indeed been observed in the above compounds. The only compound known sofar where local moment FM coexists homogeneously with SC for all temperatures below T_c is the borocarbide compound ErNi₂B₂C (Canfield and Bud'ko 1996) (sect.5). The competition between FM and superconductivity becomes more interesting if FM order is due to itinerant electrons which also form the SC state. In Hartree-Fock approximation the Stoner condition for the reduced interaction constant $\lambda = IN(0) = 1-S^{-1} \geq 1$ (S = Stoner parameter, I = exchange constant) of conduction electrons determines the existence of itinerant FM order. If the interaction is slightly above the critical value $\lambda_c = 1$ one has weak FM order such as in ZrZn₂ with large longitudinal ferromagnetic spin fluctuations. Fay and Appel (1980) have shown that in this case p-wave superconductivity may actually be mediated by the exchange of FM spin fluctuations and coexist with the small FM moments. According to this theory p-wave superconductivity should exist on both (FM and PM) sides of the critical value $\lambda_c = 1$ for some range of the interaction parameter λ . Until recently this remained only a theoretical scenario. The discovery of unconventional superconductivity under pressure in the itinerant FM UGe₂ (Saxena et al. 2000) and later for FM URhGe (Aoki et al. 2001) and the 3d FM ZrZn₂ (Pfleiderer 2001) under ambient pressure has opened this field to experimental investigation.

It became quickly clear however that the physics of UGe₂ is not as simple as suggested by the FM spin fluctuation model. Firstly the maximum of SC T_c occurs at a pressure where the FM moment per U is still $1\mu_B$ as compared to $1.5\mu_B$ at ambient pressure thus λ_c should still be far from the critical value where spin fluctuations are important. Secondly the SC phase diagram is not approximately symmetric around the critical value as expected but the region of SC lies completely inside the FM phase. This problem has been further investigated by resistivity measurements (Huxley et al. 2001) where an additional phase within the FM region appeared at lower temperature witnessed by a resistivity anomaly. Its critical temperature $T_x(p)$ precisely hits the maximum of the SC $T_c(p)$ curve as seen in fig. 43. The x-phase has been associated with a combined CDW/SDW transition. This is also suggested by electronic structure calculations (Shick and Pickett 2001) which show nesting features of the Fermi states. In addition the main FS sheet consists mostly of majority spin ($m_s = \uparrow$, $m_l = 0$) electrons. Therefore the SC pairs must have triplet character. It is suggestive that the unconventional Cooper pairing then appears close to the quantum critical point of the alledged CDW/SDW transition and therefore T_c should rather be associated with the T_x transition instead of the FM transition at T_C . However sofar no indication of a CDW/SDW order parameter below T_x has been identified in neutron diffraction (Kernavanois et al. 2001) and the subject remains open.

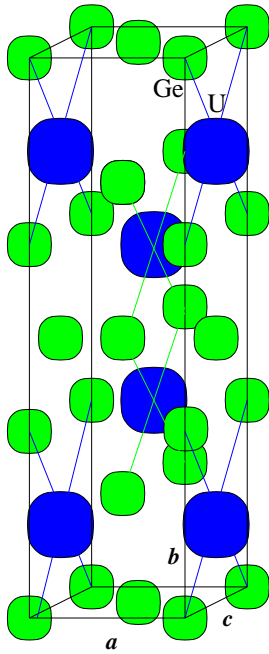


Figure 42. Conventional orthorhombic unit cell of UGe_2 with lattice parameters given by $a = 3.997\text{\AA}$, $b = 15.039\text{\AA}$ and $c = 4.087\text{\AA}$. U atoms (large spheres) form zig-zag lines along a .

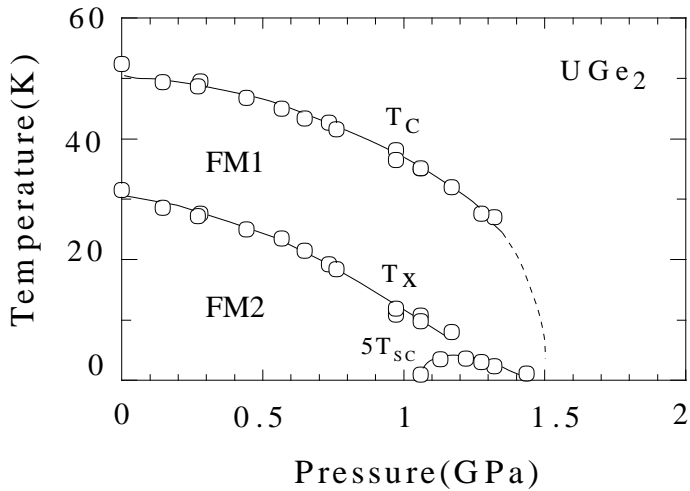


Figure 43. pressure - temperature phase diagram of UGe_2 from resistivity measurements. T_C = FM Curie temperature, T_x = boundary of new x-phase. T_{SC} = superconducting transition temperature (note scale enhancement) with optimum pressure at $p_m = 1.25$ GPa. Ferromagnetic FM1 and FM2 regions have different moments ($\simeq 1 \mu_B$ and $1.45 \mu_B$ at low T respectively) (Kobayashi et al. 2001).

Various theoretical scenarios for UGe_2 have been formulated. In the context of Ginzburg-Landau theories the symmetries of possible SC order parameters and their coupling to the FM have been discussed, e.g. (Machida and Ohmi 2001, Mineev 2002). However, as already mentioned in the context of UPt_3 the predictive power of such theories is limited. The traditional approach of microscopic theories invoking FM spin fluctuations has been extended beyond Hartree Fock with the inclusion of mode coupling terms in order to explain the asymmetric phase diagram around the critical coupling strength (Kirkpatrick et al. 2001). The new aspect of the T_x transition line was introduced by Watanabe and Miyake (2002) who, in order to comply with the experimental evidence from Kernavanois et al. (2001), interpret it as a crossover line into a region of enhanced SDW/CDW fluctuations rather than an ordered phase. When $T_x(p)$ approaches zero these fluctuations then would mediate formation of a triplet p-wave SC state.

4.3.1. Electronic structure and band magnetism

The itinerant FM UGe_2 crystallizes in the base-centered orthorhombic ZrGa_2 type structure (Cmmm) which is shown in fig. 42. It may be viewed consisting of antiphase zig-zag U chains running along the a-axis. This is also the easy axis for the FM moments ($\mu = 1.43\mu_B$ per formula unit) below the Curie temperature of $T_C = 52$ K at ambient pressure. Magnetisation and susceptibility are extremely anisotropic (Onuki et al. 1992) corresponding to almost Ising like behaviour of U-moments. The specific heat coefficient is $\gamma = 32$ mJ/molK² which corresponds to an enhancement factor of 2.7 as compared to the band mass (Shick and Pickett 2001). This points to some degree of mass renormalization by dynamic correlation effects. Individual masses observed in dHvA experiments exhibit an enhancement factor of $m^*/m \simeq 15 - 25$ compared to the free electron mass. Therefore UGe_2 is an itinerant 5f metal with sizable correlation effects but has an order of magnitude smaller effective masses than real U-heavy fermion metals.

The electronic band structure of UGe_2 has first been calculated within the LDA+U approach (Shick and Pickett 2001) where $U \simeq 0.7$ eV is a strongly screened on-site Coulomb interaction that was fitted to reproduce the proper FM ground state moment of $1.43\mu_B$. On the other hand this value is too small to reproduce the observed photoemission spectrum. The calculated Fermi surface has a main sheet which mostly consists of ($m_l=0$, $m_s = \uparrow$)-states. Bands crossing the Fermi energy have mostly U-5f majority spin character, indicating almost complete polarisation, i.e. strong FM. The LDA+U Fermi surface also displays a nesting feature for $\mathbf{Q} = (0.45, 0, 0)$ (in r.l.u.) which is due to bands that have little dispersion along b, i.e. perpendicular to the zig-zag U chains. The proper easy a axis for FM moment and a strong magnetocrystalline anisotropy of the moment due to spin orbit coupling was also correctly found. These calculations describe the ambient pressure strong band ferromagnetism in UGe_2 which is still far from the superconducting pressure region with reduced moments.

A more recent theoretical investigation of the collapse of the FM state under hydrostatic pressure and the simultaneous appearance of another instability has been given in Yaresko and Thalmeier (2003). In this study a relativistic LSDA calculation was performed for isotropically compressed lattice constants simulating the application of hydrostatic pressure p. The experimental lattice constants corresponding to $p = 0$ are given in fig. 42. In agreement with the experimental results a FM ground state with the a-axis

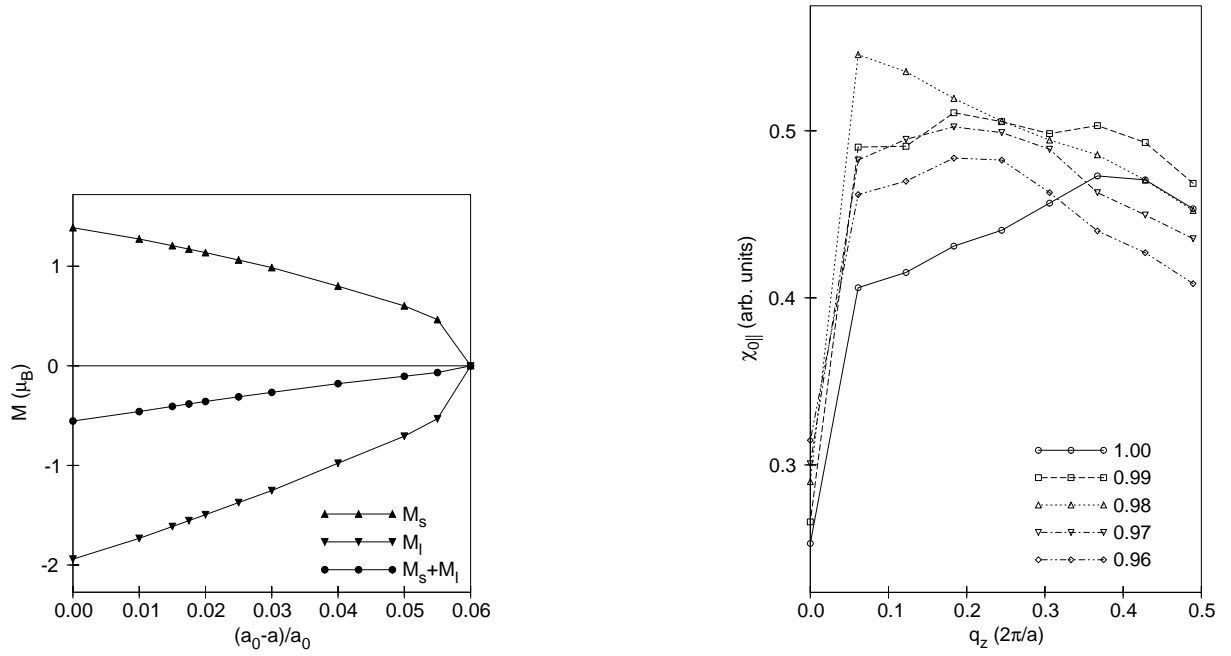


Figure 44. Left panel: calculated pressure dependence of spin (M_S), orbital (M_L) and total moment (M_S+M_L). Right panel: pressure dependence of calculated longitudinal susceptibility. The step drop at $q_z=0$ is caused by the loss of intra-band transitions due to finite q_z resolution. The enhancement of $\chi_{0||}$ under pressure for small q_z suggests the evolution of a SDW instability within the FM phase (Yaresko and Thalmeier 2003).

as easy axis is obtained. However the U spin ($-1.39 \mu_B$) and orbital ($1.94 \mu_B$) magnetic compensate partly leading to a total moment of only $0.55 \mu_B$ significantly smaller than the experimental value ($1.43 \mu_B$). This was the main reason for performing the above mentioned LDA+U calculation. However the LSDA calculation reproduces quite well the angular dependence of the cross section of a major FS sheet with an area of $F \simeq 9$ kT. The calculated cyclotron masses are about 8 m and smaller than the experimental values of 15.5 m. This confirms that UGe₂ has itinerant 5f-electrons with only moderately strong correlations.

The hydrostatic pressure simulation shows that FM U moments decrease continuously with pressure until at compression factor $x = 0.94$ only a nonmagnetic solution is obtained (fig. 44). The magnetocrystalline anisotropy energy $E_{\mathbf{M}\parallel a} - E_{\mathbf{M}\parallel b}$ also decreases upon compression. On the other hand the DOS $N(0)$ first increases to a maximum at $x \sim 0.98$ and then decreases again. In order to check whether a tendency to a CDW/SDW instability exists which might be related to the empirical observation of the T_x phase boundary inside FM the staggered static susceptibility within LSDA has been calculated (Yaresko and Thalmeier 2003). It is given by

$$\chi_{0\alpha}(\mathbf{q}, 0) = \sum_{ij, \mathbf{k}} [f(\epsilon_{i\mathbf{k}}) - f(\epsilon_{j\mathbf{k}+\mathbf{q}})] \frac{|M_{i\mathbf{k}, j\mathbf{k}+\mathbf{q}}^\alpha|^2}{\epsilon_{i\mathbf{k}} - \epsilon_{j\mathbf{k}+\mathbf{q}}} \quad (93)$$

where $\epsilon_{i\mathbf{k}}$ are the band energies, $M_{i\mathbf{k}, j\mathbf{k}+\mathbf{q}}^\alpha$ are the transition matrix elements ($\alpha = \parallel, \perp$ \mathbf{M}) and $f(\epsilon)$ is the Fermi function. The q_z wave-number dependence of $\chi_{0\perp}$ and $\chi_{0\parallel}$ has been calculated as function of the lattice compression. Whereas $\chi_{0\perp}(q_z)$ shows monotonic decrease with compression $\chi_{0\parallel}(q_z)$ is very sensitive to lattice constant change, it develops a strong enhancement at small wave vector at the same intermediate compression $x = 0.98$ where $N(0)$ also is at its maximum. This is an indication that for an intermediate compression (smaller than the critical compression $x = 0.94$ where FM vanishes) UGe₂ has a tendency to develop a long wavelength longitudinal SDW-like instability. It is possible that the tendency towards instability for the susceptibility associated with an unconventional SDW is even stronger. However it should be noted that the susceptibility enhancement does not correspond to any obvious nesting in the FS sheets obtained in LSDA calculations. This raises the question whether the observed nesting feature in the LDA+U FS of Shick and Pickett (2001) has a real physical significance to the alleged hidden order phase.

4.3.2. Coexistence of FM order and superconductivity under pressure

The experimental phase diagram of FM collapse under pressure and simultaneous appearance of superconductivity is shown in fig. 43. The critical pressure for disappearance of FM order is $p_{c2} = 16 - 17$ kbar. The SC phase appears between $p_{c1} = 10$ kbar and $p_{c2} = 16$ kbar which is also the critical pressure for the FM-PM transition. The critical temperature $T_x(p)$ of the x-phase hits the maximum of $T_c(p)$ at the optimum pressure $p_m = 12.5$ kbar. As mentioned before the nature of the order parameter in the x-phase remains elusive. The coincidence of maximum T_c with vanishing x-phase order parameter suggests that the collective bosonic excitations of the x-phase which supposedly become soft at p_m mediated superconductivity and not quantum critical FM spin fluctuations which are absent due to the persisting large FM molecular field. Associated with $T_x(p)$

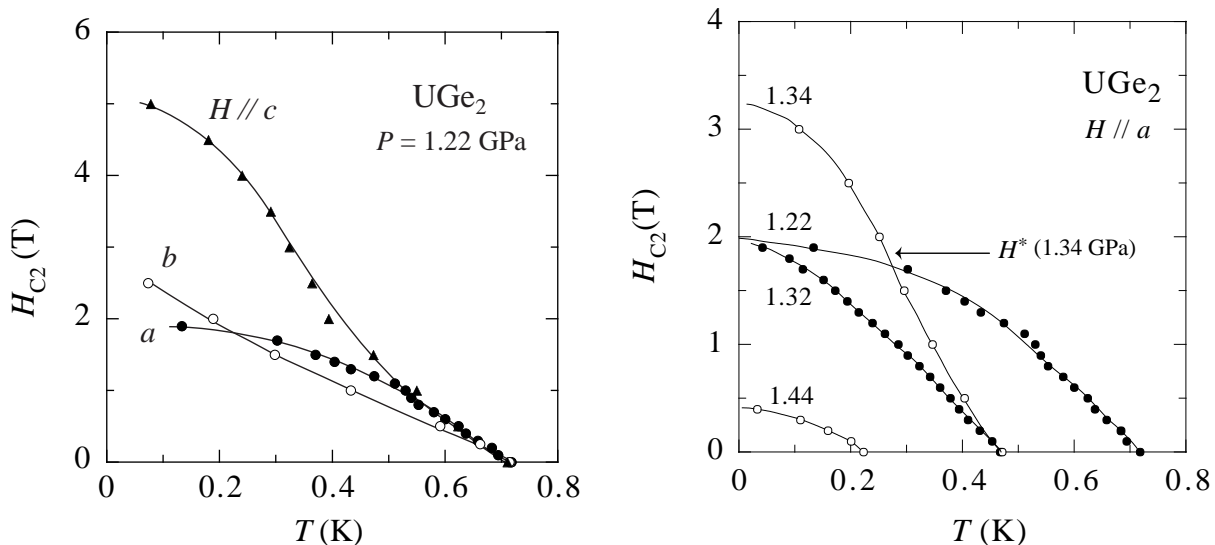


Figure 45. Left panel: H_{c2} - curves for pressure close to p_m and field along the crystal axes. Right panel: H_{c2} for field parallel to easy a-axis at four different pressures below and above $p_m = 1.25$ GPa. Unusual H_{c2} at 1.34 GPa leads to SC reentrance as function of pressure for low temperature (Kobayashi et al. 2001).

phase boundary is an abrupt first order change of the magnetic moment $\mu(p)$ around p_m whose different size distinguishes the FM2 region ($\mu(0) \simeq 1.45 \mu_B$) from the FM1 region ($\mu(p_m) \simeq 1 \mu_B$) (Pfleiderer and Huxley 2002). The connection between SC and the x-phase is also witnessed by the anomalous upper critical field behaviour around p_m which displays a reentrance behaviour as function of pressure seen in fig. 45. Apparently close to the T_x line the superconducting state is strongly stabilized as shown by the dramatically increased value of $H_{c2}(0)$. The existence of phases with ‘hidden order parameters’ which show up in thermodynamic and transport coefficients but do not appear as spin- or charge-density modulations in neutron diffraction is not uncommon for U-compounds. As discussed in the next section URu_2Si_2 has a similar phase. Two kinds of proposals for such hidden order may be considered: (i) if the U 5f electrons have a partly localised character as in the latter case the hidden order may be of quadrupolar or more generally multipolar character. (ii) If 5f-electrons are strongly itinerant, as apparently in UGe_2 , one may have an unconventional density wave order parameter which has been introduced in sect. 2. These phases have \mathbf{k} -dependent gap functions which do not belong to identity representations as in the CDW/SDW case. This type of order has also been proposed for the yet unidentified x-phase in UGe_2 and its coexistence behaviour with FM and unconventional superconductivity was studied (Varelogiannis et al. 2003).

4.3.3. Theoretical scenarios for superconductivity in UGe_2

From the previous discussion of experimental evidence the superconducting mechanism via ferromagnetic fluctuations can be ruled out since the ferromagnetic polarization at p_m where T_c is largest is still 65% of the maximum value at ambient pressure (Pfleiderer

and Huxley 2002). Therefore models based on the FM quantum critical point scenario that follow the original work of (Fay and Appel 1980) are not relevant for UGe₂. On the other hand the phenomenological classification of possible SC order parameters based on Landau expansion of the free energy is simplified by the remaining large spin polarisation of conduction electrons, only spin triplet pairing is possible in order to avoid the effect of the large exchange field.

4.3.4. Symmetry properties of gap states and Ginzburg-Landau theory

Triplet pair states are characterised by the vector gap function $\mathbf{d}(\mathbf{k})$ defined in sect. 2. Due to the constraint of equal (pseudo-) spin pairing (i.e. $\Delta_{\uparrow\downarrow} \equiv 0$) the \mathbf{d} -vector is confined to the bc-plane perpendicular to the FM moment \mathbf{M}_0 which is parallel to the easy a-axis. Neglecting the small orthorhombicity of the ab-plane the gap function can be written as (Machida and Ohmi 2001, Fomin 2001)

$$\mathbf{d}(\mathbf{k}) = f(\mathbf{k})\boldsymbol{\eta} = f(\mathbf{k})(\hat{\mathbf{a}} + i\hat{\mathbf{b}}) \quad (94)$$

Here $\boldsymbol{\eta}=(\eta_x, \eta_y, \eta_z)=(1, i, 0)$ is the vector order parameter and $f(\mathbf{k})$ the orbital part which transforms as a representation of the (approximate) tetragonal group. As in the case of UPt₃ it is assumed that the pseudo spins describing the Kramers degeneracy of quasiparticle states are only weakly coupled to the orbital momentum, then $f(\mathbf{k})$ may belong to any tetragonal representation which have typical point or line node structures. Presently there is no experimental information on the nodes. The equal spin pairing state is nonunitary, i.e. it breaks time reversal symmetry. This property is directly enforced by the nearly complete FM polarisation. Therefore the Cooper pairs have a net spin moment $\mathbf{S} = i\mathbf{d}(\mathbf{k}) \times \mathbf{d}(\mathbf{k})^*$ which aligns with the ordered FM moment. In a Ginzburg Landau expansion of the free energy it is sufficient to consider only the aligned component $\eta_+ = \eta_x + i\eta_y$ and neglect $\eta_- = \eta_x^*$ because of the large \mathbf{M}_0 even around the critical pressure. The total GL functional should then only be expanded in terms of η_+ and should also not contain \mathbf{M}_0 explicitly except in the vector potential. One obtains (Machida and Ohmi 2001) for \mathbf{H} along the c - axis ($\perp \mathbf{M}_0$),

$$f_{GL} = \alpha_0(T - T_c)|\eta_+|^2 + \frac{1}{2}\beta|\eta_+|^4 + K_1\left(\frac{d\eta_+}{dx}\right)^2 + \left(\frac{2\pi}{\phi_0}\right)^2 K_2(M_0 + \mu_0 H)^2 x^2 |\eta_+|^2 \quad (95)$$

because in this case the magnetic induction in the FM state is given by $\mathbf{B}=(0,0,\mu_0 H + M_0)$. Similar expressions hold for \mathbf{H} along a- and b-axis. Minimization of eq. (95) leads to the critical field curves close to T_c . The term $\sim M_0^2|\eta_+|^2$ only renormalizes T_c . Then one obtains the upper critical fields $H_{c2}^a \sim (T_c - T)$ and $H_{c2}^{b,c} \sim (T_c - T)^{\frac{1}{2}}$. The remarkable root singularity for $H_{c2}^{b,c}$ at T_c is due to the presence of a finite FM moment. Experimentally the critical field curves are quite anomalous close to the optimal pressure p_m although different exponents for different field directions are not observed, the H_{c2}^c -curve, however, does show an anomalous strong upturn around $0.5T_c$ (Kobayashi et al. 2001), see fig. 45. In any case a proper theory of H_{c2} has to include the influence of the hidden order parameter close to maximum T_c (fig. 43). The symmetry considerations of this section gave some constraints one should expect to hold for the SC order parameter, however the simple Landau theory

approach only indicates that H_{c2} should behave anomalous, without being able to give a quantitative account close to the optimum T_c .

4.3.5. Microscopic approaches

Aside from the FM QCP scenarios now known to be irrelevant for UGe_2 (Pfleiderer and Huxley 2002) little theoretical investigation has been undertaken so far with the exception of Watanabe and Miyake (2002). This theory starts from the assumption that $T_x(p)$ represents the phase boundary of a coupled (conventional) CDW-SDW transition. Because of the strong background FM polarisation these two order parameters have to appear simultaneously. Inversely, if one is close to the critical pressure p_m their critical fluctuations will be coupled to fluctuations in the FM polarisation by a mode-mode coupling term in the free energy, which couples the amplitudes of FM, CDW and SDW fluctuations at the commensurate nesting vector \mathbf{Q} of a n.n.n tight binding model used for the majority bands of UGe_2 . The strong coupling theory for this mechanism has been used to calculate H_{c2} and apparently qualitative anomalies like those close to p_m (fig. 45) are obtained.

However, no evidence for CDW or SDW formation central to this theory has been seen below T_x so far. On the other hand in specific heat measurements a pronounced anomaly $\Delta C(T_x)$ at 1.15 GPa suggests that $T_x(p)$ is a real phase line (Tateiwa et al. 2003). This leads one to the natural suggestions that one should look for more general particle-hole pairing ('unconventional density wave') discussed in sections 2 and 4.4 as an alternative for the phase below T_x since they do not lead to charge or magnetic superstructures (Varelogiannis et al. 2003).

4.4. A case of ‘Hidden Order’ in URu₂Si₂

This moderate HF compound ($\gamma = 110$ mJ/moleK²) has mystified both experimentalists and theorists alike since the discovery of AF order at T_m and another still unidentified (‘hidden order’) phase at T_0 which both seem to appear at the same temperature $T_0 = T_m = 17.5$ K, at least for annealed samples. In addition the compound becomes a nodal superconductor below $T_c \simeq 1.2$ K (Palstra et al. 1985, Schlabitz et al. 1986, de Visser et al. 1986). The simple tetragonal AF order with wave vector $\mathbf{Q} = (0,0,\frac{\pi}{c})$ has tiny moments $\mu \simeq 0.02\mu_B$ along c -axis (Broholm et al. 1987, Walker et al. 1993) which are of the same order as in UPt₃. However, unlike in UPt₃, very large thermodynamic effects, e.g. in specific heat ($\Delta C/T_0 \simeq 300$ mJ/molK²), thermal expansion etc., occur which are hard to reconcile with the small ordered moments. The pronounced anomalies at T_0 were interpreted as evidence for the presence of a second ‘hidden order’ parameter which cannot be seen in neutron or x-ray diffraction. Many different types of models for hidden order have been proposed, where the 5f-electrons of URu₂Si₂ are considered as essentially localized (Santini and Amoretti 1994), or itinerant (Ikeda and Ohashi 1998) or, of dual nature (Okuno et al. 1998, Sikkema et al. 1996). In the former case local quadrupoles of the CEF states are supposed to show staggered order below T_0 akin to the many examples of such order in 4f-compounds. Quadrupolar order does not break time reversal symmetry and cannot be directly seen by neutron diffraction. The small dipolar moments are considered as an unrelated secondary order parameter with accidentally the same transition temperature. In the itinerant models the order parameter is due to an unconventional pairing in the particle-hole channel leading to an unconventional SDW which has vanishing moment in the clean limit and also does not break time reversal invariance. The small staggered moments may then be induced in the condensate due to impurity scattering. Finally in the dual models one assumes a localised singlet-singlet system in interaction with the itinerant electrons to cause induced moment magnetism with small moments but large anomalies.

In all models it was previously taken for granted that both the primary ‘hidden’ order parameter and AF order coexist homogeneously within the sample. However, hydrostatic and uniaxial pressure experiments (Amitsuka et al. 1999, Amitsuka et al. 2002) have radically changed this view, showing that the order parameters exist in different parts of the sample volume; the tiny AF moment is not intrinsic but due to the small AF volume fraction under ambient pressure. Applying hydrostatic pressure or lowering the temperature increases the AF volume fraction and hence the ordered moment until it saturates at an atomic size moment of $0.4\mu_B/U$. This means that the evolution of AF arises from the increase of AF volume with pressure rather than the increase of the ordered moment μ per U-atom. This interpretation is supported by the observation of a comparatively weak increase of T_0 with pressure (Amitsuka et al. 1999).

4.4.1. Electronic structure and 5f-states

Inelastic neutron scattering (Park et al. 2002) using the time-of-flight method has shown that the valence state in URu₂Si₂ is U³⁺ corresponding to 5f², judging from the observation of the ³H₄ → ³F₂ transition of this configuration. In tetragonal (D_{4h}) symmetry the ninefold degenerate ³H₄ multiplet should be split by the CEF potential into five singlets and two doublets. There is indeed an indication of four strongly broadened CEF

transitions at energies ranging from $\delta = 5$ meV to 159 meV. However, the data are not sufficient to determine the CEF potential and states. There is a transition at 49 meV which might be associated with the Γ_3 - Γ_5^1 transition from the Γ_3 ground state which has been invoked in the model of Santini and Amoretti (1994). Earlier, low energy triple axis INS (Broholm et al. 1991) has shown that the transitions have a considerable dispersion. In addition the c-axis susceptibility exhibits clear CEF anomalies from which a CEF level scheme has been derived (Santini and Amoretti 1994). However the result is not unique and the overall splitting obtained is by a factor two smaller as compared to the above INS results. In this analysis the low energy group of CEF states consists of three singlets shown in table 6.

Table 6

Model for low lying CEF states in URu_2Si_2 (tetragonal structure as in fig. 15). The complete CEF level system for concentrated URu_2Si_2 is comprised of five singlets (the low lying states are listed with ϵ and γ being adjustable parameters) and two doublets. The dilute ($x \ll 1$) $\text{Th}_{1-x}\text{U}_x\text{Ru}_2\text{Si}_2$ system may have a different single-ion CEF level scheme with a doublet ground state (Amitsuka et al. 1994).

symmetry	CEF-state	energy (meV)
Γ_3	$ 0\rangle = \frac{1}{\sqrt{2}}(2\rangle + -2\rangle)$	0
Γ_1^1	$ 1\rangle = \epsilon 4\rangle + -4\rangle + \gamma 0\rangle$	3.8
Γ_2	$ 2\rangle = \frac{1}{\sqrt{2}}(4\rangle - -4\rangle)$	9.6

The clear evidence for CEF states supports the view of mostly localised 5f-states in URu_2Si_2 . This raises the question of the origin of HF behaviour in this compound. The specific heat coefficient in the low temperature ordered (magnetic+hidden) phase is reduced to only a moderate $\gamma = 64$ mJ/molK², 40% of the paramagnetic value and only one tenth that of typical HF values. Magnetoresistance measurements have shown that URu_2Si_2 is a compensated metal without open orbits (Ohkuni et al. 1999). Three of the closed Fermi surface sheets have been determined by dHvA experiments (Ohkuni et al. 1999). Their moderately heavy masses are in the range $m^* = 8$ -25 m which are, however, still larger by a factor ten as compared to the LDA band masses. For a nonmagnetic 5f singlet ground state system as given in table 6 there is no Kondo mechanism to generate heavy quasiparticles. It is tempting to assume that rather the same mechanism as recently proposed for UPt_3 (Zwicknagl et al. 2002) and UPd_2Al_3 (Zwicknagl et al. 2003) is important: mass renormalization through virtual excitations within a pair of low lying 5f singlet states which leads to (White and Fulde 1981)

$$\frac{m^*}{m} = 1 + N(0) \frac{2\alpha^2}{\delta} \quad (96)$$

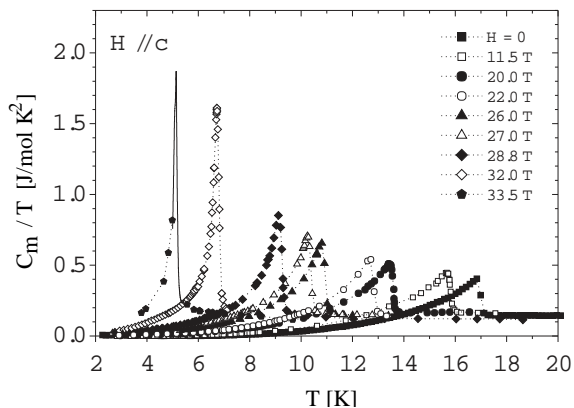


Figure 46. Magnetic specific heat C_m/T for fields up to 33.5 T (Jaime et al. 2002).

where $\alpha = \langle 0 | J_z | 1 \rangle$ is a dipolar matrix element and δ the singlet-singlet splitting. This is a simplified version of the mass renormalisation in eqs. (65),(66) with $\alpha \equiv 2a_{5f}|M|$. For several singlet pairs as in the present case one has a sum of such contributions. As discussed for UPt_3 for realistic parameters of U-compounds this mechanism may easily lead to a mass enhancement factor $\frac{m^*}{m} \simeq 10$ which would be an appropriate value for URu_2Si_2 .

4.4.2. Phase transitions, field and pressure dependence

The discrepancy between small AF moment in URu_2Si_2 and large thermodynamic anomalies has led to the postulation of a hidden (non-dipolar) order parameter. The crucial questions about its nature are: i) is the order primarily involving the localised 5f-CEF split states or the heavy itinerant conduction electrons. ii) Does the hidden order parameter break time reversal invariance or not. In the former case it may induce AF as secondary order parameter, in the latter the two order parameters are unrelated and their appearance at the same temperature $T_m = T_0$ has to be considered as accidental.

The continuous phase transition at T_0 is clearly seen in a large specific heat anomaly which becomes more pronounced in a magnetic field (fig. 46). The magnetic entropy contained in this peak is orders of magnitude larger compared to other magnetic U-compounds and alloys if one scales it with the AF ordered moment (Amitsuka et al. 2002) which proves that it must be connected to a hidden order parameter. A similar behaviour is seen in thermal expansion (Mentink et al. 1997) along a, however, the tetragonal symmetry below T_0 is preserved and no superstructure evolves (Kernavanois et al. 1999). The shape of specific heat and thermal expansion anomalies and their sharpening in an external field is reminiscent of antiferroquadrupolar (AFQ) phase transitions due to localised f-electrons known in the 4f-Ce-hexaborides and Tm-intermetallics. A quadrupolar order parameter is even under time reversal and is expected to be in competition with the dipolar AF order.

Pressure experiments have indeed found this competition. It is evident from the comparison of the pressure dependent ordered AF moment, and the position and intensity of ^{29}Si -NMR satellites. While the former increases continuously with pressure, the splitting

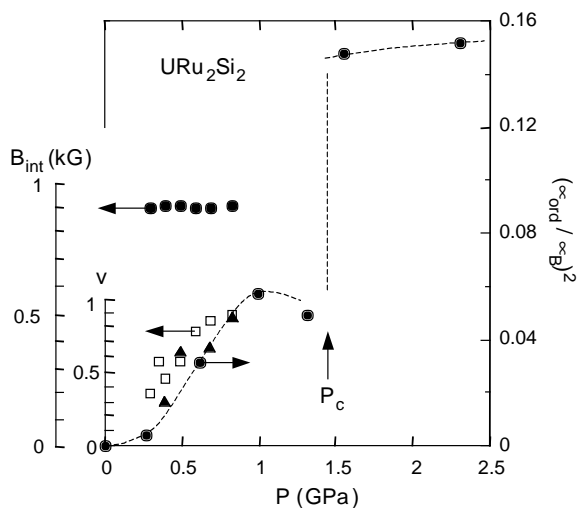


Figure 47. Evolution of AF Bragg intensity (full circles, right scale) with hydrostatic pressure. Full circles (leftmost scale) denote internal staggered field B_{int} from ^{29}Si NMR. Triangles and squares denote AF volume fraction v from the same experiment (Amitsuka et al. 2002).

which is proportional to the local 5f-moment is pressure independent, however, the split satellite intensity which is a measure of the AF volume fraction also increases with pressure (fig. 47). Analysis of these results show that the AF moment per magnetic U-site $\mu_{AF} \simeq 0.25\mu_B/U$ is not small. It is the small AF volume fraction at ambient pressure which leads to the small overall ordered moment of $0.03\mu_B$. As pressure increases the ordered moment also increases due to the increase in AF volume which continuously replaces the volume fraction with the hidden order. The replacement is complete at $p \simeq 1$ GPa. Somewhat above at p_c another phase transition takes place in the complete AF-phase leading to a sudden increase of the on-site U-moment, however we note that this has not been observed in magnetic x-ray diffraction experiments. The observed moderate increase of T_m with pressure (Amitsuka et al. 1999) is compatible with the observation of a pressure independent U-moment. Subsequent uniaxial pressure experiments (Yokoyama et al. 2002) have shown that only the [100] or [110] uniaxial pressure in the tetragonal plane leads to the increase of the AF volume fraction or destruction of the hidden order, whereas the [001] uniaxial pressure has little effect. This anisotropic behaviour under pressure suggests that the hidden order parameter is associated with the tetragonal fourfold symmetry plane.

4.4.3. Theoretical models: localised vs. itinerant

We shall not recount the many attempts to explain the broken symmetry states of URu_2Si_2 but rather concentrate on two typical examples that seem to be compatible with the recent important results of the pressure investigations just described.

AFQ order of local induced quadrupole moments

The competitive behaviour of AF and hidden order points to even time reversal sym-

metry of the latter. If one assumes that the localised 5f electrons are involved in the hidden order then the already mentioned AFQ order in the singlet CEF level scheme is the most obvious choice. This model was proposed by Santini and Amoretti (1994) and Santini (1998) and is also the most well studied one. It is an entirely localised 5f-model and is defined by the Hamiltonian

$$H = \sum_i \sum_{k,q} B_k^q O_k^q(i) + K \sum_{i \in A, j \in B} Q(i)Q(j) - \sum_i g\mu_B J_z(i)H \quad (97)$$

whose terms represent CEF potential in Stevens operator representation, quadrupolar interactions and Zeeman energy respectively. K is an effective quadrupolar inter-site exchange mediated by conduction electrons, similar as in 4f-systems (Thalmeier and Lüthi 1991). The CEF parameters B_k^q are obtained from fitting to the susceptibility which leads to the CEF states in table 6. Since the ground state is a singlet, quadrupole order can only appear as *induced* order, i.e. nondiagonal matrix elements $\langle \Gamma_3 | Q | \Gamma_1^1 \rangle \neq 0$ must be present. This is possible for quadrupole operators $Q_{\Gamma_3} = (J_x^2 - J_y^2)$ or $Q_{\Gamma_5} = (J_x J_y + J_y J_x)$. Naively this would be compatible with uniaxial pressure results which show that the hidden order parameter is most sensitive to strains within the tetragonal xy-plane. Mean field calculations were performed with eq. (97) based on the above CEF scheme under the assumption of two sublattice AFQ ordering. They give a qualitatively correct behaviour of the specific heat, thermal expansion, nonlinear and anisotropic susceptibility and magnetisation. For example, the thermal expansion exhibits step like anomalies at $T_0(H)$ which increase with field strength. This is reproduced by the model since in tetragonal symmetry ($i = a, c$) $\alpha_i = g_i \partial \langle O_2^0 \rangle / \partial T$ where $Q = O_2^0 = 3J_z^2 - J(J+1)$ and g_i is an effective magnetoelastic coupling constant. Close to T_0 this is proportional to the growth rate $\partial \langle Q \rangle^2 / \partial T$ which leads to jumps in thermal expansion coefficient $\alpha_a = (1/a)(\partial a / \partial T)$ etc. reminiscent of those in the specific heat.

In principle the AFQ order parameter may also lead to a lattice superstructure with the AFQ vector \mathbf{Q} via magnetoelastic coupling terms. This has not been found (Kernavanois et al. 1999) but may simply be too small to observe as it is the case in other AFQ compounds like CeB₆. More disturbing is the fact that in the AFQ state an external field in the ab-plane should also induce a field dependent staggered magnetisation which has not been observed either.

In the AFQ hidden order model there is no natural connection to an AF order parameter. For this purpose a dipolar interaction term has to be introduced (Santini 1998) and the resulting magnetic ordering temperature T_m is unrelated to T_0 , if they are equal this has to be interpreted as accidental. In the light of the new pressure experiments it seems that they are close at ambient pressure, slightly favoring AFQ order. For $p > 0$ $T_0(p)$ and $T_m(p)$ cross at the critical pressure p_c , stabilizing the AF local moment phase for $p > p_c$. At ambient pressure local stress around crystal imperfections might already lead to a small AF volume fraction which then increases upon applying external pressure. Such a situation may be phenomenologically described by a Landau free energy ansatz (Shah 2000)

$$f_L = \alpha_0(T - T_0(p))Q^2 + \beta Q^4 + \alpha'_0(T - T_m(p))m^2 + \beta' m^4 + \gamma_0 m^2 Q^2 \quad (98)$$

where the last term is a coupling term for AF (m) and AFQ (Q) order parameters. For $\gamma_0 > 0$ the two order parameters are in competition. If $T_m(p)$ and $T_0(p)$ are close the inclusion of inhomogeneities might then lead to a phase separation where m and Q order parameters exist in macroscopically separate volume fractions. The Landau approach has been extended by including the strain coordinates to analyze neutron diffraction results under uniaxial pressure (Yokoyama et al. 2003).

Although the AFQ scenario for the hidden order parameter seems most attractive for the explanation of macroscopic anomalies at T_0 there is no direct experimental proof. This would require the observation of either i) the induced AF magnetic order in an external field or ii) direct signature of 5f-orbital order in resonant x-ray scattering as e.g. in the AFQ phase of CeB₆ (Nakao et al. 2001).

Hidden order as unconventional density wave

A complementary view of hidden order in URu₂Si₂ starts from a completely itinerant view of 5f-electrons by describing them within a multiband extended Hubbard model (Ikeda and Ohashi 1998, Ikeda and Ohashi 1999). Naturally this approach is unable to account for the CEF signatures in specific heat, susceptibility and similar quantities. In this model the large jump $\Delta C(T_0)$ is due to a condensation of electron-hole pairs (sect. 2). Unlike conventional CDW or SDW states however the pair states belong to nontrivial anisotropic representations of the symmetry group, similar to Cooper pairs in unconventional superconductors. The symmetry classification of unconventional electron-hole pair states and their stability analysis is given in (Gulacsi and Gulacsi 1987, Schulz 1989, Ozaki 1992). In full generality this has only been done for n.n. tight binding models with perfect nesting property of 2D conduction bands $\epsilon_{\mathbf{k} \pm \mathbf{Q}} = -\epsilon_{\mathbf{k}}$ and $\mathbf{Q} = (\frac{1}{2}, \frac{1}{2}, 0)$. In the low energy corner of the U-V phase diagram (U, V = on-site and n.n. Coulomb interaction respectively) the stable state is an unconventional triplet particle-hole pair condensate ('d-SDW'). In contrast to a common SDW where the gap function $\Delta^s(\mathbf{k}) = \text{const}$ is momentum independent, in the d-wave case one has $\Delta_{s_1 s_2}^d(\mathbf{k}) = \Delta^d(\mathbf{k}) \sigma_{s_1 s_2}^z$ with

$$\Delta^d(\mathbf{k}) = i\Delta_0^d(\cos k_x - \cos k_y) \quad (99)$$

The order parameter is purely imaginary because it is connected with persistent commensurate spin currents around lattice plaquettes. This state breaks spin rotational symmetry but not time reversal symmetry because the latter inverses both current and spin direction leaving the order parameter invariant. The staggered magnetic moment in the s-or d-wave case is given by

$$M_Q^z = \sum_{\mathbf{k}\sigma} \sigma \langle c_{\mathbf{k}\sigma}^\dagger c_{\mathbf{k}+\mathbf{Q}\sigma} \rangle = \sum_{\mathbf{k}} \frac{\Delta^{d,s}(\mathbf{k})}{2E(\mathbf{k})} \text{th} \frac{E(\mathbf{k})}{2T} \quad (100)$$

where $E_{\mathbf{k}} = [\epsilon_{\mathbf{k}}^2 + \Delta_{\mathbf{k}}^2]^{\frac{1}{2}}$ is the quasiparticle energy which is fully symmetric in both s,d cases. Therefore $M_Q^z > 0$ for conventional s-SDW but $M_Q^z \equiv 0$ for d-SDW case since the sign change in eq. (99) as function of \mathbf{k} makes the integral in eq. (100) vanish for d-SDW (this notation convention is a misnomer since $M_Q^z \equiv 0$ means that there is precisely *no* 'spin density' in the d-wave case).

Despite the vanishing staggered moment in the d-SDW state there is a large BCS-like specific heat anomaly similar to the conventional s-SDW case. Therefore the d-

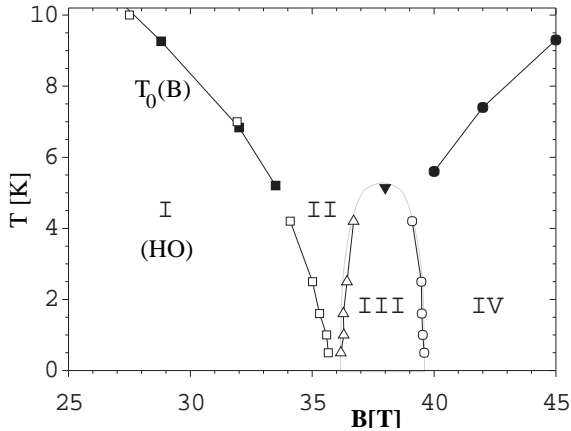


Figure 48. B-T phase diagram of hidden order (HO) phase (I), metamagnetic phase (III) and high field phase (IV). Open symbols correspond to resistivity anomalies and filled symbols to specific heat maxima. For zero field $T_0 = 17.5$ K(HO) (Jaime et al. 2002).

SDW state would naturally explain the most prominent property of the hidden order phase in URu₂Si₂. The tiny moments would then immediately appear at the hidden order transition ($T_m \equiv T_0$) around impurities, either through the creation of a s-SDW component by a proximity effect (Ikeda and Ohashi 1998) or through anisotropic exchange interactions of the condensate with magnetic impurities (Virosztek et al. 2002). In the latter case the temperature dependence of the staggered moment can be explained. The phase separation of hidden order and staggered micromagnetism is then again seen as a consequence of the sample defects and inhomogeneous impurity concentration.

4.4.4. High field phase diagram and metamagnetism

Besides pressure, magnetic fields also destroy the hidden order as can be seen from the progressive $T_0(B)$ -reduction in fig. 46. The corresponding critical field line forms the boundary to the hidden order phase (I) in fig. 48. Assuming the AFQ hidden order model of URu₂Si₂ there is an important difference to other known AFQ compounds which have a *degenerate* CEF ground state like cubic Γ_8 in CeB₆. There $T_0(B)$ first *increases* with field strength due to the lifting of orbital degeneracy. Since in URu₂Si₂ $T_0(B)$ decreases monotonously this is a strong argument for the induced AFQ order in a singlet-singlet system. At low temperatures the hidden order phase is destroyed at a field $B_0(0) = 36.1$ T. For $B > B_0(0)$ $M(B)$ exhibits multistep metamagnetic behaviour (Sugiyama et al. 1999) which may in principle be explained by the AFQ model as a field induced crossing of singlet CEF levels (Santini 1998) complemented by the effect of inter-site exchange interactions. Originally it was thought that the metamagnetic transition extends to temperatures much higher than T_0 (Sugiyama et al. 1999). Recent pulsed field experiments (Jaime et al. 2002) have shown however that the metamagnetic phase is much more confined (region III in fig. 48). Alternatively this region has also been interpreted as reentrant hidden order phase (Harrison et al. 2003). Finally above 40 T one reaches a moment of $1.5\mu_B/U$ which is much larger than the zero field value at high pressure, hence at high field not only the

AF volume fraction is maximal but also the magnetic ground state of U^{4+} has a larger moment. The structure of magnetic phases in the high field regime is still unknown.

4.4.5. Collective excitations in the ordered phase

Inelastic neutron scattering has perhaps provided the most convincing evidence that the localised 5f electron picture is a good starting point for URu_2Si_2 . In this case the dipolar CEF transition from the singlet ground state $|0'\rangle$ to excited singlet $|2'\rangle$ with dipolar matrix element $\alpha = \langle 0'|J_z|2'\rangle$ should disperse into a collective ‘magnetic exciton’ band. Here the primes indicate that the corresponding singlet states in table 6 are modified due to the presence of AF order which mixes the unprimed states with higher CEF states, without this mixing obviously α would vanish. These magnetic excitons have indeed been found (Broholm et al. 1991) as well propagating modes in a large part of the tetragonal BZ. They may be described by a similar expression as magnetic excitons for UPd_2Al_3 . The relatively large matrix element $\alpha = 1.2$ obtained from fitting to experimental results (Broholm et al. 1991) is not in contradiction to the small overall AF moment, since the latter is only an effect of the small AF volume fraction. The $|0'\rangle$ to $|1'\rangle$ singlet excitation has no dipolar matrix element, it is the excitation whose softening is governed by the quadrupolar matrix element $\alpha_Q = \langle 0'|Q|1'\rangle$ leading to the induced AFQ (hidden) order at T_0 . This quadrupolar mode does not directly appear in the dipolar response function and the INS cross section. It has been suggested that its presence can be seen indirectly through an influence on the dipolar excitation (Santini et al. 2000).

4.4.6. The superconducting state

As in other U-HF compounds the superconducting state in URu_2Si_2 with $T_c = 1.4$ K is embedded in the AF phase and here in addition in the hidden order phase with $T_0 \gg T_c$. Although there are a number of signatures for an unconventional pair state, it has attracted much less attention than the hidden order phase, possibly because there is no direct evidence for a multicomponent SC order parameter (Thalmeier 1991). The evidence for gap anisotropy is obtained from various low temperature power laws for specific heat (Hasselbach 1993) ($\sim T^2$) and NMR relaxation rate (Matsuda et al. 1996) ($\sim T^3$) which suggests the presence of line nodes. A plot of C/T vs. T is shown in fig. 9 in comparison with theoretical curves (Hasselbach 1993) obtained for gap functions allowed in the Landau theory of tetragonal superconductors (Volovik and Gor'kov 1985). The region of experimental linear T behaviour in C/T is surprisingly large. This cannot be explained within a Landau approach which is restricted to the vicinity of T_c . In addition the reduced specific heat jump $\Delta C(T_c)$ as compared to a constant gap supports the existence of a gap anisotropy with line nodes. This is also the conclusion from point contact spectroscopy (Hasselbach et al. 1992). The upper critical field curves of URu_2Si_2 show two anomalies (Keller et al. 1995): First the anisotropy ratio $B_{c2}^a/B_{c2}^c = 4$ is large, it cannot be fully explained by the anisotropy of Pauli limiting fields given by $\sqrt{\chi_c/\chi_a} \simeq \sqrt{5}$, orbital effects due to effective mass anisotropy must be involved. Furthermore, a distinct upward curvature of B_{c2}^a is observed, similar to critical fields in the borocarbide superconductors where it was associated with two band effects or alternatively anisotropic Fermi velocities. The effect of AF on B_{c2} should be negligible due to its small volume fraction.

As discussed in sect. 2 the observation of the dHvA effect far in the vortex phase

($B \ll B_{c2}$) is a sure signature of nodal superconductivity. Although oscillations of the three Fermi surface sheets in URu_2Si_2 have been seen below B_{c2} (Ohkuni et al. 1999) the amplitude falls of quite rapidly with B , especially for field along c . Therefore, these experiments are not able to confirm the existence of nodes in $\Delta(\mathbf{k})$.

4.5. Superconductivity in the non-Fermi liquid state of UBe_{13} and $\text{U}_{1-x}\text{Th}_x\text{Be}_{13}$

This cubic compound was discovered rather early (Ott et al. 1983, Ott et al. 1984) as a superconducting HF system. The U atom in this structure is embedded in an icosahedral cage of 12 Be-atoms. A global understanding of the normal state and symmetry breaking in both superconducting and magnetic state is still elusive. Firstly ‘pure’ UBe_{13} crystals do not have the highest quality as compared to e.g. UPt_3 so that the symmetry of the anisotropic SC gap functions has not been identified, furthermore the Th-doped crystals $\text{U}_{1-x}\text{Th}_x\text{Be}_{13}$ show a perplexing variety of SC and possibly also magnetic phases whose microscopic origin and order parameter symmetries are not understood. The T-x phase diagram of $\text{U}_{1-x}\text{Th}_x\text{Be}_{13}$ has been investigated with a variety of methods and the most detailed results have been obtained using the thermal expansion method (Kromer et al. 1998, Kromer et al. 2000, Kromer et al. 2002) (fig. 50). The most important question concerns the nature of the low temperature phase (C) at intermediate doping ($0.02 < x < 0.045$). This phase may either be a nonunitary SC phase with condensate magnetic moments due to unconventional Cooper pairs (Sigrist and Rice 1989) or a phase with coexisting anisotropic SC and a SDW type phase suggested by Kromer et al. (1998) on experimental grounds and already proposed in a theory by Kato and Machida (1987). In the former case one has to assume a crossing of two SC phases with two independent unconventional order parameters as function of the Th-concentration (Sigrist and Ueda 1991) and in the latter a crossing of a SC and SDW phase line. Already in the normal state UBe_{13} is a rather anomalous metal, e.g. non-Fermi-liquid (nFl) behaviour has been observed and attributed to a multichannel Kondo effect.

4.5.1. Normal state and nFl properties of UBe_{13}

The 5f-electron level in UBe_{13} is close to the Fermi level as seen from photoemission results. Therefore the HF-behaviour which sets in below a fluctuation temperature of $T^* \simeq 8 - 25$ K does not correspond well to the Kondo picture which requires 5f states to lie sufficiently removed from the Fermi energy. Nevertheless the Kondo model in its single and multichannel version has been employed for this HF compound. The specific heat coefficient is strongly enhanced with $\gamma \simeq 1\text{J/molK}^2$. Furthermore resistivity, specific heat and thermal expansion reveal the presence of a second low energy scale with $T_m \simeq 2$ K where these quantities exhibit an additional maximum anomaly. This proves that at T_m a coherent Landau FL state has not yet evolved and that the superconducting transition at $T_c \simeq 0.9$ K in UBe_{13} happens within a strongly anomalous nFl state. In fact if superconductivity is suppressed by a strong magnetic field the γ value shows a roughly logarithmic increase with decreasing temperature typical for a nFl state. No saturation of $\gamma(T)$ is observed down to lowest temperatures (Helfrich 1996). In most other U-HF compounds superconductivity is embedded in a weakly AF state. Despite a number of attempts no long range AF order has been found in UBe_{13} , μSR measurements set an upper limit of $10^{-3}\mu_B$ for the moments on U-sites.

4.5.2. The 5f-ground state of U

The observed normal state nFl behaviour raises the still controversial question of the magnetic ground state of U-atoms in UBe_{13} . The high temperature susceptibilities do not allow to distinguish between a $5f^3$ and $5f^2$ state of U. In the former case proposed in Felten et al. (1986) a Kramers degenerate magnetic Γ_6 CEF ground state and two excited Γ_8

quartets at 180 K and still higher energy were inferred from analysis of specific heat which exhibits a CEF Schottky anomaly around 80 K. In this case the HF state would be due to a conventional Kondo mechanism involving the magnetic Γ_6 localised doublet. However this picture is in conflict with the pronounced nFl anomalies mentioned above. Indeed the nFl behaviour was taken as direct evidence for a $5f^2$ configuration with a nonmagnetic Γ_3 doublet ground state which has a nonvanishing quadrupolar moment (Cox 1987, Cox 1988) whose fluctuations scatter conduction electrons. The effective Hamiltonian is of the two-channel Kondo type which leads to an overcompensation of quadrupolar moments and therefore to typical logarithmic nFl anomalies in specific heat and susceptibility at low temperatures (Schlottmann and Sacramento 1993, Zvyagin 2000). The Γ_3 quadrupolar model would predict a positive nonlinear magnetic susceptibility in χ_3 with considerable anisotropy at low temperatures, instead the opposite, namely almost isotropic, negative $\chi_3(T)$ was found (Ramirez et al. 1994). This suggests that the ground state is a magnetic Kramers doublet Γ_6 . To explain nFl behaviour one either has to invoke a magnetic multichannel Kondo effect or closeness to a quantum critical point in UBe_{13} .

4.5.3. The superconducting state in UBe_{13}

The T_c values for superconductivity which occurs in the nFl state depend considerably on the type of sample. There are two classes with ‘high’ T_c ($\simeq 0.9$ K) and ‘low’ T_c ($\simeq 0.75$) which, however, are not much different in their impurity content. Low temperature ‘power law’ dependencies give conflicting information on the node structure of the gap and no firm conclusion on whether spin singlet or triplet pairing is realized in UBe_{13} can be drawn. Therefore, these results will not be discussed further here although an axial order parameter with point nodes seems to be favored. The most direct evidence obtained sofar for unconventional superconductivity is connected with the giant ultrasonic absorption anomaly observed directly below T_c (Golding et al. 1985, Müller et al. 1986) which was attributed to collective modes or domain-wall damping due to a multicomponent order parameter (Sigrist and Ueda 1991).

The B-T phase diagram of UBe_{13} presented in fig. 49 has quite anomalous appearance: The upper critical field curve $B_{c2}(T)$ shows an inflection point around 0.45 K, furthermore deep in the superconducting regime another anomaly line $B^*(T)$ starting at $T_L = 0.7$ K has been identified both by specific heat (Helfrich 1996) and thermal expansion measurements (Kromer et al. 1998, Kromer et al. 2000). This line might be connected to the onset of magnetic correlations which, however, do not lead to long range order. This interpretation is supported by recent thermal expansion results (Kromer et al. 2000) who have shown that the line can be followed as function of Th-doping and eventually, according to this picture, long range SDW order appears above a Th concentration of $x_{c1} = 0.02$.

4.5.4. Superconducting phase diagram of Th-doped crystals

The T-x superconducting phase diagram of the thorated $\text{U}_{1-x}\text{Th}_x\text{Be}_{13}$ -crystals ($x \leq 0.10$) whose most recent version (Kromer et al. 2002), is shown in fig. 50 has attracted enormous interest because it was taken as strong evidence for unconventional superconductivity. Mainly two observations favored an interpretation in terms of exclusively SC phase transitions into SC phases denoted A,B and C in fig. 50: i) at $x_{c1} = 0.02$ a cusp-like increase of T_c into T_{c1} occurs with seemingly different T_c pressure coefficients below and above x_{c1} , suggesting that SC phases below T_c (A, $x < x_{c1}$) and T_{c1} (B, $x > x_{c1}$) are

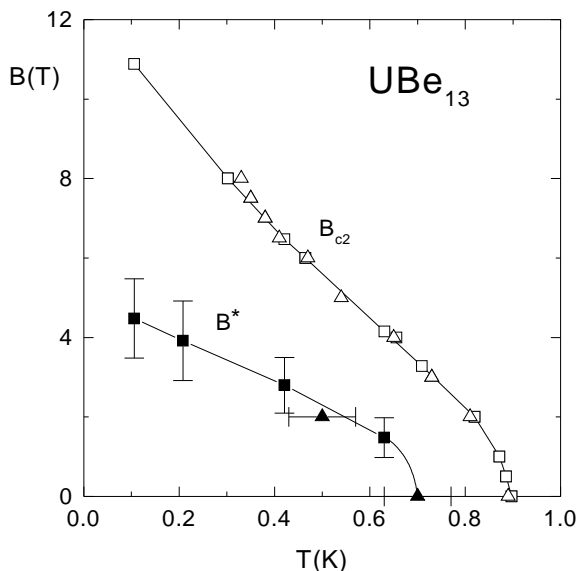


Figure 49. Upper critical field B_{c2} and magnetic anomaly line B^* obtained from specific heat (squares) and thermal expansion (triangles) experiments (Helfrich 1998, Kromer et al. 1998) for a ‘high’ T_c sample.

different. ii) Below T_{c2} for $x_{c1} < x < x_{c2}$ with $x_{c2} = 0.045$ a second superconducting transition into phase C takes place which was inferred from the sudden increase of slope in H_{c1} (Rauchschalbe et al. 1987). Furthermore in phase C magnetic moments $\mu \simeq 10^{-3}$ per U site appear according to μ SR results (Heffner et al. 1990). This lead to the suggestion that the SC order parameter in the C phase is nonunitary, i.e. Cooper pairs carry a magnetic moment which appears around impurity sites.

These observations lead to a scenario within the Ginzburg-Landau theory approach based on the basic assumption of a crossing of $T_c(\Gamma_1, x)$ and $T_c(\Gamma_5, x)$ of two different superconducting order parameters at the critical concentration x_{c1} (Sigrist and Ueda 1991). They belong to cubic O_h representations Γ_1 (fully symmetric) and Γ_5 (threefold orbital degeneracy), though different pairs of representations are also possible. Below x_{c1} (and hence also for stoichiometric UBe_{13}) $T_c(\Gamma_5, x) > T_c(\Gamma_1, x)$ and the unconventional Γ_5 (A) SC state is stable. Above x_{c1} the opposite inequality holds and the conventional Γ_1 (B) SC phase is stable immediately below T_{c1} . For lower temperature when the size of the SC order parameter increases the fourth order mixing terms in the GL functional favor a mixed $\Gamma_1 \oplus \Gamma_5$ SC state (C) which becomes stable below the transition at T_{c2} . For a specific region in the parameter space of the GL functional the mixed state may be nonunitary and therefore lead to Cooper pairs with magnetic moments. For further increase of Th-concentration enhanced pair breaking eventually leads again to a decreasing $T_c(\Gamma_1, x)$ and a second crossing at x_{c2} appears.

However, the results of recent detailed thermal expansion experiments including additional Th-concentrations have challenged this $T_c(\Gamma_5, x)$ - $T_c(\Gamma_1, x)$ crossing interpretation (Kromer 2000, Kromer et al. 2000, Kromer et al. 2002). Firstly, investigation of additional

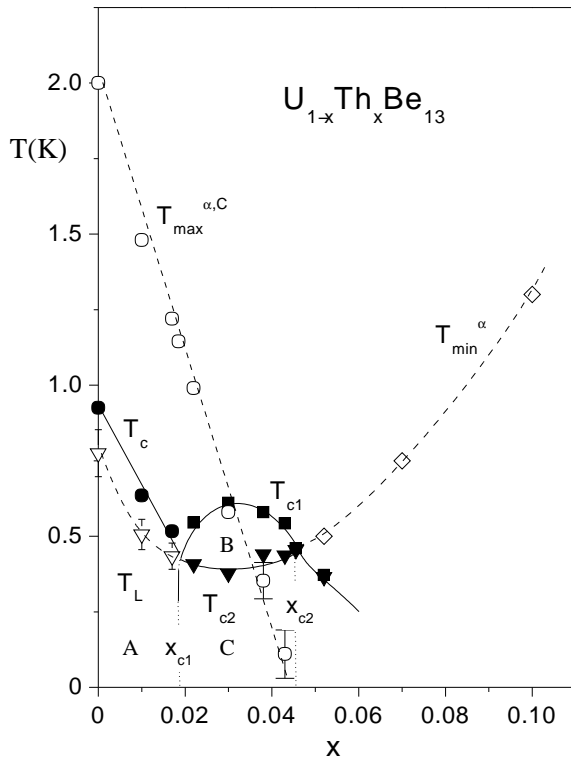


Figure 50. Superconducting phase diagram of $U_{1-x}Th_xBe_{13}$ for $x < 0.10$ (Kromer et al. 2002). full lines and symbols: thermodynamic phase boundaries; broken lines and open symbols: lines of anomalies. T_L and T_{min}^α denote line of anomalies from minimum in the thermal expansion coefficient $\alpha(T)$, $T_{max}^{\alpha,C}$ is the line of anomalies from the maximum in $C(T)$ and $\alpha(T)$. A, B and C denote distinct SC phases in the T_c -crossing model.

Th dopings has shown that pressure dependence of T_c and T_{c1} is not really different outside the critical region around x_{c1} . More importantly, however, a new line of anomalies T_L (dashed line in fig. 50) has been found that starts at the aforementioned anomaly for UBe_{13} in fig. 49 ($B^*=0$) and continues until it merges with T_{c2} for $x > x_{c1}$ and then even beyond x_{c2} . For $x = 0$ T_L was interpreted as onset temperature of magnetic correlations. The thermal expansion anomaly at T_L becomes ever sharper when x approaches x_{c1} which suggests increasing magnetic correlation length until finally at x_{c1} at the real phase transition line T_{c2} a true SDW state has evolved which continues beyond x_{c2} . In this picture then the phases A and B are the same superconducting phases and C is characterised by coexistence of the superconducting B-phase with the SDW state which also is responsible for the observed small moments ($10^{-3}\mu_B$), there is no need to assume an exocitic nonunitary SC order parameter in the C-phase. The evolution of a SDW state within the SC phase has already been proposed by Kato and Machida (1987) However in this picture the increased slope of H_{c1} below T_{c2} has no obvious explanation. Furthermore the sudden drop of flux creep rate by several orders of magnitude below T_{c2} in phase C (Dumont and Mota 2002) can be explained in the crossing scenario where the nonunitary nature of C provides an efficient mechanism for flux pinning (Sigrist and Agterberg 1999). Indeed the drop in the flux creep rate is not observed for pure UBe_{13} below T_L (Mota and Cichorek 2003).

In thermal expansion investigations it also became clear that the additional temperature scale T_{max} is continuously reduced with increasing Th-concentration. Amazingly it hits T_{c1} exactly at its maximum and (observed for $B > B_{c2}$) vanishes at x_{c2} as shown by the dashed T_{max} line in fig. 50. If this energy scale is due to magnetic excitations it suggests a close connection to the mechanism of Cooper pairing.

The discussion in this section has necessarily been rather qualitative as there is no developed microscopic theory for this complex behaviour where indeed SC and perhaps SDW order evolve in an incoherent nonstoichiometric HF metal with pronounced nFI behaviour.

5. Rare Earth Borocarbide superconductors

The superconducting class of layered transition metal borocarbides $\text{RNi}_2\text{B}_2\text{C}$ was discovered (Cava et al. 1994, Nagarajan et al. 1994) and investigated rather recently. Here R stands either for nonmagnetic Y, Lu and Sc or for lanthanide elements in a magnetic R^{3+} state. Several excellent reviews are available already (Hilscher and Michor 1999, Müller and Narozhnyi 2001), mostly focusing on the material physics and chemistry of these compounds. The crystal structure shown in fig. 51 is body centered tetragonal (space group $I4/mmm$). It consists of R-C rock salt type planes separated by Ni_2B_2 layers built from NiB_4 tetrahedra and stacked along the c-axis. More general structures with more than one R-C layer are possible (Hilscher and Michor 1999) but will not be discussed further. The nonmagnetic borocarbides have relatively high T_c 's around 15 K as seen in fig. 51. There is evidence that the superconducting mechanism is primarily of the electron-phonon (e-p) type although this cannot explain the large anisotropy of the SC gap. At first sight the layered structure is similar to the high- T_c cuprates. However, unlike the copper oxide planes the NiB_2 planes show buckling (fig. 51, left panel), as a consequence the electronic states at the Fermi level in the borocarbides do not have quasi-2D $d_{x^2-y^2}$ character and, therefore, have much weaker correlations excluding the possibility of AF spin-fluctuation mediated superconductivity. The nonmagnetic borocarbides serve as a kind of reference point to separate the fascinating effects of AF and SC order parameter coupling in the magnetic $\text{RNi}_2\text{B}_2\text{C}$. However, the former have their own peculiarities which are not yet completely understood. Foremost, despite their alleged electron-phonon nature, $\text{LuNi}_2\text{B}_2\text{C}$ and $\text{YNi}_2\text{B}_2\text{C}$ have strongly anisotropic gap functions and low energy quasiparticle states as evident from specific heat and thermal conductivity. Furthermore an anomalous upturn in H_{c2} has been observed. The magnetic $\text{RNi}_2\text{B}_2\text{C}$ are an excellent class of materials to study the effects of competition of magnetic order and superconductivity for the following reasons: The T_c 's are relatively high and their size relative to T_N varies systematically across the R-series. Especially interesting are the cases of $\text{RNi}_2\text{B}_2\text{C}$ with $\text{R} = \text{Dy}, \text{Ho}$ and Er where T_c and T_N (or T_{IC}) are not too different, leading to strong competition of the magnetic and SC order parameters. Furthermore the superconducting condensate and magnetic moments are carried by different types of electrons, namely itinerant 3d-electrons for the Ni_2B_2 layers and localized R^{3+} 4f-electrons for the R-C layers respectively. Finally they are well separated and their coupling which is of the local exchange type can be treated in a controlled perturbative way somewhat akin to the situation in the well known classes of Chevrel phase (Fischer 1990) and ternary compound (Fischer and Maple 1982) magnetic superconductors.

The antiferromagnetic molecular field establishes a periodic perturbation characterized by a length scale of the order of the Fermi wavelength $k_F^{-1} \ll \xi_0$. This implies that the spatial extent of the Cooper pairs extends over many periods of the alternating molecular field. The latter is therefore effectively averaged to zero and does not suppress superconductivity via an orbital effect. The system is invariant under the combined operation of time inversion followed by a translation with a lattice vector which allows to form Cooper pairs in a spin singlet state with vanishing (crystal) momentum in the antiferromagnetic lattice. This pair-state can be considered as a natural generalization of the pairing in time-reversed states encountered in usual non-magnetic superconductors to which it re-

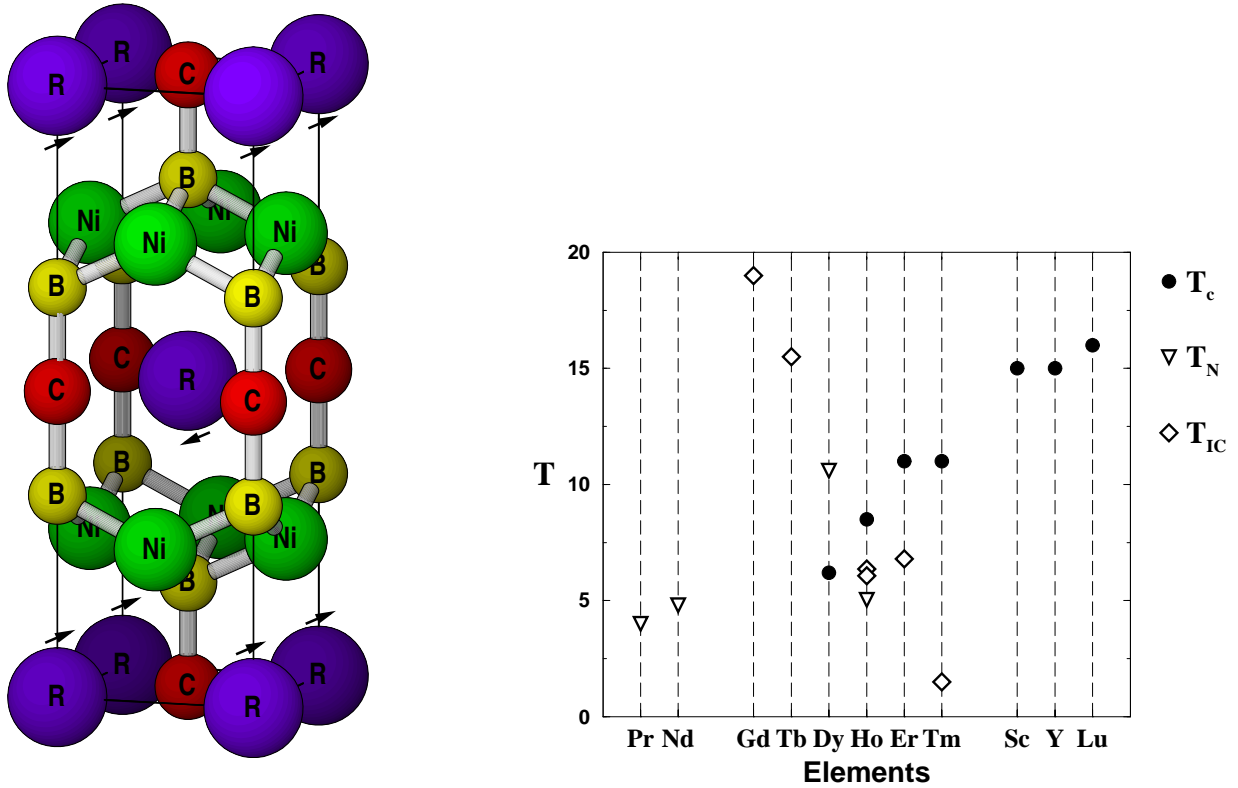


Figure 51. Left: tetragonal crystal structure (I4/mmm) of $\text{RNi}_2\text{B}_2\text{C}$. Low temperature AF2 magnetic structure with [110] easy axis is indicated by arrows. $a = b = 3.52\text{\AA}$ and $c = 10.53\text{\AA}$ for $\text{R} = \text{Ho}$. Reciprocal lattice vectors are given by $2\mathbf{a}^*$, $2\mathbf{b}^*$ and $2\mathbf{c}^*$ where $a^* = \frac{2\pi}{a}$ etc. Right: magnetic (T_{IC} : incommensurate magnetic structure, T_N : simple AF structure) and superconducting (T_c) transition temperatures in Kelvin for the $\text{RNi}_2\text{B}_2\text{C}$ series.

duces in the limit of vanishing staggered magnetization. The magnetic order does not lead to depairing (Fulde and Keller 1982).

For detailed investigation it is necessary to gain a clear understanding of the magnetic phases of $\text{RNi}_2\text{B}_2\text{C}$. A theory of the rich metamagnetic phases in the B-T phase diagram of $\text{HoNi}_2\text{B}_2\text{C}$ and $\text{DyNi}_2\text{B}_2\text{C}$ is a necessary prerequisite to comprehend the interaction effects of the two order parameters in these compounds.

The investigation of alloy series of magnetic R^{3+} dissolved in the nonmagnetic borocarbides allows one to study the pair breaking effects due to incoherent exchange scattering and its associated de Gennes scaling of T_c . One also observes ‘inverse’ de Gennes scaling (Müller and Narozhnyi 2001), i.e. the suppression of T_c by *nonmagnetic* impurities like Lu and Y in the *magnetic* $\text{RNi}_2\text{B}_2\text{C}$ superconductors which shows quite similar behaviour as function of the impurity concentration although its underlying physics is very different.

5.1. Physical properties of the nonmagnetic borocarbides

The nonmagnetic $\text{YNi}_2\text{B}_2\text{C}$ and $\text{LuNi}_2\text{B}_2\text{C}$ compounds with comparatively high T_c of 16.5 K and 15.5 K serve as reference systems for the more difficult systems $\text{RNi}_2\text{B}_2\text{C}$ with

both magnetic and superconducting phases. The electron-phonon nature of superconductivity in $\text{YNi}_2\text{B}_2\text{C}$ and $\text{LuNi}_2\text{B}_2\text{C}$ is inferred from a substantial s-wave character of the order parameter as witnessed by the appearance of a moderate Hebel-Slichter peak in the ^{13}C NMR relaxation rate (Mizuno et al. 1999). On the other hand the gap function is strongly anisotropic as can be seen both from temperature and field dependence of thermodynamic and transport quantities. At low temperatures one observes a specific heat $C_s \sim T^3$ (Hilscher and Michor 1999) and thermal conductivity $\kappa_{xx} \sim T$ (Boaknin et al. 2001) and $\kappa_{zz} \sim T^\alpha$ ($\alpha \sim 2 - 3$) indicating the presence of gap nodes (Izawa et al. 2002a). More precisely, within experimental accuracy, there must be at least a gap anisotropy of $\Delta_{min}/\Delta_{max} \leq 10^{-2}$ (Izawa et al. 2002a). For an electron-phonon superconductor this would be the largest anisotropy ever observed. This conjecture is also supported by a \sqrt{H} field dependence (Nohara et al. 1997) of the low temperature specific heat and the linear H dependence of the thermal conductivity κ_{xx} for \mathbf{H} along [001] (Boaknin et al. 2001). Since in the latter case the heat current is perpendicular to the vortices this proves that quasiparticles must be present in the inter-vortex region. This is also required to explain the observation of dHvA oscillations far in the vortex phase. Experimental evidence therefore demands a nodal gap function for borocarbides and the s+g wave model proposed in (Maki et al. 2002) fulfils the requirements. In addition it explains recent results on ultrasonic attenuation which also confirmed the existence of gap nodes in the cubic plane (Watanabe et al. 2003). In the following we will address the question of electron-phonon coupling strength, isotope effect and positive curvature in the upper critical field. Furthermore power law behaviour of the electronic specific heat and thermal conductivity as function of temperature and in addition their field-angle dependence $C_s(T, \mathbf{H})$ and $\kappa_{ij}(T, \mathbf{H})$ for $T \ll T_c$ in the vortex phase allows to discuss the nodal structure of the SC gap.

5.1.1. Evidence for electron-phonon superconductivity

The classical argument in favor of the e-p mechanism is the observation of an isotope effect characterized by the isotope exponent for a specific atom with mass M as given by $\alpha_M = -d \ln T_c / d \ln M$. However, this cannot be applied easily to complex layered superconductors, as evident from the existence of an isotope effect in the nonphononic cuprate superconductors with nonoptimal doping. A boron isotope effect has been found in $\text{YNi}_2\text{B}_2\text{C}$ ($\alpha_B = 0.2$) and $\text{LuNi}_2\text{B}_2\text{C}$ ($\alpha_B = 0.11$) much smaller than the BCS value $\alpha_M = 0.5$ and a nonphononic origin for α_B originating in the influence of boron on the charge density in the B_2Ni_2 layers has, therefore, been suggested (Drechsler et al. 2001).

The most direct support for the phonon mediated Cooper pairing is due to scanning tunneling spectroscopy (Martinez-Samper et al. 2003) which has shown the existence of a strong coupling signature in the tunneling DOS due to a soft optical phonon close to the FS nesting wave vector \mathbf{Q} . The e-p coupling constant was derived as $\lambda = 0.5-0.8$ which is compatible with the value $\lambda = 0.53$ obtained from resistivity data.

Additional support for the electron phonon mechanism comes from the comparison of thermodynamic ratios $\Delta(T_c)/\gamma T_c$ and $\Delta(0)/kT_c$ calculated in strong coupling theory and the phonon spectra measured by inelastic neutron scattering (Hilscher and Michor 1999). The strong coupling corrections of the above ratios to their BCS values are related to the logarithmic moments $\bar{\omega}$ of the phonon DOS $F(\omega)$ or more precisely of the $\alpha^2F(\omega)$ Eliash-

berg function. These moments may be directly obtained from the INS phonon DOS or indirectly from the above ratios. A comparison shows a reasonable agreement between the moments with a $T_c/\bar{\omega}$ ratio characteristic for moderately strong coupling electron phonon superconductivity. The moments are, however, much smaller than the Debye energies obtained from the phonon specific heat which again indicates that certain low lying optical phonon modes play a special role for the coupling. By varying temperature it has been found that these are soft optical phonon modes along the $[q_x, 0, 0]$ direction which involve primarily the vibration of the heavy Y or Lu atoms. The softening occurs at $q_x \sim 0.55$ (in r.l.u of $2a^*$) which corresponds to a nesting vector of the Fermi surface (Dugdale et al. 1999) where the \mathbf{q} -dependent electronic susceptibility which determines the renormalized phonon frequency becomes strongly enhanced. The special role of these optical phonons for the strong coupling effects is underlined by the moment ratio $(\bar{\omega}_{YNi_2B_2C}^{\alpha^2 F} / \bar{\omega}_{LuNi_2B_2C}^{\alpha^2 F}) \sim 1.5 \sim (M_{Lu}/M_Y)^{\frac{1}{2}}$ rather than being equal to the square root of the unit cell masses which would only be 1.16.

5.1.2. Anomalous H_{c2} -behaviour

The upper critical field in nonmagnetic $\text{LuNi}_2\text{B}_2\text{C}$ and $\text{YNi}_2\text{B}_2\text{C}$ compounds shows a peculiar positive (upward) curvature below T_c . This phenomenon is also observed in various other layered superconductors. Within the standard Ginzburg Landau description of H_{c2} for isotropic single band superconductors the slope is determined by the Fermi velocity and only a negative curvature is possible. A positive curvature can be obtained by assuming a strong anisotropy of the Fermi velocity (Drechsler et al. 2001) which may be simplified to a two band model with two Fermi velocities. The upper critical field for the two band model may be calculated within the linearized version of Eliashberg theory (Shulga et al. 1998). In this way a fit for the experimental H_{c2} -curves using a two band Fermi velocity ratio of $v_{F1} : v_{F2} = 0.97 : 3.7$ ($\text{LuNi}_2\text{B}_2\text{C}$) and $0.85 : 3.8$ ($\text{YNi}_2\text{B}_2\text{C}$) can be obtained. It also has to be assumed that there is strong e-p coupling in the v_{F1} band and sizable coupling between v_{F1} and v_{F2} bands. It should be noted that the presence of magnetic impurity scattering may change the picture (Shulga and Drechsler 2001) because an increasing scattering rate decreases the positive curvature. Thus the extraction of a unique set of parameters for the two band model from the positive H_{c2} curvature seems difficult. As expected for uniaxial crystal structures, there is an a-c anisotropy of H_{c2} but surprisingly there is also a strong fourfold anisotropy within the tetragonal ab-plane (Metlushko et al. 1997) which cannot be due to FS effects on the level of the effective mass approximation, it rather should be taken as another indication of the large gap anisotropy in the ab-plane.

5.1.3. Specific heat and thermal conductivity results

The low temperature dependence of the specific heat is apparently described by a power law behaviour $C_s \sim T^n$ with n between 2 and 3 (Hilscher and Michor 1999). Thermal conductivity κ_{xx} (Boaknin et al. 2001) clearly exhibits T-linear behaviour for $T \ll T_c$ suggesting the presence of nodal lines or second order node points as introduced below which would be compatible with $n = 2$ for the specific heat. Furthermore the investigation of field (and field-angle) dependence of $C_s(T, \mathbf{H})$ and $\kappa_{ij}(T, \mathbf{H})$ ($i, j = x, y, z$) is a powerful method to obtain information on the quasiparticle spectrum and hence on the anisotropy

properties of the gap function (sect. 2). In a conventional superconductor with isotropic gap the quasiparticles at low temperature are confined to the vortex core where they form closely spaced bound states with an energy difference Δ^2/E_F much smaller than kT . Therefore, they can be taken as a cylinder of normal state electrons of diameter ξ_0 (coherence length) which gives a field independent contribution $\xi_0^2\gamma T$ per vortex to the linear specific heat. Then in the vortex phase $\gamma(H)$ is predicted to scale with the number of vortex lines which is $\sim H$. However in superconductors with nodes the quasiparticles with momenta in the node direction can tunnel into the inter-vortex region and then their energy is Doppler shifted by the supercurrents around the vortex by an amount $\delta E = m\mathbf{v}_F \cdot \mathbf{v}_s$. As shown by Volovik (1993) this leads to a finite residual quasiparticle DOS at zero energy given by

$$N_s(0)/N_n = K\sqrt{\frac{H}{H_{c2}}} \quad (101)$$

Where K is of order unity and N_n the normal state DOS. As found later the DOS also depends on the relative angle of the field with respect to the nodal positions of the gap function. The DOS in eq.(101) leads then to a \sqrt{H} behaviour of the specific heat (Nohara et al. 1997) and also for $\kappa_{zz}(H)$ for temperatures larger than the quasiparticle scattering rate. Thermal conduction perpendicular to the vortex lines ($\mathbf{H} \parallel \mathbf{c}$) as given by $\kappa_{xx}(H)$ that starts immediately above H_{c1} for $T \ll T_c$ can only result from the presence of extended quasiparticle states outside the vortex cores and hence is a direct proof for the presence of nodal regions in the gap. To draw similar conclusions from the specific heat it is necessary to observe the \sqrt{H} behaviour for $H \ll H_{c2}$ and in connection the infinite slope of $\gamma(H)$ for $H \rightarrow 0$. The Doppler shift picture of magnetothermal properties is only an approximation. A comparison with exact quasiclassical calculations has been given in Dahm et al. (2002)

5.2. Theoretical analysis of nonmagnetic borocarbides

We briefly discuss the electronic structure and associated FS topology which is also important for the magnetic borocarbides. Our main topic here is the explanation of the quasi-unconventional SC low temperature behaviour of nonmagnetic Lu- and Y- which may be understood within a a hybrid s+g wave model for the SC gap function.

5.2.1. Electronic Structure of the Borocarbides

The crystal structure of the borocarbides is of a layered type which might one lead to expect quasi 2D features in the electronic bands. Calculations by various groups (Mattheis 1994, Pickett and Singh 1994, Rosner et al. 2001) have shown however that they have definitely 3D character which is also suggested by the rather isotropic resistivity (Fisher et al. 1997). Conduction states are composed of wide Ni-B-N-sp bands and narrow (~ 3 eV) Ni-3d bands centered about 2eV below the Fermi level which is close to a local peak of the DOS in $\text{LuNi}_2\text{B}_2\text{C}$ and $\text{YNi}_2\text{B}_2\text{C}$. The DOS peak generally decreases when Lu is replaced by progressively lighter R atoms which leads to a correspondingly smaller T_c . This also agrees with the observation that substitution of Ni with Co (hole-doping) or with Cu (electron-doping) decreases T_c (Gangopadhyay and Schilling 1996, Schmidt and Braun 1997) because the Fermi level moves away from the local peak position. Unlike in the cuprates all Ni 3d-states in the borocarbides contribute to conduction bands

at the Fermi surface which therefore consists of many sheets. In $\text{LuNi}_2\text{B}_2\text{C}$ the main sheet exhibits an important nesting feature (Dugdale et al. 1999). FS lobes along [110] direction in the tetragonal plane are connected by a nesting vector $\mathbf{Q}=(0.55,0,0)$. This in turn leads to a peak structure in the staggered susceptibility $\chi(\mathbf{q})$ (Rhee et al. 1995) at $\mathbf{q} = \mathbf{Q}$. In the $\text{RNi}_2\text{B}_2\text{C}$ the effective magnetic RKKY interaction $J(\mathbf{q})$ is proportional to $\chi(\mathbf{q})$ and therefore a-axis incommensurate magnetic order with modulation vector \mathbf{Q} is seen in Gd, Tb, Ho, Er and Tm-borocarbides which coexists with c-axis spiral order in $\text{HoNi}_2\text{B}_2\text{C}$ (sect.5.3). Further evidence of the importance of the nesting at \mathbf{Q} comes from the presence of a pronounced Kohn anomaly at wave vector \mathbf{Q} in the phonon dispersion of $\text{LuNi}_2\text{B}_2\text{C}$ (Derwenagas et al. 1995). Finally the previous conjecture of strongly different Fermi velocities in the two band model has been confirmed in electronic structure calculations for $\text{YNi}_2\text{B}_2\text{C}$ (Rosner et al. 2001).

5.2.2. Nodal structure of the superconducting gap and impurity effects

As explained before, thermodynamics and transport behaviour points to an extremely anisotropic or nodal gap function in the nonmagnetic borocarbides. A gap function compatible with reported experiments was proposed in Maki et al. (2002). It is a hybrid s+g wave gap which is fully symmetric (A_{1g}) under the tetragonal group D_{4h} and has the form

$$\Delta(\mathbf{k}) = \frac{1}{2}\Delta(1 - \sin^4 \vartheta \cos(4\phi)) \quad (102)$$

where ϑ, ϕ are the polar and azimuthal angle in \mathbf{k} -space respectively. This gap function has four second order node points at $(\vartheta, \phi) = (\frac{\pi}{2}, 0), (\frac{\pi}{2}, \pi)$ and $(\frac{\pi}{2}, \pm\frac{\pi}{2})$ (fig. 52) which dominate the quasiparticle DOS for $E \ll \Delta$ where

$$\frac{N_s(E)}{N_n} = \frac{\pi |E|}{4 \Delta} \quad (103)$$

The form of $\Delta(\mathbf{k})$ implies a fine tuning of s and g amplitudes. At its *second order* node points there is no sign change of the gap function and therefore the derivative is also zero. The resulting linear quasiparticle DOS then leads to the observed low temperature specific heat

$$\frac{C_s}{\gamma T} = \frac{27}{4\pi} \zeta(3) \left(\frac{T}{\Delta}\right) \quad (104)$$

where γ is the Sommerfeld constant. The presence of nodal points in the hybrid s+g wave gap function has no intrinsic symmetry reason but is due to a ‘fine-tuning’ of s- and g-wave amplitudes in eq. (102). For $\text{YNi}_2\text{B}_2\text{C}$ this is realised to an astonishing degree of $\Delta_{min}/\Delta_{max} \leq 0.01$. There is presently no microscopic explanation for this fine tuning but a phenomenological justification for the stability of an s+g wave order parameter for a wide range of pair potentials has been given (Yuan and Thalmeier 2003).

The nodal s+g wave gap function has a surprising behaviour when normal impurity scattering is taken into account (Yuan et al. 2003). For nodal gap functions belonging to a single nontrivial representation, like a d-wave gap there is a strong difference between scattering in the Born limit (small phase shift) and unitary limit (phase shift $\frac{\pi}{2}$). In the latter resonance scattering leads to the appearance of a residual zero field DOS resulting

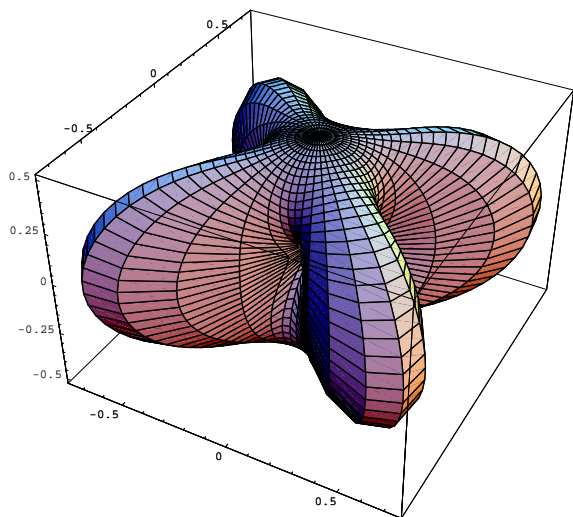


Figure 52. Polar plot of the anisotropic SC gap function $\Delta(\mathbf{k})$ of the s+g model. Nodal points are along [100] and [010] directions. (Maki et al. 2002)

in a finite specific heat coefficient for $T < \Gamma$ ($\Gamma =$ quasiparticle scattering rate). In the hybrid s+g wave case, quite the opposite behaviour, i.e. gap opening by impurity scattering, is observed which is almost identical for Born limit and unitary limit. The quasiparticle DOS including impurity scattering is given by

$$\frac{N_s(E)}{N_n} = \text{Im} \left\langle \frac{i\tilde{\omega}_n}{\sqrt{\tilde{\omega}_n^2 + \tilde{\Delta}_{\mathbf{k}}^2}} \right\rangle_{i\omega_n \rightarrow E+i\delta} \quad (105)$$

where $\tilde{\omega}_n = \omega_n + i\Sigma_0$ and $\tilde{\Delta}_{\mathbf{k}} = \Delta_{\mathbf{k}} + \Sigma_1$ are the Matsubara frequency and gap function renormalised by impurity scattering which leads to diagonal and nondiagonal self energies Σ_0 and Σ_1 respectively. For $\omega \rightarrow 0$ one finds $\tilde{\Delta} \rightarrow \frac{1}{2}\Delta + \Gamma$ where Γ is the scattering rate. In other words an energy gap ω_g immediately opens up for finite Γ as can be observed in fig. 53 which scales approximately as $\omega_g(\Gamma) = \Gamma/(1 + \frac{2\Gamma}{\Delta})$. Thus the s+g wave fine tuning is destroyed by impurity scattering and nodal quasiparticles are removed for temperatures $T < \Gamma$. This would lead to a crossover to exponential low temperature behaviour in the specific heat. Indeed this gap creation was observed in Pt-substituted $\text{Y}(\text{Ni}_{1-x}\text{Pt}_x)_2\text{B}_2\text{C}$ with $x = 0.2$ by Nohara et al. (1997) as shown in fig. 55. This remarkable behaviour, which is exactly opposite to the d-wave case where residual states at the Fermi level are created, can be traced back to the different character of first order nodes (d-wave) where the gap function changes sign and second order nodes (s+g wave) where the angular derivatives of $\Delta(\vartheta, \varphi)$ also vanish and no sign change of the gap occurs. In the first case the effect of impurity scattering averages out in the gap equation, in the second it does not, leading to a finite excitation gap ω_g .

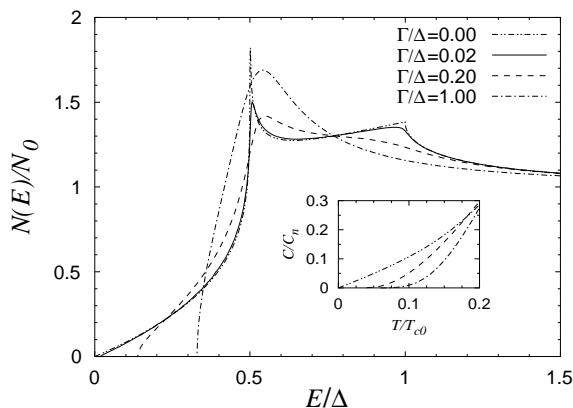


Figure 53. Normalised quasiparticle DOS for s+g wave gap in pure $\text{YNi}_2\text{B}_2\text{C}$ ($\frac{\Gamma}{\Delta} = 0$, full line) and for various scattering strengths Γ in the Born limit (for unitary limit results are quite similar). Induced excitation gap ω_g increases monotonically with Γ . The inset shows the low temperature specific heat (Yuan et al. 2003).

5.2.3. Thermodynamics and transport in the vortex phase

As discussed in sect. 2 the Volovik effect leads to a momentum *and* position dependent Doppler shift of the quasiparticle energies caused by the supercurrent flowing around the vortices. The corresponding DOS change depends both on the field strength and field direction with respect to nodal positions. For the gap model of eq.(102) the residual field induced DOS is given by (Won et al. 2003, Thalmeier and Maki 2003b)

$$\frac{N_s(0)}{N_n} = \frac{C_s}{\gamma T} = \frac{\tilde{v}\sqrt{eH}}{2\Delta} I(\theta, \phi)$$

$$I(\theta, \phi) = \frac{1}{2} \left\{ (1 - \sin^2 \theta \sin^2 \phi)^{\frac{1}{2}} + \left\{ (1 - \sin^2 \theta \cos^2 \phi)^{\frac{1}{2}} \right\} \right. \quad (106)$$

where $\tilde{v} = \sqrt{v_a v_c}$ and $I(\frac{\pi}{2}, \phi) = \max(|\sin \phi|, |\cos \phi|)$. This function has a cusp-like minimum at $\phi = n\frac{\pi}{2}$ when \mathbf{H} is sweeping over the node points. Also the residual DOS exhibits naturally the experimentally observed \sqrt{H} behaviour. For the calculation of thermal conductivity in the vortex phase of the s+g wave superconductor one has to be aware that impurity scattering immediately opens a gap $\omega_g \simeq \Gamma$. To have nodal quasiparticles for transport available one must fulfil $\omega_g \simeq \Gamma < T$. On the other hand to have an appreciable oscillation amplitude one must still be in the low temperature limit $\Gamma < T \ll \tilde{v}\sqrt{eH} \ll \Delta$. The angle dependence of the c-axis thermal conductivity in the leading order is then given by

$$\frac{\kappa_{zz}}{\kappa_n} \simeq \left(\frac{2}{\pi}\right)^2 \frac{\tilde{v}\sqrt{eH}}{\Delta} I(\theta, \phi) \quad (107)$$

i.e. in this limit to leading order it is completely determined by the angular dependent residual DOS. To determine the proper nodal positions from the maxima/minima of $\kappa_{zz}(\theta, \phi)$ it is important that the low temperature limit is reached.

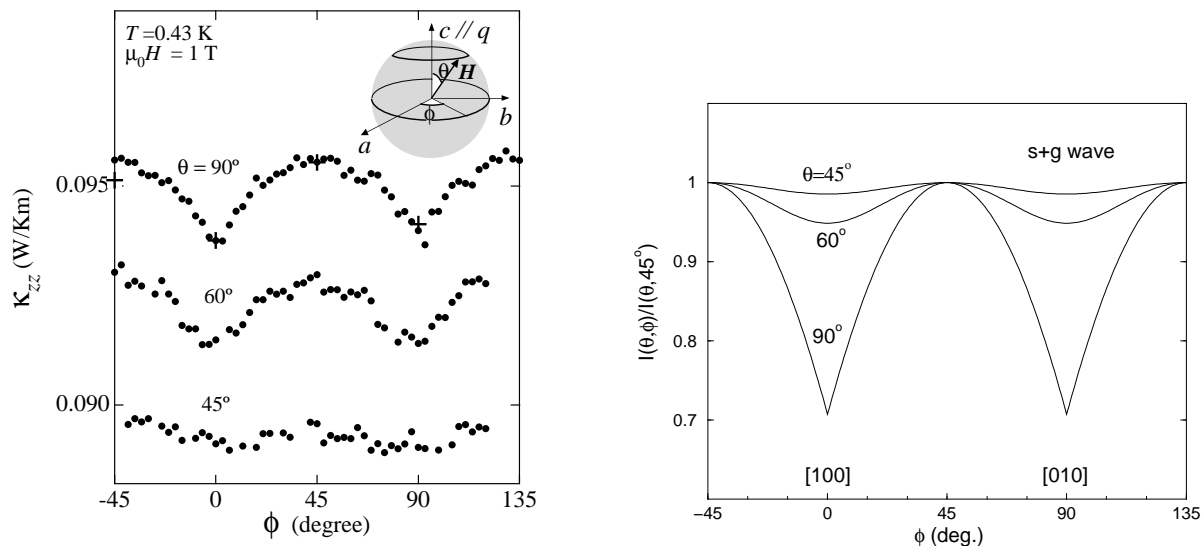


Figure 54. Left: experimental c-axis thermal conductivity of $\text{YNi}_2\text{B}_2\text{C}$ as function of azimuthal field angle ϕ for various polar field angles θ (Izawa et al 2002b). The inset shows the field geometry with \mathbf{H} being swept around c by varying ϕ and keeping θ constant. Right: theoretical normalized ϕ -dependence of angular function $I(\theta, \phi)$ which determines κ_{zz} according to eqs. (106),(107) (Thalmeier and Maki 2003).

The angular dependence of the c-axis thermal conductivity has been investigated in detail in (Izawa et al. 2002a). The geometry with heat current along c and \mathbf{H} conically swept around c is shown in the inset of fig. 54. For the in-plane field ($\theta = \frac{\pi}{2}$) pronounced cusps in $\kappa_{zz}(\frac{\pi}{2}, \phi)$ appear for $\phi = 0, \pm\pi/2$ in $\kappa_{zz}(\frac{\pi}{2}, \phi)$ as is visible in fig. 54. This is a typical signature for the existence of point nodes in the gap in the direction of the tetragonal $[100]$ and $[010]$ axes. When the polar field angle θ decreases the oscillations in $\kappa_{zz}(\theta, \phi)$ as function of azimuthal field angle ϕ are rapidly diminished. This behaviour is indeed predicted from eq. (106) as shown in fig. 54. A similar calculation for a d_{xy} -gap function $\Delta(\phi) = \Delta(\varphi) = \Delta \sin(2\varphi)$ which has line nodes in the same directions may be performed (Thalmeier and Maki 2003b). In this case no cusp appears and the amplitude of $\kappa_{zz}(\theta, \phi)$ oscillation in ϕ is almost independent of θ . This speaks strongly in favor of the s+g wave order parameter as the correct model for $\text{YNi}_2\text{B}_2\text{C}$ and possibly $\text{LuNi}_2\text{B}_2\text{C}$. It is the first confirmed case of a superconductor with (second order) node points in the gap functions. The only other known candidate is UPt_3 whose E_{2u} gap function in the B-phase is supposed to have point nodes at the poles (sect. 4.1). Similar experiments as in fig. 54 have yet to be performed for this compound. The point nodes of $\text{YNi}_2\text{B}_2\text{C}$ were found to lie along the tetragonal axis, this means that the s+g gap function in fig. 52 is rotated by 45 degrees compared to the one used in Maki et al. (2002). According to eq. (106) the ϕ dependence of the specific heat is determined by the same angular function and cusps should also appear there. This was indeed observed (Park et al. 2002) (fig. 12).

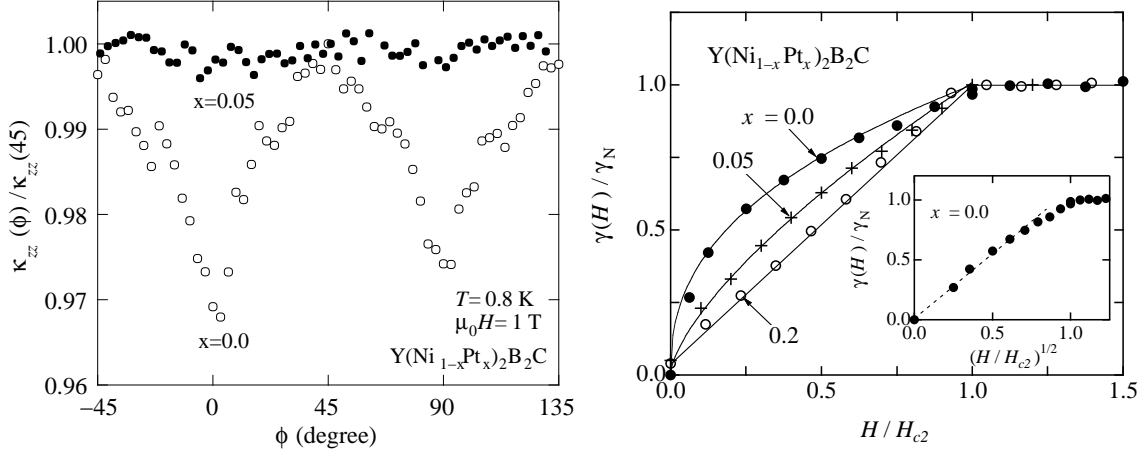


Figure 55. Left panel: Cusp-like fourfold oscillations in $\kappa_{zz}(90^\circ, \phi)$ of $\text{YNi}_2\text{B}_2\text{C}$ due to s+g wave point nodes are completely destroyed by 5% Pt-doping (Kamata 2003). Right panel: Transition from \sqrt{H} -behaviour of $\gamma(H)$ for the nodal SC at $x = 0$ to linear in H behaviour for $x = 0.2$ when a large gap has opened (Nohara et al. 1997).

In the Pt-substituted compound $\text{Y}(\text{Ni}_{1-x}\text{Pt}_x)_2\text{B}_2\text{C}$ already $x=0.05$ is sufficient to destroy the angular oscillations in $\kappa_{zz}(\theta, \phi)$ (Kamata 2003) which is again due to the rapid gap-opening for s+g wave and destruction of nodal regions by impurity scattering as shown in fig. 55.

In this section we have shown abundant experimental evidence that the nonmagnetic $\text{YNi}_2\text{B}_2\text{C}$ and possibly $\text{LuNi}_2\text{B}_2\text{C}$ have anisotropic gap functions with point nodes that can be described by a hybrid s+g wave order parameter. As a consequence the simple electron-phonon type pairing mechanism originally envisaged for the borocarbides certainly has to be supplemented, for example by strongly anisotropic Coulomb interactions, to account for the strongly anisotropic gap function found there.

5.3. Magnetic borocarbides

The magnetic 4f-electrons of lanthanides and the superconducting 3d-electrons of Ni are well separated in the RC layers and Ni_2B_2 layers of $\text{RNi}_2\text{B}_2\text{C}$. The coupling between magnetic and superconducting order parameters is weak enough to be treated as a perturbation but still strong enough to lead to pronounced effects on the SC properties. The magnetic and superconducting transition temperatures T_m and T_c of the series are shown in fig. 51. We will first discuss some of the basic observations in the series with focus on the Ho and Er borocarbides where coexistence of both order parameters is most interesting. The size of T_m and the influence of magnetism on T_c are both governed by the de Gennes factor $dG = (g-1)^2J(J+1)$ where g is the Landé factor and J the total angular momentum of the R^{3+} ion. The former suggests the RKKY interaction via Ni 3d conduction electrons of intervening Ni_2B_2 layers as the coupling mechanism for the 4f moments in RC layers. The magnetic structures exhibit a great variety which has been described and tabulated in Lynn et al. (1997) and Müller and Narozhnyi (2001) and the following gen-

eral features are observed: i) both commensurate (C) and incommensurate (IC) magnetic order parameters are present. ii) For Dy, Ho the commensurate AF structure consists of ferromagnetically ordered ab-planes stacked along the c-axis. iii) In IC structures one has two possibly coexisting type of modulations: helical modulation of stacked FM planes along the c-axis or SDW type (both longitudinal and transverse) modulation within each ab-plane with a modulation vector \mathbf{Q} close to the FS nesting vector. iv) The easy axis selected by the CEF potential is [110] (Ho,Dy), [100] (Er) or [001] (Tm).

As an example the low temperature $\text{HoNi}_2\text{B}_2\text{C}$ commensurate AF2 structure is indicated in fig. 51. In the RKKY mechanism IC modulation vectors should result from the maxima of the static electronic susceptibility $\chi(\mathbf{q})$ which has been approximately calculated by Rhee et al. (1995). It exhibits a pronounced peak at the nesting vector \mathbf{Q} of the Fermi surface which is indeed quite close to observed a-axis magnetic modulation vectors $\mathbf{Q}_a = (0.55,0,0)$ of the Gd, Tb, Ho and Er borocarbide compounds. On the other hand in $\text{HoNi}_2\text{B}_2\text{C}$ only a flat maximum is observed for wave vectors $\mathbf{q} = (0,0,q_z)$ close to the AF vector $\mathbf{Q}_{AF} = (0,0,0.5)$ so that the observed helically modulated structures along \mathbf{c}^* should not be associated with any FS nesting feature. For theoretical model calculations of stable magnetic structures it is a more sensible approach to parametrize the long range RKKY exchange interactions and compare the results with the experimentally determined field-angle dependent phase diagram at low temperature. This has been most successfully done for $\text{HoNi}_2\text{B}_2\text{C}$ (Amici and Thalmeier 1998) and $\text{ErNi}_2\text{B}_2\text{C}$ (Jensen 2002). Four of the $\text{RNi}_2\text{B}_2\text{C}$ ($R = \text{Dy, Ho, Er, Tm}$) show coexistence of superconductivity and magnetic order. As mentioned before $\text{HoNi}_2\text{B}_2\text{C}$ and $\text{DyNi}_2\text{B}_2\text{C}$ (Winzer et al. 1999) display the most spectacular interaction between superconductivity and magnetic order as already suggested by close transition temperatures T_m and T_c (fig. 51). On the other hand in $\text{ErNi}_2\text{B}_2\text{C}$ and $\text{TmNi}_2\text{B}_2\text{C}$ the SC vortex state exhibits an anomalous behaviour connected with the magnetic order. In the following we will discuss mainly $\text{HoNi}_2\text{B}_2\text{C}$ and $\text{ErNi}_2\text{B}_2\text{C}$ where most of the work has been performed sofar.

5.3.1. Metamagnetism and IC-C lock-in transition in $\text{HoNi}_2\text{B}_2\text{C}$

The metamagnetism of $\text{HoNi}_2\text{B}_2\text{C}$ has been investigated theoretically in considerable detail (Amici and Thalmeier 1998, Amici et al. 2000). First we discuss the 4f-magnetism of $\text{HoNi}_2\text{B}_2\text{C}$. This problem has two related aspects. For zero field the first IC magnetic phase with $\mathbf{Q} = (0,0,0.45)$ appears at $T_{IC} = 6$ K which has a helical modulation of the moment of FM ab-planes along c. At $T_N = 5$ K a lock-in transition occurs to the simple AF with wavevector \mathbf{Q}_{AF} and [110] easy axis which is the stable low temperature structure. In addition an a-axis modulation with wave vector \mathbf{Q}_a exists which will be neglected here. The application of a magnetic field \mathbf{H} at an angle θ with respect to the easy axis leads to the appearance of additional phases as witnessed by metamagnetic transition steps in the magnetisation curve (Canfield et al. 1997) and shown in the inset of fig. 56. At these steps some of the FM layers with moments pointing roughly opposite to the field direction align with the easy axis closest to the field direction, this leads to a stacking of FM planes with a resulting net magnetic moment. Following the magnetisation steps as function of θ one can construct the metamagnetic phase diagram (fig. 56). The observed magnetic highfield phases are listed in the caption of fig. 56.

The metamagnetism of $\text{HoNi}_2\text{B}_2\text{C}$ is caused by two conflicting interactions, namely

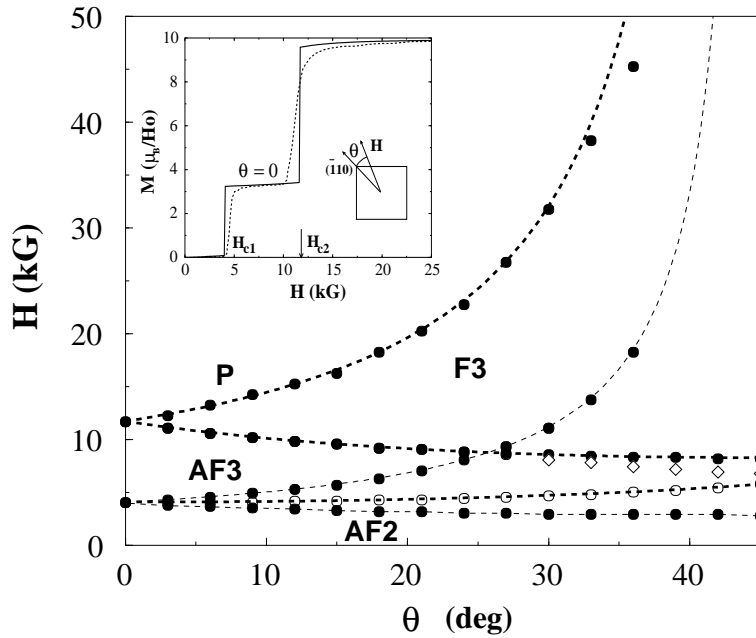


Figure 56. Inset: Experimental (dashed line) and theoretical magnetisation $M(H)$ (full line) for $\text{HoNi}_2\text{B}_2\text{C}$ with \mathbf{H} in the ab -plane at angle $\theta = 0$ with respect to the easy $[\bar{1}10]$ axis. Following the calculated magnetisation steps as function of θ leads to the theoretical phase H - θ phase diagram shown in the main figure (Amici and Thalmeier 1998). The stacking sequence of FM planes along c in the unit cell of magnetic phases is given by AF2($\uparrow\downarrow$), AF3($\uparrow\downarrow\uparrow$) (ferrimagnetic), F3($\uparrow\downarrow\rightarrow$) (noncollinear). P(\uparrow) is the homogeneously magnetised phase. The weak dashed lines denote theoretically possible intermediate phase boundaries not observed experimentally.

tetragonal CEF potential and the RKKY-interaction. Whereas the first tries to align the moments along the easy axis as determined by the CEF potential the second one prefers a helical modulation of moments with a wavevector that minimizes the exchange energy. The favored structure results from a compromise and may change with temperature and external field. The CEF potential is obtained from inelastic neutron scattering experiments (Gasser et al. 1996, Cavadini et al. 2003) by fitting the observed energies and intensities of CEF transitions to the predictions of an extended point charge model of the tetragonal CEF which determines the parameters of the model Hamiltonian H_{CEF} . Then the CEF energies and wave functions may be obtained explicitly. For Ho^{3+} ($J=8$) the 17 singlet and doublet CEF states split into two groups: A group of 13 states with energies >10 meV which is irrelevant in the interesting temperature range and four low lying tetragonal CEF states consisting of a ground state singlet Γ_4 (0 meV) and excited doublet Γ_5^* (0.15 meV) and another singlet Γ_1 (0.32 meV). The interacting Ho 4f-states are then described by

$$H_M = \sum_i [H_{CEF}(\mathbf{J}_i) - \mu_B g \mathbf{J}_i \mathbf{B}] - \frac{1}{2} \sum_{ij} J(i,j) \mathbf{J}_i \mathbf{J}_j \quad (108)$$

where the first part describes the CEF potential and Zeeman energy ($g = \frac{5}{4}$ for Ho^{3+}) and the second term the effective RKKY exchange interaction which is to be fitted empirically to reproduce the critical fields and temperatures of the metamagnetic phase diagram. In mean field (mf) approximation the dimensionless magnetisation \mathbf{m}_i has to fulfil the selfconsistency relations

$$\mathbf{m}(\mathbf{B}_i^e, T) = Tr(e^{\beta H_{mf}(\mathbf{J}, \mathbf{B}_i^e)} \mathbf{J}_i); \quad \mathbf{B}_i^e(\{\mathbf{m}_l\}, T) = g\mu_B + \sum_j J(i, j) \mathbf{m}_j \quad (109)$$

here i runs over all moments \mathbf{m}_i in the magnetic unit cell in a given magnetic structure and \mathbf{B}_i^e is the effective field experienced by the moment. Because the ab-planes are FM ordered (neglecting the \mathbf{Q}_a - modulation) these mf-equations may be solved within a simplified quasi one-dimensional model where only structures are considered that correspond to a different stacking of FM planes along c . Structures with unit cell sizes of up to 29 layers have been considered. Of all structures that are solutions of eq.(109) the stable one at a given field and temperature has to minimize the Helmholtz free energy per volume

$$f_H = f_G(\mathbf{B}) + \frac{B^2}{8\pi} - \frac{\mathbf{H} \cdot \mathbf{B}}{4\pi} = f_G(\mathbf{B}) + 2\pi M^2 - \frac{H^2}{8\pi} \quad (110)$$

where $\mathbf{B} = \mathbf{H} + 4\pi\mathbf{M}$ is assumed to be homogeneous throughout the sample with the homogeneous magnetisation per volume given by $\mathbf{M} = (g\mu_B/v_c)\bar{\mathbf{m}}_i^2$. The bar indicates the average over all moments and v_c is the chemical unit cell volume. The effective exchange parameters between 0^{th} and i^{th} FM layer, $J_i = \sum_{\{j_i\}} J(0, j)$ (j_i runs over all the sites of the i^{th} layer) are considered to be empirical parameters that are determined from the critical fields of the metamagnetic steps, from T_{IC} and from the requirement that the 1D Fourier transform $J(q_z)$ of J_i has a maximum close to the IC modulation vector \mathbf{Q} . This empirically determined exchange function $J(q_z)$ is shown in the inset of fig. 57. In this way most of the metamagnetic phases observed in $\text{HoNi}_2\text{B}_2\text{C}$ and the field angle have been explained within the CEF-RKKY-exchange model eq.(108) as shown in fig. 56 (Amici

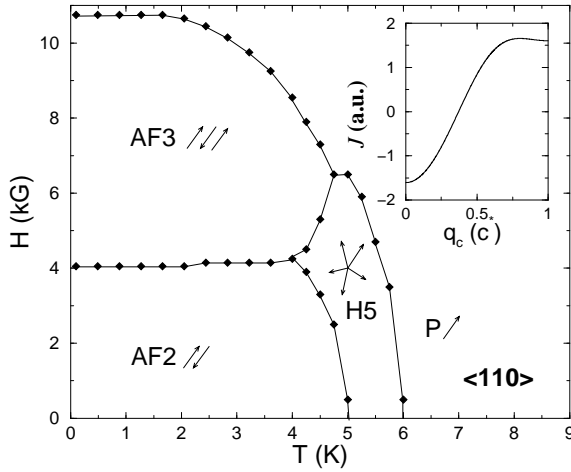


Figure 57. Calculated magnetic H-T phase diagram of $\text{HoNi}_2\text{B}_2\text{C}$ for field along the easy direction $\langle 110 \rangle$. Arrows indicate FM ordered ab-planes (easy axis $[110]$) with stacking sequence along c . The inset shows the RKKY exchange function obtained from metamagnetic critical fields with a maximum around $0.8c^*$ that corresponds to the H5 helix with $T_{IC} = 6$ K. The lock-in transition to the simple AF2 phase appears at $T_N = 5$ K (Amici et al. 2000).

and Thalmeier 1998). The exchange parameters derived theoretically in this work have been confirmed experimentally by Cavadini et al. (2003). However some discrepancies remain, especially it was found later (Campbell et al. 2000, Detlefs et al. 2000) that in the high field phase ($\uparrow\uparrow\rightarrow$) the ab-planes are no longer FM ordered so that the simplified one-dimensional model is insufficient for high fields, but it is completely adequate for studying the coexistence behaviour with superconductivity since $H_{c2}(0) \simeq 0.8$ T for $\text{HoNi}_2\text{B}_2\text{C}$ is below the critical field where the ($\uparrow\uparrow\rightarrow$) phase appears.

The inter-layer exchange parameters J_i with $i = 0-3$, or exchange function $J(q_z)$ obtained in the analysis of metamagnetism can now be used to predict the B-T phase diagram for \mathbf{H} along the easy axis $[110]$ without invoking any further empirical parameters. The solution of eq.(109) for finite temperature leads to the phase diagram shown in fig. 57. The first phase that appears at T_{IC} is determined by the maximum gain in exchange energy, it is a long wavelength commensurate helix phase H5 (FM moment of ab-plane rotating around the c -axis) with wave vector $\mathbf{Q}_{H5} = 0.802\mathbf{c}^*$ which is not too far from the true IC wave vector $\mathbf{Q} = 0.9\mathbf{c}^*$ observed in neutron diffraction. To approximate the true IC phase even better with high order C phases, one had to include still more interlayer interactions, the free energies of these phases are, however, extremely close. When temperature decreases below T_{IC} the moments $\mathbf{m}_i(T)$ increase and the CEF contribution to the free energy which grows with fourth power of the moment size becomes more important. Because it favours alignment with the easy axis directions $[110]$ etc. the helix phase becomes less favorable and finally at $T_N = 5$ K a lock-in transition to the simple commensurate AF phase takes place. There are indications from magnetic x-ray diffraction that an intermediate lock-in

to another C-phase above T_N may exist because a splitting of the IC satellite Bragg peak was observed. Such behaviour is well known from 1D ANNNI models that exhibit devil's staircase behaviour (Bak and von Boehm 1980). At temperatures below 4 K application of a magnetic field along the easy axis finally leads to a metamagnetic transition from the AF2 phase ($\uparrow\downarrow$) to the ferrimagnetic AF3 phase with unit cell ($\uparrow\downarrow\uparrow$) (fig.57).

5.3.2. Weak Ferromagnetism in $\text{ErNi}_2\text{B}_2\text{C}$

This compound becomes superconducting at $T_c = 11$ K and develops a transversely polarised SDW of Er moments below $T_{IC} = 6$ K with a propagation vector $\mathbf{Q} = (0.533, 0, 0)$ corresponding to the FS nesting vector and a moment $\mu = 7.8 \mu_B$ and an easy axis [100]. Magnetisation measurements (Canfield and Bud'ko 1996) have shown that below $T_{WFM} = 2.3$ K a remnant magnetisation exists due to the transition to a weak ferromagnetic (WFM) state with an average moment of $\mu_{WFM} = 0.33\mu_B/\text{Er}$ which persist to lowest temperatures. Therefore $\text{ErNi}_2\text{B}_2\text{C}$ is the first example of true microscopic SC/FM coexistence for all temperatures below T_c . The origin of the WFM phase has been investigated with neutron diffraction and its structure was determined (Kawano et al. 1999, Kawano-Furukawa et al. 2002). On lowering the temperature from T_N the SDW exhibits a 'squaring up' witnessed by magnetic satellite peaks and finally breaks up into commensurate AF sections separated by antiphase boundaries as shown in fig. 58. In every second layer along c the boundaries are located between the Er-bonds creating first disordered moments which finally below T_{WFM} order ferromagnetically. Because only the $z=0$ and equivalent layers of the $\text{ErNi}_2\text{B}_2\text{C}$ bcc structure carry the FM moment one obtains an *average* FM bulk moment of $\mu_{WFM} = (2/40)M_{sat} = 0.39\mu_B$ which is close to the moment from magnetisation measurements. The overall WFM structure (fig. 58) of $\text{ErNi}_2\text{B}_2\text{C}$ can be viewed as FM sheets in the bc - plane with easy axis b and stacked along a . The large stacking distance along a is the origin of the bulk WFM moment of $0.33\mu_B/\text{Er}$. As in the case of $\text{HoNi}_2\text{B}_2\text{C}$ metamagnetic transitions appear for applied field in the ab -plane. They have been explained by a similar model (Jensen 2002) including dipolar interactions. The stable zero field structure has the observed modulation vector with $|\mathbf{Q}| = 11/20$.

5.4. Coexistence of superconductivity and magnetic order

Coexistence behaviour has been studied both for stoichiometric compounds Er, Tm, Dy and Ho borocarbides as well as for pseudo-quarternary compounds $\text{R}_{1-x}\text{R}'_x\text{Ni}_2\text{B}_2\text{C}$ where R, R' are different lanthanide atoms or compounds $\text{R}(\text{Ni}_{1-x}\text{M}_x)\text{B}_2\text{C}$ with M denoting another transition metal atom. In the stoichiometric compounds the interaction of both order parameters is most dramatically seen in the upper critical field H_{c2} -anomalies, especially for $\text{HoNi}_2\text{B}_2\text{C}$ with an almost reentrant behaviour visible in fig. 59. Reentrance can finally be achieved by replacing Ni with Co around $x = 0.005$. According to sect. 5.2 this reduces the DOS at the Fermi level. As seen in fig. 59, this results in a lower T_c and destabilizes the superconducting order parameter against magnetic order, finally for $x > 0.0075$ Co reentrance disappears and superconductivity exists only below the lock-in transition at T_N which remains almost unchanged. The main effect of M substitution for Ni is therefore a T_c tuning by variation of the DOS. Lanthanide substitution like $\text{R}' = \text{Ho}$ or Dy instead of $\text{R} = \text{Lu}$ or Y has a more subtle effect. For relatively small concentrations x of the magnetic R ions T_c is reduced as expected from the Abrikosov Gor'kov

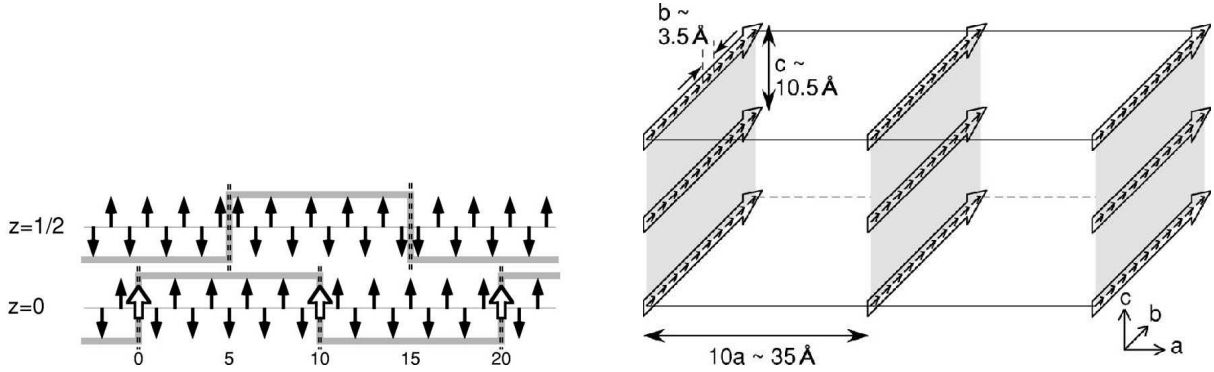


Figure 58. Left panel: WFM structure of $\text{ErNi}_2\text{B}_2\text{C}$ showing the AF moment ordering (easy axis $[010]$) along a -direction for two layers ($z = 0, 1/2$) along c . Moments residing in $z=0$ antiphase boundaries order ferromagnetically (open arrows) below T_{WFM} . Right panel. Overall WFM structure is composed of FM sheets in bc -plane stacked along a (shaded in grey and corresponding to open arrows in left panel) (Kawano-Furukawa et al. 2002).

pair breaking theory by paramagnetic impurities in a nonmagnetic host superconductor, in this case $\text{LuNi}_2\text{B}_2\text{C}$. The pair breaking, like T_m in the magnetic borocarbides, is then controlled by the de Gennes factor dG . This leads to a reduction of T_c linear in $x \cdot dG$. For large concentrations ($x > 0.5$) of magnetic ions however this concept breaks down dramatically. In fact for $x = 1$ $\text{DyNi}_2\text{B}_2\text{C}$ is superconducting and one observes a kind of ‘inverse’ de Gennes scaling of the transition temperature with $(1-x)dG$ corresponding to the concentration $(1-x)$ of *nonmagnetic* Lu impurities in the *antiferromagnetic* host superconductor $\text{DyNi}_2\text{B}_2\text{C}$ which also act like pair breakers.

5.4.1. Coexistence of helical SDW, antiferromagnetism and superconductivity in $\text{HoNi}_2\text{B}_2\text{C}$

In this subsection we discuss a microscopic model (Amici 1999, Amici et al. 2000) which successfully describes the most interesting coexistence behaviour found in $\text{HoNi}_2\text{B}_2\text{C}$. A more phenomenological approach based on GL theory has also been presented for $\text{Ho}_{1-x}\text{Dy}_x\text{Ni}_2\text{B}_2\text{C}$ in Doh et al. (1999). Firstly these compounds should more appropriately be called superconducting magnets because the magnetic and superconducting energy scales given by $E_m = kT_m$ and $E_{SC} = k^2 T_c^2 / E_F$ differ strongly. If $T_m \simeq T_c$ as in the present case then $E_{SC} / E_m = kT_c / E_F \simeq 10^{-2}$. This is due to the fact that only a fraction kT_c / E_F of conduction electrons participates in the pair formation whereas the exchange energy of all localised spins is involved in the magnetic ordering. Thus *local moment* magnetic order energetically completely dominates superconductivity whose influence on the former will therefore be neglected (Amici and Thalmeier 2001). In fact in our previous discussion this was implicitly assumed by neglecting the effect of superconductivity on the RKKY interaction via the conduction electron susceptibility. This is justified because the latter would only be affected for $|\mathbf{q}| \leq \xi_0^{-1}$ ($\xi_0 = \text{SC coherence length}$), and we discuss the competition with AF order or IC phases with modulation vectors close to \mathbf{Q}_{AF} .

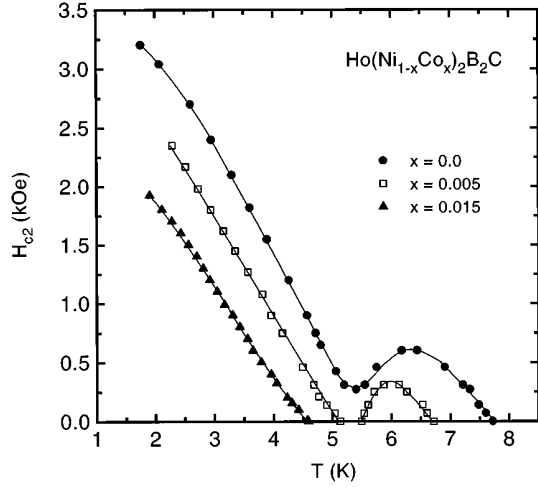


Figure 59. Upper critical field curves for $\text{HoNi}_2\text{B}_2\text{C}$ ($x = 0$) and Co-substituted compounds. For $x = 0$ one observes near reentrance around $T_N \simeq 5.3$ K. For $x = 0.005$ the reduced T_c leads to real reentrance and for $x = 0.015$ finally T_c falls below T_N and ordinary H_{c2} behaviour sets in (Schmidt and Braun 1997).

The really important microscopic coupling is then caused by the appearance of the ordered 4f local moments. According to their magnetic structure they exert an additional periodic potential on the conduction electrons. For the AF or helix structure the local 4f moments are described by

$$\langle S_{\mathbf{R}_i} \rangle = S(T)(\hat{\mathbf{a}} \cos(\mathbf{Q} \cdot \mathbf{R}_i) + \hat{\mathbf{b}} \sin(\mathbf{Q} \cdot \mathbf{R}_i)) \quad (111)$$

where $S(T)$ is the size of the ordered moments and \mathbf{Q} the helix wave vector with $\mathbf{Q} = \mathbf{Q}_{AF}$ in the AF case. The exchange interaction between the conduction and 4f-electrons then leads to an additional spin dependent periodic potential

$$H_{cf} = \frac{1}{2} IS \sum_{\mathbf{k}} (c_{\mathbf{k}+\mathbf{Q}\downarrow}^\dagger c_{\mathbf{k}\uparrow} + c_{\mathbf{k}-\mathbf{Q}\uparrow}^\dagger c_{\mathbf{k}\downarrow}) \quad (112)$$

The exchange constant I may be estimated from the RKKY expression $I^2 N(E_F) dG \simeq kT_m$ by using $N(E_F) = 4.8 \text{ eV}^{-1}$ resulting in $I \simeq 5 \text{ meV}$. The periodic exchange potential of eq. (112) has important effects on the conduction electron states, the original band energies $\epsilon_{\mathbf{k}}$ and Bloch states $c_{\mathbf{k}}$ are strongly modified close to the magnetic Bragg planes at $\pm\mathbf{Q}$ and at $\mathbf{c}^* \pm \mathbf{Q}$. The modified magnetic bands and Bloch states are obtained by a unitary transformation (Herring 1966) which mixes states (\mathbf{k}, \uparrow) and $(\mathbf{k}+\mathbf{Q}, \downarrow)$ where each pair is decoupled from the others. This leads to magnetic Bloch states given by

$$c_{\mathbf{k}+}^\dagger = u_{\mathbf{k}} c_{\mathbf{k}\uparrow}^\dagger + v_{\mathbf{k}} c_{\mathbf{k}+\mathbf{Q}\downarrow}^\dagger; \quad c_{\mathbf{k}-}^\dagger = v_{-\mathbf{k}} c_{\mathbf{k}-\mathbf{Q}\uparrow}^\dagger + u_{-\mathbf{k}} c_{\mathbf{k}\downarrow}^\dagger \quad (113)$$

with the dispersion of the magnetic band given by

$$\tilde{\epsilon}_{\mathbf{k}\pm} = \frac{1}{2}(\epsilon_{\mathbf{k}} + \epsilon_{\mathbf{k}\pm\mathbf{Q}}) + \frac{1}{2}(\epsilon_{\mathbf{k}} - \epsilon_{\mathbf{k}\pm\mathbf{Q}}) \left(1 + \frac{I^2 S^2}{(\epsilon_{\mathbf{k}} - \epsilon_{\mathbf{k}\pm\mathbf{Q}})^2} \right)^{\frac{1}{2}} \quad (114)$$

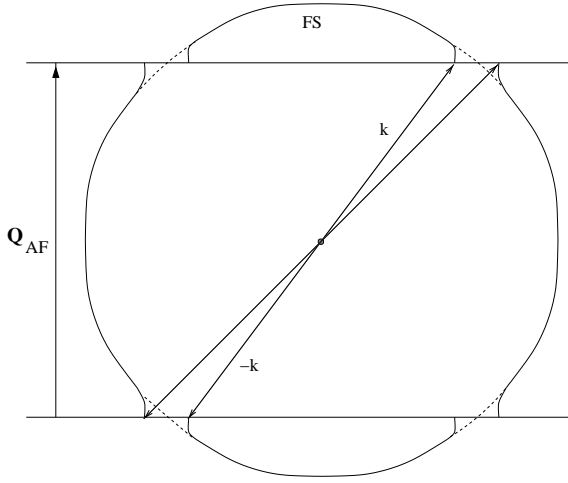


Figure 60. Schematic view of Fermi surface (FS) reconstruction around magnetic Bragg planes connected by \mathbf{Q} according to eq. (114). This leads to strong modification of SC pair potential for conduction electron states with momenta \mathbf{k} , $-\mathbf{k}$ as indicated.

The $(u_{\mathbf{k}}, v_{\mathbf{k}})$ satisfy appropriate orthonormality conditions and fulfil the relation

$$u_{\mathbf{k}}^2 - v_{\mathbf{k}}^2 = \left(\frac{(\epsilon_{\mathbf{k}} - \epsilon_{\mathbf{k}+\mathbf{Q}})^2}{(\epsilon_{\mathbf{k}} - \epsilon_{\mathbf{k}+\mathbf{Q}})^2 + 4I^2 S^2} \right)^{\frac{1}{2}} \quad (115)$$

Far away from magnetic Bragg planes $|\epsilon_{\mathbf{k}} - \epsilon_{\mathbf{k}+\mathbf{Q}}| \gg IS$ this leads to $u_{\mathbf{k}} \sim 1$ and $v_{\mathbf{k}} \sim 0$ and $\tilde{\epsilon}_{\mathbf{k}\pm} \sim \epsilon_{\mathbf{k}\pm}$ so that the original band states and energies are recovered with (\mathbf{k}, \pm) reducing to $(\mathbf{k}, \uparrow\downarrow)$ Bloch states. An illustration of the reconstructed FS is shown in fig.60. Although the effect of the exchange potential eq. (112) is confined to a small region of \mathbf{k} -vectors with $\delta k_{\perp} \leq IS/v_F$ counted from the magnetic Bragg planes, this modification proves important for superconducting properties. From the previous consideration on superconducting and magnetic energy scales it is clear that the Cooper pairs have to be constructed from the *magnetic* Bloch states. This implies that the BCS pair Hamiltonian which is expressed in terms of nonmagnetic band states has to be transformed to the new magnetic basis states. For the AF structure this has been done in (Zwicknagl and Fulde 1981) and for the more general helix phase in (Morosov 1996, Morosov 1996a). Therefore, in addition to the modification eq. (114) of band energies, the nonmagnetic BCS pair potential $V_{\mathbf{k},\mathbf{k}'}$ will be replaced by an effective pair potential between magnetic Bloch states:

$$\tilde{V}_{\mathbf{k},\mathbf{k}'} = (u_{\mathbf{k}}^2 - v_{\mathbf{k}}^2)V_{\mathbf{k},\mathbf{k}'}(u_{\mathbf{k}'}^2 - v_{\mathbf{k}'}^2) \quad (116)$$

According to eq.(115) $\tilde{V}_{\mathbf{k},\mathbf{k}'}$ vanishes if \mathbf{k} or \mathbf{k}' are located on a Bragg plane. Naturally the BCS gap equations then lead to a modified gap function. To keep the discussion of magnetic effects simple we neglect the g-wave part in eq.(102) and assume an originally isotropic s-wave gap Δ . This should not influence the qualitative coexistence behaviour.

Then the above equation leads to an additional \mathbf{k} -dependence originating in the exchange potential eq. (112) which is confined to the immediate vicinity of the Bragg planes. It is given by

$$\begin{aligned}\Delta(\mathbf{k}, T) &= (u_{\mathbf{k}}^2 - v_{\mathbf{k}}^2)\Delta(T) \\ \Delta(T) &= \int_0^{\omega_D} d\epsilon \left(V \int_{MFS} \frac{dS'}{(2\pi)^3} \frac{(u_{\mathbf{k}'}^2 - v_{\mathbf{k}'}^2)^2}{|\nabla_{\mathbf{k}'} \tilde{\epsilon}_{\mathbf{k}'}|} \right) \frac{\Delta(T)F(T)}{\sqrt{\epsilon^2 + \Delta^2(T)}}\end{aligned}\quad (117)$$

where $F_{\mathbf{k}}(T)=[1-2f_{\mathbf{k}}(T)]$ and the inner integration is taken over the reconstructed magnetic Fermi surface (MFS) corresponding to $\tilde{\epsilon}_{\mathbf{k}}$. Obviously the modified gap function $\Delta(\mathbf{k}, T)$ vanishes on node lines \perp c lying on the Bragg planes and accordingly the self consistent gap equation for $\Delta(T)$ will lead to a reduced magnitude of the gap due to the factor in the numerator of the integral in brackets. However, note that no sign change in the modified gap function $\Delta(\mathbf{k}, T)$ occurs when \mathbf{k} crosses a node line, it still belongs to a fully symmetric A_{1g} representation of the underlying AF magnetic structure. Since $(u_{\mathbf{k}}^2 - v_{\mathbf{k}}^2) \simeq 1$ almost everywhere except in the immediate vicinity of Bragg planes ($\delta k_{\perp}/k_F \leq ISN(E_F)$) the reduction of the gap amplitude is not large and helix order may coexist with superconductivity. For the special AF case this is known already from Baltensperger and Strässler (1963) and the helix case with general modulation vector \mathbf{Q} is not very different because it only has two more Bragg planes than the AF case. The second equation has the formal appearance of the BCS gap equation, however, the expression in parentheses has to be interpreted as an effective electron-phonon interaction $V_e(T)$ or dimensionless $\lambda_e(T) = N(E_F)V_e(T)$ which itself depends on the temperature via $S(T)$. Its reduction from the nonmagnetic background value $\lambda = N(E_F)V$ is due to the reconstruction of electronic states confined close to the Bragg planes. Therefore it may be treated as a perturbation linear in the small parameter $IS(T)/E_F$. One obtains

$$\delta\lambda(T) = \lambda - \lambda_e(T) = -\frac{V}{8\pi\hbar^2} \frac{k_r}{v_r v_z} IS(T) \quad (118)$$

for a FS piece without nesting features which is cut by a pair of Bragg planes with a FS radius k_r at the intersection and radial and parallel velocities v_r and v_z respectively. For a helical structure with two pairs of Bragg planes at $\pm\frac{1}{2}\mathbf{Q}$ and $\pm\frac{1}{2}(\mathbf{c}^* - \mathbf{Q})$ one has to add two corrections as in eq. (118) with different FS parameters. The main effect of the interaction of magnetic order and superconductivity described by eq. (112) has now been condensed into eq. (118). The physical consequences of the reduction of λ due to magnetic order are a reduced superconducting T_c and condensation energy which results in an anomaly in $H_{c2}(T)$ that is directly correlated with the appearance of the local moment order parameter $S(T)$. The upper critical field anomaly may approximately be calculated by using an appropriately modified BCS expression and including the magnetisation response of the local moments:

$$\begin{aligned}H_{c2}^{[110]}(T) &= B_{c2}[\lambda_e(T), T] - M^{[110]}(T) \\ H_{c2}^{[001]}(T) &= B_{c2}[\lambda_e(T), T]\end{aligned}\quad (119)$$

where $B_{c2}(\lambda_e(T), T) = B_{c2}^0(\lambda_e(T)) \cdot [1-(T/T_c(\lambda_e(T)))^2]$ is the BCS expression modified due to the T-dependence of the effective e-p coupling. The magnetisation for the [001]

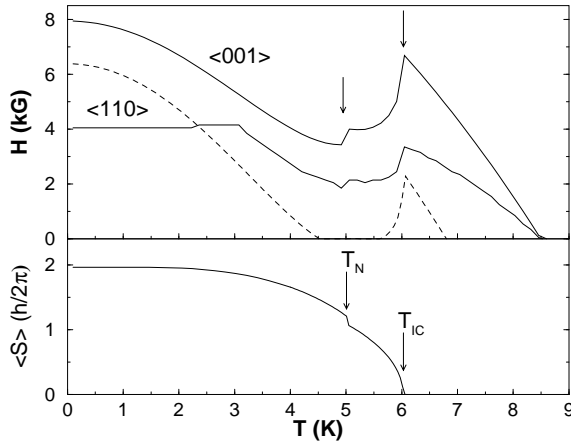


Figure 61. Lower panel: size of the magnetic order parameter (local moment amplitude) $\langle S \rangle$ vs temperature for the helix (H5) phase below T_{IC} and the AF2 phase below T_N . Upper panel: H_{c2} for two symmetry directions. For $\langle 110 \rangle$ the plateau is caused by the transition to the ferrimagnetic AF3 phase in fig. 56. The dashed line is H_{c2} along $\langle 001 \rangle$ with a reduced background T_c that simulates the effect of doping on the reentrance behaviour (Amici et al. 2000).

direction can be neglected because the 4f moments of CEF states are well constrained within the easy ab- plane. Using eqs. (118),(119) with an appropriate set of parameters for $\text{HoNi}_2\text{B}_2\text{C}$ the calculated upper critical field is shown in fig. 61. It clearly shows a pronounced depression of $H_{c2}(T)$ when magnetic order sets in. As discussed before there is no big difference in the effect of helical order (below T_{IC}) and commensurate AF order (below T_N), the overall depression is simply controlled by the increase of $S(T)$ when T decreases. At this point we mention again that in our discussion of coexistence behaviour the a^* -incommensurate magnetic modulation has been neglected. This is fully justified according to hydrostatic pressure experiments by Dertinger (2001) where it has been shown that: (i) while the a^* satellite intensity in ND decreases with pressure and vanishes at $p > 0.7$ GPa, (ii) the reentrance minimum in H_{c2} becomes even more pronounced. This proves that the a^* - modulation of moments plays no important role in the reentrance behaviour of SC, contrary to what has been claimed by many previous investigations. The [110], [001] anisotropy of H_{c2} is due to the different magnetisation response in both directions. For field lying in the easy plane $H_{c2}(T)$ exhibits a plateau which is due to the appearance of the ferrimagnetic AF2 phase above the first critical field in fig.(57). This phase has a net magnetic moment that cannot coexist with superconductivity. If the nonmagnetic background e-p coupling λ is reduced by about 10% the resulting reduction in T_c and condensation energy leads to a reentrance behaviour of $H_{c2}(T)$ as shown by the dashed curve. These features described by the theory of Amici et al. (2000), namely depression, anisotropy (plateau) and reentrance behaviour have all been observed experimentally in $\text{HoNi}_2\text{B}_2\text{C}$, the latter under Co-substitution of Ni which reduces T_c as shown in fig. 59.

5.4.2. Coexistence of superconductivity and weak ferromagnetism in $\text{ErNi}_2\text{B}_2\text{C}$

At the SDW transition of $\text{ErNi}_2\text{B}_2\text{C}$ ($T_{IC} = 6$ K) a similar but much less pronounced dip in H_{c2} as in $\text{HoNi}_2\text{B}_2\text{C}$ is observed indicating the coexistence of both types of order. Even more exciting is the observation of WFM order below $T_{WFM} = 2.3$ K which coexists with SC ($T_c = 11$ K) to the lowest temperatures. This first confirmed example of microscopic FM/SC coexistence has therefore attracted a lot of attention. Established theories (Ginzburg 1957) predict that thermodynamic coexistence in type II superconductors is only possible when the internal FM field $H_{int} \sim 4\pi M$ is smaller than H_{c2} (Fischer 1990). In $\text{ErNi}_2\text{B}_2\text{C}$ due to the large FM layer spacing (fig. 58) one estimates from μ a small $H_{int} \sim 0.5$ kG which is of the same order as H_{c1} and much smaller than $H_{c2} \sim 15$ kG (Canfield and Bud'ko 1996). Despite its smallness H_{int} does have a very peculiar effect: For applied fields H with orientation θ_a close to the c -axis the perpendicular internal field along the a direction rotates the effective field of the vortex phase to an angle θ_v towards the a -axis. Thus the vortex lattice will show a misalignment with the applied field by a small angle $\theta_v - \theta_a$. This effect has been found experimentally by Yaron et al. (1996). Theoretically this effect was considered in the context of a Ginzburg-Landau theory including the terms corresponding WFM order parameter and the coupling to SC (Ng and Varma 1997). Since the London penetration depth λ is 26 times larger than the FM layer spacing in fig. 58 (Kawano-Furukawa et al. 2001) it can still be justified to use an averaged FM moment density of saturation value $0.34\mu_B$. The tilt angle $\theta_v - \theta_a$ of vortices becomes larger at lower temperature in agreement with theoretical predictions. If the internal field H_{int} is at least somewhat larger than H_{c1} another exotic transition to a spontaneous vortex phase in zero applied field may take place. In this phase the internal field spontaneously forms a vortex lattice oriented along the a direction. Low field magnetisation measurements and small angle neutron scattering experiments (Kawano-Furukawa et al. 2001) seem to support such a possibility but the issue is not settled.

6. Rare Earth Skutterudite Superconductors

The new heavy fermion superconductor $\text{PrOs}_4\text{Sb}_{12}$ which has been discovered recently (Bauer et al. 2002) is potentially of similar interest as UPt_3 because it represents the second example of multiphase superconductivity (Izawa et al. 2003) with a critical temperature $T_c = 1.85$ K. This material belongs to the large class of RT_4X_{12} skutterudite cage compounds (R = alkaline earth, rare earth or actinide; T = Fe, Ru or Os and X=P, As or Sb) which have a bcc-filled skutterudite structure with tetrahedral space group T_h^4 (fig. 62). In this structure large voids formed by tilted T_4X_{12} octahedrons can be filled with R atoms. They are however rather loosely bound and therefore may have large anharmonic oscillations (‘rattling’) in the cage. In addition if equivalent equilibrium positions are present tunneling split states may exist. Both effects may lead to interesting low temperature elastic and transport phenomena i.e. thermoelectric effects (Sales et al. 1996, Sales 2003). Depending on the cage-filling atom this large class of compounds displays also a great variety of interesting effects of strong electron correlation. Mixed valent and heavy fermion behaviour, magnetic and quadrupolar order, non-Fermi liquid and Kondo insulating behaviour has been found, see Bauer et al. (2002), Sales (2003) and references cited therein. Recently the SC in non-stoichiometric skutterudites $\text{Pr}(\text{Os}_{1-x}\text{Ru}_x)\text{Sb}_{12}$ has been investigated throughout the whole concentration range of $0 \leq x \leq 1$ (Frederick et al. 2003). While for $x = 0$ one has an unconventional HF superconductor the $x = 1$ compound $\text{PrRu}_4\text{Os}_{12}$ on the other hand is a conventional SC with $T_c \simeq 1$ K. The type of SC changes at $x \simeq 0.6$ where the transition temperature $T_c(x)$ has a minimum value of 0.75 K. Here we will focus, however, exclusively on the HF multiphase superconductivity in $\text{PrOs}_4\text{Sb}_{12}$ ($x=0$).

6.1. Electronic structure and HF behaviour of $\text{PrOs}_4\text{Sb}_{12}$

The LDA+U band structure and Fermi surface of $\text{PrOs}_4\text{Sb}_{12}$ has been investigated by Sugawara et al. (2002) and compared with dHvA results. Three FS sheets, two of them closed and approximately spherical were identified both experimentally and in the calculation. Their dHvA masses are $m^* = 2.4 - 7.6 m$, this is considerably higher than the calculated LDA+U band masses ranging from $m_b = 0.65 - 2.5 m$. The observed dHvA masses however are still much too small compared to the thermal effective mass m^* estimated from the the extrapolated γ -value of the linear specific heat. One obtains (Vollmer et al. 2003) $\gamma = 313$ mJ/mole K^2 leading to an estimate of $m^* = 50 m$. This places $\text{PrOs}_4\text{Sb}_{12}$ among the heavy fermion metals, the first one ever observed for a Pr-compound with its $4f^2$ electronic configuration, the estimated quasiparticle bandwidth is $T^* \simeq 10$ K (Bauer et al. 2002) which is in the same range as the lowest CEF splittings. Therefore, the low temperature behaviour of $C(T)$, $\chi(T)$ and $\rho(T)$ is determined by both CEF effects and heavy quasiparticle formation and it is difficult to separate them (Maple et al. 2002). The latter is rather anomalous for a HF system since the A-coefficient in $\rho(T) = \rho_0 + AT^2$ is smaller by two orders of magnitude compared to other HF systems. The susceptibility is largely dominated by localised $4f^2$ CEF states and from the high temperature behaviour an effective Pr^{3+} moment $\mu = 2.97\mu_B$ is obtained.

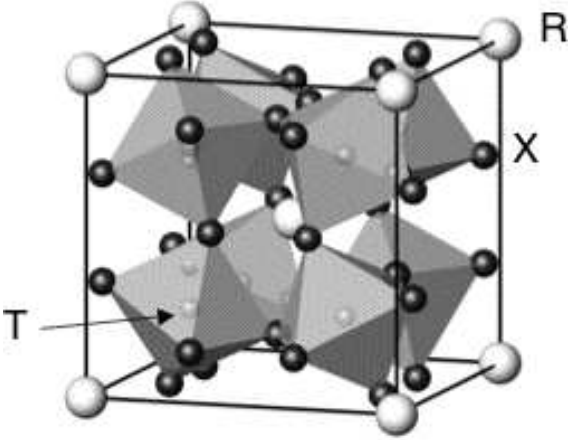


Figure 62. Cubic crystal structure of filled skutterudite RT_4X_{12} . R atoms: large circles, X atoms: middle size circles, T atoms: small circles located in the center of TX_8 octahedra (grey). For $PrOs_4Sb_{12}$ the lattice constant is $a = 9.3017\text{\AA}$.

6.2. Pr-CEF states and antiferroquadrupolar order

The CEF level scheme of Pr^{3+} is determined by a CEF potential with tetrahedral T_h symmetry. For a long time it was thought that it is equivalent to that of other cubic point groups like T_d or O_h . However, it was shown recently (Takegahara et al. 2001) that this is incorrect. Due to the absence of two types of symmetry operations the CEF potential is rather given by

$$H_{CEF} = W \left[x \left(\frac{O_4}{F(4)} \right) + (1 - |x|) \left(\frac{O_6^c}{F(6)} \right) + y \left(\frac{O_6^t}{F^t(6)} \right) \right] \quad (120)$$

where $O_4 = O_4^0 + 5O_4^4$, $O_6^c = O_6^0 - 21O_6^4$ and $O_6^t = O_6^0 - O_6^6$ are Steven's operators and for Pr^{3+} $F(4)=60$, $F(6)=1260$ and $F^t(6)=30$. For the cubic groups O_h and T_d we have $y=0$ and there is only one CEF parameter x , aside from the overall scale W , then H_{CEF} reduces to the well known form. However in tetrahedral symmetry T_h in general a second CEF parameter $y \neq 0$ appears. The consequences were analysed in detail in Takegahara et al. (2001), specifically the Γ_1, Γ_2 states of the cubic CEF case will be mixed into two inequivalent Γ_1 singlets of T_h and likewise Γ_4, Γ_5 of O_h will be mixed to become two inequivalent Γ_4 triplets of T_h where the degree of mixing depends on y . The experimental determination of the Pr^{3+} CEF level scheme has been performed under the restriction $y=0$ (i.e. assuming the cubic CEF potential), therefore, we keep the original notation of states. With this restriction the level scheme has been determined by fitting $\chi(T)$ and also directly by inelastic neutron scattering (Maple et al. 2002). The latter leads to a level scheme $\Gamma_3(0K), \Gamma_5(8.2K), \Gamma_4(133.5K), \Gamma_1(320K)$, which is close to the one obtained from $\chi(T)$. The ground state is a nonmagnetic (non-Kramers) doublet with a quadrupole moment and quadrupole matrix elements connecting to the first excited triplet state. An alternative CEF level scheme has been proposed (Aoki et al. 2002, Tayama et al. 2003)

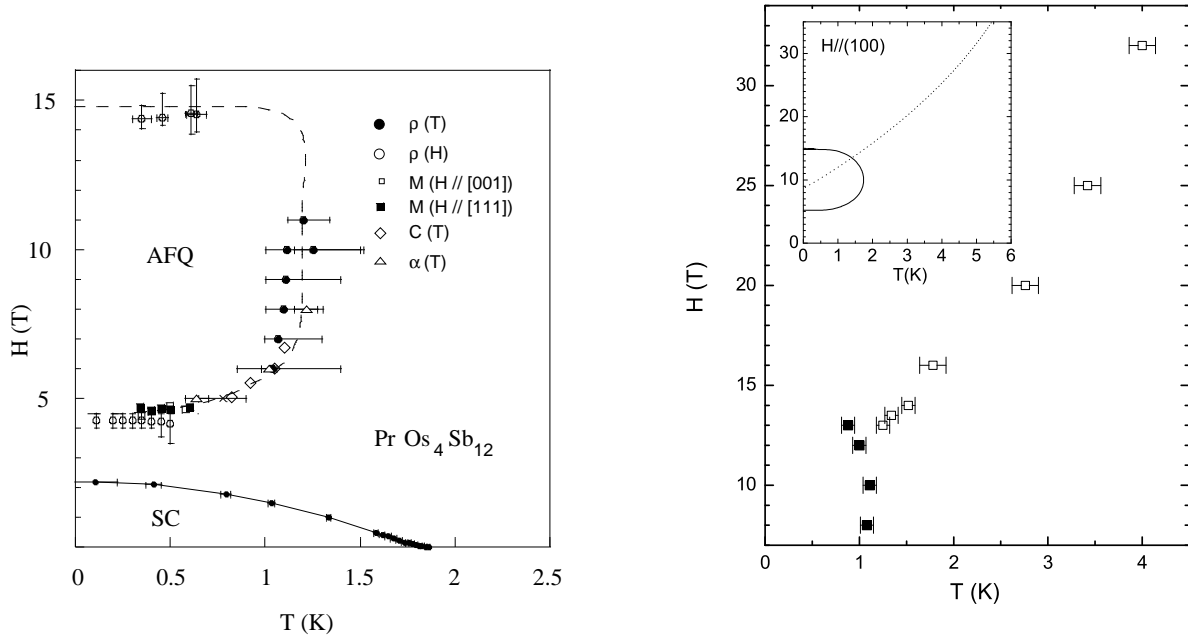


Figure 63. Left panel: complete B-T phase diagram (Maple et al. 2002) with SC regime and region of field induced order parameter which is presumably of antiferroquadrupolar (AFQ) type. Data are obtained from resistivity (ρ), magnetisation (M), specific heat (C) and thermal expansion (α) measurements. Right panel: high magnetic field phase diagram (Aoki et al. 2003) with upper part of AFQ phase (full squares) and line of high field Schottky anomaly from the Γ_1 - Γ_5 crossing. The inset shows calculation for tetrahedral CEF model.

from specific heat and magnetisation experiments. It has a singlet ground state without magnetic nor quadrupole moment, namely $\Gamma_1(0\text{K})$, $\Gamma_5(6\text{K})$, $\Gamma_4(65\text{K})$ and $\Gamma_3(111\text{K})$. The splitting energy δ ($\simeq 6 - 8.2$ K) of ground state to first excited state is also seen as a pronounced zero field Schottky anomaly sitting on top of the superconducting transition. Application of a field above the SC $H_{c2}(0) = 2.2$ T suppresses the Schottky anomaly.

However, at larger fields of $H \simeq 4$ T a new and sharper one appears at lower temperatures possibly signifying the stabilization of a long range antiferroquadrupolar ordered phase (Aoki et al. 2001, Aoki et al. 2002, Vollmer et al. 2003, Maple et al. 2003). This is summarized in the phase diagram shown in the left part of fig. 63. A detailed analysis of AFQ long range order in the high field region is still lacking, therefore it is helpful to compare with other known AFQ ordered 4f systems, where $\text{Ce}_{1-x}\text{La}_x\text{B}_6$ is certainly the most well studied one (Shiina et al. 1997). It has a Γ_8 quartet as CEF ground state which carries both quadrupole and magnetic moment. Both spontaneous AFQ and AF order are therefore observed with $T_Q > T_N$ and we consider only the former. For $x = 0.5$ the AFQ phase diagram (Nakamura et al. 1997) is quite similar to that of fig. 63, namely the AFQ phase is only induced in finite field and $T_Q(H)$ increases with field. In the $\text{Ce}_{1-x}\text{La}_x\text{B}_6$ system the AFQ order has been identified by observing the induced secondary AF order

which is induced by a homogeneous field H in the ordered AFQ background. This can be done by neutron diffraction and NMR experiments. Recent neutron diffraction results (Kohgi et al. 2003) suggest that the CEF ground state is singlet Γ_1 and the AFQ order parameter is of $O_{yz} = J_y J_z + J_z J_y$ type. Additional high field measurements on $C(T, H)$ for different field directions (Rotundu et al. 2003) also give strong evidence for the Γ_1 ground state scenario and for a $\Gamma_1 - \Gamma_5$ level crossing as origin of the field induced AFQ phase (fig. 63, right panel).

The existence of a nonmagnetic (Γ_1 or Γ_3) ground state in $\text{PrOs}_4\text{Sb}_{12}$ leads one to speculate about the origin of the observed HF behaviour since the usual Kondo lattice mechanism as in Ce-intermetallic compounds which demands a Kramers degenerate magnetic ground state cannot be at work here. In the case that Γ_3 were realised one might conjecture that instead of the exchange scattering one has aspherical Coulomb scattering from the quadrupolar degrees of freedom of the nonmagnetic Γ_3 ground state. As discussed for the isoelectronic U^{4+} -configuration in UBe_{13} in sect. 4.5 this is described by a multichannel Kondo Hamiltonian for the quadrupolar pseudo-spin. It can lead to a partial screening of the Γ_3 -quadrupole below a quadrupolar Kondo temperature T^* . At even lower temperatures logarithmic non-Fermi liquid anomalies in thermodynamic quantities should develop due to the partial screening. This cannot be confirmed due to the intervening SC transition. Therefore this quadrupolar HF mechanism for $\text{PrOs}_4\text{Sb}_{12}$ is only a conjecture. If a singlet Γ_1 ground state is realised as suggested by neutron diffraction and high field $C(T, H)$ results mentioned before one has to invoke another mechanism for heavy mass generation which is similar to the one implied in U-compounds like UPd_2Al_3 (Zwicknagl et al. 2003). It is due to mass renormalisation by the low lying Γ_1 - Γ_5 excitation, i.e. contrary to the previous scenario it is caused by off-diagonal parts of the conduction electron-CEF level interaction.

6.3. The superconducting split transition

The SC specific heat jump is superposed on the Schottky anomaly from the lowest CEF excitation at δ . Nevertheless its detailed analysis provides clear evidence for a split SC transition (Bauer et al. 2002, Vollmer et al. 2003) at $T_{c1} = 1.85$ K and $T_{c2} = 1.75$ K as shown in fig. 64. The total jump of both transitions amounts to $\Delta_{SC}C/\gamma T_c \simeq 3$ which exceeds the BCS value 1.43 for a single transition considerably. It also proves that the SC state is formed from the heavy quasiparticles that cause the enhanced γ -value. A T_c -splitting of similar size also was clearly seen in thermal expansion measurements Oeschler et al. (2003, 2003a). The two superconducting transitions in fig. 64 are reminiscent of the split transition in UPt_3 (sect. 4.1). There a twofold orbitally degenerate SC state is split by weak AF order that reduces the hexagonal symmetry to orthorhombic. This also leads to two critical field curves in the B-T phase diagram. In $\text{PrOs}_4\text{Sb}_{12}$ no such symmetry breaking field exists and the split transition has to belong to two different T_h representations of the SC order parameter or combinations thereof as discussed below. The critical field curves associated with $T_{c1,2}$ have been investigated with magnetisation (Tayama et al. 2003) and specific heat measurements from which practically parallel curves are obtained. Only the upper critical field corresponding to T_{c1} with $H_{c2}(0) \simeq 2.2$ T is shown in fig. 63.

As usual in the early stage of investigation different experiments gave inconclusive

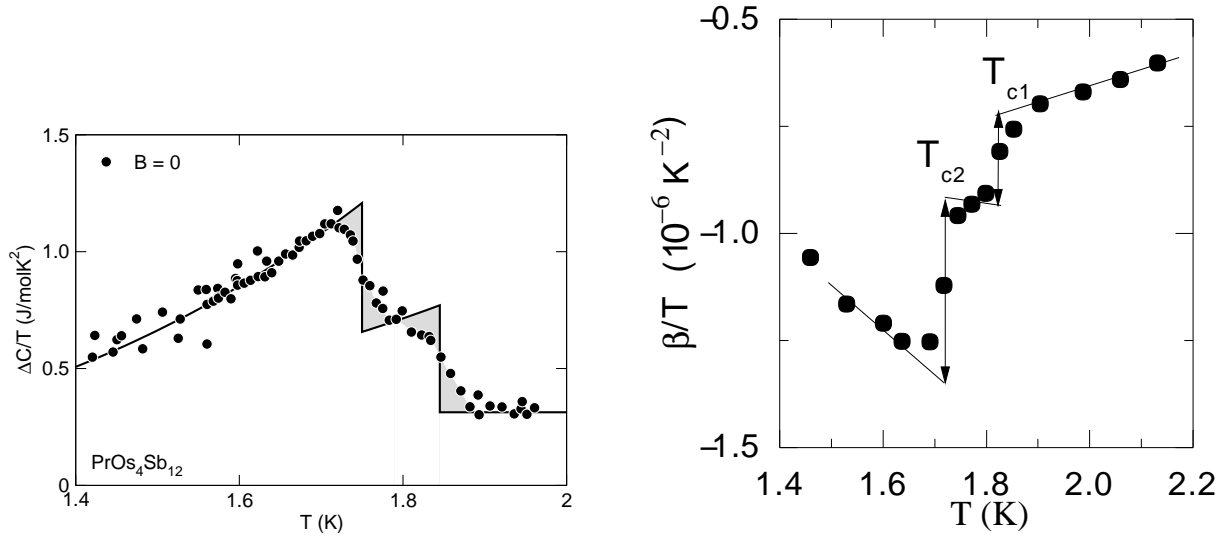


Figure 64. Left panel: electronic specific heat $\Delta C/T$ vs. temperature (Vollmer et al. 2002). Solid line is an entropy conserving construction leading to SC transitions at $T_{c1} = 1.85$ K and $T_{c2} = 1.75$. Total specific heat jump $\Delta C_{SC}/\gamma T_c \simeq 3$. Right panel: corresponding jumps in the volume thermal expansion at $T_{c1,2}$ (Oeschler et al. 2003, 2003a).

results on the question of the nature of gap anisotropy. The low temperature specific heat exhibits a $C_s(T) \sim T^n$ power law in a rather reduced range between 0.65 K and 1.2 K which points to some kind of nodal state. In Sb-NQR experiments (Kotegawa et al. 2003) the nuclear spin lattice relaxation $1/T_1$ rate was determined. It has an itinerant quasiparticle contribution that contains information on the SC nodal state below T_c and in addition a localised contribution from broadened CEF excitations which decreases exponentially for temperatures $T \ll \Delta$. There is no unique way to separate these contributions, this problem is similar to the two Knight shift contributions in the case of UPd_2Al_3 (sect. 4.2) with its isoelectronic $5f^2$ localised states. The NQR measurements did not show any evidence for a coherence peak below T_c which points to an unconventional SC state, for lower temperatures an exponential decay of T_1^{-1} in conflict with the existence of gap nodes was reported. However, this result depends critically on the subtraction procedure of the localised contribution.

6.4. Thermal conductivity in the vortex phase and multiphase superconductivity in $\text{PrOs}_4\text{Sb}_{12}$

The experiments on field-angle dependent thermal conductivity described in sect. 2 are a more powerful method to investigate the SC state. This method achieved the determination of critical field curves and the associated B-T phase diagram in $\text{PrOs}_4\text{Sb}_{12}$ (Izawa et al. 2003) and at the same time the nodal structure of the gap function has at least been partly clarified. The same geometry as for borocarbides (sect. 5) with conical field rotation around the heat current direction parallel to a cubic [001] axis was used and

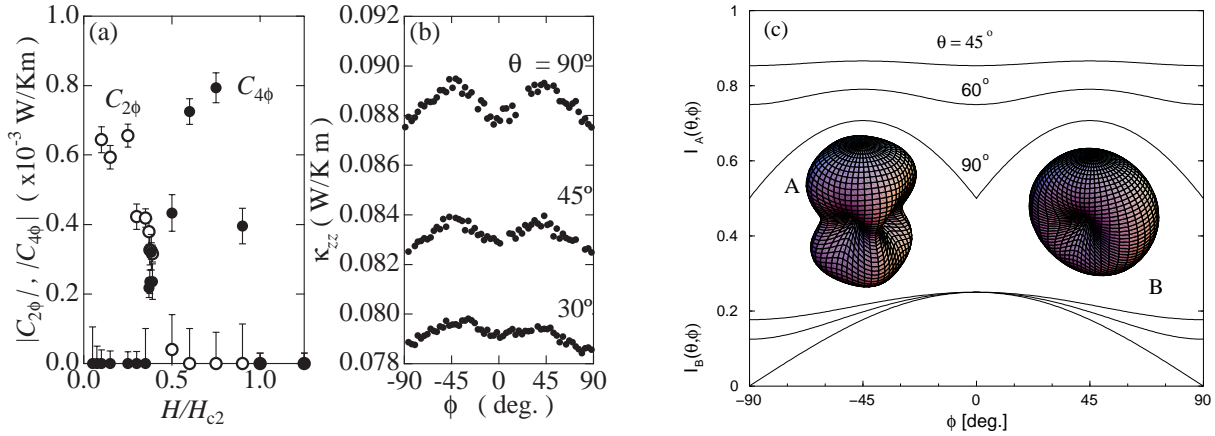


Figure 65. (a) Field dependence of the fourfold ($C_{4\phi}$) and twofold ($C_{2\phi}$) amplitudes of $\kappa_{zz}(\phi)$ oscillations in (b) as function of field strength at $T = 0.52$ K. Sharp transition at $H^* = 0.4H_{c2}$ from twofold to fourfold oscillation is seen. (b) Fourfold oscillations from experiment for different polar field angle θ (Izawa et al. 2003). (c) Calculated angular variation of κ_{zz} as function of azimuthal field angle ϕ exhibiting fourfold (A) and twofold (B) oscillations ($\theta =$ polar field angle). The inset shows polar plots of A- and B-phase gap functions with four and two point nodes respectively (Maki et al. 2002b).

measurements in the whole temperature range from 0.3 K up to T_{c1} were performed. The azimuthal angle dependence of κ_{zz} was found to be approximately of the empirical form

$$\kappa_{zz}(\theta, \phi, H, T) = \kappa_0 + C_{2\phi}(\theta, H, T) \cos 2\phi + C_{4\phi}(\theta, H, T) \cos 4\phi \quad (121)$$

containing both twofold and fourfold rotations in ϕ . The ϕ dependence for $H = 1.2$ T is shown in fig. 65 for a few polar angles θ . It exhibits clearly a dominating fourfold oscillation. Since the amplitude rapidly decreases with θ similar as in the borocarbides this may be interpreted as evidence for *point nodes* in $\Delta(\mathbf{k})$ along the [100] and [010] cubic axes. Surprisingly, when the field is lowered to $H^* = 0.8$ T $\ll H_{c2}$ a rather sudden change from a fourfold to a twofold oscillation in ϕ as shown in fig. 65 is observed which is interpreted as at transition to a different SC state with only two point nodes along [010]. The second critical field H^* can be followed to higher temperatures, although with rapidly decreasing oscillation amplitudes $C_{2\phi}$ and $C_{4\phi}$. Apparently the second critical field curve $H^*(T)$ ends at the lower critical temperature T_{c2} observed already in the second specific heat jump at zero field.

This allows one to construct a B-T phase diagram for $\text{PrOs}_4\text{Sb}_{12}$ shown in fig. 66. Most importantly one has two distinct regions with A- and B-phase superconductivity characterised by four and two point nodes along cubic axis [100] and [010]. In the applied geometry the field is swept around the [001] axis, and therefore possible nodes along this direction cannot be detected. Additional experiments with a sweep axis orthogonal to [001] would be necessary. Furthermore, three different domains (orientation of the node directions) of A- and B-phase are possible. Apparently for the sample investigated a specific domain has been selected, possibly by internal strain effects. From the B-T

Table 7

Even parity basis functions for SC gap in tetrahedral (T_h) symmetry. (symbols used: $\psi_i^\Gamma(\mathbf{k})$ and $\psi_i^{\Gamma'}(\mathbf{k})$ (i=1-d) are second (l=2) and fourth degree (l=4) basis functions respectively, d denotes the degeneracy and Γ_2 and Γ_3 are complex conjugate combinations of E_1 and E_2 components)

d	Γ	$\psi_i^\Gamma(\mathbf{k})$	$\psi_i^{\Gamma'}(\mathbf{k})$
1	$A(\Gamma_1)$	1	$k_x^4 + k_y^4 + k_z^4$
2	$E(\Gamma_2, \Gamma_3)$	$(2k_z^2 - k_x^2 - k_y^2, k_x^2 - k_y^2)$	$(2k_z^4 - k_x^4 - k_y^4, k_x^4 - k_y^4)$
3	$T(\Gamma_5)$	$(k_y k_z, k_z k_x, k_x k_y)$	$(k_y k_z k_x^2, k_z k_x k_y^2, k_x k_y k_z^2)$

phase diagram fig. 66 we conclude that $\text{PrOs}_4\text{Sb}_{12}$ is the second pure multiphase HF superconductor found after UPt_3 . There is, however, no crossing of critical field lines and a corresponding tetracritical point in $\text{PrOs}_4\text{Sb}_{12}$ as was observed in fig. 29 for UPt_3 .

6.5. Gap models for SC A- and B-phases of $\text{PrOs}_4\text{Sb}_{12}$

The observation of a different nodal structure in the A- and B-phases raises the question of the symmetry of the gap function in $\text{PrOs}_4\text{Sb}_{12}$. Various proposals have been made in (Maki, Won, Thalmeier, Yuan, Izawa and Matsuda 2003, Goryo 2003, Miyake et al. 2003, Ichioka et al. 2003) based on an empirical approach and compatible with the observed point nodes. The gap function may be expanded in terms of basis functions $\psi_i^\Gamma(\mathbf{k})$ which transform like representations Γ of the crystal symmetry group (i=1-d is the degeneracy index, the index l denoting the degree of Γ is suppressed). So far there is no information from NMR Knight shift or H_{c2} - Pauli limiting effects whether $\text{PrOs}_4\text{Sb}_{12}$ has spin singlet or triplet pairing. In the singlet case the gap function should then be given by

$$\Delta(\mathbf{k}) = \sum_{\Gamma, i} \eta_i^\Gamma \psi_i^\Gamma(\mathbf{k}) \equiv \Delta f(\mathbf{k}) \quad (122)$$

where the form factor $f(\mathbf{k})$ is normalized to one and Δ is the temperature dependent maximum gap value. In the spirit of the Landau theory only a *single* representation with the highest T_c should be realized and for $T \geq T_c$ the free energy may then be expanded in terms of possible invariants of the order parameter components (Volovik and Gor'kov 1985) η_i^Γ which are determined by Landau parameters $\alpha^\Gamma(T)$ and β_i^Γ . The node structure is then fixed by the specific symmetry class of $\Delta(\mathbf{k})$ defined by the set of η_i^Γ . However the pure second (l=2) and fourth (l=4) degree representations in tetragonal T_h symmetry which are given in table 7 cannot realize a gap function with the observed nodal structure, and therefore, one has to consider the possibility of hybrid order parameter models. A striking example of such a hybrid gap function (s+g wave model) has already been discussed in the previous section for the nonmagnetic borocarbide superconductor $\text{Y}(\text{Lu})\text{Ni}_2\text{B}_2\text{C}$. The symmetry classification of table 7 suggests the following simple proposal for a hybrid gap function $\Delta(\mathbf{k}) = \Delta f(\mathbf{k})$ for $\text{PrOs}_4\text{Sb}_{12}$ which has the the observed nodes along the cubic axis, excluding the still hypothetical ones along [001]:

$$\begin{aligned} \text{A-phase } \Delta(\mathbf{k}) &= \Delta(1 - k_x^4 - k_y^4) \\ \text{B-phase } \Delta(\mathbf{k}) &= \Delta(1 - k_y^4) \end{aligned} \quad (123)$$

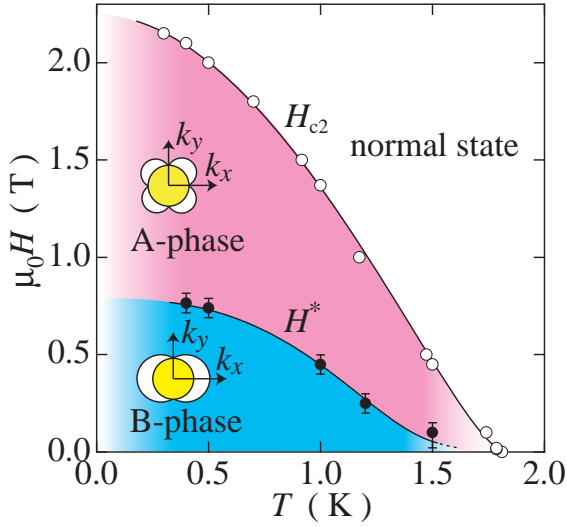


Figure 66. B-T phase diagram of $\text{PrOs}_4\text{Sb}_{12}$ exhibiting B-phase with twofold symmetry and A-phase with fourfold symmetry in a cubic plane. The A-phase and B-phase gap symmetries are indicated. They have four and two point nodes in a cubic plane respectively (Izawa et al. 2003).

According to table 7 A- and B-phase are superpositions of A and E representations with planar and axial symmetry respectively. They are threefold degenerate and particular domains with nodes in the $k_y k_z$ -plane (A) or along k_y (B) have been chosen. This selection might be realised due to internal strains in the SC sample. Polar plots of A,B-phase gap functions are shown in the inset of fig. 65. The magnetothermal conductivity in the vortex state of phases A, B in the limit $\Gamma < T \ll \Delta$ can be calculated as described in sect. 2 and the result for κ_{zz} is

$$\frac{\kappa_{zz}}{\kappa_n} = \left(\frac{2}{\pi}\right)^2 \frac{v\sqrt{eH}}{\Delta} I_{A,B}(\theta, \phi) \quad (124)$$

with the angular dependent functions $I_i(\theta, \phi)$ ($i=A,B$) given by

$$\begin{aligned} I_A(\theta, \phi) &= \frac{1}{2}[(1 - \sin^2 \theta \sin^2 \phi)^{\frac{1}{2}} + (1 - \sin^2 \theta \cos^2 \phi)^{\frac{1}{2}}], \\ I_B(\theta, \phi) &= \frac{1}{4}(1 - \sin^2 \theta \sin^2 \phi)^{\frac{1}{2}} \end{aligned} \quad (125)$$

For in plane field ($\theta = \pi/2$) one has $I_A(\theta, \phi) = |\sin \phi| + |\cos \phi|$ and $I_B(\theta, \phi) = |\cos \phi|$, their leading Fourier components vary like $\cos 4\phi$ and $\cos 2\phi$ respectively in accordance with the empirical expressions in eq. (121). However, the above equations really predicts cusps at $\phi = n(\pi/2)$ (fig. 65(c)) analogous to the situation in the borocarbides and not the smooth minima as seen in fig. 65(b). Therefore, the existence of cusps cannot be safely inferred from the experimental results in fig. 65, this would necessitate measurements at lower temperatures. Also experiments with variation of the polar angle θ have to

be performed to check the possible existence of node points along [001]. Finally μSR experiments show indications of the presence of magnetic moments in the SC phase which is interpreted, similarly as in $U_{1-x}Th_xBe_{13}$ as evidence for a nonunitary triplet SC state (Aoki et al. 2003). This has also been claimed from a recent penetration depth study (Chia et al. 2003).

As a preliminary conclusion it seems clear that $PrOs_4Sb_{12}$ is a very unconventional multiphase HF superconductor of potentially the same interest as UPt_3 . Recalling that heavy quasiparticles are presumably caused by coupling with virtual quadrupolar excitations from the nonmagnetic 5f ground state one is lead to speculate that SC in $PrOs_4Sb_{12}$ might also imply the presence of an unprecedented pairing mechanism based on the exchange of quadrupolar fluctuations. In addition to the spin-fluctuation and magnetic-exciton exchange mechanism this would be the third possibility for Cooper pair formation at work in heavy fermion compounds. However, at the moment the quadrupolar SC mechanism in $PrOs_4Sb_{12}$ is still a conjecture.

7. Summary and Outlook

During the past decade a number of exciting and often unanticipated broken symmetry states and associated physical effects have been discovered in lanthanide and actinide intermetallic compounds. Prominent among them are superconductivity characterized by highly anisotropic unconventional order parameters and superconductivity coexisting with ferromagnetic order as well as the hidden order of unconventional density waves. A further example is the inhomogeneous superconducting phase appearing in an applied field which has been predicted theoretically a long time ago. A general hallmark of these systems is the coexistence and the competition of various different cooperative phenomena such as superconductivity and itinerant spin density wave magnetism.

The wealth of experimental data is only partly understood. To describe the low-temperature ordered phases, the determination of the type and symmetry of order parameters is of central importance. The latter restrict the possible excitations in the ordered phases and hence determine the low-temperature properties. Order parameters given in terms of expectation values of physical observables like spin- and charge-densities can be directly measured e.g. by x-ray and neutron diffraction. The magnetic phases in lanthanide and actinide compounds are therefore rather well characterized. This, however, is not the case for hidden order like quadrupolar ordering or unconventional density waves.

Superconductivity corresponds to an off-diagonal long range order parameter which is not directly observable and it is not surprising that the type of pairing is still a matter of controversy in many heavy fermion compounds. Considerable progress has, however, been made recently in detecting unconventional order parameter symmetries. Angle-resolved studies of thermodynamic and transport properties in the vortex phase determine the position of the order parameter nodes relative to the crystal axes. These results help to strongly reduce the number of symmetry-allowed superconducting candidate states.

Important information about the material properties relevant for superconductivity is gained from the temperature and frequency dependence of thermodynamic and transport properties. Experiments indicate severe deviations from the universal behavior predicted by weak-coupling BCS theory. The current theoretical analysis of experimental data which relies on standard weak-coupling theory can yield only qualitative results. A quantitative treatment must account for strong-coupling effects. This, however, requires a microscopic picture of the normal state, i.e., the quasiparticles and their interactions.

A microscopic picture for the strongly renormalized quasiparticles has finally emerged for the actinide compounds. The hypothesis of the dual character of the 5f-electrons is translated into a calculational scheme which reproduces both the Fermi surfaces and the effective masses determined by dHvA experiments without adjustable parameter. The method yields also a model for the residual interaction leading to the various instabilities of the normal phase. The next step will be to develop an appropriate Eliashberg-type theory. The dual model approach should also provide insight into the mysterious hidden order phases of U-compounds.

In Ce-based compounds, the Cooper pairs are formed by heavy quasiparticles with predominantly 4f-character which arise through the Kondo effect in the periodic lattice. This picture has been confirmed in detail by dHvA and high-resolution photoemission studies. The strongly renormalised quasiparticles can be successfully reproduced by a semiphe-

nomenological ansatz. Despite the efforts to implement modern many-body methods for strong correlations into realistic electronic structure calculations there is still no general concept for quantitative microscopic calculations. In particular, the subtle interplay between local and intersite effects continues to challenge theorists. The latter may lead to long-range order of local moments while the former favor the formation of a Fermi liquid state at low temperatures.

Many heavy fermion materials are on the verge of magnetic instability. By application of pressure and magnetic field, these materials can be tuned through a quantum critical point from a metallic antiferromagnet into a paramagnet. This may also trigger a transition to an unconventional SC state. Much effort has been devoted to the study of the behavior in the vicinity of the quantum critical point. Experimental data exhibit universality with unusual critical exponents. The theoretical picture, however, is highly controversial at present.

Superconductivity, magnetism and hidden order in lanthanide and actinide compounds pose an ongoing challenge. These compounds serve as model systems to study strong correlations in a broader context.

Acknowledgement

We have benefitted from discussions and suggestions from many colleagues, especially we would like to thank for collaboration and support from J. W. Allen, A. Amici, N. E. Christensen, T. Dahm, P. Fulde, K. Izawa, G. G. Lonzarich, K. Maki, Y. Matsuda, E. Runge, N. Sato, R. Shiina, F. Steglich, G. Varelogiannis, H. Won, A. Yaresko, and Q. Yuan.

G. Zwirner would like to acknowledge hospitality of the Max-Planck-Institute for the Chemical Physics of Solids, Dresden.

References

- Abrikosov, A. A.: 1988, *Fundamentals of the theory of metals*, North-Holland.
- Abrikosov, A. A., Gorkov, L. P. and Dzyaloshinski, I. E.: 1975, *Methods of Quantum Field Theory in Statistical Physics*, Dover, New York.
- Adenwalla, S., Lin, S. W., Ran, Q. Z., Zhao, Z., Ketterson, J. B., Sauls, J. A., Taillefer, L., Hinks, D. G., Levy, M. and Sarma, B. K.: 1990, *Phys. Rev. Lett.* **65**, 2298.
- Aeppli, G., Bucher, E., Broholm, C., Kjems, J. K., Baumann, J. and Hufnagl, J.: 1988, *Phys. Rev. Lett.* **60**, 615.
- Aeppli, G., Goldman, A., Shirane, G., Bucher, E. and Lux-Steiner, M.-C.: 1987, *Phys. Rev. Lett.* p. 808.
- Albers, R., Boring, A. M. and Christensen, N. E.: 1986, *Phys. Rev. B* **33**, 8116.
- Albessard, A. K., Ebihara, T., Umehara, I., Satoh, K., Onuki, Y., Aoki, H., Uji, S. and Shimizu, T.: 1993, *Physica B* **186-188**, 147.
- Allen, J. W.: 1992, *Resonant Photoemission of Solids with Strongly Correlated Electrons*, Vol. 1 of *Synchrotron Radiation Research: Advances in Surface and Interface Science*, Plenum Press, New York, chapter 6, p. 253.
- Alver, U., Goodrich, R. G., Harrison, N., Hall, D. W., Palm, E. C., Murphy, T. P., Tozer, S. W., Pagliuso, P. G., Moreno, N. O., Sarrao, J. L. and Fisk, Z.: 2001, *Phys. Rev. B* **64**, 180402–1.
- Amici, A.: 1999, *Magnetic order and superconductivity in $\text{HoNi}_2\text{B}_2\text{C}$ and related borocarbide compounds*, PhD thesis, Technical University Dresden.
- Amici, A. and Thalmeier, P.: 1998, *Phys. Rev. B* **57**, 10648.
- Amici, A. and Thalmeier, P.: 2001, Rare earth transition metal borocarbides (nitrides): Superconducting, magnetic and normal state properties, in K.-H. Müller and V. Narozhnyi (eds), *NATO Science Series II*, Vol. 14, Kluwer Academic Publishers, Dordrecht, p. 297.
- Amici, A., Thalmeier, P. and Fulde, P.: 2000, *Phys. Rev. Lett.* **84**, 1800.
- Amitsuka, H., Sato, M., Metoki, N., Yokohama, M., Kuwahara, K., Sakakibara, T., Morimoto, H., Kawarazaki, S., Miyako, Y. and Mydosh, J. A.: 1999, *Phys. Rev. Lett.* **83**, 5114.
- Amitsuka, H., Yokoyama, M., Miyazaki, S., Tenya, K., Sakakibara, T., Higemoto, W., Nagamine, K., Matsuda, K., Kohori, Y. and Kohara, T.: 2002, *Physica B* **312-313**, 390.
- Anderson, P. W.: 1984a, *Phys. Rev. B* **30**, 1549.

- Anderson, P. W.: 1984b, "Basic Notions of Condensed Matter Physics", Vol. 55 of *Frontiers in Physics*, Benjamin.
- Annett, J. F.: 1990, *Adv. Phys.* **39**, 83.
- Aoki, D., Huxley, A., Ressouche, E., Braithwaite, D., Flouquet, J., Brison, J.-P. and Lhotel, E.: 2001, *Nature* **413**, 613.
- Aoki, H., Uji, S., Albessard, A. K. and Onuki, Y.: 1993, *Phys. Rev. Lett.* **71**, 2110.
- Aoki, Y., Namiki, T., Ohsaki, S., Saha, S. R., Sugawara, H. and Sato, H.: 2002, *J. Phys. Soc. Jpn.* **71**, 2098.
- Aoki, Y., Tsuchiya, A., Kanayama, T., Saha, S. R., Sugawara, H., Sato, H., Higemoto, W., Koda, A., Ohishi, K., Nishiyama, K. and Kadono, R.: 2003, *Phys. Rev. Lett.* **91**, 067003.
- Bak, P. and von Boehm, J.: 1980, *Phys. Rev. B* **21**, 5297.
- Baltensperger, W. and Strässler, S.: 1963, *Phys. Kondens. Mater.* **1**, 20.
- Barash, Y. S., Svidzinskii, A. A. and Mineev, V. P.: 1997, *JETP Lett.* .
- Bardeen, J., Cooper, L. N. and Schrieffer, J. R.: 1957, *Phys. Rev.* **108**, 1175.
- Basletic, M., Korin-Hamzic, B. and Maki, K.: 2002, *Phys. Rev. B* **65**, 235117.
- Bauer, E. D., Frederick, N. A., Ho, P.-C., Zapf, V. S. and Maple, M. B.: 2002, *Phys. Rev. B* **65**, 100506(R).
- Bauer, E., Hilscher, G., Michor, H., Paul, C. and Scheidt, E. W.: 2003, *cond-mat/0308083* .
- Benfatto, L., Caprara, S. and Castro, C. D.: 2000, *Eur. Phys. J. B* **17**, 95.
- Berk, N. and Schrieffer, J. R.: 1966, *Phys. Rev. Lett.* **17**, 433.
- Berlinsky, A. J., Fetter, A. L., Franz, M., Kallin, C. and Soininen, P. I.: 1995, *Phys. Rev. Lett.* **75**, 2200.
- Bernhoeft, N.: 2000, *Eur. Phys. J. B* **13**, 685.
- Bernhoeft, N. and Lonzarich, G. G.: 1995, *J. Phys.: Condens. Matter* **7**, 7325.
- Bernhoeft, N., Sato, N., Roessli, B., Aso, N., Hiess, A., Lander, G. H., Endoh, Y. and Komatsubara, T.: 1998, *Phys. Rev. Lett.* **81**, 4244.
- Bianchi, A., Movshovich, R., Capan, C., Lacerda, A., Pagliuso, P. G. and Sarrao, J. L.: 2003, *cond-mat/0304420* .
- Bianchi, A., Movshovich, R., Oeschler, N., Gegenwart, P., Steglich, F., Thompson, J. D., Pagliuso, P. G. and Sarrao, J. L.: 2002, *Phys. Rev. Lett.* **89**, 137002.

- Biasini, M.: 2003, *J. Magn. Magn. Mater.* . to appear.
- Bilbro, G. and McMillan, W. L.: 1976, *Phys. Rev. B* **14**, 1887.
- Blount, E.: 1985, *Phys. Rev. B* **32**, 2935.
- Boaknin, E., Hill, R. W., Proust, C., Lupien, C., Taillefer, L. and Canfield, P. C.: 2001, *Phys. Rev. Lett.* **87**, 237001.
- Böhm, A., Grauel, A., Sato, N., Schank, C., Geibel, C., Komatsubara, T., Weber, G. and Steglich, F.: 1992, *Int. J. Mod. Phys. B* **7**, 34.
- Braithwaite, D., Fukuhara, T., Demuer, A., Sheikin, I., Kambe, S., Brison, J.-P., Maezawa, K., Naka, T. and Flouquet, J.: 2000, *J. Phys.: Condens. Matter* **12**, 1339.
- Brandt, E. H.: 1995, *Rep. Prog. Phys.* **58**, 1465.
- Brison, J. P., Keller, N., Lejay, P., Tholence, J. L., Huxley, A., Bernhoeft, N. R., Buzdin, A., Fak, B., Flouquet, J., Schmidt, L., Stepanov, A., Fisher, R. A., Phillips, N. and Vettier, C.: 1994, *Physica B* **199-200**, 70.
- Broholm, C., Kjems, J. K., Buyers, W. J. L., Matthews, P., Palstra, T. T. M., Menovsky, A. A. and Mydosh, J. A.: 1987, *Phys. Rev. Lett.* **58**, 1467.
- Broholm, C., Lin, H., Matthews, P. T., Mason, T. E., Buyers, W. J. L., Collins, M. F., Menovsky, A. A., Mydosh, J. A. and Kjems, J. K.: 1991, *Phys. Rev. B* **43**, 12809.
- Bruls, G., Weber, D., Wolf, B., Thalmeier, P., Lüthi, B., de Visser, A. and Menovsky, A.: 1990, *Phys. Rev. Lett* **65**, 2294.
- Bruls, G., Wolf, B., Finsterbusch, D., Thalmeier, P., Kouroudis, I., Sun, W., Assmus, W., Lüthi, B., Lang, M., Gloos, K., Steglich, F. and Modler, R.: 1994, *Phys. Rev. Lett.* **72**, 1754.
- Buchholtz, L. J. and Zwicknagl, G.: 1981, *J. Phys. Condens. Matter* **23**, 5788.
- Buyers, W. J. L. and Holden, T. M.: 1985, Handbook on the Physics and Chemistry of the Actinides, Elsevier Science Publishers B. V., Amsterdam.
- Campbell, A. J., Paul, D. M. and McIntyre, G. J.: 2000, *Phys. Rev. B* **61**, 5872.
- Canfield, P. C. and Bud'ko, S. L.: 1996, *Physica C* **262**, 249.
- Canfield, P. C., Bud'ko, S. L., Cho, B. K., Lacerda, A., Farrell, D., Johnston-Halperin, E., Kalatsky, V. and Pokrovsky, V. L.: 1997, *Phys. Rev. B* **55**, 970.
- Caspary, R., Hellmann, P., Keller, M., Wassilew, C., Köhler, R., Sparn, G., Schank, C., Geibel, C., Steglich, F. and Phillips, N. E.: 1993, *Phys. Rev. Lett.* **71**, 2146.

- Cava, R. J., Tagaki, H., Zandbergen, H. W., Krajewski, J. J., Jr., W. F. P., Siegrist, T., Batlogg, B., van Dover, R. B., Felder, R. J., Mizuhashi, K., Lee, J. O., Eisaki, H. and Uchida, S.: 1994, *Nature* **367**, 252.
- Cavadini, N., Schneider, M., Allenspach, P., Canfield, P. C. and Bourges, P.: 2003, *Europhys. Lett.* **63**, 597.
- Chakravarty, S., Kee, H.-Y. and Nayak, C.: 2001, *Int. J. Mod. Phys. B* **15**, 2901.
- Chakravarty, S., Laughlin, R. B., Morr, D. K. and Nayak, C.: 2001a, *Phys. Rev. B* **63**, 94503.
- Chia, E. E., Salamon, M. B., Sugawara, H. and Sato, H.: 2003, *cond-mat/0308454* .
- Chitra, R. and Kotliar, G.: 2000, *Phys. Rev. Lett.* **84**, 3678.
- Choi, C. and Sauls, J.: 1991, *Phys. Rev. Lett.* **66**, 484.
- Coleman, P.: 1999, *Physica B* **259-261**, 353.
- Condon, E. U. and Shortley, G. H.: 1957, *The Theory of Atomic Spectra*, Cambridge University Press, Cambridge.
- Continentino, M. A.: 2001, *Quantum Scaling in Many-Body Systems*, World Scientific Publishing, Singapore.
- Cox, D. L.: 1987, *Phys. Rev. Lett.* **59**, 1240.
- Cox, D. L.: 1988, *J. Magn. Magn. Mater* **76-77**, 53.
- Cox, D. L. and Zawadowski, A.: 1999, *Exotic Kondo effects in retals: Magnetic ions in a crystalline electric field and tunnelling centres*, Taylor and Francis.
- Custers, J., Gegenwart, P., Wilhelm, H., Neumaier, K., Tokiwa, Y., Trovarelli, O., Geibel, C., Steglich, F., Pepin, C. and Coleman, P.: 2003, *Nature* **424**, 524.
- Dahm, T.: 2001, *unpublished* .
- Dahm, T., Graser, S., Iniotakis, C. and Schopohl, N.: 2002, *Phys. Rev. B* **66**, 144515.
- Dahm, T., Maki, K. and Won, H.: 2000, *cond-mat/006301* .
- Dahm, T. and Tewordt, L.: 1995, *Phys. Rev. Lett.* **74**, 793.
- de Visser, A., Kayzel, F. E., Menovsky, A. A., Franse, J. J. M., van der Berg, J. and Nieuwenhuys, G. J.: 1986, *Phys. Rev. B* **34**, 8168.
- Degiori, L.: 1999, *Rev. Mod. Phys.* **71**, 687.
- Demuer, A., Sheikin, I., Brathwaite, D., Fak, B., Huxley, A., Saymon, S. and Flouquet, J.: 2001, *J. Magn. Magn. Mat.* **226-230**, 17.

- Denlinger, J. D., Gweon, G.-H., Allen, J. W., Olson, C. G., Maple, M. B., Sarrao, J. L., Armstrong, P. E., Fisk, Z. and Yamagami, H.: 2001, *J. Electron Spectrosc. Relat. Phenom.* **117 & 118**, 347.
- Dertinger, A.: 2001, *Supraleitung un Magnetismus in Holmium-Nickel-Borkarbid vom Strukturtyp $\text{LuNi}_2\text{B}_2\text{C}$* , PhD thesis, University of Bayreuth.
- Dervenagas, P., Bullock, M., Zarestky, J., Canfield, P. C., Chao, B. K., Harmon, B., Goldman, A. I. and Stassis, C.: 1995, *Phys. Rev. B* **52**, 9839.
- Detlefs, C., Bourdarot, F., Bourlet, P., Dervenagas, P., Bud'ko, S. L. and Canfield, P. C.: 2000, *Phys. Rev. B* **61**, R14916.
- Doh, H., Sigrist, M., Cho, B. and Lee, S.-I.: 1999, *Phys. Rev. Lett.* **83**, 5350.
- Doniach, S.: 1977, *Physica B* **91**, 231.
- Dóra, B., Maki, K., Korin-Hamzic, B., Basletic, M., Virosztek, A., Kartsovnik, M. V. and Müller, H.: 2002, *Europhys. Lett.* **60**, 737.
- Dóra, B. and Virosztek, A.: 2001, *Eur. Phys. J. B* **22**, 169.
- Drechsler, S. L., Rosner, H., Shulga, S. V., Opahle, I., Eschrig, H., Freudenberger, J., Fuchs, G., Nenkov, K., Müller, K., Bitterlich, H., Löser, W., Behr, G., Lipp, D. and Gladun, A.: 2001, *Physica C* **364-365**.
- Dressel, M., Kasper, N., Petukhov, K., Gorshunov, B., Grüner, G., Huth, M. and Adrian, H.: 2002, *Phys. Rev. Lett.* **88**, 186404.
- Dugdale, S. B., Alam, M. A., Wilkinson, I., Hughes, R. J., Fisher, I. R., Canfield, P. C., Jarlborg, T. and Santi, G.: 1999, *Phys. Rev. Lett.* **83**, 4824.
- Dumont, E. and Mota, A. C.: 2002, *Phys. Rev. B* **65**, 144519.
- Efremov, D., Hasselmann, N., Runge, E. K. R., Fulde, P. and Zwicknagl, G.: 2003, *cond-mat/0303414*.
- Ehm, D., Reinert, F., Nicolay, G., Schmidt, S., Hüfner, S., Claessen, R., Eyert, V. and Geibel, C.: 2001, *Phys. Rev. B* **64**, 235104-1.
- Eskildsen, M. R., Dewhurst, C. D., Hoogenboom, B. W., Petrovic, C. and Canfield, P. C.: 2003, *Phys. Rev. Lett.* **90**, 187001.
- Fak, B., Flouquet, J., Lapertot, G., Fukuhara, T. and Kadowaki, H.: 2000, *J. Phys. Condens. Matter.* **12**, 5423.
- Fay, D. and Appel, J.: 1980, *Phys. Rev. B* **22**, 3173.
- Fazekas, P.: 1999, *Lecture Notes on Electron Correlations and Magnetism*, Vol. 5 of *Series in Modern Condensed Matter Physics*, World Scientific, Singapore.

- Felten, R., Steglich, F., Weber, G., Rietschel, H., Gompf, F., Renker, B. and Beuers, J.: 1986, *Europhys. Lett.* **2**(323).
- Feyerherm, R., Amato, A., Gygax, F. N., Schenck, A., Geibel, C., Steglich, F., Sato, N. and Komatsubara, T.: 1994, *Phys. Rev. Lett.* **73**, 1849.
- Fischer, O.: 1990, *Magnetic Superconductors*, Vol. 5, North Holland, Amsterdam.
- Fischer, O. and Maple, M. B. (eds): 1982, Vol. 32 and 34 of *Topics in Current Physics*, Springer Verlag, Berlin.
- Fisher, I. R., Cooper, J. R. and Canfield, P. C.: 1997, *Phys. Rev. B* **56**, 10820.
- Fisher, R. A., Kim, S., Woodfield, B. F., Phillips, N. E., Taillefer, L., Hasselbach, K., Flouquet, J., Giorgi, A. L. and Smith, J. L.: 1989, *Phys. Rev. Lett.* **62**, 1411.
- Fomin, I. A.: 2001, *JETP Letters* **74**, 111.
- Frederick, N. A., Do, T. D., Ho, P. C., Butch, N. P., Zapf, V. S. and Maple, M. B.: 2003, *cond-mat/0307059* .
- Frigeri, P., Agterberg, D., Koga, A. and Sigrist, M.: 2003, *cond-mat/0311354* .
- Frings, P. H., Franse, J. J. M., deBoer, F. R. and Menovsky, A.: 1983, *J. Magn. Magn. Mater.* **31-34**, 240.
- Fujimori, S., Ino, A., Okane, T., Fujimori, A., Harima, H., Aoki, D., Ikeda, S., Shishido, H., Haga, Y., Tokiwa, Y. and Onuki, Y.: 2002a, *Physica B* **312-313**, 132.
- Fujimori, S., Okane, T., Okamoto, J., Mamiya, K., Muramatsu, Y., Fujimori, A., Harima, H., Aoki, D., Ikeda, S., Shishido, H., Tokiwa, Y., Haga, Y. and Onuki, Y.: 2003, *Phys. Rev. B* **67**, 144507.
- Fulde, P.: 1995, *Electron Correlations in Molecules and Solids*, third edn, Springer Verlag, Berlin.
- Fulde, P. and Keller, J.: 1982, "Topics of Current Physics" *Superconductivity in Ternary Compounds*, Vol. 34, Springer, Berlin, chapter Theory of Magnetic Superconductors.
- Fulde, P., Keller, J. and Zwicknagl, G.: 1988, Theory of heavy fermion systems, in F. Seitz, D. Turnbull and H. Ehrenreich (eds), *Solid State Physics*, Vol. 41, Academic Press, New York, p. 1.
- Fulde, P. and Zwicknagl, G.: 1990, Pairbreaking in superconductors, in J. G. Bednorz and K. A. Müller (eds), *Earlier and Recent Aspects of Superconductivity*, Vol. 90, Springer-Verlag, Heidelberg.
- Gangopadhyay, A. K. and Schilling, J. S.: 1996, *Phys. Rev. B* **54**, 10107.
- Garnier, M., Purdie, D., Breuer, K., Hengsberger, M. and Baer, Y.: 1997, *Phys. Rev. B* **56**, R11399.

- Garnier, M., Purdie, D., Breuer, K., Hengsberger, M. and Baer, Y.: 1998, *Phys. Rev. B* **58**, 3515.
- Gasser, U., Allenspach, P., Fauth, F., Henggeler, W., Mesot, J., Furrer, A., Rosenkranz, S., Vorderwisch, P. and Buchgeister, M.: 1996, *Z. Phys. B* **101**, 345.
- Gaulin, B. D., Mao, M., Wiebe, C. R., Qiu, Y., Shapiro, S. M., Broholm, C., Lee, S.-H. and Garrett, J. D.: 2002, *Phys. Rev. B* **66**, 174520.
- Gegenwart, P., Kromer, F., Lang, M., Sparn, G., Geibel, C. and Steglich, F.: 1999, *Phys. Rev. Lett.* **82**, 1293.
- Gegenwart, P., Langhammer, C., Geibel, C., Helfrich, R., Lang, M., Sparn, G., Steglich, F., Horn, R., Donnevert, L., Link, A. and Assmus, W.: 1998, *Phys. Rev. Lett.* **81**, 1501.
- Geibel, C., Schank, C., Thies, S., Kitazawa, H., Bredl, C. D., Böhm, A., Rau, M., Grauel, A., Caspary, R., Helfrich, R., Ahlheim, U., Weber, G. and Steglich, F.: 1991a, *Z. Phys. B* **84**, 1.
- Geibel, C., Thies, S., Kczorowski, D., Mehner, A., Grauel, A., Seidel, B., Ahlheim, U., Helfrich, R., Petersen, K., Bredl, C. D. and Steglich, F.: 1991, *Z. Phys.* **83**, 305.
- Georges, A., Kotliar, G., Krauth, W. and Rozenberg, M. J.: 1996, *Rev. Mod. Phys.* **68**, 13.
- Ginzburg, V.: 1957, *JETP* **4**, 153.
- Golding, B., Bishop, D. J., Batlogg, B., Haemmerle, W. H., Fisk, Z., Smith, J. L. and Ott, H. R.: 1985, *Phys. Rev. Lett.* **55**, 2479.
- Goll, G., v. Löhneysen, H., Zapf, V. S., Bauer, E. D. and Maple, M. B.: 2003, *Acta Physica Polonica* **34**, 575.
- Goremychkin, E. A. and Osborn, R.: 1993, *Phys. Rev. B* **47**, 14280.
- Gorkov, L.: 1987, *Sov. Sci. Rev. Sect. A* **9**, 1.
- Gor'kov, L. P. and Sokol, A.: 1992, *Phys. Rev. Lett.* **69**, 2586.
- Goryo, J.: 2003, *Phys. Rev. B* **67**, 184511.
- Graf, M. J., Yip, S.-K. and Sauls, J. A.: 1996, *Phys. Ref. B* **53**, 15147.
- Graf, M. J., Yip, S.-K. and Sauls, J. A.: 1999, *J. Low Temp. Phys.* **114**, 257.
- Graf, M. J., Yip, S.-K. and Sauls, J. A.: 2000, *Phys. Rev. B* **62**, 14393.
- Grauel, A., Böhm, A., Fischer, H., Geibel, C., Köhler, R., Modler, R., Schank, C., Steglich, F. and Weber, G.: 1992, *Phys. Rev. B* **46**, 5818.

- Grewe, N. and Steglich, F.: 1991, *Handbook on the Physics and Chemistry of Rare Earths*, Vol. 14, Elsevier Science Publishers B. V., Amsterdam, chapter Heavy Fermions, p. 343.
- Grin', Y. N., Yarmolyuk, Y. P. and Gladyshevskii, E. I.: 1979, *Sov. Phys. Crystallogr.* **24**, 137.
- Grosche, F. M., Agarwal, P., Julian, S. R., Wilson, N. J., Haselwimmer, R. K. W., , Lister, S. J. S., Mathur, N. D., Carter, F. V., Saxena, S. S. and Lonzarich, G. G.: 2000, *J. Phys. Condens. Matter.* **12**, L533.
- Grosche, F. M., Julian, S. R., Mathur, N. D. and Lonzarich, G. G.: 1996, *Physica B* **223** & **224**, 50.
- Grüner, G.: 1994, *Density waves in solids*, Frontiers in physics, Addison-Wesley.
- Gulacsi, Z. and Gulacsi, M.: 1987, *Phys. Rev. B* **36**, 699.
- Gunnarsson, O. and Schönhammer, K.: 1983, *Phys. Rev. B* **28**, 4315.
- Harima, H. and Yanase, A.: 1991, *Journal of The Physical Society of Japan* **60**, 21.
- Harrison, N., Jaime, M. and Mydosh, J. A.: 2003, *Phys. Rev. Lett.* **90**, 096402.
- Hasselbach, K.: 1993, *Phys. Rev. B* **47**, 509.
- Hasselbach, K., Kirtley, J. R. and Lejay, P.: 1992, *Phys. Rev. B* **46**, 5826.
- Hayden, S. M., Taillefer, L., Vettier, C. and Flouquet, J.: 1992, *Phys. Rev. B* **46**, 8675.
- Heffner, R. H., Cooke, D. W., Giorgi, A. L., Hutson, R. L., Schillaci, M. E., Remp, H. D., Smith, J. L., Willis, J. O., Maclaughlin, D. E., Boekman, C., Licht, R. L., Oostens, J. and Denison, A. B.: 1989, *Phys. Rev. B* **39**, 11345.
- Heffner, R. H. and Norman, M. R.: 1996, *Comments in Cond. Matter Phys.* **17**, 361.
- Heffner, R. H., Smith, J. L., Willis, J. O., Birrer, P., Baines, C., Gygax, F. N., Hitti, B., Lippelt, E., Ott, H. R., Schenk, A., Knetsch, E. A., Mydosh, J. A. and MacLaughlin, D. E.: 1990, *Phys. Rev. Lett.* **65**(2816).
- Hegger, H., Petrovic, C., Moshopolou, E. G., Hundley, M. F., Sarrao, J. L., Fisk, Z. and Thompson, J. D.: 2000, *Phys. Rev. Lett.* **84**, 4986.
- Helfrich, R.: 1996, PhD thesis, TU Darmstadt.
- Herring, C.: 1966, *Magnetism. A Treatise on Modern Theory and Materials*, Vol. V of *Magnetism, A treatise on Modern Theory and Materials*, Academic Press, New York.
- Hertz, J. A.: 1976, *Phys. Rev. B* **14**, 1165.
- Hess, D. W., Tokuyasu, T. A. and Sauls, J. A.: 1989, *J. Phys. Condens. Matter* **1**, 8135.

- Hessert, J., Huth, M., Jourdan, M., Adrian, H., Rieck, C. T. and Scharnberg, K.: 1997, *Physica B* **230-232**, 373.
- Hewson, A. C.: 1993, *The Kondo Problem to Heavy Fermions*, Cambridge University Press.
- Hilscher, G. and Michor, H.: 1999, *Studies in High Temperature Superconductors*, Vol. 28, Nova Science Publishers, pp. 241–286.
- Hiroi, M., Sera, M., Kobayashi, N., Haga, Y., Yamamoto, E. and Onuki, Y.: 1997, *J. Phys. Soc. Jpn.* **66**, 1595.
- Hirschfeld, P., Vollhardt, D. and Wölfle, P.: 1986, *Solid State Commun.* **59**, 111.
- Hotta, T.: 1993, *J. Phys. Soc. Jpn.* **62**, 278.
- Hunt, M., Meeson, P., Probst, P. A., Reinders, P., Springford, M., Assmus, W. and Sun, W.: 1990, *J. Phys. C* **2**, 6859.
- Huxley, A., Sheikin, I., Ressouche, E., Kernavanois, N., Braithwaite, D., Calemczuk, R. and Flouqut, J.: 2001, *Phys. Rev. B* **63**, 144519–1.
- Ichioka, M., Nakai, N. and Machida, K.: 2003, *J. Phys. Soc. Jpn.* **72**, 1322.
- Ikeda, H. and Ohashi, Y.: 1998, *Phys. Rev. Letts.* **81**, 3723.
- Ikeda, H. and Ohashi, Y.: 1999, *Phys. Rev. Lett.* **82**, 5173.
- Inada, Y., Ishiguro, A., Kimura, J., Sato, N., Sawada, A., Komatsubara, T. and Yamagami, H.: 1995, *Physica B* **206-207**, 33.
- Inada, Y., Yamagami, H., Haga, Y., Sakurai, K., Tokiwa, Y., Honma, T., Yamamoto, E., Onuki, Y. and Yanagisawa, T.: 1999, *J. Phys. Soc. Jpn.* **68**, 3643.
- Ishida, K., Okamoto, K., Kawasaki, Y., Kitaoka, Y., Troarelli, O., Geibel, C. and Steglich, F.: 2002, *Phys. Rev. Lett.* **89**, 107202.
- Izawa, K., Kamata, K., Nakajima, Y., Matsuda, Y., Watanabe, T., Nohara, M., Takagi, H., Thalmeier, P. and Maki, K.: 2002a, *Phys. Rev. Lett.* **89**, 137006.
- Izawa, K., Nakajima, Y., Goryo, J., Matsuda, Y., Osaki, S., Sugawara, H., Sato, H., Thalmeier, P. and Maki, K.: 2003, *Phys. Rev. Lett.* **90**, 1170013.
- Izawa, K., Takahashi, H., Yamaguchi, H., Matsuda, Y., Suzuki, M., Sasaki, T., Fukase, T., Yoshida, Y., Settai, R. and Onuki, Y.: 2001a, *Phys. Rev. Lett.* **86**, 2653.
- Izawa, K., Yamaguchi, H., Matsuda, Y., Shishido, H., Settai, R. and Onuki, Y.: 2001, *Phys. Rev. Lett.* **87**, 05700.
- Izawa, K., Yamaguchi, H., Sasaki, T. and Matsuda, Y.: 2002, *Phys. Rev. Lett.* **88**, 027002.

- Izyumov, Y. A.: 1999, *Physics -Uspekhi* **42**, 215.
- Jaccard, D., Behnia, K. and Sierro, J.: 1992, *Phys. Lett. A* **163**, 475.
- Jaime, M., Kim, K. H., Jorge, G., McCall, S. and Mydosh, J. A.: 2002, *Phys. Rev. Lett.* **89**, 287201.
- Jayprakash, C., Krishna-murthy, H.-R. and Wilkins, J. W.: 1981, *Phys. Rev. Lett.* **47**, 737.
- Jayprakash, C., Krishna-murthy, H.-R. and Wilkins, J. W.: 1982, *J. Appl. Phys.* **53**, 2142.
- Jensen, J.: 2002, *Phys. Rev. B* **65**, 140514.
- Jensen, J. and Mackintosh, A. R.: 1991, *Rare Earth Magnetism Structures and Excitations*, Clarendon Press, Oxford.
- Jones, B. and Varma, C. M.: 1987, *J. Magn. Magn. Mater.* **63 & 64**, 251.
- Jourdan, M., Huth, M. and Adrian, H.: 1999, *Nature* **398**, 47.
- Joynt, R.: 1990, *J. Phys. Condens. Matter* **2**, 3415.
- Joynt, R. and Taillefer, L.: 2002, *Rev. Mod. Phys.* **74**, 237.
- Kadanoff, L. and Falko, C.: 1964, *Phys. Rev. A* **136**, A1170.
- Kaganov, M. I. and Lifshits, I. M.: 1979, *Sov. Phys. Usp.* **22**, 904.
- Kamata, K.: 2003, Master's thesis, University of Tokyo.
- Kato, M. and Machida, K.: 1987, *J. Phys. Soc. Jpn.* **56**, 2136.
- Kato, M. and Machida, K.: 1988, *Phys. Rev. B* **37**, 1510.
- Kawano-Furukawa, H., Habuta, E., Nagata, T., Nagao, M., Yoshizawa, H., Furukawa, N., Takeya, H. and Kadowaki, K.: 2001, *cond-mat/0106273*.
- Kawano-Furukawa, H., Takeshita, H., Ochiai, M., Nagata, T., Yoshizawa, H., Furukawa, N., Takeya, H. and Kadowaki, K.: 2002, *Phys. Rev. B* **65**, 180508.
- Kawano, H., Takeya, H., Yoshizawa, H. and Kadowaki, K.: 1999, *J. Phys. Chem. Solids* **60**, 1053.
- Kawasaki, S., Mito, T., Kawasaki, Y., q. Zheng, G., Kitaoka, Y., Shishido, H., Araki, S., Settai, R. and Onuki, Y.: 2002, *Phys. Rev. B* **66**, 054521.
- Kee, H.-Y., Kim, Y. B. and Maki, K.: 2000, *Phys. Rev. B* **62**, 5877.
- Keller, N., Brison, J. P., Lejay, P., Tholence, J. L., Huxley, A., Schmidt, L., Buzdin, A. and Flouquet, J.: 1995, *Physica B* **206-207**, 568.
- Kernavanois, N., de Réotier, P. D., Yaouanc, A., Sanchez, J.-P., Liß, K. D. and Lejay, P.: 1999, *Physica B* **259-261**, 648.

- Kernavanois, N., Grenier, B., Huxley, A., Ressouche, E., Sanchez, J. P. and Flouquet, J.: 2001, *Phys. Rev. B* **64**, 174509.
- Kimura, N., Komatsubara, T., Aoki, D., Onuki, Y., Haga, Y., Yamamoto, E., Aoki, H. and Harima, H.: 1998, *J. Phys. Soc. Jpn.* **67**, 2185.
- King, C. A. and Lonzarich, G. G.: 1991, *Physica B* **171**, 161.
- Kirkpatrick, T. R., Belitz, D., Vojta, T. and Narayanan, R.: 2001, *Phys. Rev. Lett.* **87**, 127003.
- Kita, H., Dönni, A., Endoh, Y., Kakurai, K., Sato, N. and Komatsubara, T.: 1994, *J. Phys. Soc. Jpn.* **63**, 726.
- Kitaoka, Y., Tou, H., Ishida, K., Kimura, N., Onuki, Y., Yamamoto, E., Haga, Y. and Maezawa, K.: 2000, *Physica B* **281 & 282**, 878.
- Knöpfle, K., Mavromaras, A., Sandratskii, L. M. and Kübler, J.: 1996, *J. Phys. Condens. Matter* **8**, 901.
- Kobayashi, T. C., Hanazono, K., Tateiwa, N., Amaya, K., Haga, Y., Settai, R. and Onuki, Y.: 2001, *cond-mat/0107548*.
- Kohgi, M., Iwasa, K., Nakajima, M., Metoki, N., Araki, S., Bernhoeft, N., Mignot, J.-M., Gukasov, A., Sato, H., Aoki, Y. and Sugawara, H.: 2003, *J. Phys. Soc. Jpn.* **72**, 1002.
- Kohori, Y., Yamato, Y., Iwamoto, Y., Kohara, T., Bauer, E. D., Maple, M. B. and Sarrao, J. L.: 2001, *Phys. Rev. B* **64**, 134526.
- Koike, Y., Metoki, N., Kimura, N., Yamamoto, E., Haga, Y., Onuki, Y. and Maezawa, K.: 1998, *J. Phys. Soc. Jpn* **67**, 1142.
- Konno, R. and Ueda, K.: 1989, *Phys. Rev. B* **40**, 4329.
- Korin-Hamzic, B., Basletic, M. and Maki, K.: 2002, *Europhys. Lett.* **59**, 298.
- Kotegawa, H., Yogi, M., Imamura, Y., Kawasaki, Y., Zheng, G.-Q., Kitaoka, Y., Ohsaki, S., Sugawara, H., Aoki, Y. and Sato, H.: 2003, *Phys. Rev. Lett.* **90**, 027001.
- Krimmel, A., Fischer, P., Roessli, B., Maletta, H., Geibel, C., Schank, C., Grauel, A., Loidl, A. and Steglich, F.: 1992, *Z. Phys. B* **86**, 161.
- Kromer, F.: 2000, PhD thesis, TU Dresden.
- Kromer, F., Helfrich, R., Lang, M., Steglilch, F., Langhammer, C., Bach, A., Michels, T., Kim, J. and Stewart, G.: 1998, *Phys. Rev. Lett.* **81**, 4476.
- Kromer, F., Lang, M., Oeschler, N., Hinze, P., Langhammer, C. and Steglich, F.: 2000, *Phys. Rev. B* **62**, 12477.

- Kromer, F., Oeschler, N., Tayama, T., Tenya, K., Cichorek, T., Lang, M., Steglich, F., Kim, J. S. and Stewart, G. R.: 2002, *J. Low Temp. Phys.* **126**, 815.
- Kübert, C. and Hirschfeld, P. J.: 1998, *Solid State Commun.* **105**, 459.
- Kuramoto, Y. and Kitaoka, Y.: 2000, *Dynamics of Heavy Electrons*, Vol. 105 of *International Series of Monographs in Physics*, Clarendon Press, Oxford.
- Kyogaku, M., Kitaoka, Y., Asayama, K., Geibel, C., Schank, C. and Steglich, F.: 1993, *J. Phys. Soc. Jpn.* **62**, 4016.
- Landau, L. D.: 1956, *Sov. Phys. JETP* **3**, 920.
- Landau, L. D.: 1957, *Soviet Physics - JETP* **32**, 59.
- Landau, L. D.: 1958, *Soviet Physics - JETP* **35**, 97.
- Lang, M. and Müller, J.: 2003, *The Physics of Superconductors*, Vol. 2, Springer Verlag, chapter "Organic Superconductors", to appear, cond-mat/0302157.
- Layzer, A. and Fay, D.: 1971, *Int. J. Mag.* **1**, 135.
- Layzer, A. and Fay, D.: 1974, *Solid State Commun.* **14**, 599.
- Liu, W., Dolg, M. and Fulde, P.: 1998, *Inorg. Chem.* **37**, 1067.
- Lonzarich, G. G.: 1988, *J. Magn. Magn. Mat.* **76 / 77**, 1.
- Lundin, U., Sandalov, I., Eriksson, O. and Johansson, B.: 2000, *Phys. Rev. B* **62**, 16 370.
- Lussier, B., Ellman, B. and Taillefer, L.: 1996, *Phys. Rev. B* **53**, 5145.
- Lynn, J. W., Skanthakumar, S., Huang, Q., Sinha, S. K., Hossain, Z., Gupta, L. C., Nagarajan, R. and Godart, C.: 1997, *Phys. Rev. B* **55**, 6548.
- Machida, K.: 1981, *J. Phys. Soc. Jpn.* **50**, 2195.
- Machida, K. and Matsubara, T.: 1981, *J. Phys. Soc. Jpn.* **50**, 3231.
- Machida, K., Nishira, T. and Ohmi, T.: 1999, *J. Phys. Soc. Jpn.* **68**, 3364.
- Machida, K. and Ohmi, T.: 1998, *J. Phys. Soc. Jpn.* **65**, 4018.
- Machida, K. and Ohmi, T.: 2001, *Phys. Rev. Lett.* **86**, 850.
- Machida, K., Ozaki, M. and Ohmi, T.: 1989, *J. Phys. Soc. Jpn.* **58**, 4116.
- Mackenzie, A. P. and Maeno, Y.: 2003, *Rev. Mod. Phys.* **75**, 657.
- Maki, K., Dora, B., Kartsovnik, M., Virosztek, A., Korin-Hamzic, B. and Basletic, M.: 2003, *Phys. Rev. Lett* **90**, 256402.

- Maki, K., Dora, B. and Virosztek, A.: 2003a, *cond-mat/0306567* .
- Maki, K. and Thalmeier, P.: 2003, *Physica C* **388**, 521.
- Maki, K., Thalmeier, P. and Won, H.: 2002, *Phys. Rev. B* **65**, 140502(R).
- Maki, K. and Won, H.: 1996, *J. Phys. I France* **6**, 2317.
- Maki, K., Won, H., Thalmeier, P., Yuan, Q., Izawa, K. and Matsuda, Y.: 2003, *Europhys. Lett.* **64**, 496.
- Malterre, D., Grioni, M. and Baer, Y.: 1996, *Adv. Phys.* **45**, 299.
- Maple, M. B., Ho, P.-C., Frederick, N. A., Zapf, V. S., Yuhasz, W. M. and Bauer, E. D.: 2003, *Acta Phys Pol. B* **34**, 919.
- Maple, M. B., Ho, P.-C., Zapf, V. S., Frederick, N. A., Yuhasz, E. D. B. W. M., Woodward, F. M. and Lynn, J. W.: 2002, *J. Phys. Soc. Jpn.* **71**, 23.
- Marabelli, F., Wachter, P. and Franse, J. J. M.: 1987, *J. Magn. Magn. Mat.* **63-64**, 377.
- Martinez-Samper, Suderow, H., Vieira, S., Brison, J. P., Luchier, N., Lejay, P. and Canfield, P. C.: 2003, *Phys. Rev. B.* **64**, 020503.
- Mason, T. E. and Aeppli, G.: 1997, *Matematisk-fysiske Meddelelser* **45**, 231.
- Mathur, N. D., Grosche, F. M., Julian, S. R., Walker, I. R., Freye, D. M., Haselwimmer, R. K. W. and Lonzarich, G. G.: 1998, *Nature* **394**, 39.
- Matsuda, K., Kohori, Y. and Kohara, T.: 1996, *J. Phys. Soc. Jpn.* **65**(679).
- Matsuda, K., Kohori, Y. and Kohara, T.: 1997, *Phys. Rev. B.* **55**, 15223.
- Matsuda, Y. and Izawa, K.: 2003, *Acta Physica Polonica B* **34**, 579.
- Mattheis, L. F.: 1994, *Phys. Rev. B* **49**, R13279.
- McMahan, A. K., Held, K. and Scalettar, R. T.: 2003, *Phys. Rev. B* **67**, 075108.
- McMullen, G. J., Julian, S. R., Doiron-Leyraud, N., Huxley, A., Bergemann, C., Flouquet, J. and Lonzarich, G. G.: 2001. to be published.
- Mentink, S. A. M., Wyder, U., Perenboom, J. A. A. J., de Visser, A., Menovsky, A. A., Nieuwenhuys, G. J., Mydosh, J. A. and Mason, T. E.: 1997, *Physica B* **230-232**, 74.
- Metlushko, V., Welp, U., Koshelev, A., Aranson, I., Crabtree, G. W. and Canfield, P. C.: 1997, *Phys. Rev. Lett.* **79****17**, 1738.
- Metoki, N.: 2001, *J. Phys. Soc. Jpn.* **70**, 11.
- Metoki, N., Haga, Y., Koike, Y. and Onuki, Y.: 1998, *Phys. Rev. Lett.* **80**, 5417.

- Michel, L.: 1980, *Rev. Mod. Phys.* **52**, 617.
- Millis, A. J.: 1993, *Phys. Rev. B* **48**, 7183.
- Millis, A. J., Sachdev, S. and Varma, C. M.: 1988, *Phys. Rev. B* **37**, 4975.
- Mineev, V. P.: 2002, *Phys. Rev. B* **66**, 134504.
- Mineev, V. P. and Samokhin, K. V.: 1999, *Introduction to Unconventional Superconductivity*, Gordon and Breach Science Publishers.
- Miyake, K., Kohno, H. and Harima, H.: 2003, *J. Phys. Condens. Matter* **15**, L275.
- Miyake, K., Schmitt-Rink, S. and Varma, C. M.: 1986, *Phys. Rev. B* **34**, 6554.
- Mizuno, K., Saito, T., Fudo, H., Koyama, K., Endo, K. and Deguchi, H.: 1999, *Physica B* **259-261**, 594.
- Monthoux, P., Balatsky, A. V. and Pines, D.: 1991, *Phys. Rev. Lett.* **67**, 3448.
- Monthoux, P. and Lonzarich, G. G.: 1999, *Phys. Rev. B* **59**, 14598.
- Monthoux, P. and Lonzarich, G. G.: 2001, *Phys. Rev. B* **63**, 054529.
- Monthoux, P. and Lonzarich, G. G.: 2002, *Phys. Rev. B* **66**, 224504.
- Monthoux, P. and Pines, D.: 1994, *Phys. Rev. B* **49**, 4261.
- Morin, P., Vettier, C., Flouquet, J., Konczykowski, M., Lasailly, Y., Mignot, J.-M. and Welp, U.: 1988, *J. Low Temp. Phys.* **70**, 377.
- Moriya, T.: 1985, *Spin Fluctuations in Itinerant Electron Magnets*, Springer Verlag, Berlin.
- Moriya, T. and Takimoto, T.: 1995, *J. Phys. Soc. Jpn.* **64**, 960.
- Moriya, T. and Ueda, K.: 2000, *Adv. Phys.* **49**, 555.
- Morosov, A. I.: 1996, *Sov. Phys. JETP* **83**, 1084.
- Morosov, A. I.: 1996a, *Sov. Phys. JETP Lett.* **63**, 734.
- Mota, A. C. and Cichorek, T.: 2003, *to be published* .
- Movshovich, R., Graf, T., Mandrus, D., Thompson, J. D. and J. L. Smith, a. Z. F.: 1996, *Phys. Rev. B* **53**, 8241.
- Müller, K.-H. and Narozhnyi, V. N.: 2001, *Rep. Prog. Phys.* **64**, 943.
- Müller, V., Maurer, D., Scheidt, E. W., Roth, C., amd E. Bucher, K. L. and Bömmel, H. E.: 1986, *Solid State Commun.* **57**, 319.

- Nagarajan, N., Mazumda, C., Hossain, Z., Dhar, S. K., Gopalakrishnan, K. V., Gupta, L. C., Godart, C., Padalia, B. D. and Vijayaraghavan, R.: 1994, *Phys. Rev. Lett.* **72**, 274.
- Nakajima, S.: 1973, *Prog. Theor. Phys.* **50**, 1101.
- Nakamura, S., Suzuki, O., Goto, T., Sakatsume, S., Matsumara, T. and Kunii, S.: 1997, *J. Phys. Soc. Jpn.* **66**, 552.
- Nakao, H., Magishi, K., Wakabayashi, Y., Murakami, Y., Koyama, K., Hirota, K., Endoh, Y. and Kunii, S.: 2001, *J. Phys. Soc. Jpn.* **70**, 2892.
- Nersesyan, A. A., Japaridze, G. I. and Kimeridze, I. G.: 1991, *J. Phys. Condens. Matter* **3**, 3353.
- Nersesyan, A. A. and Vachnadze, G. E.: 1989, *J. Low Temp. Phys.* **77**, 293.
- Ng, T. K. and Varma, C. M.: 1997, *Phys. Rev. Lett.* **78**, 3745.
- Nohara, M., Isshiki, M., Takagi, H. and Cava, R.: 1997, *J. Phys. Soc. Jpn.* **66**, 1888.
- Norman, M. R.: 1991, *Phys. Rev. B* **43**, 6121.
- Norman, M. R.: 1994, *Phys. Rev. B* **50**, 6904.
- Norman, M. R., Albers, R. C., Boring, A. M. and Christensen, N. E.: 1988, *Solid State Commun.* **68**, N245.
- Norman, M. R. and Hirschfeld, P. J.: 1996, *Phys. Rev. B* **53**, 5706.
- Nozières, P.: 1974, *J. Low Tempo. Phys.* **17**, 31.
- Ocana, R. and Esquinazi, P.: 2002, *Phys. Rev. B* **66**, 064525.
- Oeschler, N., Gegenwart, P., Steglich, F., Frederick, N. A., Bauer, E. D. and Maple, M. B.: 2003, *Acta Phys. Pol. B* **34**, 959.
- Oeschler, N., Weickert, F., Gegenwart, P., Thalmeier, P., Steglich, F., Bauer, E. D. and Maple, M. B.: 2003a, *preprint* .
- Ohkuni, H., Inada, Y., Tokiwa, Y., Sakurai, K., Settai, R., Honma, T., Haga, Y., Yamamoto, E., Onuki, Y., Yamagami, H., Takahashi, S. and Yanagisawa, T.: 1999, *Philosophical Magazine B* **79**, 1045.
- Ohmi, T. and Machida, K.: 1996, *J. Phys. Soc. Jpn.* **65**, 4018.
- Ohmi, T. and Machida, K.: 1996a, *J. Phys. Soc. Jpn.* **65**(3456).
- Okuno, Y., Narikiyo, O. and Miyake, K.: 1998, *J. Phys. Soc. Jpn.* **67**, 2469.
- Onuki, Y., Ukon, I., Yun, S. W., Umeharhara, I., Satoh, K., Fukuhara, T., Sato, H., Takayanagi, S., Shikama, M. and Ochiai, A.: 1992, *J. Phys. Soc. Jpn.* **61**, 293.

- Ott, H. R.: 1987, Vol. XI, Elsevier, Amsterdam, p. 215.
- Ott, H. R. and Fisk, Z.: 1987, *Handbook on the Physics and Chemistry of the Actinides*, Vol. 5, North-Holland, p. 85.
- Ott, H. R., Rudigier, H., Fisk, Z. and Smith, J. L.: 1983, *Phys. Rev. Lett.* **50**, 1595.
- Ott, H. R., Rudigier, H., Rice, T. M., Ueda, K., Fisk, Z. and Smith, J. L.: 1984, *Phys. Rev. Lett.* **82**(1915).
- Ozaki, M.: 1992, *Int. Journal of Quantum Chemistry* **42**, 55.
- Ozaki, M. and Machida, K.: 1985, *Prog. Theor. Phys.* **74**, 221.
- Palstra, T. T. M., Menovsky, A. A., vandenBerg, J., Dirkmaat, A. J., Res, P. H., Nieuwenhuys, G. J. and Mydosh, J. A.: 1985, *Phys. Rev. Lett.* **55**, 2727.
- Pao, C. H. and Bickers, N. E.: 1994, *Phys. Rev. Lett.* **72**, 1870.
- Park, J.-G., McEwen, K. A. and Bull, M. J.: 2002, *Phys. Rev. B* **66**, 094502.
- Park, T., Salamon, M. B., Choi, E. M., Kim, H. J. and Lee, S.-I.: 2003, *Phys. Rev. Lett.* **90**, 177001.
- Petrovic, C., Budko, S. L., Kogan, V. G. and Canfield, P. C.: 2002, *Phys. Rev. B* **67**, 054534.
- Petrovic, C., Movshovich, R., Jaime, M., Pagliuso, P. G., Hundley, M. F., Sarrao, J. L., Fisk, Z. and Thompson, J. D.: 2001, *Europhys. Lett.* **53**, 354.
- Petrovic, C., Pagliuso, P. G., Hundley, M. F., Movshovich, R., Sarrao, J. D., Thompson, J. D., Fisk, Z. and Monthoux, P.: 2001a, *J. Phys.:Condens. Matter* **13**, L337.
- Pfleiderer, C.: 2001, *J. Magn. Magn. Mat.* **226-230**, 23.
- Pfleiderer, C. and Huxley, A. D.: 2002, *Phys. Rev. Lett.* **89**, 147005-1.
- Pickett, W. E. and Singh, D. J.: 1994, *Phys. Rev. Lett.* **72**, 3702.
- Pollmann, F. and Zwicknagl, G.: 2003. unpublished.
- Pulst, U.: 1993, PhD thesis, TH Darmstadt.
- Ramirez, A. P., Chandra, P., Coleman, P., Fisk, Z., Smith, J. L. and Ott, H. R.: 1994, *Phys. Rev. Lett.* **73**, 3018.
- Rauchschwalbe, U., Steglich, F., Stewart, G. R., amd P. Fulde, A. L. G. and Maki, K.: 1987, *Europhysics Letters* **3**, 751.
- Regnault, L. P., Erkelens, W. A. C., Rossat-Mignot, J., Lejay, P. and Flouquet, J.: 1988, *Phys. Rev. B* **38**, 4481.

- Rhee, J. Y., Wang, X. and Harmon, B. N.: 1995, *Phys. Rev. B* **51**, 15585.
- Rieck, C. T., Scharnberg, K. and Schopohl, N.: 1991, *J. Low. Temp. Phys.* **84**, 381.
- Rosch, A.: 1999, *Phys. Rev. Lett.* **82**, 4280.
- Rosner, H., Drechsler, S.-L., Koepfner, K., Opahle, I. and Eschrig, H.: 2001, Rare earth transition metal borocarbides (nitrides): Superconducting, magnetic and normal state properties, in K.-H. Müller and V. Narozhnyi (eds), *NATO Science Series II*, Kluwer Academic Publishers, Dordrecht.
- Rotundu, C. R., Tsuji, H., Takano, Y., Andracka, B., Sugawara, H., Aoki, Y. and Sato, H.: 2003, *cond-mat/0305182*.
- Runge, E., Albers, R. A., Christensen, N. E. and Zwicknagl, G.: 1995, *Phys. Rev. B* **51**.
- Sachdev, S.: 1999, *Quantum Phase Transitions*, Cambridge University Press.
- Saint-James, D., Thomas, E. J. and Sarma, G.: 1969, *Type II Superconductivity*, Pergamon Press, Oxford.
- Sales, B. C.: 2003, *Handbook on the Physics and Chemistry of the Rare Earths*, Vol. 33, Elsevier, chapter 211, p. 1.
- Sales, B. C., Mandrus, D. and Williams, R. K.: 1996, *Science* **272**, 1325.
- Sandratskii, L. M. and Kübler, J.: 1994, *Phys. Rev. B* **50**.
- Santini, P.: 1998, *Phys. Rev. B* **57**, 5191.
- Santini, P. and Amoretti, G.: 1994, *Phys. Rev. Lett.* **73**, 1027.
- Santini, P., Amoretti, G., Caciuffo, R., Bourdarot, F. and Fak, B.: 2000, *Phys. Rev. Lett.* **85**, 654.
- Sarrao, J. L., Thompson, J. D., Moreno, N. O., Morales, L. A., Wastin, F., Rebizan, J., Boulet, P., Colineau, E. and Lander, G. H.: 2003, *J. Phys. Condens. Matter* **15**, 52775.
- Sato, N.: 1993, *unpublished*.
- Sato, N., Aso, N., Lander, G. H., Roessli, B., Komatsubara, T. and Endoh, Y.: 1997, *J. Phys. Soc. Jpn.* **66**, 1884.
- Sato, N., Aso, N., Lander, G. H., Roessli, B., Komatsubara, T. and Endoh, Y.: 1997a, *J. Phys. Soc. Jpn.* **66**, 2981.
- Sato, N. K., Aso, N., Miyake, K., Shiina, R., Thalmeier, P., Varelogiannis, G., Geibel, C., Steglich, F., Fulde, P. and Komatsubara, T.: 2001, *Nature* **410**, 340.
- Sato, N., Koga, N. and Komatsubara, T.: 1996, *J. Phys. Soc. Jpn.* **65**, 1555.

- Sauls, J. A.: 1994, *Advances in Physics* **43**, 113.
- Saxena, S. S., Agarwal, P., K.Ahllan, Grosche, F. M., Haselwimmer, R. W. K., Steiner, M. J., Pugh, E., Walker, I. R., Julian, S. R., Monthoux, P., Lonzarich, G. G., Huxley, A., Shelkin, I., Braithwaite, D. and Flouquet, J.: 2000, *Nature* **406**, 587.
- Scalapino, D. J.: 1995, *Physics Reports* **250**, 329.
- Scharnberg, K., Walker, D., Monien, H., Tewordt, L. and Klemm, R.: 1986, *Solid State Commun.* **60**, 535.
- Schlabitz, W., Bauman, J., Politt, B., Rauchschwalbe, U., Mayer, H. M., Ahlheim, U. and Bredl, C. D.: 1986, *Z. Phys. B* **52**, 171.
- Schlottmann, P. and Sacramento, P.: 1993, *Adv. Phys.* **42**, 641.
- Schmidt, H. and Braun, H. F.: 1997, *Phys. Rev. B* **55**, 8497.
- Schmitt-Rink, S., Miyake, K. and Varma, C. M.: 1986, *Phys. Rev. Lett.* **57**, 2575.
- Schoenes, J., Vogt, O., Löhle, J., Hulliger, F. and Mattenberger, K.: 1996, *Phys. Rev. B* **53**, 14987.
- Schrieffer, J. R.: 1964, *Theory of Superconductivity*, Benjamin, Reading, Massachusetts.
- Schuberth, E. A., Strickler, B. and Andres, K.: 1992, *Phys. Rev. Lett.* **68**, 117.
- Schulz, H.: 1989, *Phys. Rev. B* **39**, 2940.
- Shah, N.: 2000, *Phys. Rev. B* **61**, 564.
- Shick, A. B. and Pickett, W. E.: 2001, *Phys. Rev. Lett.* **86**, 300.
- Shiina, R.: 2001. private communication.
- Shiina, R., Shiba, H. and Thalmeier, P.: 1997, *J. Phys. Soc. Jpn.* **66**, 1741.
- Shishido, H., Settai, R., Aoki, D., Ikeda, S., Nakawaki, H., Nakamura, N., Iizuka, T., Inada, Y., Sugiyama, K., Takeuchi, T., Kindo, K., Kobayashi, T. C., Haga, Y., Harima, H., Aoki, Y., Namiki, T., Sato, H. and Onuki, Y.: 2002, *J. Phys. Soc. Japan* **71**, 162.
- Shivaram, B. S., Jeong, Y. H., Rosenbaum, T. F., Hinks, D. G. and Schmitt-Rink, S.: 1987, *Phys. Rev. B* **35**, 5372.
- Shulga, S. V. and Drechsler, S.-L.: 2001, Rare earth transition metal borocarbides (nitrides): Superconducting, magnetic and normal state properties, *in* K.-H. Müller and V. Narozhny (eds), *NATO Science SeriesII*, Kluwer Academic Publishers, Dordrecht.
- Shulga, S. V., Drechsler, S.-L., Fuchs, G., Müller, K. H., Winzer, K. H., Heinecke, M. and Krug, K.: 1998, *Phys. Rev. Lett.* **80**, 1730.

- Si, Q.: 2001, *J. Magn. Magn. Mat.* **226-230**, 30.
- Si, Q., Rabello, S., Ingersent, K. and Smith, J. L.: 2001, *Nature* **413**, 804.
- Si, Q., Smith, J. L. and Ingersent, K.: 1999, *Int. J. of Mod. Phys. B* **13**, 2331.
- Sigrist, M. and Agterberg, D.: 1999, *Prog. Theor. Phys.* **102**, 965.
- Sigrist, M. and Rice, T. M.: 1989, *Phys. Rev. B* **39**, 2200.
- Sigrist, M. and Ueda, K.: 1991, *Rev. Mod. Phys.* **63**, 239.
- Sikkema, A. E., Buyers, W. J. L., Affleck, I. and Gan, J.: 1996, *Phys. Rev. B* **54**, 9322.
- Smith, J. L. and Si, Q.: 2000, *Phys. Rev. B* **61**, 5184.
- Söderlind, P., Ahuja, R., Eriksson, O., Johansson, B. and Wills, J. M.: 2000, *Phys. Rev. B* **61**, 8119.
- Steglich, F.: 1985, in T. Kasuya and T. Saso (eds), *Theory of Heavy Fermions and Valence Fluctuations*, Springer Verlag, Berlin, p. 3.
- Steglich, F., Aarts, J., Bredl, C., Lieke, W., Meschede, D., Franz, W. and Schäfer, H.: 1979, *Phys. Rev. Lett.* **43**, 1892.
- Steglich, F., Gegenwart, P., Geibel, C., Hinze, P., Lang, M., Langhammer, C., Sparn, G., Tayama, T., Trovarelli, O., Sato, N., Dahm, T. and Varelogiannis, G.: 2001, *More is different- fifty years of condensed matter physics*, Princeton University Press, chapter 13, p. 191.
- Steglich, F., Gegenwart, P., Geibel, C., Hinze, P., Lang, M., Langhammer, C., Sparn, G. and Trovarelli, O.: 2000a, *Physica B* **280**, 349.
- Steglich, F., Gegenwart, P., Helfrich, R., C.Langhammer, Hellmann, P., Donnevert, L., Geibel, C., Lang, M., Sparn, G., Assmus, W., Stewart, G. R. and Ochiai, A.: 1997, *Z. Phys. B* **103**, 235.
- Steglich, F., Rauchschalbe, U., Gottwick, U., Mayer, H. M., Sparn, G., Grewe, N. and Poppe, U.: 1985, *J. Appl. Phys.* **57**, 3054.
- Steglich, F., Sato, N., Tayama, T., Lühmann, T., Langhammer, C., Gegenwart, P., Hinze, P., Geibel, C., Lang, M., Sparn, G. and Assmus, W.: 2000, *Physica C* **341-348**, 691.
- Stewart, G. R.: 2001, *Rev. Mod. Phys.* **73**, 797.
- Stewart, G. R., Fisk, Z., Willis, J. O. and Smith, J. L.: 1984, *Phys. Rev. Lett.* **52**, 679.
- Stockert, O., Faulhaber, E., Zwicknagl, G., Stuesser, N., Jeevan, H., Cichorek, T., Loewenhaupt, R., Geibel, C. and Steglich, F.: 2003, *preprint* .
- Suderow, H., Brison, J. P., Huxley, A. D. and Flouquet, J.: 1997, *J. Low Temp. Phys.* **108**, 11.

- Sugawara, H., Osaki, S., Saha, S. R., Aoki, Y., Sato, H., Inada, Y., Shishido, H., Settai, R., Onuki, Y., Harima, H. and Oikawa, K.: 2002, *Phys. Rev. B* **66**, 220504(R).
- Sugiyama, K., Nakashima, M., Ohkuni, H., Kindo, K., Haga, Y., Haga, Y., Honma, T., Yamamoto, E. and Onuki, Y.: 1999, *J. Phys. Soc. Jpn.* **68**, 3394.
- Sun, Y. and Maki, K.: 1995, *Europhys. Lett.* **32**, 335.
- Taillefer, L. and Lonzarich, G. G.: 1988, *Phys. Rev. Lett.* **60**, 1570.
- Taillefer, L., Newbury, R., Lonzarich, G. G., Fisk, Z. and Smith, J. L.: 1987, *J. Magn. Magn. Mat.* **63 & 64**, 372.
- Takahashi, T., Sato, N., Yokoya, T., Chainani, A., Morimoto, T. and Komatsubara, T.: 1995, *J. Phys. Soc. Japan* **65**, 156.
- Takegahara, K., Harima, H. and Yanase, A.: 2001, *J. Phys. Soc. Jpn.* **70**, 1190.
- Takeuchi, T., Inoue, T., Sugiyama, K., Aoki, D., Tokiwa, Y., Haga, Y., Kindo, K. and Onuki, Y.: 2001, *J. Phys. Soc. Japan* **70**, 877.
- Tateiwa, N., Kobayashi, T. C., Amaya, K., Haga, Y., Settai, R. and Onuki, Y.: 2003, *Acta Phys. Pol. B* **34**, 515.
- Tateiwa, N., Sato, N. and Komatsubara, T.: 1998, *Phys. Rev. B* **58**, 11131.
- Tautz, F. S., Julian, S. R., McMullen, G. J. and Lonzarich, G. G.: 1995, *Physica B* **206-207**, 29.
- Tayama, T., Sakakibara, T., Sugawara, H., Aoki, Y. and Sato, H.: 2003, *J. Phys. Soc. Jpn.* **72**, 1516.
- Thalmeier, P.: 1991, *Phys. Rev. B* **44**.
- Thalmeier, P.: 1994, *Z. Phys. B* **95**, 39.
- Thalmeier, P.: 1996, *Z. Phys. B* **100**, 387.
- Thalmeier, P.: 2002, *Eur. Phys. J. B* **27**, 287.
- Thalmeier, P. and Lüthi, B.: 1991, *Handbook on the Physics and Chemistry of Rare Earths*, Vol. 14, North-Holland, chapter 96, p. 225.
- Thalmeier, P. and Maki, K.: 2002, *Europhysics Letters* **58**, 119.
- Thalmeier, P. and Maki, K.: 2003a, *Phys. Rev. B* **67**, 092510–1.
- Thalmeier, P. and Maki, K.: 2003b, *Acta Physica Polonica B* **34**, 557.
- Thalmeier, P., Wolf, B., Weber, D., Bruls, G., Lüthi, B. and Menovsky, A. A.: 1991, *Physica C* **175**, 61.

- Thompson, J. D., Movshovich, R., Fisk, Z., Bouquet, F., Curro, N. J., Fisher, R. A., Hammel, P. C., Hegger, H., Hundley, M. F., Jaime, M., Pagliuso, P. G., Petrovic, C., Phillips, N. E. and Sarrao, J. L.: 2001, *J. Magn. Magn. Mat.* **226-230**, 5.
- Tou, H., Ishida, K. and Kitaoka, Y.: 2003, *cond-mat/0308562* .
- Tou, H., Kitaoka, Y., Asayama, K., Geibel, C., Schank, C. and Steglich, F.: 1995, *J. Phys. Soc. Jpn.* **64**, 725.
- Tou, H., Kitaoka, Y., Ishida, K., Asayama, K., Kimura, N., Onuki, Y., Yamamoto, E., Haga, Y. and Maezawa, K.: 1998, *Phys. Rev. Lett.* **80**, 3129.
- Tou, H., Kitaoka, Y., Kimura, N., Onuki, Y., Yamamoto, E. and Maezawa, K.: 1996, *Phys. Rev. Lett.* **77**, 1374.
- Trappmann, T., v. Löhneysen, H. and Taillefer, L.: 1991, *Phys. Rev. B* **43**, 13714.
- Tsuei, C. C. and Kirtley, J. R.: 2000, *Rev. Mod. Phys.* **72**, 969.
- Tsuneto, T.: 1961, *Phys. Rev.* **121**, 406.
- Ueda, K. and Rice, T. M.: 1985, *Phys. Rev. B* **31**, 7114.
- v. Löhneysen, H.: 1994, *Physica B* **197**, 551.
- van Dijk, N. H.: 1994, *Dilatometry of Heavy-Fermion Superconductors*, PhD thesis, Universiteit van Amsterdam.
- van Dijk, N. H., de Visser, A., Franse, J. J. M., Holtmeier, S., Taillefer, L. and Flouquet, J.: 1993, *Physica B* **186-188**, 267.
- van Dijk, N. H., Fak, B., Charvolin, T., Lejay, P. and Mignot, J. M.: 2000, *Phys. Rev. B* **61**, 8922.
- van Harlingen, D. J.: 1995, *Rev. Mod. Phys.* **67**, 515.
- Varelogiannis, G., Thalmeier, P. and Tsonis, S.: 2003, *cond-mat/0306106* .
- Vekhter, I., Hirschfeld, P. J. and Nichols, E. J.: 2001, *Phys. Rev. B* **64**, 064513.
- Virosztek, A., Maki, K. and Dóra, B.: 2002, *Int. J. Mod. Phys. B* **16**, 1667.
- Vollhardt, D. and Wölfle, P.: 1990, *The superfluid phases of ^3He* , Taylor and Francis, New York.
- Vollmer, R., Faißt, A., Pfeiderer, C., v. Löhneysen, H., Bauer, E. D., Ho, P. C. and Maple, M. B.: 2003, *Phys. Rev. Lett.* **90**, 57001.
- Volovik, G. E.: 1993, *JETP Lett.* **58**, 469.
- Volovik, G. E. and Gor'kov, L. P.: 1985, *Sov. Phys. JETP* **61**, 843.

- Walker, I. R., Grosche, F. M., Freye, D. M. and Lonzarich, G. G.: 1997, *Physica C* **282**, 303.
- Walker, M. B., Buyers, W. J. L., Tun, Z., Que, W., Menovsky, A. A. and Garrett, J. D.: 1993, *Phys. Rev. Lett.* **71**, 2630.
- Watanabe, S. and Miyake, K.: 2002, *J. Phys. Soc. Jpn.* **71**, 2489.
- Watanabe, T., Nohara, M., Hanaguri, T. and Takagi, H.: 2003. preprint.
- White, R. and Fulde, P.: 1981, *Phys. Rev. Lett.* **47**, 1540.
- Wilson, K. G.: 1975, *Rev. Mod. Phys.* **47**, 773.
- Winzer, K., Peng, Z. and Krug, K.: 1999, *Physica B* **259-261**, 586.
- Won, H. and Maki, K.: 1995, *Europhys. Lett.* **30**, 421.
- Won, H. and Maki, K.: 2000, *cond-mat/004105* .
- Won, H. and Maki, K.: 2001a, *Europhysics Letters* **56**, 729.
- Won, H. and Maki, K.: 2001b, *Vortices in Unconventional Superconductors and Superfluids*, Springer, Berlin.
- Won, H., Maki, K., Haas, S., Oeschler, N., Weickert, F. and Gegenwart, P.: 2003a, *cond-mat/0306548* .
- Won, H., Yuan, Q., Thalmeier, P. and Maki, K.: 2003, *Brazilian Journal of Physics* **33**.
- Wu, W. C. and Joynt, R.: 2002, *Phys. Rev. B* **65**, 104502.
- Yanase, Y., Jujo, T., Nomura, T., Ikeda, H., Hotta, T. and Yamada, K.: 2003, *cond-mat/0309094* .
- Yang, G. and Maki, K.: 1999, *Europhys. Lett.* **48**, 208.
- Yang, G. and Maki, K.: 2001, *Eur. Phys. J. B* **21**, 61.
- Yang, X. and Nayak, C.: 2002, *Phys. Rev. B* **65**, 064523.
- Yaouanc, A., de Réotier, P. D., Gubbens, P. C. M., Kaiser, C. T., Menovsky, A. A., Mihalik, M. and Cottrell, S. P.: 2002, *Phys. Rev. Lett.* **89**, 147001.
- Yaresko, A. and Thalmeier, P.: 2003, *preprint* .
- Yaron, U., Gammel, P. L., Ramirez, A. P., Huse, D. A., Bishop, D. J., Goldman, A. I., Stassis, C., Canfield, P. C., Mortensen, K. and Eskildsen, M. R.: 1996, *Nature* **382**, 236.
- Yip, S. K., Li, T. and Kumar, P.: 1991, *Phys. Rev. B* **43**, 2742.

- Yokoyama, M., Amitsuka, H., Tenya, K., Watanabe, K., Kawarazaki, S., Yoshizawa, H. and Mydosh, J. A.: 2003, *cond-mat/0311199*.
- Yokoyama, M., Amitsuka, H., Watanabe, K., Kawarazaki, S., Yoshizawa, H. and Mydosh, J. A.: 2002, *J. Phys. Soc. Jpn* **71**, 264.
- Yuan, Q., Chen, H.-Y., Won, H., Lee, S., Maki, K., Thalmeier, P. and Ting, C. S.: 2003, *Phys. Rev. B* **68**, 174510.
- Yuan, Q. and Thalmeier, P.: 2003, *Phys. Rev. B* **68**, 174501.
- Zheng, G. q., Tanabe, K., Mito, T., Kawasaki, S., Kitaoka, Y., Aoki, D., Haga, Y. and Onuki, Y.: 2001, *Phys. Rev. Lett.* **86**, 4664.
- Zvyagin, A. A.: 2000, *Phys. Rev. B* **63**, 014503.
- Zwicknagl, G.: 1988, *J. Magn. Magn. Mat.* **76 & 77**, 16.
- Zwicknagl, G.: 1992, *Adv. Phys.* **41**, 203.
- Zwicknagl, G.: 1993, *Physica Scripta T* **49**, 34.
- Zwicknagl, G.: 1999, *Physica B* **259-261**, 1105.
- Zwicknagl, G. and Fulde, P.: 1981, *Z. Phys. B* **43**, 23.
- Zwicknagl, G. and Pulst, U.: 1993, *Physica B* **186**, 895.
- Zwicknagl, G., Runge, E. and Christensen, N. E.: 1990, *Physica B* **163**, 97.
- Zwicknagl, G., Yaresko, A. and Fulde, P.: 2003, *Phys. Rev. B* **68**, 052508.
- Zwicknagl, G., Yaresko, A. N. and Fulde, P.: 2002, *Phys. Rev. B* **65**, 081103(R).

Index

- antiferromagnetic order, 35, 93
 - PrOs₄Sb₁₂, 152
 - UPt₃, 80, 82
- antiferroquadrupolar order, 118, 151
- B-T phase diagram
 - CeCu₂Si₂, 60
 - HoNi₂B₂C, 142
 - PrOs₄Sb₁₂, 152, 157
 - UPt₃, 85
 - URu₂Si₂, 121
- band structure, 14, 18, 19, 56, 95, 109, 133, 150
- BCS ratio, 40, 66
- Blount's theorem, 30, 88
- borocarbides, 34, 129
- Ce₂RhIn₈, 65
- CeCoIn₅, 64–66
- CeCu₂(Si_{1-x}Ge_x)₂, 37, 61
- CeCu₂Ge₂, 55
- CeCu₂Si₂, 12, 36
- CeIrIn₅, 65
- CeM₂X₂, 55
- CeMIn₅, 64
- CeNi₂Ge₂, 55, 61
- CePd₂Si₂, 55, 61
- CeRh₂Si₂, 55
- CeRhIn₅, 65
- CeRu₂Ge₂, 57
- CeRu₂Si₂, 58
- charge density wave, 26, 31, 49
- coexistence, 26, 32, 35, 37, 143, 144, 149
- conventional pairing, 29, 32, 49
- Coulomb interaction, 16, 23, 75
- crystalline electric field excitations, 59, 75, 98, 116, 141, 151
- d-wave gap, 33, 36, 37, 44, 47, 50, 66, 68
- de Haas-van Alphen effect, 57, 116
 - UPd₂Al₃, 96
 - UPt₃, 77
- Doppler shift, 45, 136
- dual model, 13, 73, 96
- DyNi₂B₂C, 144
- E_{2u}-model, 85, 87
- effective interaction, 23, 25, 27, 103, 146
- electron-electron pairing, 21, 49
- electron-hole pairing, 21, 31
- electron-phonon superconductivity, 131
- Eliashberg equations, 102, 104
- ErNi₂B₂C, 143, 144, 149
- Fermi liquid, 18, 20, 124
- Fermi liquid parameters, 20, 21
- Fermi surface, 33, 52, 57
 - CeCu₂Si₂, 59
 - CeRu₂Si₂, 57
 - UPd₂Al₃, 96
 - UPt₃, 74
- Fermi velocity, 18
- Fermi wave vector, 18
- ferromagnetic order, 107–109, 143, 144, 149
- FFLO phase, 67, 68
- form factor, 36, 40
- free energy, 83, 119, 141
- gap equations, 31, 35
- gap function, 27, 31, 86, 134, 155, 156
- gap nodes, 34, 44, 134
- giant diamagnetism, 51
- Ginzburg-Landau theory, 29, 84, 113
- heavy fermions, 11, 12, 14, 18, 59, 73, 74, 150
- hidden order, 31, 49, 112, 115, 120
- high-T_c, 23
- HoNi₂B₂C, 139, 140, 144
- Hubbard model, 22
- Hund's rules, 17
- hybridisation, 11, 15
- hydrostatic pressure, 81, 82, 109, 148
 - UGe₂, 108
 - URu₂Si₂, 118
- impurity scattering, 45, 135

- incommensurate order, 37, 62, 139, 141
- induced moment magnetism, 98
- inelastic neutron scattering
 - UPd₂Al₃, 101
 - URu₂Si₂, 122
- jj-coupling, 30, 74
- Knight shift, 42, 94
 - UPt₃, 89
- Kondo lattice, 10, 70
- Kondo resonance, 11, 124
- Kondo temperature, 11
- Landau levels, 51, 52
- Landau parameters, 83
- LaRu₂Si₂, 58
- LuNi₂B₂C, 130
- magnetic exciton, 92, 98, 100, 122
- magnetostriction
 - UPt₃, 85
- magnetotransport, 44, 50–52, 90, 155
- mass enhancement, 14, 75, 97, 116
- metamagnetism, 121, 139, 142
- multiphase superconductivity, 73, 154
- nesting property, 33, 36, 50, 62, 120, 134
- neutron diffraction, 50
 - CeCu₂Si₂, 62
- non-Fermi liquid state, 124
- nuclear magnetic resonance, 42, 89
- order parameter, 26
- phase shifts, 19, 20
- point nodes, 87, 91, 137, 138
- power laws, 39, 43
- PrOs₄Sb₁₂, 150
- quantum critical point, 13, 61, 69, 113
- quasiparticle DOS, 33, 39, 45, 52, 104, 133, 135
 - YNi₂B₂C, 136
- quasiparticle excitations, 32, 36
- quasiparticle tunneling, 131
 - UPd₂Al₃, 102, 103
- reentrance behaviour, 112, 145, 148
- RKKY interaction, 70, 100, 141, 142
- RNi₂B₂C, 35, 129, 138
- s+g wave gap, 134, 135, 138
- singlet CEF state, 15, 59
- singlet pairing, 21, 27, 30, 31, 43, 66, 78, 87
- skutterudites, 34, 150
- specific heat, 38, 39, 132
 - CeCoIn₅, 67
 - PrOs₄Sb₁₂, 154
 - U_{1-x}Th_xBe₁₃, 127
 - UPt₃, 81
 - URu₂Si₂, 40, 117
 - YNi₂B₂C, 46
- spin density wave, 26, 31, 37, 49
- spin fluctuation, 20, 69, 107
- spin orbit coupling, 30, 77, 89
- strong coupling effects, 66, 104, 131
- superclean limit, 45
- susceptibility, 100, 110, 111
 - UPd₂Al₃, 93
- symmetry group, 28
- T_c-splitting, 81–83, 153
- tetracritical point, 84
- Th_{1-x}U_xRu₂Si₂, 116
- thermal conductivity, 38, 40, 47, 132, 136, 154, 157
 - CeCoIn₅, 47
 - UPt₃, 89
 - YNi₂B₂C, 137
- thermal expansion, 119
 - PrOs₄Sb₁₂, 154
 - U_{1-x}Th_xBe₁₃, 125–127
 - UPt₃, 85
- tight binding model, 35, 50
- time reversal symmetry, 28, 38, 50, 113, 120
- triplet pairing, 21, 27, 30, 31, 43, 78, 87, 105, 113
- U_{1-x}Th_xBe₁₃, 124
- UBe₁₃, 124
- UGe₂, 107

ultrasonic attenuation, 41
 UPt₃, 42
unconventional pairing, 29, 31, 32, 49,
 120
UNi₂Al₃, 105
unitary state, 83
UPd₂Al₃, 13, 15, 92
upper critical field, 43, 84, 113, 132
 CeCoIn₅, 67
 HoNi₂B₂C, 145, 148
 UBe₁₃, 126
 UGe₂, 112
UPt₃, 15, 73
URu₂Si₂, 49, 115

Volovik effect, 45
vortex phase, 38, 44, 67, 90, 136, 149, 157

Wiedemann-Franz law, 53

Y(Ni_{1-x}Pt_x)₂B₂C, 135, 138
YbRh₂Si₂, 70
YNi₂B₂C, 130